



CAROLINA PENTEADO NATIVIDADE MORETO

**GEOCRONOLOGIA U-Pb E Re-Os APLICADA À EVOLUÇÃO METALOGENÉTICA
DO CINTURÃO SUL DO COBRE DA PROVÍNCIA MINERAL DE CARAJÁS**

CAMPINAS

2013



UNIVERSIDADE ESTADUAL DE CAMPINAS
INSTITUTO DE GEOCIÊNCIAS

NÚMERO: 466/2013

CAROLINA PENTEADO NATIVIDADE MORETO

**“GEOCRONOLOGIA U-Pb E Re-Os APLICADA À EVOLUÇÃO METALOGENÉTICA
DO CINTURÃO SUL DO COBRE DA PROVÍNCIA MINERAL DE CARAJÁS”**

ORIENTADORA: PROFA. DRA. LENA VIRGÍNIA SOARES MONTEIRO

CO-ORIENTADOR: PROF. DR. ROBERTO PEREZ XAVIER

TESE DE DOUTORADO APRESENTADA AO INSTITUTO DE GEOCIÊNCIAS DA UNICAMP NO PROGRAMA DE GEOCIÊNCIAS PARA OBTENÇÃO DO TÍTULO DE DOUTORA EM CIÊNCIAS NA ÁREA DE CONCENTRAÇÃO GEOLOGIA E RECURSOS NATURAIS.

ESTE EXEMPLAR CORRESPONDE À VERSÃO FINAL DA TESE DEFENDIDA PELA ALUNA CAROLINA PENTEADO NATIVIDADE MORETO, ORIENTADA PELA PROFA. DRA. LENA VIRGÍNIA SOARES MONTEIRO E CO-ORIENTADA PELO PROF. DR. ROBERTO PEREZ XAVIER

CAMPINAS

2013

FICHA CATALOGRÁFICA ELABORADA POR
CÁSSIA RAQUEL DA SILVA – CRB8/5752 – BIBLIOTECA “CONRADO PASCHOALE” DO
INSTITUTO DE GEOCIÊNCIAS
UNICAMP

M817g	<p>Moreto, Carolina Penteado Natividade, 1985- Geocronologia U-Pb e Re-Os aplicada à evolução metalogénética do Cinturão Sul do cobre da Província Mineral de Carajás / Carolina Penteado Natividade Moreto-- Campinas,SP.: [s.n.], 2013.</p> <p>Orientador: Lena Virgínia Soares Monteiro. Coorientador: Roberto Perez Xavier. Tese (doutorado) - Universidade Estadual de Campinas, Instituto de Geociências.</p> <p>1. Carajás, Serra dos (PA) 2. Depósitos de óxido de Fe-Cu-Au – Carajás, Serra dos (PA) 3. Geocronologia. 4. Cráttons – Amazônia. I. Monteiro, Lena Virginia Soares, 1970- II. Xavier, Roberto Perez, 1958- III. Universidade Estadual de Campinas, Instituto de Geociências. IV. Título.</p>
-------	-----------------------------------------------------------------------------------------------------------------------------------------------------------------------------------------------------------------------------------------------------------------------------------------------------------------------------------------------------------------------------------------------------------------------------------------------------------------------------------------------------------------------------------------------------------------------------------------------------------------------------------------------------------------------------------------------------------------------------------------------------------------

Informações para a Biblioteca Digital

Título em inglês: U-Pb and Re-Os geochronology applied to the metallogenetic evolution of the Southern Copper Belt of the Carajás Mineral Province.

Palavras-chaves em inglês:

Carajás, Serra dos (PA)

Iron oxide-Cu-Au deposits – Carajás, Serra dos (PA)

Geochronology

Craton – Amazon

Área de concentração: Geologia e Recursos Naturais

Titulação: Doutora em Ciências

Banca examinadora:

Lena Virgínia Soares Monteiro (Orientador)

Márcio Martins Pimentel

Elton Luiz Dantas

Ticiano José Saraiva dos Santos

Maria José Maluf de Mesquita

Data da defesa: 05-08-2013

Programa de Pós-graduação em Geociências



UNIVERSIDADE ESTADUAL DE CAMPINAS
INSTITUTO DE GEOCIÊNCIAS
PROGRAMA DE PÓS GRADUAÇÃO EM GEOCIÊNCIAS
ÁREA DE GEOLOGIA E RECURSOS NATURAIS

AUTORA: Carolina Penteado Natividade Moreto

"Geocronologia U-Pb e Re-Os aplicada à evolução metalogenética do Cinturão Sul do Cobre da Província Mineral de Carajás"

ORIENTADORA: Profa. Dra. Lena Virginia Soares Monteiro

CO-ORIENTADOR: Prof. Dr. Roberto Perez Xavier

Aprovada em: 05/ 08/ 2013

EXAMINADORES:

Profa. Dra. Lena Virginia Soares Monteiro

Prof. Dr. Ticiano José Saraiva dos Santos

Prof. Dr. Elton Luiz Dantas

Prof. Dr. Márcio Martins Pimentel

Profa. Dra. Maria José Maluf de Mesquita

Four handwritten signatures are shown, each above a horizontal line. From top to bottom: 1. A signature that appears to be "Lena V. Soares Monteiro" followed by "Presidente". 2. A signature that appears to be "Ticiano José Saraiva dos Santos". 3. A signature that appears to be "Elton Luiz Dantas". 4. A signature that appears to be "Márcio Martins Pimentel". 5. A signature that appears to be "Maria José Maluf de Mesquita".

Campinas, 05 de agosto de 2013

Dedico esse trabalho ao meu companheiro Wagner, aos meus pais José Luiz e Stella, ao meu irmão Bruno e minha cunhada Sonja pela compreensão e apoio durante esses anos.

AGRADECIMENTOS

Agradeço primeiramente à Deus, por todas as oportunidades que tive em minha vida e, nesse contexto acadêmico, em poder desenvolver um trabalho de doutorado numa instituição tão importante.

Devo total gratidão à minha orientadora, profa. Dra. Lena Monteiro, pela valiosa oportunidade que me foi dada, pela confiança, pelo conhecimento e aprendizado, pela dedicação, e por todo o apoio e incentivo para realização deste trabalho. Todas as palavras que eu escrever aqui não serão suficientes para expressar minha gratidão por ter sido sua orientada. Além de excelente orientadora, uma amiga em que se pode confiar sempre.

Ao meu co-orientador prof. Dr. Roberto Perez Xavier por todo o incentivo, apoio e aprendizado, e por ter me apresentado à geologia econômica.

À FAPESP, pela concessão da minha bolsa de doutorado (processo 2009/18371-0) e reserva técnica.

À VALE (Companhia Vale do Rio Doce), em particular aos geólogos Márcio Godoy, Benevides Aires, Cleive Ribeiro e Fabrício pelo apoio logístico durante as etapas de campo.

Ao INCT/Geociam (CNPq/MCT/FAPESPA), CNPq (processos 555065/2006-5, 472549/2009-0), FAPESP (processos 03/09584-3, 03/07453-9, 03-11163-603/01159-1), e FAPESPA/VALE pelo apoio financeiro.

To Dr. Robert Creaser from the University of Alberta, Canada, for accepting my visit and for allowing myself to accompany the Re-Os analyses. To Dr. Andrew Dufrane for the assistance with the LA-MC-ICPMS analyses in monazite and sphene.

To Dr. Tony Kemp, from the University of Western Australia, for performing the *in situ* U-Pb LA-ICPMS analyses in zircon.

Aos professores do IGe pelos anos de aprendizado, em especial aos profs. Drs. Lena Monteiro, Roberto Xavier, Ticiano Santos, Elson Oliveira, Alvaro Crôsta, Wanilson Silva, e Carlos Roberto de Souza Filho.

Aos profs. Drs. Márcio Pimentel, Elton Dantas, Ticiano Santos e Maria José Mesquita por participarem como examinadores na defesa da tese e terem contribuído com críticas e sugestões para o aprimoramento desse documento.

Aos profs. Drs. Ticiano Santos, Colombo Tassinari e Peter Hackspacher pela participação como examinadores no exame de qualificação e pelas revisões e críticas importantes.

Ao prof. Dr. Davis C. de Oliveira (UFPA) pelo apoio logístico, que foi essencial para a realização das etapas de campo.

Ao coordenadore da pós-graduação em Geociências do Ige/UNICAMP até 2013, Prof. Dr. Wanilson Luiz Silva, pelo auxílio financeiro que viabilizou etapas de campo e participação em eventos científicos.

Ao Dr. Kei Sato, pelo grande auxílio com as análises U-Pb SHRIMP IIe em zircão no Laboratório de Geocronologia de Alta Resolução do IG/USP.

À Val, por tudo que ela nos auxilia e com tanto carinho e eficiência. A pós-graduação não existiria sem ela. E também aos funcionários da pós, Gorete, Valdir e Rafael e Vinicius.

À Dra. Erica Tonetto pelo grande auxílio com a imagens de MEV no Ige/UNICAMP.

Ao Dailto por ter me auxiliado nesses anos. Aos demais funcionários do Ige/UNICAMP, em especial à Helena, Neide, Alba, Lúcia, Cida, Mônica, Seu Aníbal, Guerreiro, Jô, D. Raimunda, Zezé, Cristiano, Ednalva, Laércio, Maurícia, e D. Irani, pela ajuda e consideração durante esses anos. E também às meninas que mantém nosso ambiente de trabalho sempre em ordem, em especial à Cláudia, Elaine e Madalena.

Aos professores e colegas que participaram das etapas de campo em Carajás, em especial à Profa. Dra. Lena, Prof. Dr. Caetano Juliani, André, Gustavo, Marco e Soraya.

Principalmente ao meu companheiro e amigo Wagner Amaral, que esteve ao meu lado em todos os momentos (alegrias e dificuldades), me auxiliando em tudo que precisei. Pela compreensão e carinho ao longo dos últimos 2 anos e meio que, em função da distância, não foram dos mais fáceis. Pelas discussões geológicas também.

Aos meus pais José Luiz e Maria Stella, por terem sempre acreditado em mim e por terem me apoiado incondicionalmente sempre que precisei. Ao meu irmão Bruno e minha cunhada Sonja, que apesar da distância, estão sempre em meus pensamentos. Muitas saudades de vocês.

À minha prima Luciana por ter tido muita paciência comigo, principalmente nos momentos em que estive ausente trabalhando (muitos)... À todos os meus familiares, da família Penteado Natividade e da família Moreto, em especial às minhas tias (Lucia e Isa) e minhas avós, que sempre estiveram ao meu lado. Saudades dos que não estão mais encarnados nessa vida.

À Ana, por ser um exemplo de vida a ser seguido por todos.

Às minhas queridas amigas Fernanda Lourenço e Maria Fernanda Grisolia pela amizade sincera, companheirismo e cumplicidade, mesmo com a distância física que nos separa.

Aos pais do Wagner, Sr. Gilberto e Maria Inês, pelo convívio muito agradável. E também ao Luiz, Simone, Laís e Lara.

À todos os colegas da pós-graduação, em especial ao Rafa Assis, Matheus, Danilo, Zé Henrique, Gustavo, Marco, Verônica, Maurício, Paula, Paulo, Cleyton, Marquinhos, Sam, Érica, Fábio, Ethiane, Bruno, Lucília, Téo, Mariana, Anderson, Juanita, Elena, Renan, Alice, Mani e Tiara. Ao Rafa Assis, por ter compartilhado os momentos “poderia estar.... mas...”, e que diga-se de passagem foram muitos! Aos amigos de outras instituições, como a Soraya, pelos inúmeros momentos de aprendizado e risadas.

Aos integrantes do grupo de pesquisa em Carajás (Avante Carajás), e em Evolução Crustal e Metalogênese (PAAF incluída). E não, Carajás não é um grande pôrfiro!

Às minhas queridas amigas desde os tempos de colégio, em especial à Mirelle, Luana e Bia e também à Dani e Bruna, por tantos anos de convívio e alegrias. À minha amiga Marina também, por ter me apoiado e por ter sido compreensiva com meu sumiço nos últimos meses.

À Nani, por sempre me ajudar em casa, e pelas boas risadas.

E por fim, à minhas companheiras de muitos dias e noite escrevendo artigos e a tese: Mel e Pandora!

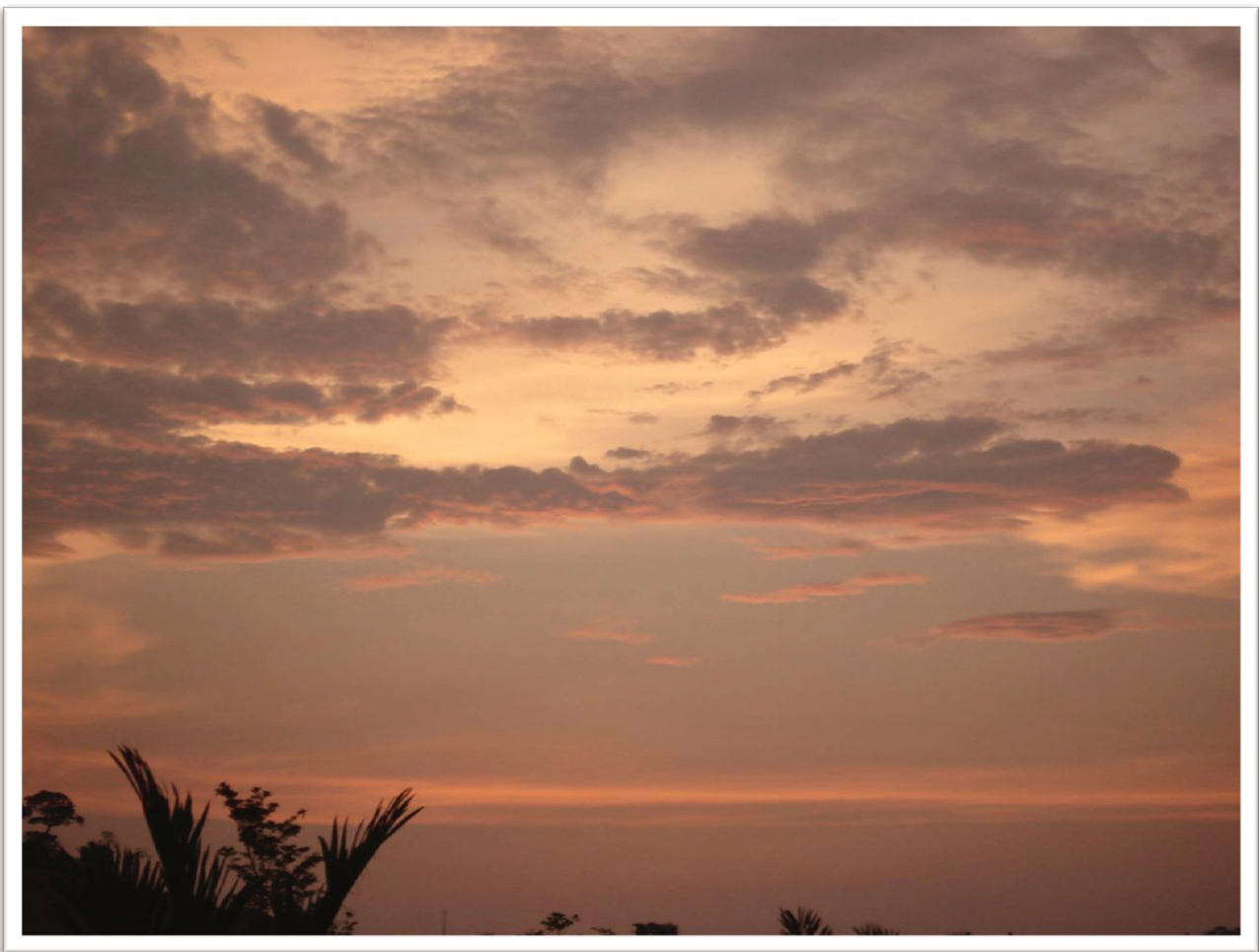
SÚMULA CURRICULAR

Carolina Penteado Natividade Moreto

Geóloga (2007), Mestre (2010) e Doutora (2013) pela Universidade Estadual de Campinas - UNICAMP. Possui experiência na área de Geociências, com ênfase em geologia econômica, petrologia ígnea e metamórfica, e geologia de campo. Atualmente atua como professora substituta das disciplinas “Petrologia Magmática”, “Petrologia Metamórfica” e “Mapeamento Geológico de áreas Cristalinas”, junto ao Departamento de Petrologia e Metalogenia da Universidade Estadual Paulista “Júlio de Mesquita Filho”, Campus Rio Claro, São Paulo.

Realizou o mestrado (2007-2009) com ênfase em estudos geocronológicos (metodologia U-Pb em zircão) no depósito de óxido de ferro-Cu-Au Bacaba, Província Mineral de Carajás, Pará, o que lhe rendeu diversas publicações em congressos e simpósios nacionais e internacionais, e a publicação de um artigo científico no periódico *Mineralium Deposita* (2011).

Também realizou o doutorado (2010-2013) na Província Mineral de Carajás, onde desenvolveu estudos isotópicos (metodologias U-Pb LA-ICPMS em monazita, U-Pb SHRIMP IIe em zircão, e Re-Os em molibdenita) em diversos depósitos do tipo óxido de ferro-Cu-Au, tais como Sossego, Castanha, Bacuri e Bacaba. Neste período, publicou mais de uma dezena de resumos nos principais congressos e simpósios no Brasil e no exterior. Submeteu, recentemente, dois artigos a periódicos internacionais.



....Pós pôr do sol na região de Serra Dourada. Grande privilégio...



UNIVERSIDADE ESTADUAL DE CAMPINAS
INSTITUTO DE GEOCIÊNCIAS

**GEOCRONOLOGIA U-Pb E Re-Os APLICADA À EVOLUÇÃO METALOGENÉTICA
DO CINTURÃO SUL DO COBRE DA PROVÍNCIA MINERAL DE CARAJÁS**

RESUMO

Tese de Doutorado
Carolina Penteado Natividade Moreto

O Cinturão Sul do Cobre, Província Carajás, hospeda diversos depósitos de óxido de ferro-cobre-ouro (*iron oxide-copper-gold* ou IOCG), tais como Sossego (corpos Sequeirinho-Pista-Baiano e Sossego-Currall), Cristalino, Alvo 118, Bacuri, Bacaba, Castanha, Visconde e Jatobá, que estão localizados ao longo de uma zona de cisalhamento com direção WNW-ESSE, no contato sul entre a Bacia Carajás e as rochas do embasamento. Mapeamento geológico aliado a estudos geocronológicos (U-Pb *SHRIMP* IIe e LA-ICPMS) permitiram a caracterização dos litotipos hospedeiros de depósitos IOCG na porção centro-oeste do Cinturão Sul do Cobre, incluindo: (1) unidades neoarqueanas de 2,74 Ga (Pórfiro Castanha, granito granofílico Sossego e intrusivas máficas); (2) unidades mesoarqueanas entre 2,87 Ga a 2,84 Ga (Tonalito Campina Verde, Trondjemito Rio Verde e Granito Serra Dourada); (3) rochas metavulcânicas félscicas de 2,97 Ga associadas à lentes de rochas metaultramáficas; (4) rochas graníticas mesoarqueanas de 3,0 Ga (Tonalito Bacaba e Granito Sequeirinho). Alteração hidrotermal que afeta essas rochas consiste em alteração sódica regional (albita, escapolita e óxidos de ferro), sódico-cálcica (albita-actinolita), potássica (feldspato potássico-biotita), clorítica (clorita) e hidrolítica (sericita-muscovita-hematita-quartzo), silicificação e formação de epidoto-calcita-clorita. Os depósitos IOCG, entretanto, exibem variações dos padrões de distribuição das zonas de alteração hidrotermal, apontando para níveis crustais distintos de instalação dos sistemas hidrotermais, com formação de corpos de magnetita maciça e actinolítitos em depósitos mais profundos (corpos Sequeirinho-Pista-Baiano e depósito Castanha) e zonas de alteração clorítica e hidrolítica nos mais rasos (corpos Sossego-Currall e depósito Alvo 118). Datação de cristais de monazita hidrotermal (U-Pb LA-MC-ICPMS) e molibdenita (Re-Os NTIMS) dos corpos Sequeirinho e Pista, e dos depósitos Bacuri e Bacaba, forneceram idades entre 2,71 a 2,68 Ga, enquanto que monazita hidrotermal dos corpos Sossego e Currall resultaram em idades entre 1,90 a 1,88 Ga. Adicionalmente, cristais de molibdenita do depósito Bacuri e de monazita do depósito Bacaba indicaram idades em 2,76 Ga e 2,05 Ga, respectivamente. Esses dados sugerem que múltiplos eventos hidrotermais neoarqueanos e paleoproterozóicos foram responsáveis pela alteração hidrotermal e mineralização cuprífera no Cinturão Sul do Cobre. O desenvolvimento de sistemas hidrotermais IOCG profundos (Sequeirinho-Pista, Bacaba, Bacuri, Visconde e Castanha) no Neoarqueano (2,71-2,68 Ga), associados a extensas zonas de escapolita, foi relacionado a reativações das zonas de cisalhamento em função da inversão tectônica da Bacia Carajás. No Orosiriano (1,9-1,87 Ga), a instalação de sistema(s) hidrotermal(is) IOCG em níveis crustais mais rasos resultou na formação de novos depósitos (Alvo 118) e corpos de minério (Sossego-Currall), possivelmente relacionados à fontes de calor devido à colocação dos granitos do tipo-A da província. Esse evento teria resultado em (re)mobilização do minério e sobreposição de estágios hidrotermais, tal como o desenvolvimento de alteração hidrolítica sobre alteração escapolítica preexistente. Assim, o Cinturão Sul do Cobre apresenta um notável registro de recorrência de eventos hidrotermais ao longo do tempo geológico, responsável pela formação de depósitos IOCG de classe mundial.

Palavras chaves: Depósitos de óxido de Fe-Cu-Au – Carajás, Serra dos (PA); Carajás, Serra dos (PA); Geocronologia; Cráttons – Amazônia;



UNIVERSITY OF CAMPINAS
INSTITUTE OF GEOSCIENCES

**U-Pb AND Re-Os GEOCHRONOLOGY APPLIED TO THE METALLOGENETIC
EVOLUTION OF THE SOUTHERN COPPER BELT OF THE CARAJÁS
MINERAL PROVINCE**

ABSTRACT

PhD Thesis
Carolina Penteado Natividade Moreto

The Southern Copper Belt, Carajás Province, hosts several iron oxide–copper–gold (IOCG) deposits, including the Sossego (Sequeirinho-Pista-Baiano and Sossego-Currall orebodies), Cristalino, Alvo 118, Bacuri, Bacaba, Castanha, Visconde, and Jatobá deposits. These deposits are situated within a WNW–ESE shear zone in the southern contact between the Carajás Basin and basement rocks. Geological mapping combined with geochronological studies (U-Pb SHRIMP IIe and LA-ICPMS) allowed the characterization of the host rocks of the IOCG deposits in the central-west part of the Southern Copper Belt, which include: (1) 2.74 Ga Neoarchean units (Castanha Porphyry, Sossego granophytic granite and mafic intrusive rocks); (2) 2.87-2.84 Ga Mesoarchean units (Campina Verde Tonalite, Rio Verde Trondhjemite and the Serra Dourada Granite); (3) 2.97 Ga felsic metavolcanic rocks associated with metaultramafic lenses; (4) 3.0 Ga Mesoarchean granitic rocks (Bacaba Tonalite and Sequeirinho Granite). Hydrothermal alteration that affects these rocks consist in regional sodic (albite, scapolite and iron oxides), sodic-calcic (albite-actinolite), potassic (potassium feldspar and biotite), chlorite, and hydrolytic (sericite-muscovite-hematite-quartz) alterations, silicification, and epidote-calcite-chlorite formation. However, the IOCG deposits display variations in the distribution of the hydrothermal alteration zones, pointing to distinct crustal levels in which the deposits were installed. Massive magnetite-rich and actinolite-rich bodies are recognized in deeper-emplaced deposits (Sequeirinho-Pista-Baiano orebodies and Castanha deposit), while chlorite and hydrolytic alteration zones are identified in shallower-emplaced deposits (Sossego-Currall orebodies and Alvo 118 deposit). Dating of hydrothermal monazite (U-Pb LA-MC-ICPMS) and molybdenite (Re-Os NTIMS) from the Sequeirinho and Pista orebodies and the Bacuri and Bacaba deposits rendered ages of ca. 2.71 to 2.68 Ga, whilst hydrothermal monazite from the Sossego and Currall orebodies yielded ages of ca. 1.90 to 1.87 Ga. Additionally, molybdenite crystals from Bacuri and monazite from Bacaba provided the ages of 2.76 Ga and 2.05 Ga, respectively. These data suggest that multiple discrete Neoarchean and Paleoproterozoic hydrothermal events were responsible for hydrothermal alteration and ore formation at the Southern Copper Belt. The development of deep IOCG hydrothermal systems (Sequeirinho-Pista, Bacaba, Bacuri, Visconde, and Castanha) at the Neoarchean (2.71-2.68 Ga), related to extensive scapolite-rich zones, was linked to the reactivation of shear zones due to the tectonic inversion of the Carajás basin. In the Orosinian (1.90-1.87 Ga), the establishment of IOCG hydrothermal system(s) in shallower crustal levels resulted in the formation of new deposits (Alvo 118) and orebodies (Sossego-Currall). This event was possibly associated with heat sources due to the emplacement of A-type granites at the province. This event would have caused ore re(mobilization) and overprint of hydrothermal alteration zones, with the formation of hydrolytic alteration over previously formed scapolite-rich zones. Therefore, the Southern Copper Belt presents an excellent example of recurrence of hydrothermal systems along the geological time, responsible for the genesis of world-class IOCG deposits.

Keywords: Iron oxide Cu-Au deposits – Carajás, Serra dos (PA); Carajás, Serra dos (PA); Geochronology; Craton – Amazon

SÚMARIO

AGRADECIMENTOS	ix
SÚMULA CURRICULAR	xi
RESUMO	xv
ABSTRACT	xvii
SUMÁRIO	xix
ÍNDICE DE FIGURAS	xxv
ÍNDICE DE TABELAS	xxxiii
1. INTRODUÇÃO	01
2. OBJETIVOS.....	03
3. MÉTODOS.....	04
4. CONTEXTO GEOLÓGICO REGIONAL: DOMÍNIO CARAJÁS	06
4.1. Embasamento.....	07
4.2. Unidades supracrustais: Bacia Carajás	09
4.3. Rochas intrusivas	10
4.4. Modelos evolutivos.....	11
5. DEPÓSITOS DE ÓXIDO DE FERRO-COBRE-OURO DA PROVÍNCIA CARAJÁS	12
6. OS DEPÓSITOS DE ÓXIDO DE FERRO-COBRE-OURO DO CINTURÃO SUL DO COBRE	18
6.1. Sossego	19
6.2. Cristalino.....	22
6.3. Alvo 118	24
6.4. Bacaba.....	27
6.5. Castanha.....	30
6.6. Bacuri.....	31
6.7. Visconde	33
7. SÍNTESE DOS ARTIGOS.....	34
7.1. Artigo I “Paleoproterozoic overprint on Archean iron oxide-copper-gold system at the Sossego deposit, Carajás Province: Re-Os and U-Pb geochronological evidence”	34

7.2. Artigo II “Timing of multiple Iron oxide Cu-Au systems in the Southern Copper Belt, Carajás Province, Brazil: U-Pb zircon and monazite and Re-Os molybdenite geochronology”	36
 ANEXOS.....	39
 ANEXO 1: Artigo “ <i>Paleoproterozoic overprint on Archean iron oxide-copper-gold system at the Sossego deposit, Carajás Province: Re-Os and U-Pb geochronological evidence</i> ”	41
Abstract.....	43
1. Introduction.....	44
2. Geological Setting of the Carajás Province	46
3. Timing of IOCG formation at the Carajás Province.....	50
4. Analytical Procedures	54
4.1 U-Pb LA-ICPMS, zircon.....	54
4.2 U-Pb LA-MC-ICPMS, monazite.....	55
4.3 U-Pb SHRIMP IIe, zircon	56
4.4 Re-Os, molybdenite.....	57
5. Sossego deposit.....	57
5.1 Sequeirinho-Baiano-Pista Orebodies	59
5.1.1 Host rocks.....	60
5.1.2 Hydrothermal alteration	65
5.1.3 Ore stage.....	65
5.1.4 Nature of the hydrothermal fluids and isotopic signatures	69
5.2 Sossego- Curral Orebodies.....	71
5.2.1 Host rocks.....	71
5.2.2 Hydrothermal alteration	73
5.2.3 Ore stage.....	73
5.2.4 Nature of the hydrothermal fluids and isotopic signatures	75
6. U-Pb and Re-Os Results	76
6.1 Sequeirinho orebody	77
6.1.1 Host rocks.....	77
6.1.2 Ore samples	81

6.2 Pista orebody	81
6.2.1 Host rocks.....	81
6.2.2 Ore samples	82
6.3 Sossego-Curral orebodies.....	82
6.3.1 Host rocks.....	82
6.3.2 Ore samples	84
7. Discussions	84
7.1 Meso- and Neoarchean magmatism in the Sossego deposit area.....	84
7.2 Metallogenetic evolution of the Sossego deposit.....	86
7.3 IOCG Metallogenesis in the Carajás Province.....	96
8. Conclusions.....	98
Acknowledgments	100
REFERENCES	100
Appendix.....	111

ANEXO 2: Artigo “ <i>Timing of multiple Iron oxide Cu-Au systems in the Southern Copper Belt, Carajás Province, Brazil: U-Pb zircon and monazite and Re-Os molybdenite geochronology</i> ”	119
Abstract.....	121
1. Introduction.....	123
2. Geological Setting of the Carajás Province	125
3. Iron oxide-copper-gold deposits from the Southern Copper Belt.....	132
4. Analytical Procedures	137
4.1 U-Pb SHRIMP IIe, zircon	138
4.2 U-Pb LA-MC-ICPMS, monazite.....	138
4.3 Re-Os, molybdenite.....	139
5. The host rocks of the IOCG deposits from the Southern Copper Belt	140
5.1 Felsic subvolcanic rocks.....	140
5.2 Mafic intrusive rocks.....	144
5.3 Mafic metavolcanic rocks	145
5.4 Meta-ultramafic rocks	146
5.5 Granitic rocks	146
5.5.1 Serra Dourada Granite.....	146

5.5.2 Campina Verde Tonalite	149
5.5.3 Bacaba Tonalite.....	150
5.5.4 Other units	151
6. IOCG deposits and hydrothermal alteration in the Southern Copper Belt	152
6.1 Host rocks of the Bacaba, Castanha and Bacuri IOCG deposits.....	153
6.2 Sodic alteration.....	153
6.2.1 Albite alteration.....	153
6.2.2 Scapolite alteration.....	155
6.3 Na-Ca alteration and Fe metasomatism	156
6.4 Potassic alteration (biotite) and chlorite formation	157
6.5 Tourmaline formation	158
6.6 Potassic alteration (potassium feldspar).....	158
6.7 Silicification	159
6.8 Epidote, calcite and chlorite formation	159
6.9 Ore stage.....	160
6.9.1 Bacaba deposit.....	160
6.9.2 Castanha deposit.....	161
6.9.3 Bacuri deposit.....	162
7. U-Pb and Re-Os results.....	163
7.1 Host rocks.....	164
7.1.1 Quartz-feldspar porphyries.....	164
7.1.2 Serra Dourada Granite.....	164
7.1.3 Campina Verde Tonalite	167
7.2 IOCG deposits	167
7.2.1 Bacaba deposit.....	167
7.2.2 Bacuri deposit.....	169
8. Discussions	169
8.1 Meso- and Neoarchean magmatism in the Southern Copper Belt	169
8.2 Significance of the meta-ultramafic rocks	172
8.3 Geochronological data from the Bacaba and Bacuri deposits.....	174
8.4 Timing and evolution of the IOCG hydrothermal systems of the Southern Copper Belt.....	176
9. Conclusions.....	184

Acknowledgments	186
REFERENCES	187
Appendix.....	199
8. CONSIDERAÇÕES FINAIS: Síntese da evolução metalogenética do Cinturão	
Sul do Cobre.....	203
REFERÊNCIAS BIBLIOGRÁFICAS	209

ÍNDICE DE FIGURAS

Figura 1. Mapa geológico do Domínio Carajás e áreas adjacentes (modificado de Vasquez et al., 2008a), mostrando a localização do Cinturão Sul do Cobre (retângulo em azul).....	08
Figura 2. Mapa geológico da porção centro-oeste do Cinturão Sul do Cobre, mostrando os depósitos Sossego (corpos Sequeirinho e Sossego), Bacaba, Castanha, Bacuri e Visconde (modificado de VALE).....	14
Figura 3. Síntese dos dados geocronológicos dos depósitos IOCG e rochas hospedeiras da Província Carajás, e principais eventos tectônicos e magmáticos registrados na província. Referências: (1) Silva et al. (2005); (2) Tassinari et al. (2003); (3) Réquia et al. (2003); (4) Machado et al. (1991); (5) Pimentel et al. (2003); (6) Galarza and Macambira (2002b); (7) Marshick et al. (2005); (8) Galarza et al. (2008); (9) Tallarico et al. (2005); (10) Tallarico (2003); (11) Neves (2006); (12) Moreto et al. (Anexo 1); (13) Marshick et al. (2003); (14) Soares et al., 2001; (15) Huhn et al. (1999b); (16) Silva et al. (2012); (17) Moreto et al. (2011); (18) Moreto et al (Anexo 2). A anfibolito; amp anfibólio; Au ouro; B basalto; bn bornita; bt biotite; cco chalcocita; cpy calcopirita; Da dacito; Di diorito; FM rocha metavulcânica félscica; G granito; GG granito granofírico; Gb gabbro; Gn gneiss; mz monazita; mgt magnetita; moly molibdenita; T tonalito; tour turmalina; WR rocha total; zr zircão.....	16
Figura 4. A. Mapa geológico simplificado da área da Mina Sossego (modificado de VALE por Monteiro et al. 2008a); B. Distribuição esquemática das zonas de alteração hidrotermais na Mina Sossego (Monteiro et al. 2008a).....	20
Figura 5. Seção esquemática dos corpos Sequeirinho e Sossego, mostrando a distribuição das zonas de alteração hidrotermais e temperaturas e assinatura isotópica de oxigênio dos fluidos hidrotermais estimadas para cada estágio de alteração (Monteiro et al. 2008a).....	21
Figura 6. A. Mapa geológico do depósito Cristalino. B. Seção geológica simplificada do depósito Cristalino (VALE).....	23
Figura 7: Mapa geológico simplificado do depósito Alvo 118 (VALE).....	25
Figura 8. Principais estágios de alteração hidrotermal no depósito Alvo 118: (1) Alteração sódica (albita) em granito; (2) Cloritização fissural em granito albitizado; (3) Alteração potássica (biotita) e cloritização. Veios com quartzo e calcita posteriores; (4) Alteração potássica (biotita) e cloritização (brechada) com matriz preenchida por quartzo, calcita e apatita; (5) Cloritização superposta por alteração potássica com feldspato potássico; (6) Brecha mineralizada com calcopirita e bornita; (7) Brecha com matriz preenchida por calcita e quartzo, cortada por veios de hematita; (8) Brecha com matriz preenchida por feldspato potássico, cortada por veios de fluorita. (Torresi et al., 2012)	26

Figura 9. Seção esquemática mostrando as rochas hospedeiras do depósito Bacaba e a distribuição das zonas de alteração hidrotermal (Moreto et al., 2011 modificado de Augusto et al., 2008)	27
Figura 10. Principais feições das rochas hospedeiras alteradas e mineralizadas do depósito Bacaba (Furo de sondagem BACD 15). Abreviações: Ab: albita; Act: actinolita; Bt: biotita; Chl: clorita; Cpy: calcopirita; Ep: epidoto; Kfs: feldspato potássico; Mt: magnetita; Ser: sericita; Tour: turmalina.....	29
Figura 11. Seção geológica do depósito Castanha, mostrando as principais rochas hospedeiras e zona mineralizada (modificado de VALE)	31
Figura 12. Seção geológica simplificada do depósito Bacuri (modificado de VALE).....	31

ANEXO 1: Artigo “Paleoproterozoic overprint on Archean iron oxide-copper-gold system at the Sossego deposit, Carajás Province: Re-Os and U-Pb geochronological evidence”

Fig. 1. Geological map of the Carajás Domain (Vasquez et al. 2008) A) Location in Brazil; B) Location of the Carajás Domain at the Carajás Province; C) Geological map of the Carajás Domain (Vasquez et al. 2008). Abbreviations: BD: Bacajá Domain; CD: Carajás Domain; RMD: Rio Maria Domain..	47
Fig. 2. A) Simplified geologic map of the Sossego deposit showing the location of the Sequeirinho, Pista, Baiano, Sossego and Curral, orebodies (Monteiro et al. 2008a modified from a VALE company figure); B) Schematic distribution of the hydrothermal alteration zones in the Sossego deposit (Monteiro et al. 2008a).....	58
Fig. 3. A) Geological map and B) Simplified cross-section of the Sequeirinho orebody of the Sossego IOCG deposit (VALE company figure).	60
Fig. 4. Characteristic features of the host rocks of the Sequeirinho-Pista-Baiano (A-F) and Sossego-Curral orebodies (G-H). A) Sequeirinho Granite with sodic alteration (albite) and chlorite alteration (SOS 22/107.45); B) Sequeirinho Granite with sodic alteration (albite-hematite) and incipient potassic alteration (biotite) (SOS 259/177.40); C) Sequeirinho Granite with silicification and fissure-style chlorite alteration (SOS 450/13); D) clinopyroxene norite from the Sequeirinho orebody with sodic-calcic alteration (hastingsite) (SOS 35); E) Pista Metavolcanic rock with sodic alteration (albite) and silicification defining the mylonitic foliation (SOS 364/138.35); F) Pista Metavolcanic rock with pervasive albite-quartz alteration and chlorite alteration in veins (SOS 475/167); G) Sossego granophyric granite with hydrolytic alteration consisting of muscovite-chlorite-hematite-epidote (SOS 35/406); H) gabbro from the Curral orebody with silicification and sodic alteration defining the mylonitic foliation (SOS 35/30). Mineral abbreviations: Ab: albite, Bt: biotite, Chl: chlorite, Qtz: quartz.....	62

Fig. 5. Characteristic features of hydrothermal alteration and ore, according to Monteiro et al. (in press). A-J) Sequeirinho orebody and the K-R) Sossego orebody; A) Open pit of the Sequeirinho orebody in 2009; B) View of the benches, in which the rocks are cut by shear zones and affected by sodic alteration; C) Pervasive Na-alteration characterized mainly by pinkish albite; D) Na-altered rock affected by Na–Ca alteration represented by actinolite, epidote, and albite; E) Na–Ca altered rock cut by actinolite-rich areas; F) Coarse-grained apatite crystals associated with actinolite; G) Breccia with matrix filled by hematite and fragments of Na–Ca altered rock; H) Breccia with matrix filled by magnetite and clasts of actinolite-rich rock; I) Ore containing chalcopyrite, magnetite and calcite; J) High-grade ore breccia containing clasts of magnetite and actinolite in a chalcopyrite-rich matrix; K) Wall rock of the Sossego orebody(2004) cut by chalcopyrite veins, replaced by malachite; L) Ore breccia with matrix filled by chalcopyrite and fragments of intensively chlorite- and biotite-altered rock; M) Chalcopyrite disseminations associated with calcite; N) Potassically altered rock with red potassium feldspar cut by later veins of chlorite; O) Chlorite alteration overprinting albite-rich zones from early Na alteration; P) Mineralized breccia with calcite-rich matrix (+ chalcopyrite, quartz, apatite, actinolite, chlorite) enclosing fragments of previously altered rocks (potassic alteration); Q) Chalcopyrite veins with subordinate chlorite and calcite; R) Coarse-grained apatite crystals with associated calcite. Mineral abbreviations: Ab: albite, Act: actinolite, Ap: apatite, Bt: biotite, Cc: calcite, Chl: chlorite, Cpy: chalcopyrite, Ep: epidote, Hm: hematite, Kfs: potassium feldspar, Mgt: magnetite, Qtz: quartz..... 66

Fig. 6. BSE (A and B) and CL (C and D) images of high-grade ore breccia from the Sequeirinho orebody. A) Monazite inclusions in apatite grains; B) Monazite inclusions in apatite and actinolite crystals; C) Apatite crustals in the matrix of ore breccia; and D) Monazite inclusions in apatite crystals. Greenish-yellow areas in CL images show hydrothermally altered parts of the apatite, in which REE was removed and formed monazite crystals. Darker green areas correspond to more preserved parts of the apatite grain and black areas represent chalcopyrite... 68

Fig. 7. Characteristic features of ore samples from the Sequeirinho-Pista-Baiano (A-F) and Sossego-Currall orebodies (G-I). A) Cu-Au ore from the Sequeirinho orebody (SOS 39J); B) Cu-Au ore from the Sequeirinho orebody (SOS 259/270); C) Pista felsic metavolcanic rock with sodic alteration (albite), chlorite alteration and silicification (SOS 364/76.84). This sample (SOS 364/76.84) contains D) molybdenite crystals associated with silicified zones; E) Pista felsic metavolcanic rock with sodic alteration (albite) cut by chlorite-rich zones (SOS 364/160.9) Sulfide veins containing F) molybdenite crystals cut the rock (SOS 364/160.9). G) Cu-Au ore from the Sossego orebody (Min-Cp-SOS); H) Cu-Au ore from the Sossego orebody (SOS 315/255.1); I) Cu-Au ore from the Curral orebody (SOS 106/84). Mineral abbreviations: Ab:

<i>albite, Act: actinolite, Ap: apatite, Bt: biotite, Cc: calcite, Chl: chlorite, Cpy: chalcopyrite, Mgt: magnetite, Moly: molybdenite, Qtz: quartz.....</i>	70
Fig. 8. A) Geological map and B) Simplified cross-section of the Sossego orebody of the Sossego IOCG deposit (modified from a VALE company figure).....	72
Fig. 9. Characteristic features of the Sossego (A and B) and Curral (C to E) high-grade ore breccia. A) Ore and ore-related minerals, such as chalcopyrite, pyrite, magnetite, actinolite, apatite and siegenite. Reflected light; B) Euhedral inclusions of monazite inside an apatite crystal; C) D) and E) Monazite inclusions in apatite and chalcopyrite crystals within the matrix of ore breccia. Photos B to E are backscattered electron (BSE) images. Mineral abbreviations: Cpy: chalcopyrite, Mz: monazite.	74
Fig. 10. BSE and CL images of zircon of the host rocks and ore samples of the Sequeirinho-Pista-Baiano orebodies (A-S) and host rocks of the Sossego-Curral (T-X) orebodies. $^{207}\text{Pb}/^{206}\text{Pb}$ ages are indicated in the image where analyses were done. A and C) BSE and B) CL images of zircon from the Sequeirinho Granite (SOS 22/107.45); D-E) BSE images of zircon from the Sequeirinho Granite (SOS 259/177.40); F-H) CL images of zircon from the Sequeirinho Granite (SOS 450/13); I-K) CL images of zircon from gabbronorite from the Sequeirinho orebody (SOS 35); L-N) CL images of zircon from Sequeirinho ore (SOS 39J); O-P) CL images of zircon from the Pista Metavolcanic rock (SOS 475/167); Q-S) CL images of zircon from the Pista Metavolcanic rock (SOS 364/138.35); T-V) BSE images of zircon from the Sossego granophyric granite (SOS 35/406); W-X) CL images of zircon from gabbro from the Curral orebody (SOS 35/30).	79
Fig. 11. $^{206}\text{Pb}^{238}\text{U}$ vs. $^{207}\text{Pb}^{235}\text{U}$ diagrams for the Sequeirinho-Pista-Baiano host rocks (A-F; gray diagrams) and ore (G-H; yellow diagrams). A) Sequeirinho Granite with sodic and chlorite alterations (SOS 22/107.45); B) Sequeirinho Granite with sodic and potassic alterations (SOS 259/177.40); C) Sequeirinho Granite with potassic alteration (SOS 450/13); D) gabbronorite from the Sequeirinho orebody (SOS 35); E) Pista Metavolcanic rock (SOS 364/138.35); F) Pista Metavolcanic rock (SOS 475/167); G) Sequeirinho ore (SOS39J); H) Sequeirinho ore (SOS 259/270). In all the host rocks (A-F) and ore sample SOS 39 J (G) zircon was the analyzed mineral. In the Sequeirinho ore sample SOS 259/270 (H) monazite was analyzed.	80
Fig. 12. $^{206}\text{Pb}^{238}\text{U}$ vs. $^{207}\text{Pb}^{235}\text{U}$ diagrams for the Sossego-Curral host rocks (A and B; gray diagrams) and ore (C-E; yellow diagrams). A) Sossego granophyric granite with sodic alteration (SOS 35/406.88); B) gabbro from the Curral orebody (SOS 35/30); C) Sossego ore (Min-Cp-SOS); D) Sossego ore (SOS 315/255.1); E) Curral ore (SOS 106/84). In both host rocks (A and B), zircon was the analyzed mineral, whereas in the ore samples (C-E) monazite was analyzed.	83
Fig. 13. Summary of geochronological data for IOCG deposits and their host rocks and main tectonic and magmatic events recorded in the province. The data obtained in this study is	

included. Data source: (1) Silva et al. (2005); (2) Tassinari et al. (2003); (3) Réquia et al. (2003); (4) Machado et al. (1991); (5) Pimentel et al. (2003); (6) Galarza and Macambira (2002b); (7) Marshick et al. (2005); (8) Galarza et al. (2008); (9) Tallarico et al. (2005); (10) Tallarico (2003); (11) Neves (2006); (12) Moreto et al., this study; (13) Marschik et al. (2003); (14) Soares et al., 2001; (15) Huhn et al. (1999b); (16) Silva et al. (2012); (17) Moreto et al. (2011). A amphibolite; amp amphibole; Au gold; B basalt; bn bornite; bt biotite; cco chalcocite; cpy chalcopyrite; Da dacite; Di diorite; FM felsic metavolcanic rock; G granite; GG granophyric granite; Gb gabbro; Gn gneiss; mz monazite; mgt magnetite; moly molybdenite; T tonalite; tour tourmaline; WR whole rock; zr zircon..... 92

Fig. 14. Schematic diagram showing the metallogenetic evolution of the Sossego deposit in time. A) Formation of the Sequeirinho-Pista-Baiano orebodies at 2.71-2.68 Ga in the interception of WNW-ESE and NE-SW ductile shear zones; B) Formation of the vertical pipe-like Sossego-Currall orebodies at 1.90-1.88 Ga after exhumation of the Neoarchean IOCG systems. 94

ANEXO 2: Artigo “Timing of multiple Iron oxide Cu-Au systems in the Southern Copper Belt, Carajás Province, Brazil: U-Pb zircon and monazite and Re-Os molybdenite geochronology”

Fig. 1. Geological map of the Carajás Domain (Vasquez et al. 2008a) A) Location in Brazil; B) Location of the Carajás Domain at the Carajás Province; C) Geological map of the Carajás Domain (Vasquez et al. 2008a). Abbreviations: BD: Bacajá Domain; CD: Carajás Domain; RMD: Rio Maria Domain... 126

Fig. 2. Geological map of the central west part of the Southern Copper Belt (modified from VALE company)..... 141

Fig. 3. Characteristic features, field aspects, and photomicrographs of the felsic subvolcanic, mafic volcanic and intrusive, and meta-ultramafic rocks from the area. A) Late quartz-feldspar porphyry dikes; B) Quartz-feldspar porphyry with blue quartz megacrysts. Zircon grains from this sample (GMCL 54) were analyzed by U-Pb SHRIMP IIe; C) Outcrop of the quartz-feldspar porphyry altered by potassic alteration (biotite), scapolite and quartz alterations; D) Castanha quartz-feldspar porphyry with millimeter-scale megacrysts of blue quartz and feldspar; E) Castanha quartz-feldspar porphyry. Zircon grains from this sample (CASP 02/424.9) were analyzed by U-Pb SHRIMP IIe; F) Castanha quartz-feldspar porphyry with euhedral bipyramidal quartz megacrysts. Note the feldspar megacrysts in the center, which correspond to hydrothermal albite with chessboard texture; G) Castanha quartz-feldspar porphyry (CASP 02/424.9) with scapolite and biotite (sodic and potassic alterations, respectively) altering the feldspar in the fine-grained matrix; H) An outcrop of gabbronorite; I) Fine- to medium-grained gabbro sample with preserved subophitic texture; J) Porphyritic diabase with up to 3 centimeter-

long plagioclase phenocrysts; K) Diopsidic norite with recognizable subophitic texture; L) Amphibolite with hydrothermal hastingsite; M) A basalt outcrop. Fractures with random directions are filled by fine-grained amphibole; N) Basalt; O) Abandoned copper (malachite) prospect, in which the orebody were hosted by a granite (Serra Dourada Granite) and a meta-ultramafic lens along a shear zone; P) S-C structures in the granite (Serra Dourada Granite) along the shear zone where the copper prospect from Fig. 7O is located; Q) Chlorite-tremolite mylonite. Note the centimeter-scale tremolite crystals; R) Meta-ultramafic rock with chlorite, talc and tremolite. Mineral abbreviations: Chl: chlorite, Di: diopside, Hs: hastingsite, Mgt: magnetite, Tlc: talc, Tr: tremolite... 142

Fig. 4. Characteristic features, field aspects, and photomicrographs of the felsic intrusive rocks from the area. A) Typical outcrop of the Serra Dourada Granite; B) Serra Dourada Granite with medium-grained phaneritic facies; C) Serra Dourada Granite with porphyritic facies. Zircon grains from this sample (GMCL 40) were analyzed by U-Pb SHRIMP IIe; D) Serra Dourada Granite with micrographic facies, consisting of the intergrowth of alkali feldspar and quartz; E) Serra Dourada Granite (sample GMCL 40) in thin section. Feldspar crystals are saussuritized. F) Serra Dourada Granite (sample GMCL 40) with biotite partially altered to chlorite; G) Exposure of Serra Dourada Granite and the Campina Verde Tonalite in an abandoned quarry for grit; H) The Campina Verde Tonalite with elongated mafic enclaves due to deformation; I) Foliated and medium-grained Campina Verde Tonalite. Zircon grains from this sample (GMCL 01) were analyzed by U-Pb SHRIMP IIe; J) Isotropic and medium-grained Campina Verde Tonalite. Zircon grains from this sample (GMCL 66) were analyzed by U-Pb SHRIMP IIe; K) Campina Verde Tonalite (sample GMCL 01). Plagioclase crystals is slightly deformed and with irregular polysynthetic twinning; L) Campina Verde Tonalite (sample GMCL 66) partially altered by potassic alteration. Biotite alters the plagioclase rims and in fractures; M) Hydrothermal hastingsite in the Campina Verde Tonalite; N) Outcrop of the Bacaba Tonalite altered by potassic and chlorite alteration along fractures; O) and P) Fine-grained Bacaba Tonalite; Q) Xingu Complex; R) Rio Verde Trondhjemite. Mineral abbreviations: Bt: biotite, Chl: chlorite, Hs: hastingsite, Pl: plagioclase, Zr: zircon..... 148

Fig. 5. Simplified cross sections of the A) Bacaba; B) Castanha; and C) Bacuri deposits (modified from VALE company)..... 152

Fig. 6. Characteristic features, field aspects, and photomicrographs of the hydrothermal alteration in the rocks from the area. A-B), G), and P-Q) Sodic alteration with albite formation; C-F) and L) Sodic alteration with scapolite formation; H) Sodic-calcic alteration; I-M) Potassic alteration with biotite -(chlorite-quartz); N) Potassic alteration with potassium feldspar; O) Silicification; P-R) Epidote alteration. A) Albite-quartz -(potassium feldspar) veins altering the Serra Dourada Granite; B) Pervasive albite alteration in the Serra Dourada Granite; C-D)

Scapolite disseminations and in veins and veinlets altering a diabase; E) Scapolite crystal with radial texture filling a fracture plane of the Serra Dourada Granite; F) Scapolite filling the matrix of a hydrothermal breccia with fragments of the Bacaba Tonalite; G) Sodic alteration altering the microcline megacrysts of the Castanha quartz-feldspar porphyry, and forming an albite crustal with chessboard texture. Biotite alteration overprint the albite alteration; H) Actinolite-albite (sodic-calcic alteration) overprinting a sodic alteration (albite) in the Serra Dourada Granite; I) Biotite -(chlorite) filling fractures on the Bacaba Tonalite; J) Intense biotite and chlorite alteration on the Serra Dourada Granite. The igneous mineralogy and texture is completely modified, except for small areas preserved from alteration; K) Mylonite consisting of biotite, chlorite and quartz; L) Biotite, scapolite and quartz altering the matrix of the Castanha quartz-feldspar mylonite along the protomylonitic foliation; M) Biotite altering the plagioclase rim and along a fracture of the feldspar in the Campina Verde Tonalite; N) Diabase with selective potassic alteration, in which the igneous plagioclase are replaced by potassium feldspar; O) Quartz stockwork; P) Epidote vein surrounded by albite alteration cutting the Campina Verde Tonalite; Q) Epidote veins cutting the albite altered Rio Verde Trondhjemite; R) Allanite formed during a late epidote-chlorite-calcite alteration in the Serra Dourada Granite.

Mineral abbreviations: Ab: albite, Act: actinolite, Al: allanite, Bt: biotite, Chl: chlorite, Ep: epidote, Kfs: potassium feldspar, Mgt: magnetite. Qtz: quartz, Scp: scapolite..... 154

Fig. 7. Characteristic features of the ore and hydrothermally altered samples selected for geochronological studies. A) Ore from the Bacaba deposits hosted by the Bacaba Tonalite (sample BACD 25/229.25); B) Serra Dourada Granite in the Bacaba deposit area intensively affected by albite alteration and silicification (sample BACD 15/237.4); C) Sample from the Bacuri deposit pervasively affected by chlorite and biotite alteration, and with chalcopyrite and scapolite disseminations (sample BRID 07/115.42); D) Serra Dourada Granite in the Bacuri deposit area altered by silicification, and by discrete biotite and chlorite alteration (sample BRID 01/45). Molybdenite and chalcopyrite are coeval with biotite formation. Mineral abbreviations: Ab: albite, Bt: biotite, Chl: chlorite, Cpy: chalcopyrite, Kfs: potassium feldspar, Moly: molybdenite, Qtz: quartz, Scp: scapolite..... 161

Fig. 8. BSE images showing monazite crystals in hydrothermally altered and ore samples from the Bacaba and Bacuri deposits. A) and B) Monazite inclusions in apatite crystals. Chalcopyrite and apatite fills the matrix of the copper ore breccia. Bacaba deposit (sample BACD 25/229.25); C) Large monazite crystal (> 200 µm) included in hydrothermal albite. Serra Dourada Granite affected by sodic alteration and silification (BACD 15/237.4); D) Monazite included in hydrothermal albite and biotite from sodic and potassic alteration, respectively. Sample from the Bacuri deposit pervasively affected by chlorite and biotite alteration (BRID 07/115.42). Mineral

<i>abbreviations: Ab: albite, Bt: biotite, Cpy: chalcopyrite, Kfs: potassium feldspar, Mgt: magnetite, Mz: monazite.</i>	162
Fig. 9. CL images of zircon from the felsic rocks dated by U-Pb SHRIMP IIe. $207\text{Pb}/206\text{Pb}$ ages are indicated in the image where analyses were done. A-C) Quartz-feldspar porphyry (sample GMCL 54A); D-F) Castanha quartz-feldspar porphyry (sample CASD 02/424.9); G-I) Serra Dourada Granite (sample GMCL 40A); J-L) Campina Verde Tonalite (sample GMCL 01); M-O) Campina Verde Tonalite (sample GMCL 66).	165
Fig. 10. $^{206}\text{Pb}^{238}\text{U}$ vs. $^{207}\text{Pb}^{235}\text{U}$ diagrams for zircon from the felsic rocks dated by U-Pb SHRIMP IIe. A) Quartz-feldspar porphyry (sample GMCL 54A); B) Castanha quartz-feldspar porphyry (sample CASD 02/424.9); C) Serra Dourada Granite (sample GMCL 40A); D) Campina Verde Tonalite (sample GMCL 01); E) Campina Verde Tonalite (sample GMCL 66).	166
Fig. 11. $^{206}\text{Pb}^{238}\text{U}$ vs. $^{207}\text{Pb}^{235}\text{U}$ diagrams for monazite from hydrothermally altered rocks and ore from the Bacaba and Bacuri deposits. A) and B) Cu ore from the Bacaba deposit (sample BACD 25/229.25). Two different concordia ages (diagrams A and B) from distinct monazite populations were obtained for this sample; C) Serra Dourada Granite affected by sodic alteration (albite) and silicification (BACD 15/237.4); D) Sample from the Bacuri deposit with biotite, chlorite and scapolite alteration (BRID 07/115.42).	168
Fig. 12. A summary of geochronological data for IOCG deposits from the Southern Copper Belt and their host rocks, and the main tectonic and magmatic events recorded in the Carajás province. The data obtained in this study is included. Data source: (1) Marschik <i>et al.</i> (2003); (2) Neves (2006); (3) Moreto <i>et al.</i> (<i>submitted</i>); (4) Soares <i>et al.</i> (2001); (5) Huhn <i>et al.</i> (1999b); (6) Tallarico (2003); (7) Moreto <i>et al.</i> (<i>this study</i>); (8) Moreto <i>et al.</i> (2011); (9) Silva <i>et al.</i> (2012). amp amphibole; cpy chalcopyrite; Da dacite; Di diorite; FM felsic metavolcanic rock; G granite; GG granophyric granite Gb gabbro; mz monazite; moly molybdenite; P quartz-feldspar porphyry; T tonalite; zr zircon.	178
Fig. 13. Schematic diagram showing the magmatic and metallogenetic evolution of the Southern Copper Belt in time, from 3.0 to 1.88 Ga.....	181

ÍNDICE DE TABELAS

Tabela 1. Dados geocronológicos disponíveis na literatura para os depósitos IOCG do Cinturão Sul do Cobre e rochas hospedeiras.....	18
Tabela 2. Síntese dos dados geocronológicos para os corpos Sequeirinho, Pista, Sossego e Curral.....	35
Tabela 3. Síntese dos dados geocronológicos obtidos para as rochas do Cinturão Sul do Cobre e depósitos Bacuri e Bacaba.....	37

ANEXO 1: Artigo “Paleoproterozoic overprint on Archean iron oxide-copper-gold system at the Sossego deposit, Carajás Province: Re-Os and U-Pb geochronological evidence”

Table 1 Available geochronological data for IOCG deposits and their host rocks from the Carajás Domain	51
Table 2 Main characteristics of the Sequeirinho-Pista-Baiano and Sossego-Curral orebodies of the Sossego deposit.....	59
Table 3 Synthesis of geochronological data for the Sequeirinho, Pista, Sossego and Curral orebodies	77
Table 4 Summary of Re-Os molybdenite data from the Pista orebody.....	82

Appendix

Supplementary Table 1 Summary of U-Pb LA-ICPMS zircon data from the host rocks of the Sequeirinho and Sossego orebodies.....	112
Supplementary Table 2 Summary of U-Pb SHRIMP IIe zircon data from the host rocks of the Sequeirinho, Pista and Sossego orebodies, and an ore sample from the Sequeirinho orebody	114
Supplementary Table 3 Summary of U-Pb LA-MC-ICPMS monazite data from ore samples of the Sequeirinho, Sossego and Curral orebodies	116

ANEXO 2: Artigo “Timing of multiple Iron oxide Cu-Au systems in the Southern Copper Belt, Carajás Province, Brazil: U-Pb zircon and monazite and Re-Os molybdenite geochronology”

Table 1 Available geochronological data for the Carajás Domain.....	127
Table 2 Main characteristics of the IOCG deposits from the Southern Copper Belt	133
Table 3 Available geochronological data for the IOCG deposits and their host rocks from the Southern Copper Belt.....	136
Table 4 Synthesis of geochronological data obtained in this study.....	163
Table 5 Summary of Re-Os molybdenite data from the Bacuri deposit.....	169

Appendix

Supplementary Table 1 Summary of U-Pb SHRIMP IIe zircon data.....	200
Supplementary Table 2 Summary of the U-Pb LA-MC-ICPMS monazite data	202

1. INTRODUÇÃO

A Província Carajás destaca-se mundialmente por apresentar a maior quantidade conhecida de importantes depósitos de óxido de ferro-cobre-ouro (*iron oxide-copper-gold* ou IOCG; Hitzman *et al.*, 1992; Hitzman, 2000). Os depósitos IOCG de Carajás são também considerados os únicos de classe mundial de idade arqueana (Réquia *et al.*, 2003; Tassinari *et al.*, 2003; Tallarico *et al.*, 2005; Groves *et al.*, 2010; Xavier *et al.*, 2010), refletindo a particular evolução da Província Carajás. Entre os depósitos dessa classe destacam-se Salobo (1,112 Bt @ 0.69% Cu e 0.43 g/t Au; VALE, 2012), Igarapé Bahia-Alemão (219 Mt @ 1.4% Cu e 0.86 g/t Au; Tavaza, 1999; Tallarico *et al.*, 2005), Sossego (355 Mt @ 1.1 % Cu e 0.28 g/t Au; Lancaster Oliveira *et al.*, 2000), Cristalino (482 Mt @ 0.65% Cu e 0.06 g/t Au; NCL Brasil, 2005) e Alvo 118 (170 Mt @ Cu e 0.3 g/t Au; Rigon *et al.*, 2000), além de vários outros depósitos em avaliação.

As minas de cobre Sossego e Salobo, operadas pela VALE, foram as primeiras da província a entrarem em produção, em 2004 e 2011, respectivamente. A Mina Salobo, a 30 km ao norte da Serra de Carajás, localiza-se ao longo do sistema de falha transcorrente Cinzento, próximo ao limite norte entre a Bacia Carajás e as rochas do embasamento. Na parte norte da província, no Cinturão Norte do Cobre, são também conhecidos outros depósitos IOCG, tais como Igarapé Bahia/Alemão, Gameleira, Pojuca, Paulo Alfonso, Furnas, Polo e Igarapé Cinzento/Alvo GT46.

A Mina Sossego localiza-se no contato sul entre a Bacia Carajás e as rochas mesoarqueanas do embasamento (Moreto, 2010; Oliveira *et al.*, 2010; Moreto *et al.*, 2011; Feio *et al.*, 2012a), no chamado Cinturão Sul do Cobre, que compreende uma zona de cisalhamento com mais de 130 km de extensão. Outros depósitos de classe mundial (Cristalino e Alvo 118) e de menor tonelagem (Castanha, Bacaba, Bacuri, Visconde e Jatobá) também são situados ao longo dessa faixa. Com exceção dos dois primeiros, os demais depósitos ainda estão em fase de avaliação pela VALE, e dados sobre teor e tonelagem não foram divulgados.

Apesar da relevância e do potencial metalogenético do Cinturão Sul do Cobre, trabalhos de mapeamento geológico sistemático são escassos no entorno dos depósitos IOCG. A caracterização das rochas hospedeiras dos depósitos IOCG, feita a partir da descrição de testemunhos de sondagem, é dificultada pela intensa alteração hidrotermal e deformação

associada, que obliteram, por vezes por completo, a textura e mineralogia original das rochas. Nesse sentido, uma caracterização detalhada da natureza das rochas hospedeiras dos depósitos IOCG fazia-se necessária para uma melhor compreensão da evolução de cada depósito.

A Mina Sossego é notável por apresentar corpos de minério com padrões de alteração hidrotermal semelhantes aos formados em diferentes níveis crustais em sistemas IOCG mundiais (Monteiro *et al.*, 2008a). Nos corpos Sequeirinho-Pista-Baiano, alteração sódico-cálcica e corpos de magnetititos, típicos de depósitos IOCG profundos (Hitzman, 2000; Williams *et al.*, 2005) são predominantes, enquanto alteração potássica, clorítica e hidrolítica, análogas às reconhecidas em sistemas rasos, são identificadas nos corpos Sossego-Curril. Os demais depósitos de classe mundial, Alvo 118 e Cristalino, compartilham características geológicas comuns aos dos corpos da Mina Sossego, com a predominância de alteração potássica e clorítica no primeiro (Torresi *et al.*, 2012) e de alteração sódico-cálcica no depósito Cristalino (Huhn *et al.*, 1999a).

Os depósitos Bacaba, Castanha, Bacuri e Visconde localizam-se entre 8 a 15 km a nordeste da Mina Sossego e associam-se a extenso halo de escapolitização (Augusto *et al.*, 2008; Moreto *et al.*, 2011). De maneira geral, todos esses depósitos registram sobreposição de alteração sódica regional (albita-escapolita), alteração potássica e cloritização, alteração sódico-cálcica (actinolita) local, formação de óxidos de ferro, e formação tardia de sericita, epidoto e carbonatos (Augusto *et al.*, 2008, Monteiro *et al.*, 2008a; Moreto *et al.*, 2011; Pestilho, 2011, Craveiro *et al.*, 2012a; Melo *et al.*, Submetido). Alguns desses depósitos apresentam características peculiares, tais como espessos corpos de rocha rica em magnetita e actinolita no depósito Castanha (Pestilho, 2011), que assemelham-se aos reconhecidos nos corpos Sequeirinho-Pista-Baiano da Mina Sossego.

As características particulares de cada depósito IOCG do Cinturão Sul do Cobre, somadas aos estudos de inclusões fluidas e isótopos estáveis (Monteiro *et al.*, 2008a; Ribeiro, 2008; Carvalho, 2009; Melo, 2010; Pestilho, 2011; Torresi *et al.*, 2012; Craveiro *et al.*, 2012b) sugerem que esses depósitos foram formados em níveis estruturais distintos, e que os fluidos hidrotermais foram provenientes de múltiplas fontes ou interagiram com componentes magmáticos e externamente derivados em diferentes proporções. Contudo, ainda não é possível, a luz dos dados disponíveis, associar esses depósitos a distintas porções de um único sistema hidrotermal ou a vários sistemas com histórias evolutivas distintas.

Adicionalmente, uma comparação mais detalhada entre os depósitos do Cinturão Sul do Cobre é limitada pela escassez de dados geocronológicos que permitam avaliar a contemporaneidade entre os estágios de mineralização nesses depósitos. As datações mais confiáveis disponíveis na literatura são referentes ao depósito Alvo 118 (U-Pb SHRIMP IIe em xenotima hidrotermal) que apontam para uma idade paleoproterozóica ($1,869 \pm 7$ Ma, Tallarico, 2003) para a formação do minério. Os demais dados disponíveis foram obtidos pela sistemática Pb-Pb em sulfetos (calcopirita) e, apesar dos grandes erros associados, apontam para um evento no Neoarqueano nos depósitos Cristalino e Visconde e no corpo Sequeirinho (ca. 2,74 Ga a 2,53 Ga; Soares *et al.*, 2001; Neves, 2006; Silva *et al.*, 2012). No corpo Sossego uma idade mesoproterozóica (ca. 1,5 Ga) foi obtida em calcopirita (Pb-Pb; Neves, 2006), porém interpretada como sem significado geológico.

Adicionalmente, o intervalo de idades reportado para os depósitos do Cinturão Sul do Cobre é mais amplo que o considerado para o Cinturão Norte do Cobre, com base em idades obtidas pelos métodos Re-Os em molibdenita (Salobo; Réquia *et al.*, 2003) e U-Pb SHRIMP em monazita (Igarapé Bahia; Tallarico *et al.*, 2005). Esses depósitos seriam relacionados a um único evento metalogenético IOCG em ca. 2,57 Ga, associado à instalação de sistema magmático-hidrotermal regional (Grainger *et al.*, 2008; Groves *et al.*, 2010).

2. OBJETIVOS

O presente projeto de doutorado teve como principais objetivos a:

- I. Caracterização geológica da porção centro-oeste do Cinturão Sul do Cobre, na área dos depósitos IOCG Bacaba, Bacuri, Castanha e Visconde;
- II. Determinação das idades de cristalização das rochas hospedeiras desses depósitos e do depósito Sossego, além das demais rochas presentes na porção centro-oeste do Cinturão Sul do Cobre;
- III. Delimitação do (s) intervalo (s) de idade (s) de formação das mineralizações IOCG e dos estágios de alteração hidrotermal nos depósitos do Cinturão Sul do Cobre;
- IV. Estabelecimento de modelos evolutivos para os depósitos do Cinturão Sul do Cobre a partir dos dados geocronológicos inéditos apresentados nesse estudo e de outros dados disponíveis na literatura, considerando relações com os principais eventos geológicos regionais do Domínio Carajás.

3. MÉTODOS

As etapas metodológicas estão listadas abaixo. Os métodos analíticos específicos utilizados nos laboratórios (e.g., U-Pb SHRIMP IIe, LA-ICPMS e Re-Os NTIMS) estão detalhados nos procedimentos analíticos dos artigos em anexo (Anexos 1 e 2).

Revisão Bibliográfica:

Revisão bibliográfica foi realizada com enfoque em estudos geocronológicos aplicados à depósitos minerais no Brasil e em outras províncias metalogenéticas no mundo. Também foi enfatizada a leitura de trabalhos sobre depósitos IOCG e modelos genéticos. Adicionalmente, trabalhos relacionados à evolução crustal da Província Carajás, de outras províncias minerais no mundo também foram priorizados.

Trabalhos de campos:

Trabalhos de campo foram realizados em três etapas, nos períodos entre 14 a 28/07/2009, 12 a 28/07/2011, e 10 a 23/07/2012. Nessas etapas de campo foi realizado mapeamento geológico na região a leste do depósito Sossego, na porção centro-oeste do Cinturão Sul do Cobre, entre as coordenadas 601900 e 627300E, e 9285600 e 9296000N.

Petrografia em luz transmitida e refletida:

Estudos petrográficos foram realizados no Instituto de Geociências da Universidade Estadual de Campinas (UNICAMP) em amostras inalteradas das rochas hospedeiras e também com diferentes graus e estágios de alteração hidrotermal dos depósitos Sossego, Castanha, Bacaba e Bacuri. Adicionalmente, estudos petrográficos também foram feitos nas amostras coletadas em campo, nas adjacências desses depósitos. Microfotografias foram obtidas por sistema de captura de imagens acoplado ao microscópio.

Preparação de amostras e separação mineral:

Essa etapa incluiu separação de fases minerais datáveis pelo método U-Pb, tais como zircão, titanita e monazita, e por Re-Os, como molibdenita e calcopirita. Ao longo do doutorado foram preparadas 53 amostras para geocronologia U-Pb, das quais 17 amostras não apresentaram

minerais passíveis de datação. Essa etapa foi realizada nos laboratórios de Preparação de Amostras e de Concentração Mineral do Instituto de Geociências da UNICAMP. Os minerais foram concentrados a partir de métodos gravimétricos e magnéticos convencionais, seguindo as etapas descritas abaixo:

- Britagem em britador de mandíbulas;
- Moagem em moinho vibratório por tempo que varia de 15 segundos a 1 minuto, dependendo da dureza da amostra;
- Peneiramento em peneiras de nylon de 250 µm de abertura;
- Bateamento manual;
- Separação magnética através do separador isodinâmico Frantz;
- Separação manual dos grãos em lupa binocular.

Microscopia Eletrônica de Varredura:

O microscópio eletrônico de varredura do Instituto de Geociências da UNICAMP foi utilizado com a finalidade de auxiliar na caracterização (estruturas e texturas internas, morfologia, dentre outras) de fases minerais datáveis, tais como monazita, titanita e zircão.

Estágio de pesquisa e aquisição de dados no exterior:

No período entre 14 de abril a 31 de maio de 2012 foi realizado um estágio na *University of Alberta*, em Edmonton, Canadá, supervisionado pelos professores Dr. Robert Creaser e Dr. Andy DuFrane. O objetivo desse estágio consistiu no acompanhamento da preparação das amostras e aquisição de resultados isotópicos Re-Os NTIMS em molibdenita e calcopirita. Adicionalmente, análises em grãos de monazita e titanita pelo método U-Pb LA-ICP-MS também foram realizadas. Foi possível acompanhar todo o procedimento analítico de dissolução isotópica dos sulfetos e separação e concentração do Re e Os para posterior análise no NTIMS.

Geocronologia:

Os dados geocronológicos inéditos foram obtidos nos anos de 2011 e 2012. Em 2011, 3 lâminas de amostras de rochas hospedeiras do depósito Sossego foram analisadas pelo método LA-ICP-MS U-Pb in situ em zircão na *James Cook University*, Austrália. Durante o período de estágio no Canadá, 3 amostras de molibdenita, duas amostras de calcopirita e uma amostra de pirrotita dos

depósitos Sossego e Bacuri foram analisadas pelo método Re-Os NTIMS no *Radiogenic Isotope Facility da University of Alberta*, Canadá. Diferentemente dos cristais de molibdenita, as amostras de calcopirita e pirrotita não produziram resultados confiáveis, uma vez que as diversas alíquotas desses minerais (quatro por amostra) forneceram idades consideravelmente distintas, entre 528 a 3.126 Ma (amostra de minério do depósito Castanha) e 470 a 549 Ma (amostra de minério do corpo Sequeirinho). Adicionalmente, sete amostras de monazita e outras sete de titanita de amostras de minério dos diversos depósitos IOCG foram analisadas pelo método U-Pb LA-ICP-MS também na *University of Alberta*. Os grãos de monazita geraram resultados muito confiáveis, o que não foi observado nos cristais de titanita, que mostraram uma grande perda de Pb. Essa abertura do sistema isotópico não produziu grãos alinhados ao longo de uma discordia, mas sim extremamente dispersos. Assim sendo, não foi possível obter idades de intercepto superior, que poderiam ser interpretadas como a idade de cristalização/rehomogeneização dos cristais de titanita. Em dezembro de 2011 e 2012, cristais de zircão de 11 amostras de rochas hospedeiras dos depósitos Sossego, Bacaba, Castanha e Bacuri foram analisadas no Laboratório de Geocronologia de Alta Resolução do Centro de Pesquisas Geocronológicas (CPGeo) da Universidade de São Paulo, pelo método U-Pb SHRIMP IIe em zircão. Todas as amostras analisadas geraram idades concordância.

4. CONTEXTO GEOLÓGICO REGIONAL: DOMÍNIO CARAJÁS

A Província Carajás, considerada parte da Província Amazônia Central na proposta de compartimentação tectônica do Cráton Amazônico de Tassinari e Macambira (1999, 2004), foi individualizada na proposta de Santos *et al.* (2000) e Santos (2003) e adotada por Vasquez *et al.* (2008a).

A Província Carajás, que compreende o núcleo crustal mais antigo do Cráton Amazônico, foi formada e estabilizada tectonicamente no Arqueano (Teixeira *et al.*, 1989; Tassinari, 1996; Tassinari e Macambira, 1999, 2004). É subdividida em dois domínios tectônicos, Carajás, ao norte, e Rio Maria, ao sul (Vasquez *et al.*, 2008a), limitados por uma descontinuidade regional de direção aproximada E-W.

O Domínio Carajás (Fig. 1) destaca-se por apresentar depósitos gigantes de minério de Ferro de alto teor, a maior quantidade conhecida no planeta de depósitos IOCG de classe mundial e um dos raros exemplos mundiais de depósito de ouro-EGP associado a rochas

metassedimentares, representado por Serra Pelada, que se tornou famoso na década de 1980 devido à intensa atividade garimpeira. Adicionalmente, depósitos cupro-auríferos sem associação com óxidos de Ferro ou polimetálicos, depósitos de cromo e níquel-EGP associados a intrusões máfico-ultramáficas acamadas, depósitos manganesíferos sedimentares e depósitos lateríticos de ouro, níquel e bauxita apresentam grande importância econômica.

O Domínio Carajás (Vasquez *et al.*, 2008a), previamente denominado de Cinturão de Cisalhamento Itacaiúnas por Araújo *et al.* (1988), inclui a Bacia Carajás e, em sua parte sul, uma faixa denominada de Subdomínio de Transição (Dall'Agnol *et al.*, 2006; Feio *et al.*, 2012a), na qual o possível embasamento Mesoarqueano da bacia é predominante.

4.1 Embasamento

No Domínio Carajás, o embasamento arqueano é formado por rochas metamorfisadas em fácies anfibolito a granulito atribuídas ao Complexo Xingu (Silva *et al.*, 1974), composto por gnaisses tonalíticos a trondjemíticos, migmatitos e anfibolitos, e ao Complexo Pium com ortogranulitos máficos a félscos, cujos protólitos teriam idades de cristalização de 3.002 ± 14 Ma (U-Pb SHRIMP zircão; Pidgeon *et al.*, 2000). Segundo Machado *et al.* (1991), ao menos duas fases de migmatização podem ser identificadas nas rochas do Complexo Xingu. O último episódio de migmatização, associado à deformação regional (2.859 ± 2 Ma e 2.860 ± 2 Ma; U-Pb em zircão; Machado *et al.*, 1991) seria coevo ao evento de granulitização das rochas do Complexo Pium (2.859 ± 9 Ma, U-Pb SHRIMP zircão; Pidgeon *et al.*, 2000). Ainda segundo Machado *et al.*, (1991), em 2.851 Ma novos cristais de zircão teriam se formado em gnaisses do Complexo Xingu em função de possível atividade hidrotermal de amplitude regional.

Estudos recentes (Gomes, 2003; Moreto, 2010; Moreto *et al.*, 2011; Silva, 2011; Feio *et al.*, 2012a) na área do embasamento a sul da Bacia Carajás, no entanto, sugerem que é possível individualizar unidades mesoarquenas distintas nas áreas antes atribuídas ao Complexo Xingu, o que restringe a ocorrência desse complexo na Província Carajás. Entre tais unidades geológicas, incluem-se: (1) ca. 3,0 Ga – Tonalito Bacaba (Moreto *et al.*, 2011); (2) 2,96-2,93 Ga - Granito Canaã dos Carajás, de afinidade cálcio-alcalina, e rochas mais antigas do Trondjemito Rio Verde (Feio *et al.*, 2012a); (3) 2,87-2,83 Ga - Trondjemito Rio Verde e os granitos predominantemente cálcio-alcalinos Cruzadão e Serra Dourada (Moreto *et al.*, 2011; Feio *et al.*,

2012a). Adicionalmente, Barros *et al.* (2010) reinterpretou a idade U-Pb em zircão de ca. 2,86 Ga de Machado *et al.* (1991), atribuída à migmatização, como relativa à idade de cristalização de alguns dos granitóides foliados da região de Serra Leste.

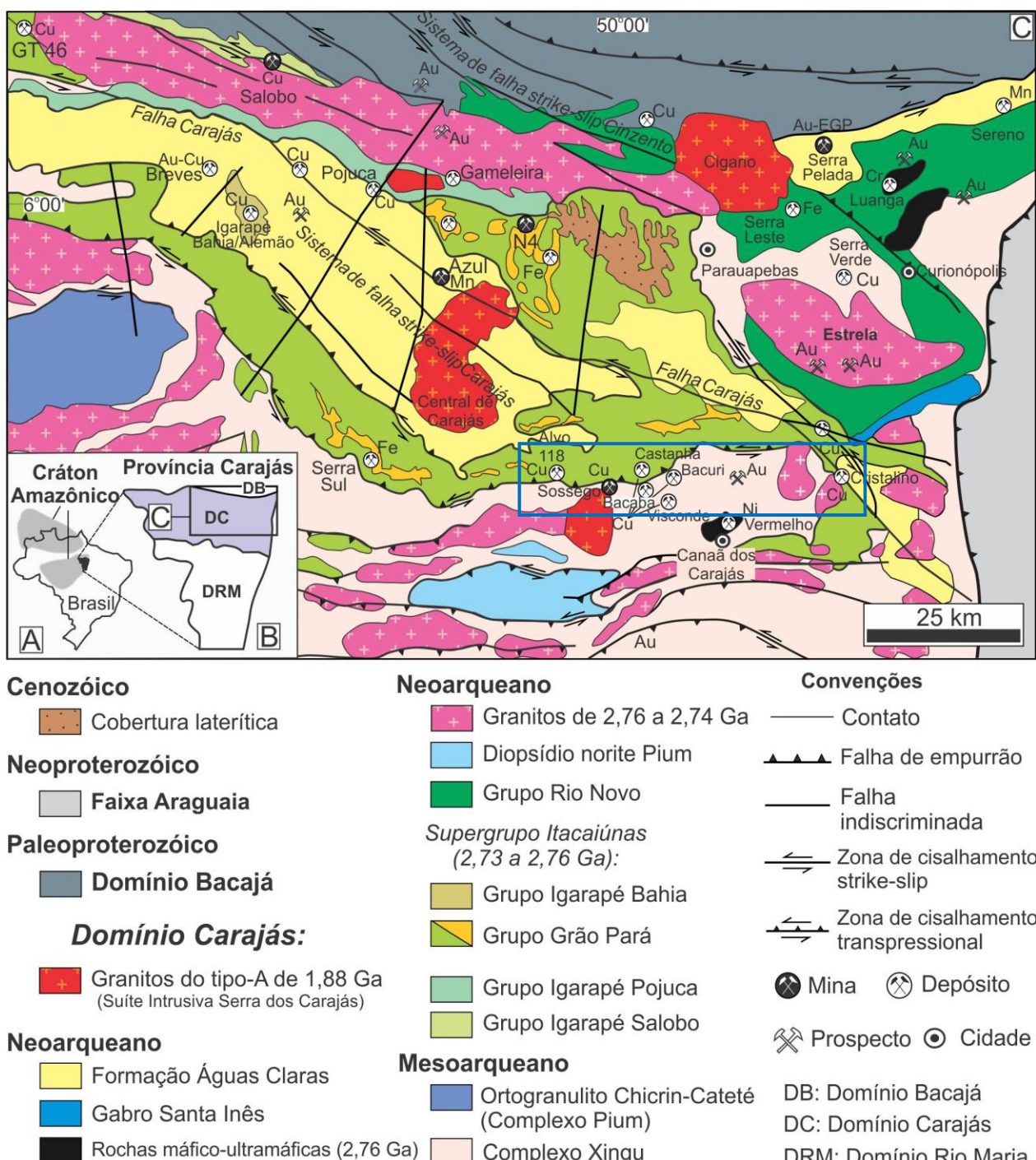


Figura 1. Mapa geológico do Domínio Carajás e áreas adjacentes (modificado de Vasquez et al., 2008a), mostrando a localização do Cinturão Sul do Cobre (retângulo em azul).

Na localidade-tipo do Complexo Pium, também foram individualizadas rochas ígneas, tais como noritos, gabros e dioritos (Oliveira *et al.*, 2010), sob a denominação de Diopsídio-norito Pium (Vasquez *et al.*, 2008a). Os ortogranulitos, enderbitos e charnockitos que ocorrem ao longo do rio Cateté, nas proximidades da aldeia indígena Chicrim, anteriormente considerados por Araújo e Maia (1991) como parte do Complexo Pium, foram separados por Ricci e Carvalho (2006) e Vasquez *et al.* (2008a), e denominados de Ortogranulito Chicrim-Cateté.

4.2 Unidades supracrustais: Bacia Carajás

As rochas da Bacia Carajás (Fig. 1) encontram-se em inconformidade com as rochas do embasamento, e correspondem a sequências metavulcano-sedimentares do Grupo Rio Novo (Hirata *et al.*, 1982) e do Supergrupo Itacaiúnas (Wirth *et al.*, 1986; DOCEGEO, 1988; Machado *et al.*, 1991), além da Formação Águas Claras, metassedimentar (Araújo *et al.*, 1988; Nogueira *et al.*, 1995). O Grupo Rio Novo, localizado na porção nordeste do Domínio Carajás (Fig. 1), inclui anfíbolitos, xistos, metagrauvacas, rochas metavulcânicas tholeiíticas e gabros (Hirata *et al.* 1982). O Supergrupo Itacaiúnas (Wirth *et al.*, 1986; DOCEGEO, 1988) é constituído pelo Grupo Grão Pará, na base, e pelo Grupo Igarapé Bahia, no topo. As rochas (meta-)vulcânicas basais do Grupo Grão Pará (Formação Parauapebas) possuem caráter bimodal, englobando metabasaltos e metariolitos (2.758 ± 39 Ma, U-Pb em zircão, Wirth *et al.*, 1986; 2.759 ± 2 Ma, U-Pb zircão, Machado *et al.*, 1991). Formações ferríferas bandadas (Formação Carajás) localizam-se estratigráficamente acima das rochas vulcânicas basais, e são cobertas por derrames basálticos e rochas metassedimentares. O Grupo Igarapé Bahia, aflorante em uma janela estrutural dentro da Formação Águas Claras, inclui rochas metavulcânicas, metapiroclásticas (2.747 ± 1 Ma, Pb-Pb zircão, Galarza e Macambira, 2002a) e formações ferríferas (DOCEGEO, 1988). Os grupos Igarapé Salobo (gnaisses, anfíbolitos, xistos, quartzitos; DOCEGEO, 1988) e Igarapé Pojuca (rochas metavulcânicas básicas e intermediárias, *chert*, formações ferríferas bandadas, xistos e gabros; DOCEGEO, 1988) foram inicialmente incluídos no Supergrupo Itacaiúnas por DOCEGEO (1988). Contudo, dados geocronológicos obtidos por Machado *et al.*, (1991) apontam que esses grupos possivelmente são mais antigos que 2,84 Ga.

O Supergrupo Itacaiúnas é parcialmente recoberto pela Formação Águas Claras, representada por meta-conglomerados, meta-arenitos, mármore dolomítico, filito carbonoso e sericita quartzitos, que refletem sedimentação marinha rasa a fluvial (Nogueira *et al.*, 1995). Esta

unidade tem idade limitada ao Arqueano em função de ser cortada por sill de metagabro datado em 2.645 ± 12 Ma (Dias *et al.*, 1996) e 2.708 ± 37 Ma (Mougeot *et al.* 1996a). Contudo, idades Pb-Pb em sulfetos diagenéticos presentes em meta-arenitos de ca. 2,06 Ga foram obtidas por Mougeot *et al.* (1996b) e consideradas por Fabre *et al.* (2011) evidência de idade paleoproterozóica para a Formação Águas Claras.

4.3 Rochas intrusivas

Intrusões acamadas representadas pelo Complexo Máfico-Ultramáfico Luanga (Machado *et al.*, 1991), localizado na Serra Leste, e pela Suíte Intrusiva Cateté (e.g., Serra da Onça, Serra do Puma, Serra do Jacaré-Jacarezinho, Vermelho e Igarapé Carapanã; Macambira e Vale, 1997; Macambira e Ferreira Filho, 2002; Ferreira Filho *et al.*, 2007), no Sub-domínio de Transição, hospedam importantes mineralizações de níquel e EGP (Ferreira Filho *et al.*, 2007). O Complexo Luanga apresenta evidências de metamorfismo em fácies xisto verde (Ferreira Filho *et al.*, 2007), diferentemente da Suíte Cateté, que não apresenta indícios de deformação ou metamorfismo (Macambira e Vale, 1997). Idade U-Pb em zircão em 2.763 ± 6 Ma foi obtida para anortosito do Complexo Luanga (Machado *et al.*, 1991), enquanto um gábrico do Corpo Onça foi datado em 2.766 ± 6 Ma (U-Pb SHRIMP zircon; Lafon *et al.*, 2000).

O magmatismo granítico neoarqueano (ca. 2,75 a 2,74 Ga), restrito ao Domínio Carajás, foi responsável pela formação de granitos alcalinos a metaluminosos, foliados, similares aos do tipo-A, que são compreendidos pelas suítes Plaquê, Planalto, Estrela, Igarapé Gelado, Serra do Rabo e Pedra Branca (Huhn *et al.*, 1999b; Avelar *et al.*, 1999; Barbosa, 2004; Barros *et al.*, 2004; 2009; Sardinha *et al.*, 2006; Feio *et al.*, 2012a,b). Granitos alcalinos, peralcalinos a metaluminosos, mesozonais, com augita como máfico principal, representados pelos granitos Old Salobo e Itacaiúnas (ca. 2,57 Ga, Machado *et al.* 1991, Souza *et al.* 1996) foram caracterizados apenas na parte norte do domínio, nas proximidades do sistema de falha *strike-slip* Cinzento (Fig. 1).

O magmatismo paleoproterozóico (ca. 1,88 Ga), presente por toda a Província Carajás, é representado por granitos alcalinos a sub-alcalinos do tipo A e metaluminosos a levemente peraluminosos, que inclui a Suíte Intrusiva Serra dos Carajás no Domínio Carajás (granitos Central de Carajás, Young Salobo, Cigano, Pojuca, Breves, e Rio Branco) e pela Suíte Intrusiva Jamon (granitos Jamon, Musa, Redenção, Seringa e Bannach) no Domínio Rio Maria (Machado

et al., 1991; Lindenmayer e Teixeira, 1999; Tallarico, 2003; Dall’Agnol *et al.*, 1999a,b, 2005; Dall’Agnol e Oliveira, 2007).

4.4 Modelos evolutivos

A estrutura dominante da Serra dos Carajás foi definida inicialmente por Beisiegel *et al.* (1973) como um sinclinório com eixo WNW-ESE, reinterpretado por Araújo *et al.* (1988) como associado a uma estrutura em flor positiva. Rosière *et al.* (2006) consideram que as estruturas das serras Norte e Sul seriam relacionadas a um par antiformal-sinormal em forma de “S”, denominado de Dobra Carajás.

A complexa configuração estrutural da Bacia Carajás também foi atribuída ao desenvolvimento de zonas de cisalhamento de alto mergulho com direção regional E-W e WNW-ESE representadas na porção norte pelos sistemas de falha *strike-slip* Carajás e Cinzento (Araújo e Maia, 1991) (Fig. 1). De acordo com Araújo et al. (1988), a estrutura sigmoidal de Carajás teria se formado durante transtração dextral das rochas do embasamento, o que teria favorecido a abertura de uma bacia do tipo *pull-apart*, além do desenvolvimento dos sistemas de falha Carajás, Cinzento de Araraquara. Essa bacia teria sido preenchida pela sequência de rochas vulcânicas e sedimentares do Supergrupo Itacaiúnas, e por sedimentos da Formação Águas Claras no topo. Após o término da deposição, transpressão sinistral teria causado inversão tectônica da bacia e criação de uma estrutura em flor positiva no sistema de falha transcorrente Carajás.

O modelo de reativação tectônica proposto por Pinheiro e Holdsworth (1997), Holdsworth e Pinheiro (2000) e Domingos (2009), sugere uma evolução distinta para a área. Nesse modelo, o Supergrupo Itacaiúnas e a Formação Águas Claras teriam sido depositados entre 2,76-2,74 Ga em uma bacia intracratônica sob um embasamento intensamente deformado em ca. 2,85 Ga sob transpressão sinistral regional de alta temperatura. Sob regime de extensão regional (transtração rúptil) em ca. 2.8-2.7 Ga, as rochas vulcão-sedimentares teriam sido acomodadas por subsidência tectônica ao formato atual da estrutura sigmoidal de Carajás. Os sistemas de falha *strike-slip* Carajás e Cinzento teriam se formado durante esse evento. Domingos (2009) sugere que a inversão tectônica da Bacia Carajás teria iniciado em ca. 2,70 Ga e durado até ca. 2,60 Ga, sob atuação de regime transpressional sinistral. Adicionalmente, Pinheiro e Holdsworth (1997) propõem que os sistemas de falha *strike-slip* Carajás e Cinzento preservam evidências diretas e indiretas de diversas fases de reativações dextrais e sinistrais a partir de 2,7 Ga. A Falha Carajás

(Fig. 1), por exemplo, teria sido formada durante uma dessas fases de reativação, sob transpressão sinistral rúptil. Domingos, (2009) também sugere uma fase tardia de extensão crustal (transtracção) em ca. 1,8 Ga, que teria favorecido colocação de diques e plútôns anorogênicos (e.g., Suite Intrusiva Serra dos Carajás; Fig. 1).

Wirth *et al.* (1986), Gibbs *et al.* (1986), DOCEGEO (1988), Macambira (2003) e Tallarico *et al.* (2005) também sugerem que a formação da Bacia Carajás estaria relacionada a abertura de um rifte continental. As idades das intrusões acamadas mafico-ultramáficas do Complexo Luanga, próximas às do vulcanismo bimodal do Grupo Grão Pará apontam, segundo Ferreira Filho *et al.* (2007), que tais intrusões correspondem a câmeras magnáticas associadas ao rifteamento.

Meirelles (1986), Dardenne *et al.* (1988), Meirelles e Dardenne (1991), Teixeira (1994), Lobato *et al.*, (2005), Silva *et al.*, (2005) e Teixeira *et al.* (2010), no entanto, sustentam a hipótese de que a bacia teria se formado em ambiente de arco vulcânico associada a mecanismo de subducção, o que seria evidenciado pela afinidade cálcio-alcalina de alto potássio dos basaltos do Supergrupo Itacaiúnas e rochas intrusivas. Zucchetti (2007) considera que tais características poderiam refletir vulcanismo extravasado sobre crosta continental atenuada, em ambiente de retro-arco desenvolvido em ca. 2,76 Ga. Nesse modelo de evolução geotectônica, colisão continente-continente em ca. 2,74 Ga teria sido responsável pela justaposição dos domínios Rio Maria e Carajás (Teixeira *et al.*, 2010).

5. DEPÓSITOS DE ÓXIDO DE FERRO-COBRE-OURO DA PROVÍNCIA CARAJÁS

A Província Carajás contém uma das maiores concentrações de depósitos IOCG de alta tonelagem do mundo (Monteiro *et al.* 2008a). Os depósitos IOCG são restritos ao Domínio Carajás e situam-se majoritariamente ao longo ou próximo de importantes descontinuidades crustais representadas pelos contatos norte e sul entre a Bacia Carajás e as rochas do embasamento. Tais contatos são definidos por zonas de cisalhamento de expressão regional (> 130 km de extensão) com orientação aproximada WNW-ESE. No limite norte da bacia, denominado de Cinturão Norte do Cobre, ao longo do sistema de falha transcorrente Cinzento, os depósitos Salobo, Igarapé Bahia-Alemão, Gameleira, Pojuca, Paulo Alfonso, Furnas, Polo, e Igarapé Cinzento/Alvo GT46 são conhecidos. O Cinturão Sul do Cobre, foco desse estudo,

hospeda os depósitos Sossego, Cristalino, Alvo 118, Bacaba, Castanha, Bacuri, Visconde, e Jatobá.

A primeira associação dos depósitos cupríferos com a classe IOCG, definida por Hitzman *et al.* (1992), foi proposta por Huhn e Nascimento (1997), sendo adotada por outros autores (Réquia *et al.*, 2003; Tallarico *et al.*, 2005; Monteiro *et al.*, 2008a,b; Xavier *et al.*, 2010; Teixeira *et al.*, 2010). Essa classificação baseia-se em um conjunto de atributos compartilhados pelos depósitos, tais como:

- I. Enriquecimentos em óxido de ferro, Cu, Au, ETRL, P, Ni, Co, e, em alguns casos, Ag, Mo, U, Th, Y, Pd, Zn, Te e Sn, análogos aos descritos em depósitos da classe IOCG em outras províncias mundiais (Hitzman, 2000; Williams *et al.*, 2005; Grainger *et al.*, 2008);
- II. Proximidade com intrusões maficas (diorito, gабro, noritos) e felsicas;
- III. Estágios iniciais de alteração hidrotermal característicos de depósitos formados em níveis crustais relativamente profundos, controlados por zonas de cisalhamento regionais e foliação milonítica, associados à circulação de fluidos quentes ($> 550^{\circ}\text{C}$) e hipersalinos, incluindo alteração sódica com albita, escapolitização, alteração sódico-cálcica e formação de magnetititos;
- IV. Alteração potássica ($< 450^{\circ}\text{C}$) com biotita e feldspato potássico espacialmente associada com as zonas mineralizadas;
- V. Cloritização, alteração cálcica tardia (clorita-epidoto-calcita) ou hidrolítica (sericitita-hematita) desenvolvidas a menores temperaturas ($< 350^{\circ}\text{C}$) e condições rúpteis, coevas com a precipitação do minério nas porções mais rasas do(s) sistema hidrotermal(is);
- VI. Amplo intervalo de temperaturas de homogeneização ($100\text{--}570^{\circ}\text{C}$) e salinidades (0 a 69% eq. peso NaCl) em inclusões fluidas de minerais de ganga relacionados aos minerais de minério, indicando predominância de fluidos magmáticos iniciais e variável grau de mistura com fluidos de origens diversas durante o estágio de deposição do minério (Rosa, 2006; Carvalho, 2009; Xavier *et al.*, 2010).

No Cinturão Sul do Cobre (Fig. 2), os depósitos de classe mundial, Sossego, Cristalino e Alvo 118, e os vários outros menores (Bacaba, Bacuri, Castanha, Visconde, e Jatobá) apresentam uma evolução paragenética semelhante (Augusto *et al.*, 2008; Melo, 2011; Pestilho, 2011; Torresi *et al.*, 2012; Craveiro *et al.*, 2012a). O depósito de Sossego é notável por apresentar padrões de alteração hidrotermal semelhantes aos reconhecidos em sistemas IOCG formados em diferentes

níveis crustais (Monteiro *et al.*, 2008a). A extensiva alteração sódica, sódica-cálcica e os corpos de magnetita-apatita associados à milonitização caracterizados no Corpo Sequeirinho são típicos de depósitos formados em níveis crustais mais profundos (Hitzman 2000; Williams *et al.*, 2005). Esse padrão também é semelhante ao caracterizado por Pestilho (2011) no depósito Castanha, no qual expressivos corpos com magnetita com envelope de actinolítitos foram caracterizados em zonas distais, e alteração potássica com biotita nas zonas proximais em relação aos corpos de minério. Os padrões de alteração hidrotermal do Corpo Sossego, análogos aos descritos no depósito Alvo 118 por Torresi *et al.* (2012), com predominância de alteração potássica e cloritização, são característicos de níveis crustais intermediários a rasos.

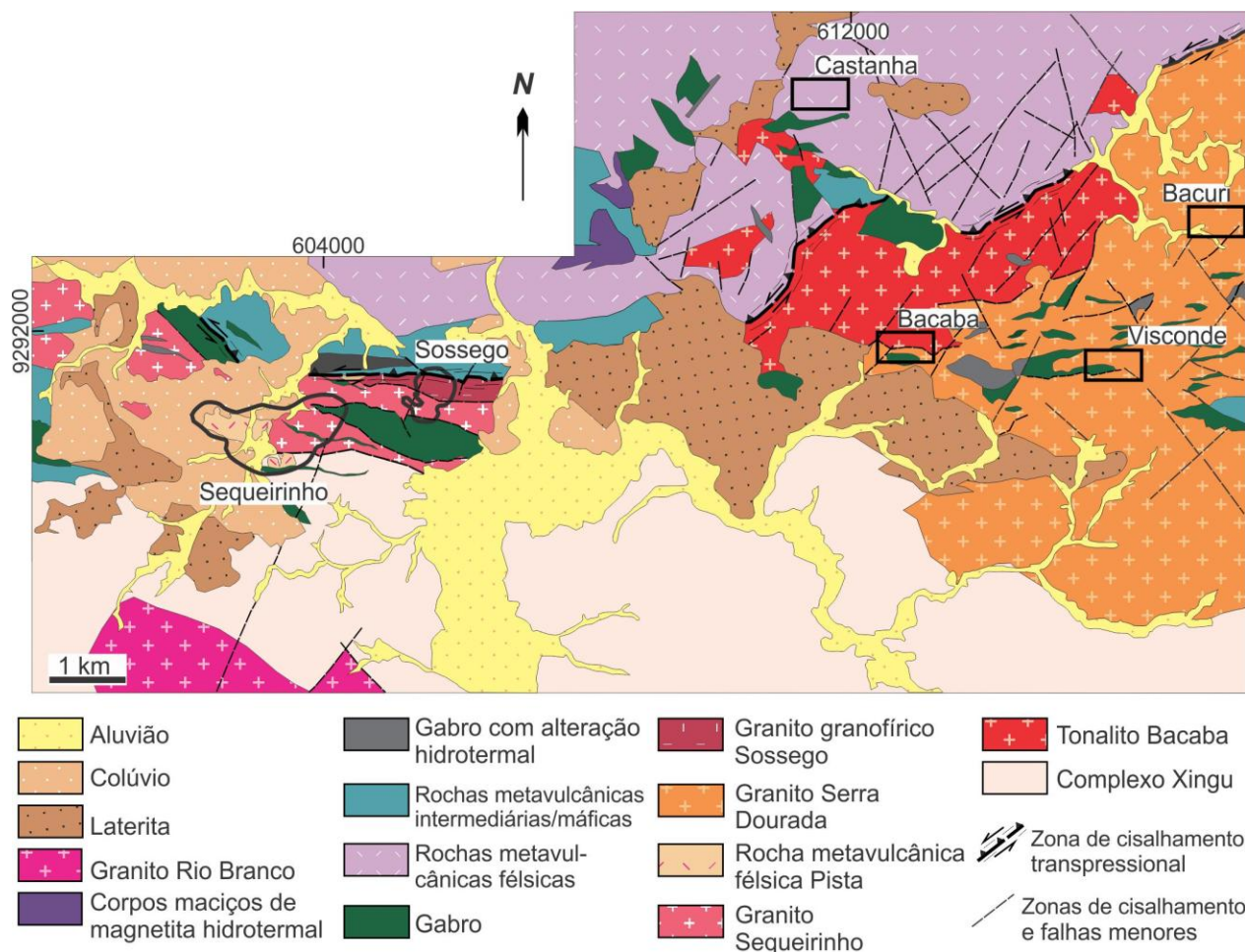


Figura 2. Mapa geológico da porção centro-oeste do Cinturão Sul do Cobre, mostrando os depósitos Sossego (corpos Sequeirinho e Sossego), Bacaba, Castanha, Bacuri e Visconde (modificado de VALE).

Alguns depósitos apresentam predominância de componentes magmáticos e contribuição muito limitada de fluidos externos, como o depósito de Castanha (Pestilho, 2011), o que é

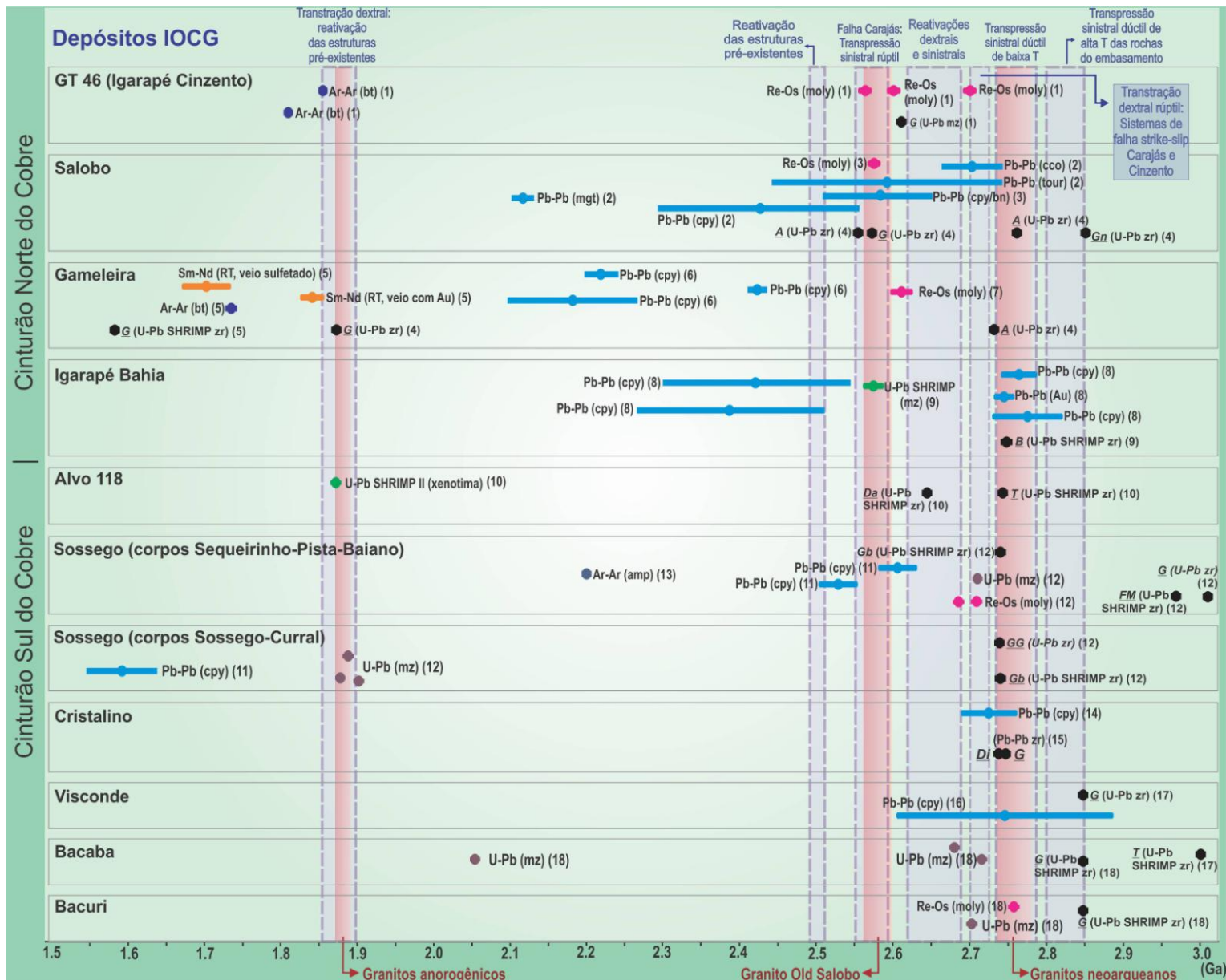
evidenciado pela ausência de fluidos de baixa salinidade ou com menores valores de $\delta^{18}\text{O}$ que os tipicamente magmáticos. Nesse depósito, a presença de brechas com pirrotita, calcopirita, pirita, pentlandita evidenciam também enriquecimentos em Ni e Co, associados ao Cu, Fe, P e ETR (Pestilho, 2011).

No entanto, a participação de fluidos superficiais (água meteórica e salmouras derivadas da água do mar) parece ter sido importante em depósitos desenvolvidos em níveis crustais mais rasos (Alvo 118, Torresi *et al.*, 2012; Corpo Sossego; Monteiro *et al.*, 2008a) e intermediários (Corpo Sequeirinho, Bacaba, Bacuri; Augusto *et al.*, 2008; Pestilho, 2011), e seria responsável por favorecer a deposição do cobre transportado como complexos cloretados pelos fluidos metalíferos, devido à diminuição de temperatura e salinidade.

No Cinturão Norte do Cobre, algumas diferenças em relação aos depósitos IOCG da parte sul são notáveis. O depósito de Salobo difere dos demais por apresentar minerais de mais alta temperatura (fayalita, granada e sillimanita) associados a zonas de cisalhamento dúcteis (Lindenmayer, 2003). Embora o papel de um sistema magmático-hidrotermal para a gênese do Salobo tenha sido enfatizado (Réquia *et al.*, 2003; Grainger *et al.*, 2008; Groves *et al.*, 2010), isótopos de boro ($\delta^{11}\text{B} = 14$ a 26,5‰, Xavier *et al.*, 2008a) em turmalina revelaram também a participação de componentes não-magmáticos para o sistema hidrotermal, que poderiam ser associados tanto com fluidos hidrotermais de fundo oceânico como da água do mar modificada. Tais componentes podem refletir estágios iniciais vulcano-sedimentares ou influxo da água do mar durante a evolução do sistema magmático-hidrotermal, sugerindo um sistema mais complexo, com contribuições de componentes de múltiplas fontes.

A gênese dos depósitos IOCG de Carajás tem sido relacionada a três eventos de alojamento de granitos identificados no Domínio Carajás (Fig. 3): (i) ca. 2,75-2,74 Ga (Huhn *et al.*, 1999b; Galarza *et al.*, 2003); (ii) ca. 2,57 Ga (Réquia *et al.*, 2003; Tallarico *et al.*, 2005; Grainger *et al.*, 2008), e (iii) ca. 1,88 Ga (Pimentel *et al.*, 2003; Tallarico, 2003).

A importância das intrusões graníticas neoárqueanas (ca. 2,57 Ga), semelhantes aos granitos Old Salobo e Itacaiúnas, para o estabelecimento dos sistemas magmático-hidrotermais IOCG de Carajás foi proposta por alguns autores (Réquia *et al.*, 2003; Tallarico *et al.*, 2005; Grainger *et al.*, 2008; Groves *et al.*, 2010), com base em dados geocronológicos como Re-Os em molibdenita (Salobo, Réquia *et al.*, 2003) e U-Pb SHRIMP em monazita (Igarapé Bahia, Tallarico *et al.*, 2005) (Fig. 3).



«Figura 3. Síntese dos dados geocronológicos dos depósitos IOCG e rochas hospedeiras da Província Carajás, e principais eventos tectônicos e magmáticos registrados na província. Referências: (1) Silva et al. (2005); (2) Tassinari et al. (2003); (3) Réquia et al. (2003); (4) Machado et al. (1991); (5) Pimentel et al. (2003); (6) Galarza and Macambira (2002b); (7) Marshick et al. (2005); (8) Galarza et al. (2008); (9) Tallarico et al. (2005); (10) Tallarico (2003); (11) Neves (2006); (12) Moreto et al. (Anexo 1); (13) Marshick et al. (2003); (14) Soares et al., 2001; (15) Huhn et al. (1999b); (16) Silva et al. (2012); (17) Moreto et al. (2011); (18) Moreto et al (Anexo 2). A anfibolito; amp anfibólito; Au ouro; B basalto; bn bornita; bt biotite; cco chalcocita; cpy calcopirita; Da dacito; Di diorito; FM rocha metavulcânica felsica; G granito; GG granito granofílico; Gb gabbro; Gn gneiss; mz monazita; mgt magnetita; moly molibdenita; T tonalito; tour turmalina; WR rocha total; zr zircão.

Entretanto, essa idade também é contestada, uma vez que o magmatismo de ca. 2,57 Ga é extremamente restrito no Domínio Carajás, e presente somente no Cinturão Norte do Cobre. Segundo Teixeira et al. (2010), essa idade seria próxima da atribuída a mais uma das reativação do sistema de falha *strike-slip* Cinzento (2.555 ± 4 Ma; Machado et al., 1991) ao longo do qual situa-se o depósito de Salobo. Idades mais antigas (2.705 ± 42 Ma; Pb-Pb em calcocita) e mais novas (2.112 ± 12 Ma; Pb-Pb em magnetita) que as da colocação do granito Old Salobo, reportadas por Tassinari et al. (2003), apontam para uma evolução mais complexa, que poderia inclusive incluir sobreposição de evento hidrotermal no Paleoproterozóico.

No Cinturão Sul do Cobre, a quantidade de dados geocronológicos é menor quando comparada aos depósitos do Cinturão Norte do Cobre (Tabela 1). Datações por métodos mais precisos são restritas ao depósito Alvo 118 (U-Pb SHRIMP em xenotima hidrotermal; Tallarico, 2003), que forneceram idade paleoproterozóica ao minério (ca. 1,87 Ga; Tallarico, 2003). Sistemática Pb-Pb por dissolução total de calcopirita foi aplicada aos depósitos Sossego (corpos Sequeirinho e Sossego), Cristalino e Visconde. Com exceção do Corpo Sossego que forneceu a idade de 1,59 Ga, interpretada por Neves (2006) como sem significado geológico, os dados isotópicos nos demais depósitos compreenderam um intervalo de idades neoarqueanas, variando de 2,74 a 2,70 Ga nos depósitos Cristalino e Visconde (Soares et al., 2001; Silva et al., 2012), e 2,53 Ga no corpo Sequeirinho (Neves, 2006). Essas idades são relativamente imprecisas e associadas a grandes intervalos de erros, mas foram interpretadas como relacionadas ao magmatismo de 2,74 Ga presente na província, a exemplo das intrusões da Suíte Planalto (Soares et al., 2001; Neves, 2006; Silva et al., 2012). A idade do Corpo Sequeirinho foi atribuída à processos de abertura do sistema isotópico em funções de eventos tectono-termais posteriores (Neves, 2006).

6. DEPÓSITOS DE ÓXIDO DE FERRO-COBRE-OURO DO CINTURÃO SUL DO COBRE

Os depósitos IOCG de Cinturão Sul do Cobre (e.g., Sossego, Cristalino, Alvo 118, Bacaba, Castanha, Bacuri, Visconde e Jatobá) concentram-se ao longo de uma faixa de deformação correspondente ao contato da Bacia Carajás com as unidades mesoarquenas do embasamento (Fig. 2), tais como o Granito Serra Dourada (ca. 2,86 Ga; Moreto *et al.*, 2011) e o Tonalito Bacaba (ca. 3,0 Ga; Moreto *et al.*, 2011), entre outras.

Tabela 1. Dados geocronológicos disponíveis na literatura para os depósitos IOCG do Cinturão Sul do Cobre e rochas hospedeiras

Rocha/Mineral	Idade (Ma)	Método	Referência
Sossego			
Corpos Sequeirinho-Pista-Curräl			
Minério			
Anfibólio associado ao minério	2.199 ± 13	Ar-Ar	Marschik <i>et al.</i> , 2003
calcopirita	2.530 ± 25; 2.608 ± 25	Pb-Pb	Neves, 2006
brecha	2.578 ± 29	Sm-Nd, RT	Neves, 2006
Corpos Sossego-Curräl			
Minério			
calcopirita	1.592 ± 45	Pb-Pb	Neves, 2006
Cristalino			
Rochas hospedeiras			
Diorito Cristalino	2.738 ± 6	Pb-Pb, Zr	Huhn <i>et al.</i> , 1999b
Granito Planalto	2.747 ± 2	Pb-Pb, Zr	Huhn <i>et al.</i> , 1999b
Minério			
Calcopirita e pirita	2.700 ± 29* (*MSWD=656)	Pb-Pb	Soares <i>et al.</i> , 2001
Alvo 118			
Rochas hospedeiras			
Dique dacítico	2.645 ± 9	U-Pb, Zr (*)	Tallarico, 2003
Dique riolítico	2.654 ± 9	U-Pb, Zr (*)	Tallarico, 2003
Tonalito Alvo 118	2.743 ± 3	U-Pb, Zr (*)	Tallarico, 2003
Minério			
xenotima	1.868 ± 7, 1.869 ± 7	U-Pb (*)	Tallarico, 2003
Visconde			
Rochas hospedeiras			
Granito Serra Dourada	2.860 ± 22	U-Pb, Zr	Moreto <i>et al.</i> , 2011
Minério			
calcopirita	2.747 ± 140	Pb-Pb	Silva <i>et al.</i> , 2012

Abreviações : (*): SHRIMP; RT: rocha total; Zr: zircão.

6.1 Sossego

A Mina Sossego (Figs. 4 e 5), operada pela VALE, representou o primeiro depósito IOCG a entrar em produção no Brasil, em 2004. É constituído por dois grupos de corpos de minério (Sequerinho-Baiano-Pista e Sossego-Currall) com distintas associações minerais, estilos e intensidade de alteração hidrotermal (Fig. 5), que podem refletir intensidade variável de processos de interação fluido-rocha e distintos níveis crustais (Monteiro *et al.*, 2008a,b). Os corpos Sequeirinho e Baiano são hospedados pelo Granito Sequeirinho e por gabronorito, enquanto que o corpo Pista é hospedado por rocha metavulcânica félítica intercalada a lentes de rocha metaultramáfica. Os corpos Sossego e Currall são hospedados pelo granito granofílico Sossego e pelas mesmas rochas gabróicas hospedeiras do Corpo Sequeirinho.

Nos corpos Sequerinho-Baiano-Pista podem ser reconhecidas zonas de alteração sódica (albita-hematita) e sódica-cálcica (actinolita-albita-titanita-epidoto-alanita) associadas com a formação de corpos maciços de magnetita-(apatita), envelopados por zonas constituídas predominantemente por actinolita (Monteiro *et al.*, 2008a). Zonas de alteração potássica são restritas, mas ocorrem espacialmente relacionadas às brechas mineralizadas, cortando as zonas de alteração sódico-cálcica.

Os corpos Sossego-Currall, entretanto, apresentam evidências de alteração potássica mais intensa, caracterizada pela formação de feldspato potássico e biotita rica em cloro, que substituem minerais do granito granofílico hospedeiro das mineralizações. Alteração clorítica predomina em halos externos e alteração hidrolítica com sericita, hematita e quartzo, típicas de partes bastante rasas de sistemas IOCG, foram reconhecidas apenas nesses corpos.

A mineralização cupro-aurífera no depósito Sossego associa-se a brechas hidrotermais. No Corpo Sequeirinho, tais brechas apresentam predominância de calcopirita na matriz envolvendo fragmentos de actinolítitos/magnetítitos e de cristais de actinolita, apatita e magnetita, comumente também hidrotermalizados (Monteiro *et al.*, 2008a,b). A mineralização de cobre-ouro foi tardia e relacionada a sistemas de falhas de direção NE (Morais e Alkmim, 2005; Domingos, 2009). No Corpo Sossego, as brechas ocorrem associadas a *pipes* verticais com expressão circular em superfície. Apresentam fragmentos da rocha hospedeira hidrotermalizada envolvidos por magnetita e matriz com calcopirita, carbonatos e quartzo com texturas de preenchimento de espaços abertos (Monteiro *et al.*, 2008a,b), que denotam condições rúpteis.

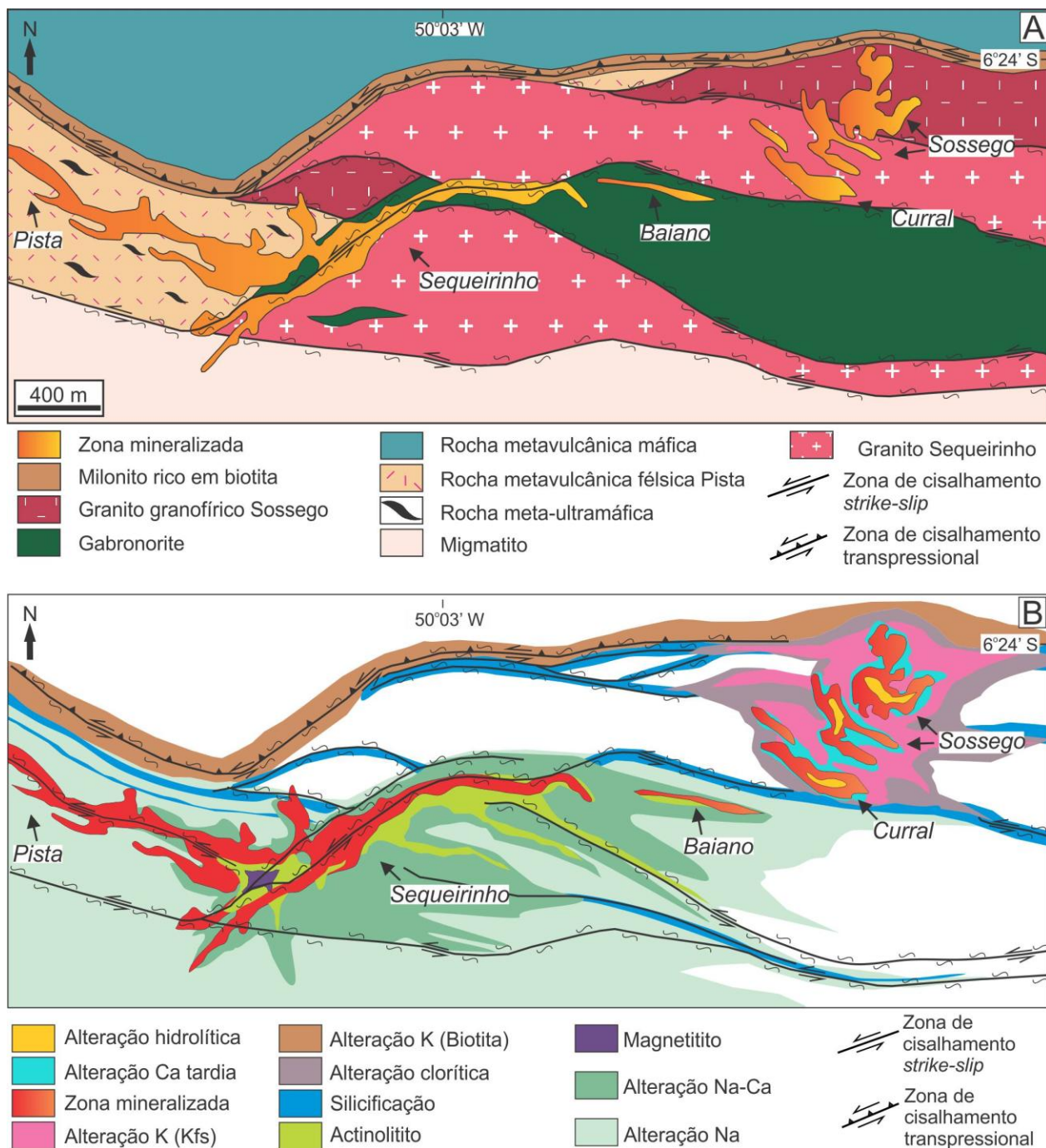


Figura 4. A. Mapa geológico simplificado da área da Mina Sossego (modificado de VALE por Monteiro et al. 2008a); B. Distribuição esquemática das zonas de alteração hidrotermais na Mina Sossego (Monteiro et al. 2008a).

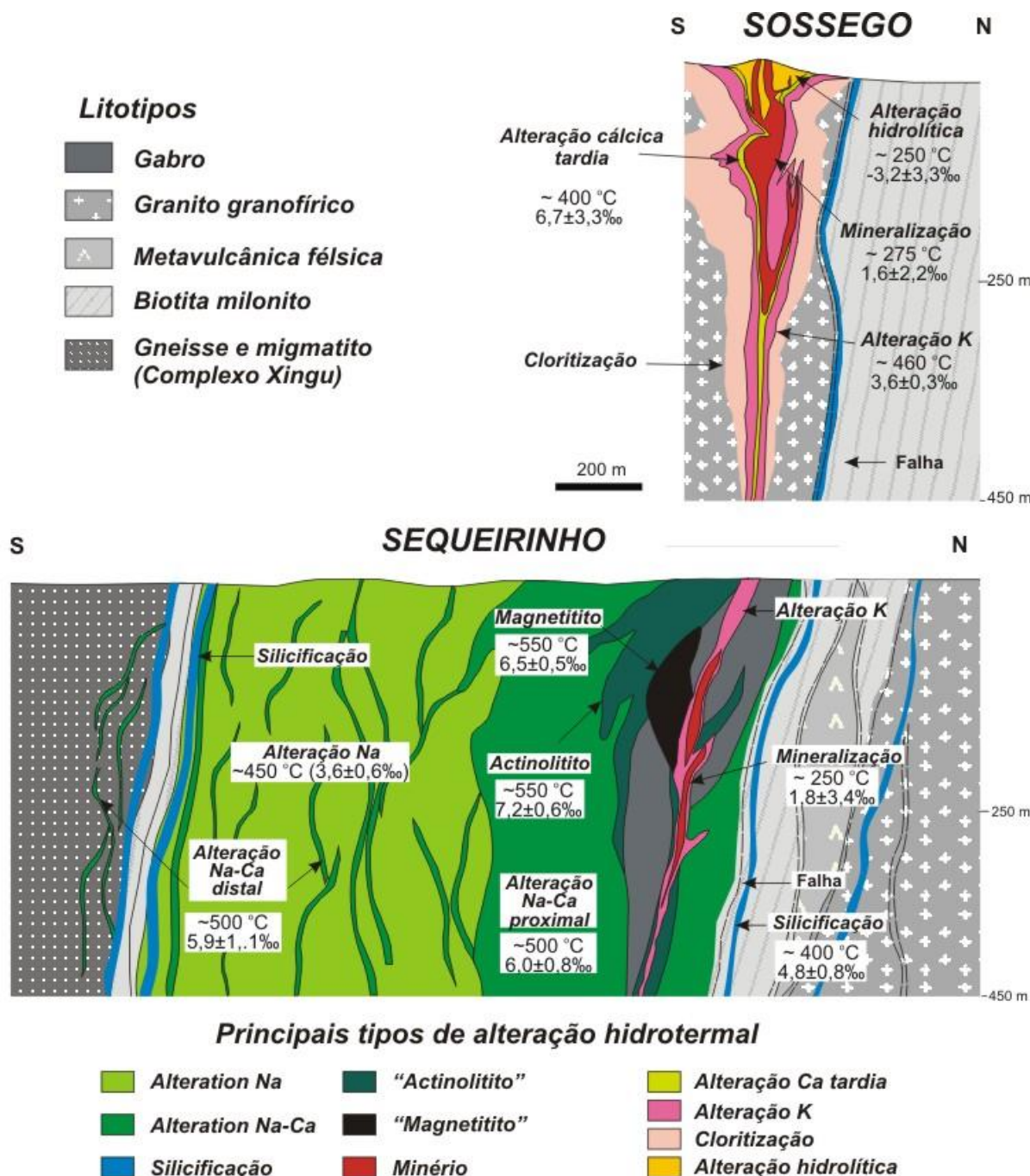


Figura 5. Seção esquemática dos corpos Sequeirinho e Sossego, mostrando a distribuição das zonas de alteração hidrotermais e temperaturas e assinatura isotópica de oxigênio dos fluidos hidrotermais estimadas para cada estágio de alteração (Monteiro et al. 2008a).

A mineralização de cobre-ouro, tanto no Corpo Sequeirinho como no Corpo Sossego, é representada pela associação de calcopirita com pirita, siegenita, millerita, vaesita, ouro, Pd-melonita e, subordinadamente, hessita, cassiterita, esfalerita, galena e molibdenita. Apatita, monazita, epidoto, alanita, actinolita e clorita comumente associam-se aos sulfetos e indicam que

o estágio de mineralização nos diferentes corpos foi associado a menores temperaturas (~ 300 °C) em relação àquelas registradas pelas associações de alteração sódica e sódico-cálcica (~ 550 °C) ou potássica (> 450 °C). Assinatura isotópica de oxigênio do fluido hidrotermal ($\delta^{18}\text{O}_{\text{fluido}} = -1,8 \pm -3,4\text{\%}$) em equilíbrio com fases minerais presentes nas brechas mineralizadas indica introdução de fluidos meteóricos durante o estágio de mineralização, principalmente no Corpo Sossego (Monteiro *et al.*, 2008a).

Episódios de descompressão relacionados com sobrepressão de fluidos podem ter originado as brechas mineralizadas, permitindo o influxo de fluidos meteóricos canalizados em falhas, causando a deposição do minério devido à diluição e resfriamento dos fluidos metalíferos quentes (~ 550 °C) associados aos estágios iniciais de alteração.

O depósito Sossego distingue-se por apresentar zonas mineralizadas e de alteração hidrotermal semelhantes às reconhecidas mundialmente como formadas em níveis crustais distintos, possibilitando a reconstituição vertical do zoneamento em um sistema hidrotermal IOCG. As porções mais profundas, representadas principalmente pelo Corpo Sequeirinho, caracterizam-se pela predominância de alteração sódica e sódico-cálcica. Zonas de alteração potássica, que cortam as áreas de alteração sódico-cálcicas, predominam nos corpos Sossego-Currall, e gradam lateralmente para zonas de cloritização nos níveis crustais mais rasos (Fig. 5).

Composições isotópicas de enxofre de calcopirita ($\delta^{34}\text{S} = 2,2$ a $7,6\text{\%}$) foram obtidas por Monteiro *et al.* (2008a) para os diferentes corpos de minério do depósito Sossego. De modo geral, valores de $\delta^{34}\text{S}$ mais elevados ($\delta^{34}\text{S} = 4,9 \pm 2,4\text{\%}$) que aqueles característicos de enxofre magmático ($\delta^{34}\text{S} = 0 \pm 1\text{\%}$) podem refletir origem do enxofre a partir de reservatórios superficiais com sulfato ou lixiviação de enxofre das rochas hospedeiras (Monteiro *et al.*, 2008a).

6.2 Cristalino

O depósito Cristalino (482 Mt @ 0.65% Cu e 0.06 g/t Au; NCL Brasil, 2005) (Fig. 6) é hospedado por rochas metavulcânicas félsicas, intermediárias e máficas metamorfisadas em fácies xisto verde a anfibolito (Huhn *et al.*, 1999a; Ribeiro, 2008), em formações ferríferas bandadas do Grupo Grão Pará, e em corpos intrusivos da Suíte Planalto e do Diorito Cristalino (Huhn *et al.*, 1999b). Os estágios de alteração hidrotermal reconhecidos no depósito incluem silicificação sincrônica à milonitzação, seguida por alteração sódica (albita e escapolita) e potássica (biotita e microclínio). Assim como no depósito Sossego, a alteração hidrotermal

proximal aos corpos de minério é representada pela formação de anfibólio (hastingsita, actinolita e grunerita) e magnetita. Posteriormente, houve a superposição de intensa alteração clorítica com epidoto, apatita, alanita e turmalina, contemporânea ao estágio de mineralização (Huhn *et al.*, 1999a).

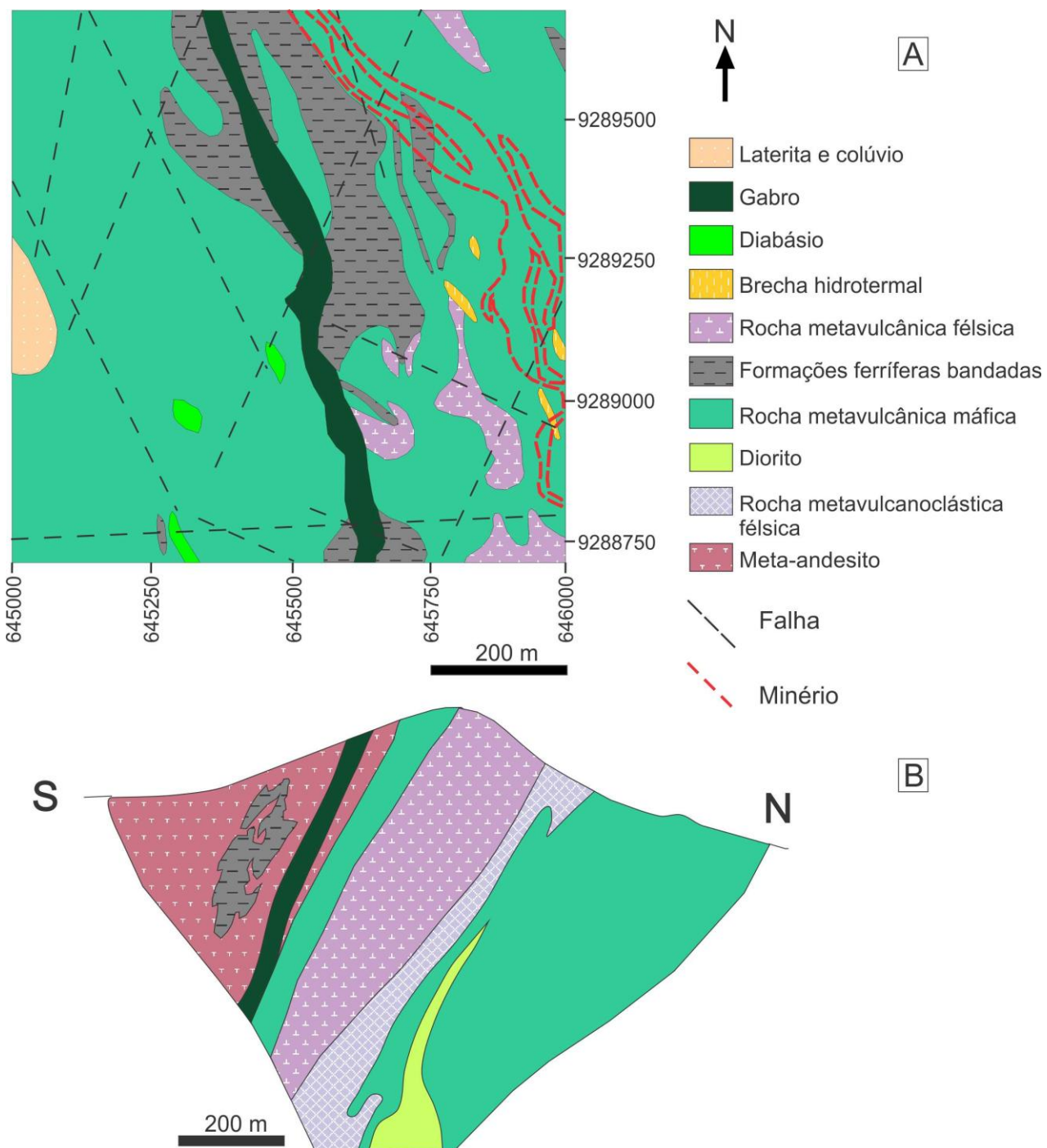


Figura 6. A. Mapa geológico do depósito Cristalino. B. Seção geológica simplificada do depósito Cristalino (VALE).

O minério de cobre–ouro associa-se a brechas quartzo–carbonáticas, veios, *stockworks* e, mais subordinadamente, disseminações nas rochas hospedeiras. Consiste em calcopirita, pirita, magnetita, marcassita, bravoita, cobaltita, millerita, vaesita e ouro, com quantidades subordinadas de hematita, bornita, covellita, calcocita, molibdenita e esfalerita (Huhn *et al.*, 1999a).

Valores de $\delta^{34}\text{S}_{(\text{CDT})}$ entre 0,6 a 1,5‰, obtidos por Ribeiro (2008), foram interpretados como próximos aos do enxofre do manto e ao do campo dos MORB. Dados de $\delta^{13}\text{C}_{(\text{PDB})}$ (-7,2 a -4,4‰) e de $\delta^{18}\text{O}_{(\text{SMOW})}$ (+8,1 a +9,3‰) em carbonatos foram interpretados como similares às razões isotópicas de carbonatitos primários (Ribeiro, 2008).

6.3 Alvo 118

O depósito Alvo 118 (170 Mt @ 1.0 wt% Cu, 0,3 g/t Au; Rigon *et al.*, 2000) (Figs. 7 e 8) é hospedado por rocha metavulcânica máfica e félscica, gábro e tonalito (2.743 ± 3 Ma; Pb-Pb SHRIMP II em zircão; Tallarico, 2003), que são truncados por diques porfiríticos de composição dacítica e riolítica (2.645 ± 9 Ma e 2.654 ± 9 Ma, Pb-Pb SHRIMP II em zircão; Tallarico, 2003). Com exceção dos diques tardios, os demais litotipos apresentam, das zonas distais em direção às zonas mineralizadas, alteração sódica inicial (albita e escapolita), seguida por alteração potássica com biotita ou feldspato potássico acompanhada pela formação de magnetita, cloritização associada à mineralização de Cu-Au, silicificação, carbonatização e epidotização em menor proporção (Fig. 8; Torresi *et al.*, 2012).

Deformação rúptil atuou durante a formação do minério resultando em corpos brechados e zona de *stockwork* com textura de preenchimento de espaço abertos. Estes são compostos por quartzo, calcita, fluorita, apatita, alanita e fosfatos de ítrio. Os minerais de minério são representados por calcopirita, bornita, hematita e magnetita além de pequenas quantidades de ouro nativo, calcocita, galena, esfalerita, cassiterita e minerais com Bi-Te-Au-Ag (Torresi *et al.*, 2012). A assinatura geoquímica do minério é caracterizada por enriquecimento em Fe-Cu-Au-(Te-Ag-Pb-Sn)-P-F-ETR e difere do depósito de Sossego pela ausência de fases minerais com Co-Ni-Pd e presença de F (Bortholoto, 2007; Xavier *et al.*, 2008b).

Ao contrário dos demais depósitos IOCG de Carajás, o depósito Alvo 118 possui enriquecimento em ETRP, concentrados em apatita e silicatos de Be-B-ETRP pobres em Al do grupo da gadolinita, não descritos em sistemas IOCG de outras partes do mundo (Xavier *et al.*, 2008b).

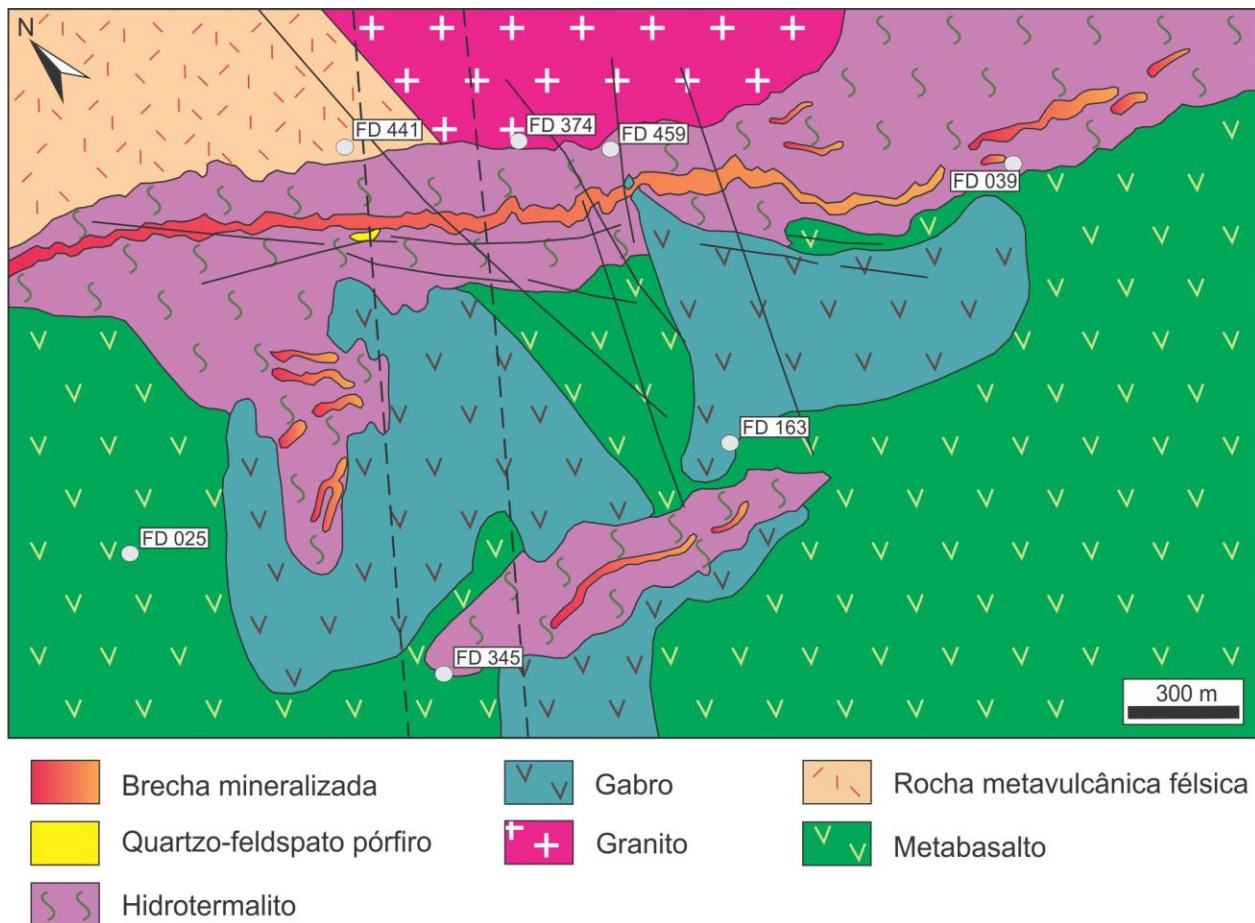


Figura 7: Mapa geológico simplificado do depósito Alvo 118 (VALE).

Inclusões aquosas bifásicas associadas a menos de 10% de inclusões fluidas são predominantes em quartzo e calcita da matriz da brecha e veios mineralizados (Torresi *et al.*, 2012). A ampla variação dos valores de $\delta^{18}\text{O}$ do fluido (13,7 a 2,1‰; a 350 °C) estimados a partir de calcita (ganga) sugerem o envolvimento de fluidos enriquecidos em ^{18}O , com possível contribuição magmática, porém modificados devido às interações com as rochas encaixantes, além de importante componente meteórico pouco modificado. Assinatura isotópica de enxofre ($\delta^{34}\text{S}_{\text{CP}} = 5,1$ a 6,3‰) indica fontes de enxofre isotopicamente mais pesado que o esperado para fontes magmáticas ou mantélicas, sugerindo origem a partir de reservatórios superficiais (Torresi *et al.*, 2012).

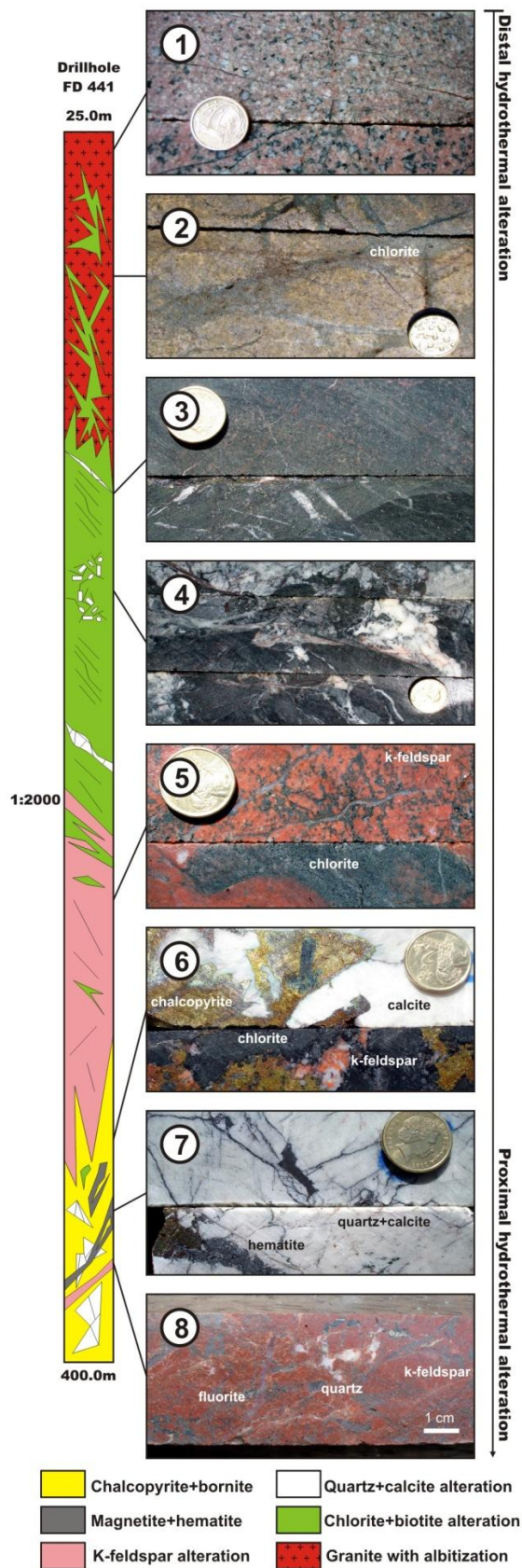


Figura 8. Principais estágios de alteração hidrotermal no depósito Alvo 118: (1) Alteração sódica (albita) em granito; (2) Cloritização fissural em granito albitizado; (3) Alteração potássica (biotita) e cloritização. Veios com quartzo e calcita posteriores; (4) Alteração potássica (biotita) e cloritização (brechada) com matriz preenchida por quartzo, calcita e apatita; (5) Cloritização superposta por alteração potássica com feldspato potássico; (6) Brecha mineralizada com calcopirita e bornita; (7) Brecha com matriz preenchida por calcita e quartzo, cortada por veios de hematita; (8) Brecha com matriz preenchida por feldspato potássico, cortada por veios de fluorita. (Torresi et al., 2012)

6.4 Bacaba

O depósito Bacaba, situado a 10 km a leste da Mina Sossego, é hospedado por rochas gabróicas e graníticas variavelmente hidrotermalizadas (Figs. 9 e 10), que incluem o Granito Serra Dourada com idade em 2.860 ± 22 Ma (U–Pb LA–ICPMS em zircão; Moreto *et al.*, 2011) e o Tonalito Bacaba com idade ao redor de 3,0 Ga ($3.001,2 \pm 3,6$ Ma; $2.990,9 \pm 5,8$ Ma e $3.004,6 \pm 9$ Ma; U–Pb LA–ICP–MS em zircão; Moreto *et al.*, 2011). Diferentemente da maioria dos depósitos IOCG de Carajás, a clara associação espacial desse depósito com rochas graníticas, permitiu averiguar que suas rochas hospedeiras félscicas (Granito Serra Dourada e Tonalito Bacaba) não foram responsáveis pelo estabelecimento do sistema magnético–hidrotermal associado com a gênese do depósito (Moreto, 2010; Moreto *et al.*, 2011).

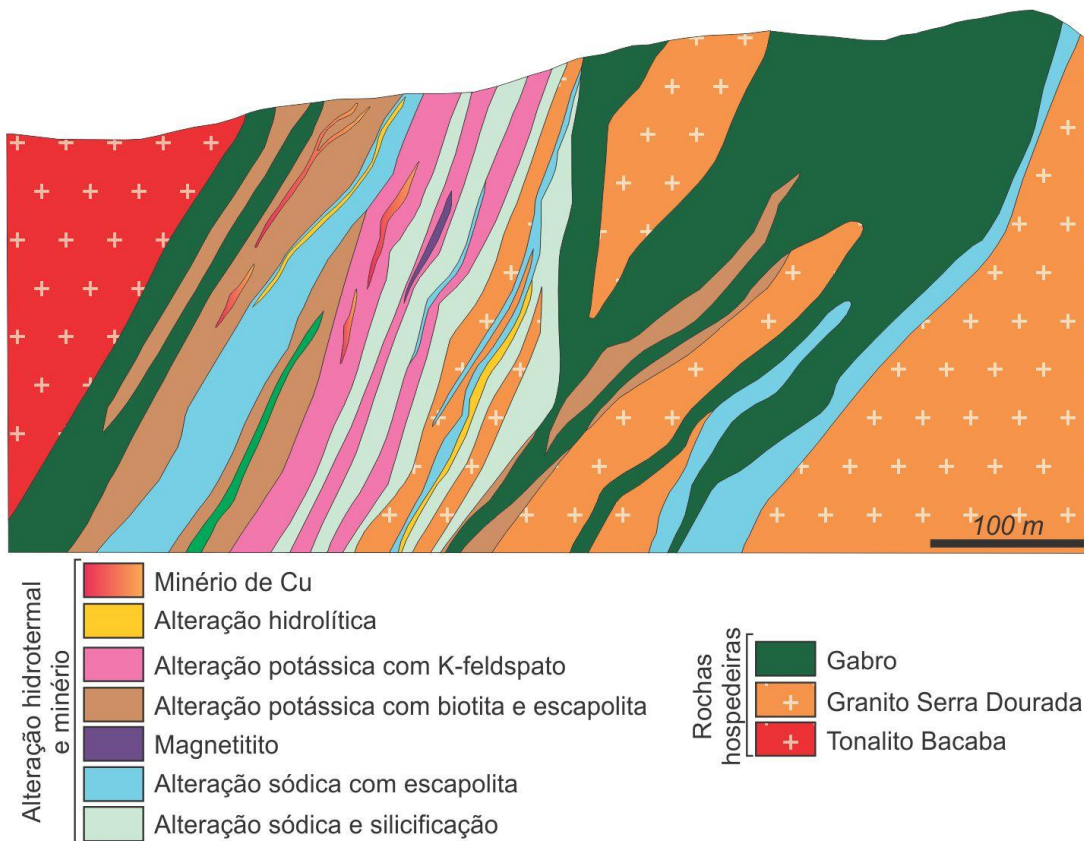


Figura 9. Seção esquemática mostrando as rochas hospedeiras do depósito Bacaba e a distribuição das zonas de alteração hidrotermal (Moreto *et al.*, 2011 modificado de Augusto *et al.*, 2008).

A sequência de alteração hidrotermal (Fig. 10) presente tanto nas rochas félscicas quanto no gabbro inicia-se por alteração sódica, representada por albitização (albita e hematita) e por intensa escapolitização (escapolita marialítica, magnetita, quartzo e fluorita), seguida por alteração potássica (feldspato potássico, biotita, turmalina, potássio-cloro hastingsita) e formação

de magnetita, cloritização/epidotização, mineralização cuprífera e sericitização tardia (Augusto *et al.*, 2008). A evolução paragenética do depósito Bacaba é semelhante à descrita para o depósito de Sossego, principalmente no Corpo Sequeirinho (Monteiro *et al.*, 2008a,b), sendo a principal diferença representada pela predominância de escapolita marialítica no depósito Bacaba, que ocorre em veios e extensas zonas de substituição.

O principal mineral de minério é calcopirita que ocorre associada com bornita e calcocita e, subordinadamente, galena, teluretos (melonita, hessita, altaita) e óxidos (magnetita, hematita, uraninita, cassiterita). A assinatura geoquímica do minério é caracterizada por enriquecimento em Cu-Fe-Ni-Co-Te-Ag-Pb-U-Sn, além de significativos conteúdos de ETR, Th e P evidenciados pela ocorrência de minerais de ganga (alanita, apatita, monazita, cheralita; Augusto *et al.*, 2008).

Augusto *et al.* (2008) e Monteiro *et al.* (2008a,b) consideram que o depósito Bacaba e o depósito Sossego representariam porções diferentes de mesmo sistema hidrotermal. A comparação das características desses depósitos com o modelo teórico proposto por Hitzman *et al.* (1992) sugere que o depósito Bacaba, notadamente pela escapolitização mais intensa, teria sido formado em zonas mais profundas e distais em relação ao depósito de Sossego. Essas zonas de escapolitização estariam relacionadas com o fluxo de fluidos metalíferos hipersalinos, que poderiam representar um halo distal ao redor dos corpos maiores de minério, reconhecidos no depósito Sossego. Neste contexto, as zonas de maior concentração de minério estariam associadas a falhas que teriam permitido a entrada de fluidos mais frios e de baixa salinidade (e.g., meteóricos) em maior escala, aumentando a eficiência da deposição do minério.

Entretanto, a escassez de dados geocronológicos robustos limita uma compreensão mais detalhada desses sistemas, assim como a avaliação dessa possível cogeneticidade. Alternativamente, cada um desses depósitos poderiam representar sistemas hidrotermais distintos, porém com uma história evolutiva similar. Neste caso, a recorrência de sistemas hidrotermais ao longo da mesma área seria responsável pela configuração atual desses depósitos IOCG.

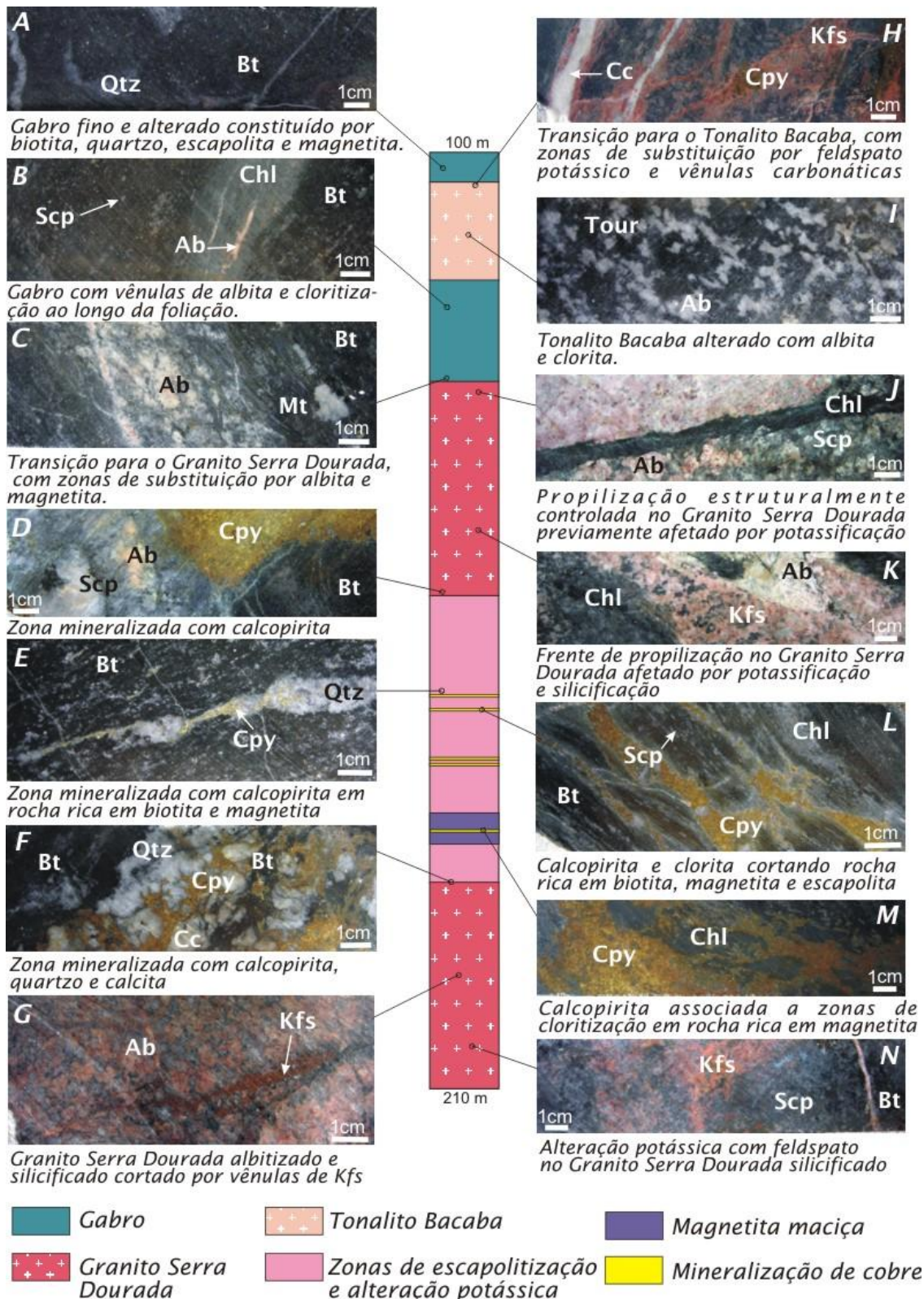


Figura 10. Principais feições das rochas hospedeiras alteradas e mineralizadas do depósito Bacaba (Furo de sondagem BACD 15). Abreviações: Ab: albita; Act: actinolita; Bt: biotita; Chl: clorita; Cpy: calcopirita; Ep: epidoto; Kfs: feldspato potássico; Mt: magnetita; Ser: sericita; Tour: turmalina.

6.5 Castanha

O depósito Castanha (Fig. 11), situado à 9 km a NE do depósito Sossego, é hospedado por rocha subvulcânica félscica, denominada de quartzo-feldspato pórfiro Castanha (Pestilho, 2011) e por corpos de gábro. A sucessão dos estágios de alteração hidrotermal compreende albitização, escapolitização, alteração sódica-cálcica (com predominância de actinolita), formação de óxidos de ferro, alteração potássica, formação de turmalina, sericitização, cloritização, epidotização e carbonatização.

O estágio de mineralização, considerado tardio em relação à evolução do sistema hidrotermal, é associado ao estágio de carbonatização. O minério ocorre na forma de veios, zonas de *stockwork* e brechas hidrotermais, sendo constituído por calcopirita, pirrotita, magnetita, pentlandita, esfalerita, molibdenita e marcassita (Pestilho, 2011). A assinatura geoquímica do minério é caracterizada por enriquecimento de Cu-Fe-Zn-Ni-(Co-Pb-Mo-Pd) associada à ETR, U e P.

Dados petrográficos e microtermométricos de Pestilho (2008) possibilitaram a caracterização de um fluido inicial hipersalino (13,9 a >39,4% peso eq. NaCl) que teria transportado os metais em complexos cloretados. Outro fluido mais tardio, relativamente menos salino (13,9 a 24% peso eq. NaCl) e distinto de fluidos meteóricos também foi identificado. Os prováveis mecanismos de deposição do minério de cobre, sob condições relativamente redutoras, teriam sido resultado de múltiplos processos, tais como, redução do sulfato contido no fluido, aumento do pH devido à formação dos carbonatos e diminuição da salinidade concomitante à redução da temperatura (Pestilho, 2008).

De acordo com Pestilho (2011), a precipitação do minério teria ocorrido em temperatura entre 350 °C e 420 °C. As composições isotópicas de oxigênio dos fluidos em equilíbrio com calcita ($\delta^{18}\text{O}_{\text{fluido}} = 4,6$ a 7,3‰ SMOW), quartzo ($\delta^{18}\text{O}_{\text{fluido}} = 5,8\text{\textperthousand}$ SMOW) e biotita ($\delta^{18}\text{O}_{\text{fluido}} = 6,6\text{\textperthousand}$ SMOW) dos veios mineralizados do depósito Castanha indicam a predominância de fonte magmáticas, inclusive durante o estágio de mineralização.

Os valores de $\delta^{34}\text{S}$ em sulfetos (1,8 a 3,0‰) (Pestilho, 2011) são próximos aos esperados para enxofre magmático ou de origem mantélica ($\delta^{34}\text{S} = 0 \pm 1\text{\textperthousand}$), de modo análogo ao verificado em relação ao Corpo Pista, do depósito Sossego. Assim como no corpo Pista, a presença de pirrotita indica que o fluido mineralizante esteve no campo de estabilidade do H₂S. Dessa forma, as razões isotópicas de enxofre refletem os valores de $^{34}\text{S}_{\Sigma\text{S}}$ e, portanto, a fonte do enxofre, que

poderia ter sido relacionada a fluidos derivados do magma ou da lixiviação das rochas ígneas, incluindo o Pórfiro Castanha.

6.6 Bacuri

O depósito Bacuri (Fig. 12) localiza-se cerca de 16 km a NE da Mina Sossego. Estudos realizados por Melo *et al.* (Submetido) sugerem que o depósito Bacuri também apresenta características semelhantes a de outros depósitos IOCG caracterizados mundialmente (Williams *et al.*, 2005; Hitzman, 2000), tais como: (i) minério de cobre associado a óxido de ferro (magnetita); (ii) enriquecimento em ETR, presentes na apatita, monazita e alanita; (ii) intensa alteração hidrotermal sódica, incluindo albitização e escapolitização, potássica e clorítica; (iii) forte controle estrutural.

A zona central do depósito é caracterizada pela presença de clorita milonitos (clorititos) que são produtos de intensa deformação e alteração hidrotermal da principal rocha hospedeira do depósito Bacuri, o Pórfiro dacítico Bacuri, intrusivo em rochas maficas, e no Granito Serra Dourada (Fig. 12).

O depósito Bacuri apresenta evidências de albitização inicial e incipiente, seguida por intensa escapolitização e alteração potássica com biotita, concomitante ao desenvolvimento de foliação milonítica, resultando em escapolita-biotita milonitos. Esses estágios de alteração foram seguidos por alteração potássica por feldspato potássico e formação de magnetita, cloritização, mineralização cuprífera, representada pela calcopirita, além de sericitização tardia (Melo *et al.*, Submetido).

O minério de cobre, constituído predominantemente por calcopirita, é disseminado, associado com intensa cloritização e intensa alteração potássica com feldspato potássico. Também pode ser venular, confinado em vênulas com feldspato potássico, e filoniano, associado a veios de quartzo com grandes concentrações de calcopirita.

A evolução caracterizada por Melo *et al.* (Submetido) no depósito Bacuri evidencia: (i) circulação de fluidos hipersalinos e quentes, que teriam transportado metais como complexos cloretados, em escala regional ao longo de falhas; (ii) intensa interação fluido-rocha resultando em litotipos fortemente modificados (clorititos); (iii) mecanismos de deposição do minério a partir da redução de sulfato presente no fluido, associado possivelmente com diluição e

decréscimo de temperatura do fluido mineralizante; (iv) possível evolução do sistema hidrotermal associada com a exumação progressiva do sistema.

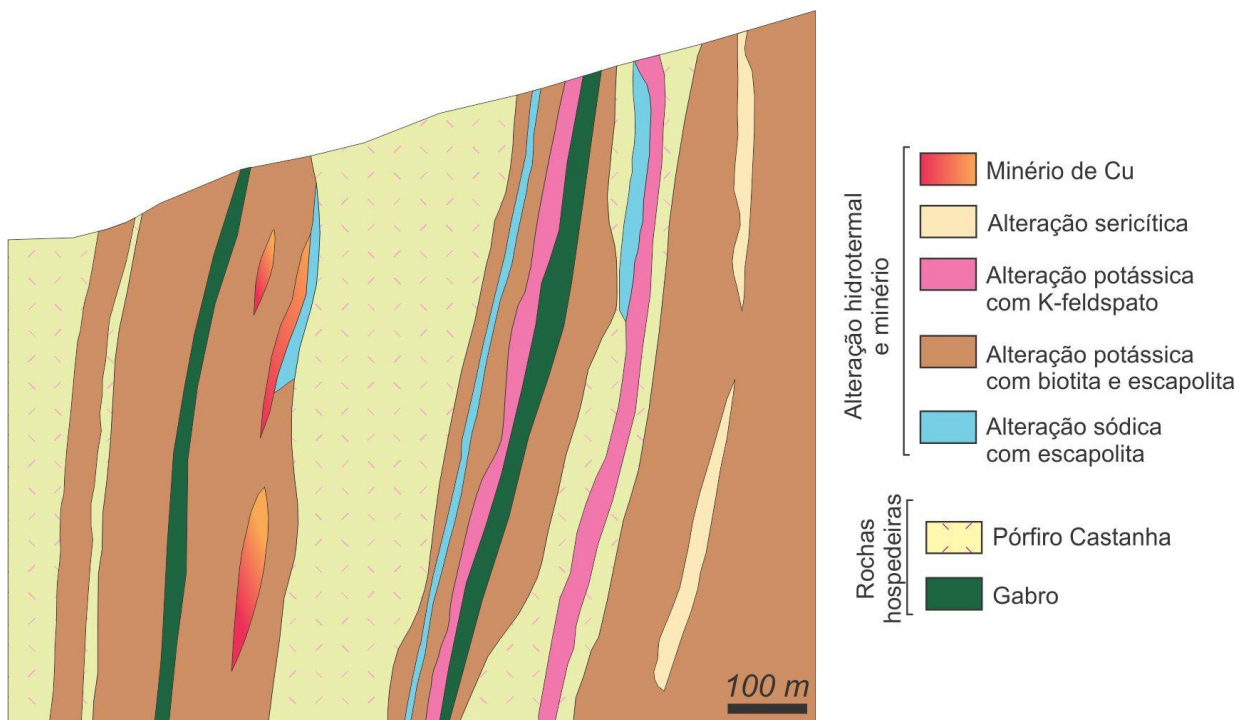


Figura 11. Seção geológica do depósito Castanha, mostrando as principais rochas hospedeiras e zona mineralizada (modificado de VALE).

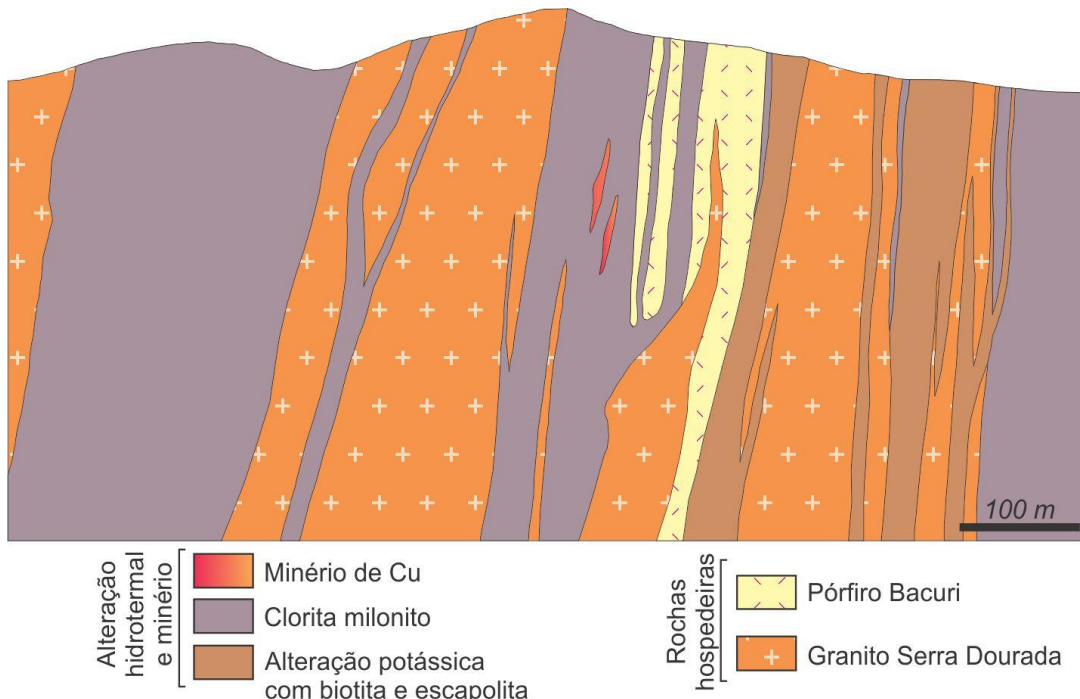


Figura 12. Seção geológica simplificada do depósito Bacuri (modificado de VALE).

6.7 Visconde

O depósito Visconde situa-se a aproximadamente 14 km a leste do deposito Sossego, e a sul dos depósitos Bacaba, Castanha e Bacuri. É hospedado pelo Granito Serra Dourada, que também hospeda os depósitos Bacaba e Bacuri, por quartzo pôrfiro, rochas vulcânicas, intrusivas maficas e rochas metaultramáficas (Craveiro *et al.*, 2012a).

Segundo Craveiro *et al.* (2012a), sob condições dúctil-rúpteis a rúpteis a evolução do sistema hidrotermal foi responsável por alteração sódica inicial, sódica-cálcica (albita-escapolita-anfibólio-turmalina), seguida por alteração potássica (feldspato potássico e biotita rica em cloro), retomando, em seguida, novamente o caráter sódico-cálcico (albita, epidoto, apatita e fluorita) para posteriormente assumir característica cálcio-magnesiana (clinocloro, actinolita, carbonatos e talco).

Os corpos de minério são representados por veios e brechas constituídos por calcopirita-bornita, além de disseminações de calcopirita + pirita \pm molibdenita \pm pentlandita. Os sulfetos teriam sido precipitados na transição da alteração potássica para a cálcio-magnesiana, tendo apatita, actinolita, epidoto, calcita, gipsita e fluorita como principais minerais de ganga. A assinatura geoquímica do minério denota enriquecimento em Cu-Fe-ETR-Ni-Co-Mo-Ca-P-Mg-Nb-Tb-Y-Zn-Se-Au (Craveiro *et al.*, 2012a).

Dados microtermométricos (Craveiro *et al.*, 2012b) apontam para três fluidos aquosos distintos: 1) fluido inicial, hipersalino (25-58% eq. peso de NaCl), com temperaturas de homogeneização variadas, incluindo as mais elevadas observadas ($Th = 480\text{-}160^\circ\text{C}$). Esse fluido estaria associado aos estágios de alteração sódico-cálcica e potássica; 2) fluido com menor salinidade (8-30% eq. em peso de NaCl) e temperaturas ($Th = 350\text{-}160^\circ\text{C}$); 3) fluido não saturado (6-19% eq. em peso de NaCl) e com $Th < 300^\circ\text{C}$. Os fluidos 2 e 3 teriam sido aprisionados em inclusões tardias, posteriores ao evento de mineralização.

Os complexos de Cu, Fe, Au e ETR teriam sido transportados pelo fluido hipersalino que, ao longo do processo hidrotermal, incorporou espécies de S. Em torno de 350°C , a mistura do fluido 1 (quente e metalífero) com fontes superficiais, ao longo de zonas de cisalhamento meso a neoarqueanas, teria resultado em diluição e subsequente precipitação de sulfetos (Craveiro *et al.*, 2012b).

7. SÍNTESE DOS ARTIGOS

São apresentados, nessa tese de doutorado, dois artigos científicos a serem submetidos, logo após o exame de defesa, a periódicos internacionais indexados a serem definidos. Uma síntese de cada artigo é apresentada a seguir.

7.1. Artigo I “*Paleoproterozoic overprint on Archean iron oxide-copper-gold system at the Sossego deposit, Carajás Province: Re-Os and U-Pb geochronological evidence*”

Esse primeiro artigo (Anexo 1) tem como foco uma caracterização mais detalhada das rochas hospedeiras do depósito Sossego (corpos Sequeirinho-Baiano-Pista e Sossego-Currall) previamente reportadas por Monteiro *et al.* (2008a) e Carvalho (2009). Para tanto, foram enfatizados estudos geocronológicos (U-Pb SHRIMP IIe e LA-ICPMS em zircão) com a finalidade de determinar as idades de cristalização das rochas hospedeiras do Sossego. Adicionalmente objetivou-se compreender a (s) idade (s) de formação dos distintos corpos de minério. Priorizou-se a datação de fases minerais hidrotermais formadas durante os estágios de alteração hidrotermal e mineralização, tais como monazita e molibdenita. Os métodos isotópicos U-Pb LA-MC-ICPMS e Re-Os NTIMS foram empregados, fornecendo resultados muito confiáveis.

Os resultados geocronológicos apresentados nesse artigo estão resumidos na Tabela 2. Como pode ser observado, as rochas hospedeiras do depósito Sossego possuem idades que variam do Measoarqueano (ca. 3,0 Ga, Granito Sequeirinho; 2,97 Ga, Metavulcânica félsica Pista) ao Neoarqueano (2,74 Ga, granito granofírico Sossego e gabronorito). O Granito Sequeirinho corresponde à uma das unidades geológicas mais antigas já caracterizadas na Província Carajás. O magmatismo em 2,74 Ga tem uma característica marcante bimodal. A rocha metavulcânica Pista, que ocorre intercalada à lentes de rochas metaultramáficas, assemelha-se à porções dos *greenstone belts* do Domínio Rio Maria, com idades entre 3,0-2,97 Ga (e.g., Gradaús e Lagoa Seca; Macambira e Lancelot, 1996; Pimentel e Machado, 1994; Tassinari *et al.*, 2005). Tais similaridades poderiam sugerir que a rochas hospedeira do corpo Pista representariam lascas alóctones desses *greenstone belts*.

Tabela 2. Síntese dos dados geocronológicos para os corpos Sequeirinho, Pista, Sossego e Curral.

Rocha	Mineral	Método	Idade (Ma)	MSWD
Corpo Sequeirinho				
Rochas hospedeiras				
Granito Sequeirinho (SOS 259/177,4)	zircão	U-Pb LA-ICPMS	3.010 ± 21	0,81
Granito Sequeirinho (SOS 22/107,45)	zircão	U-Pb LA-ICPMS	3.014 ± 22	2,5
Granito Sequeirinho (SOS 450/13)	zircão	U-Pb SHRIMP IIe	$2.989 \pm 5,2$	3,5
gabronorito (SOS 35)	zircão	U-Pb SHRIMP IIe	$2.739 \pm 5,9$	1,4
Minério				
Brecha (SOS 39J)	zircão	U-Pb SHRIMP IIe	$3.076 \pm 5,3$	1,5
Brecha (SOS 259/270)	monazita	U-Pb LA-MC-ICPMS	$2.712,3 \pm 4,7$	1,6
Corpo Pista				
Rochas hospedeiras				
Rocha metavulcânica Pista (SOS 364/138,35)	zircão	U-Pb SHRIMP IIe	2.968 ± 15	10,7
Rocha metavulcânica Pista (SOS 475/167)	zircão	U-Pb SHRIMP IIe	$2.979 \pm 5,3$	0,28
Minério				
Rocha metavulcânica Pista silicificada (SOS 364/76,84)	molibdenita	Re-Os NTIMS	2.685 ± 11	
Rocha metavulcânica Pista albitizada (SOS 364/160,9)	molibdenita	Re-Os NTIMS	2.710 ± 11	
Corpo Sossego				
Rochas hospedeiras				
granito granofírico Sossego (SOS 35/406,88)	zircão	U-Pb LA-ICPMS	2.740 ± 26	11,4
Minério				
Brecha (Min-Cp-SOS)	monazita	U-Pb LA-MC-ICPMS	$1.878,9 \pm 4,1$	1,3
Brecha (SOS 315/255,1)	monazita	U-Pb LA-MC-ICPMS	$1.904 \pm 5,2$	1,2
Corpo Curral				
Rochas hospedeiras				
gabro (SOS 35/30)	zircão	U-Pb SHRIMP IIe	$2.739,1 \pm 4,2$	2,1
Minério				
Brecha (SOS 106/84)	monazita	U-Pb LA-MC-ICPMS	$1.889,8 \pm 8,5$	2,7

Em relação aos eventos responsáveis pela gênese do depósito Sossego, os dados isotópicos sugerem que os grupos de corpos de minério Sequeirinho-Pista-Baiano e Sossego-Curral não são cogenéticos, mas sim foram formados com um intervalo de tempo de aproximadamente 820 Ma. A gênese dos corpos Sequeirinho-Pista-Baiano teria ocorrido durante o intervalo 2,71-2,68 Ga, enquanto Sossego-Curral teriam se formado durante o Paleoproterozóico (1,90-1,88 Ga) após exumação progressiva dos sistemas arqueanos. Tais resultados apontam para recorrência de eventos hidrotermais no depósito Sossego, que possivelmente teriam lixiviado e remobilizado metais e elementos dos depósitos Neorqueanos e

reconcentrados nos corpos Paleoproterozócos, que possuem menor tonelagem e maior teor de Cu e Au.

7.2. Artigo II “*Timing of multiple Iron oxide Cu-Au systems in the Southern Copper Belt, Carajás Province, Brazil: U-Pb zircon and monazite and Re-Os molybdenite geochronology*”

O segundo artigo (Anexo 2) tem como principais enfoques a: (1) caracterização geológica da porção centro-oeste do Cinturão Sul do Cobre, no entorno dos depósitos Bacaba, Castanha, Bacuri e Visconde; (2) obtenção das idades de cristalização das rochas intrusivas félsicas presentes nessa área (método U-Pb SHRIMP IIe); (3) determinação da (s) idade (s) do (s) evento (s) responsáveis pela gênese do minério nos depósitos Bacaba e Bacuri, a partir da datação de monazita hidrotermal e molibdenita; e (4) integração dos dados obtidos nesse estudo com àqueles obtidos para o depósito Sossego (Artigo 1; Anexo 1), além de outros disponíveis na literatura, com a finalidade de caracterizar a evolução metalogenética do Cinturão Sul do Cobre.

Os dados geocronológicos apresentados no segundo artigo estão resumidos na Tabela 3. De maneira similar ao observado no depósito Sossego, mais de um sistema hidrotermal está associado à gênese dos depósitos Bacaba e Bacuri. Nesse último, um estágio de alteração inicial foi responsável pela precipitação de molibdenita em 2,76 Ga, evento que precede o principal estágio de mineralização no Bacuri, também datado em ca. 2,70 Ga. No depósito Bacaba o estágio inicial de alteração sódica teria ocorrido ao redor de 2,71 Ga, enquanto que o evento mineralizante IOCG seria pouco mais jovem (2,68 Ga). Esse intervalo entre 2,71-2,68 Ga é similar ao intervalo de idades de alteração hidrotermal e formação dos corpos Sequeirinho e Pista, depósito Sossego (Artigo 1; Anexo 1), e próximo às idades Pb-Pb (calcopirita) obtidas para os depósitos Cristalino e Visconde (Soares *et al.*, 2001; Silva *et al.*, 2012). Apesar dos erros elevados associados às idades Pb-Pb, esse conjunto de dados geocronológicos aponta para um importante intervalo neoarqueano (2,71-2,68 Ga) de mineralização no Cinturão Sul do Cobre.

Adicionalmente, a formação de cristais hidrotermais de monazita no Paleoproterozóico (2,05 Ga) no depósito Bacaba evidencia um episódio de alteração hidrotermal tardio. Entretanto, a idade riaciana desse novo evento de metassomatismo difere das idades do evento mineralizante Orosiriano (1,90-1,88 Ga) bem definido nos corpos Sossego e Curral (Artigo 1; Anexo 1) e Alvo 118 (Tallarico, 2003).

Tabela 3. Síntese dos dados geocronológicos obtidos para as rochas do Cinturão Sul do Cobre e depósitos Bacuri e Bacaba.

Rocha	Mineral	Método	Idade (Ma)	MSWD
Rochas hospedeiras e regionais				
Quartzo-feldspato pôrfiro (GMCL 54A)	zircão	U-Pb SHRIMP IIe	$2.740,9 \pm 4,7$	1,08
Quartzo-feldspato pôrfiro Castanha (CASF 02/424,90)	zircão	U-Pb SHRIMP IIe	$2.744,8 \pm 4$	0,18
Granito Serra Dourada (GMCL 40A)	zircão	U-Pb SHRIMP IIe	$2.848 \pm 5,5$	1,5
Tonalito Campina Verde (GMCL 01)	zircão	U-Pb SHRIMP IIe	$2.876 \pm 6,8$	5,6
Tonalito Campina Verde (GMCL 66)	zircão	U-Pb SHRIMP IIe	$2.876 \pm 5,2$	6,9
Depósito Bacuri				
Rocha com alteração potássica (biotita) e clorítica (BRID 07/115,42)	monazita	U-Pb LA-MC-ICPMS	$2.703,0 \pm 5,8$	3,9
Minério hospedado pelo Granito Serra Dourada (BRID 01/45)	molibdenita	Re-Os NTIMS	2.758 ± 11	-
Depósito Bacaba				
Minério hospedado pelo Tonalito Bacaba (BACD 25/229,25)	monazita	U-Pb LA-MC-ICPMS	2.681 ± 11	3
			$2.054,1 \pm 8,8$	10,2
Granito Serra Dourada albitizado e silicificado (BACD 15/237,4)	monazita	U-Pb LA-MC-ICPMS	$2.716,4 \pm 8,4$	2,4

ANEXOS

Anexo 01

Artigo:

***Paleoproterozoic overprint on Archean iron oxide -copper-gold system
at the Sossego deposit, Carajás Province: Re-Os and U-Pb
geochronological evidence***

Carolina P. N. Moreto et al.

Abstract

The Sossego iron oxide–copper–gold (IOCG) deposit is situated within a WNW–ESE shear zone in the Southern Copper Belt of the Carajás Province, Brazil. The Sossego deposit consists of two major groups of orebodies (Pista–Sequeirinho–Baiano and Sossego–Curral) with distinct hydrothermal alteration assemblages, styles and intensity. U–Pb (SHRIMP IIe and LA–ICPMS) geochronology of the host rocks reveal ages that vary from Mesoarchean (ca. 3.0 Ga Sequeirinho Granite and 2.97 Ga Pista felsic metavolcanic rock) to Neoarchean (ca. 2.74 Ga Sossego granophyric granite and gabbronorite). Dating of hydrothermal monazite (U-Pb LA-MC-ICPMS) and molybdenite (Re-Os NTIMS) from the Sequeirinho and Pista orebodies rendered ages of ca. 2.71 to 2.68 Ga, whilst hydrothermal monazite from the Sossego and Curral orebodies yielded the ages of ca. 1.90 to 1.88 Ga. These data suggest a complex evolutional history for the Sossego deposit, in which multiple mineralizing events were responsible for IOCG ore genesis. The Sequeirinho-Pista-Baiano orebodies, characterized by scapolite-, magnetite-(apatite), actinolite-rich zones, represent deep-emplaced bodies formed at 2.71-2.68 Ga. The shallow-emplaced Sossego-Curral orebodies, with predominant potassic and chlorite alteration, were developed at 1.90-1.88 Ga, after progressive exhumation of the Neoarchean IOCG systems. The sources of heat for the establishment of the 2.71-2.68 Ga IOCG forming interval are interpreted to be related to tectonic inversion of the Carajás Basin at ca. 2.7 Ga, under ductile sinistral transpression with NNE-directed oblique shortening. This inversion promoted the reactivation of regional shear zones, in which the Sossego deposit is located. The recurrence of the Paleoproterozoic (1.90-1.88 Ga) events is likely associated with fluid circulation along crustal discontinuities, reworking and metal leaching from the Neoarchean deposits and the country rocks, and ore reconcentration. The widespread ca. 1.88 Ga magmatism in the Carajás Province possibly provided heat for regional fluid circulation.

Keywords: Sossego deposit, IOCG deposits, Carajás Province, U-Pb geochronology, Re-Os geochronology

1. Introduction

The Carajás Province is located in the eastern part of the Amazon Craton, NW Brazil, and corresponds to a Mesoarchean crustal nucleus stabilized during the Neoarchean (Teixeira et al., 1989; Tassinari, 1996; Tassinari and Macambira, 1999, 2004). This province hosts numerous different types of deposits, such as high-grade giant iron deposits (Tolbert et al., 1971; Dardenne and Schobbenhaus, 2001), orogenic gold deposits (Oliveira and Leonards, 1990; Villas and Santos, 2001), the main tungsten reserve in NW Brazil (Rios et al., 1998, 2003), Au-PGE associated with metasedimentary rocks (Moroni et al. 2001; Cabral et al., 2002a,b), chromium and Ni-PGE associated with ultramafic layered intrusions (Diella et al., 1995; Ferreira Filho et al., 2007), Cu-Au polymetallic deposits (Villas and Santos, 2001; Tallarico et al., 2004; Marschik et al., 2005), sedimentary manganese deposits (Silva, 1988; Dardenne and Schobbenhaus, 2001), and lateritic Au, Ni and bauxite (Alves et al., 1986; Macambira and Tassinari, 1998; Klein and Carvalho, 2008). The Carajás Province also hosts the largest amount of world-class iron oxide-copper-gold (IOCG) deposits in the world, which are the only Archean representatives of this deposit class currently known (Réquia et al., 2003; Tassinari et al., 2003; Tallarico et al., 2005; Groves et al., 2010; Xavier et al., 2010; 2012). A recent review of the mineral deposits of the Carajás Province was made by Monteiro et al. (in press).

The IOCG deposits of the Carajás Province are mainly located in two different sectors, situated along, or close to, two important regional shear zones. The Northern Copper Belt hosts the Salobo (1.112 Bt @ 0.69% Cu and 0.43 g/t Au; Vale, 2012), Igarapé Bahia-Alemão (219 Mt @ 1.4% Cu and 0.86 g/t Au; Tavaza, 1999; Tallarico et al., 2005), Gameleira, Pojuca, Paulo Alfonso, Furnas, Polo, and Igarapé Cinzento/Alvo GT46 deposits. The Southern Copper Belt includes the Sossego (355 Mt @ 1.1% Cu and 0.28 g/t Au; Lancaster Oliveira et al., 2000), Cristalino (482 Mt @ 0.65% Cu and 0.06 g/t Au; NCL Brasil, 2005), Alvo 118 (170 Mt @ Cu and 0.3 g/t Au; Rigon et al., 2000), Bacaba, Castanha, Visconde, Bacuri, and Jatobá deposits.

The distribution of hydrothermal alteration zones in a single deposit reveals spatial zoning as an important feature of the Carajás IOCG deposits. The Sossego deposit is composed of two groups of orebodies (Sequeirinho-Baiano-Pista and Sossego-Curril) and is distinctive in this aspect because it appears to contain mineralized zones similar to those recognized worldwide as formed at a range of depths, providing a vertical view of a major IOCG hydrothermal system.

The deeper portion of the deposit, represented mainly by the Sequeirinho orebody, has undergone regional sodic (albite-hematite) and sodic-calcic (actinolite-hastingsite-albite) alterations. This latter is associated with massive magnetite bodies (magnetites) enveloped by apatite- and actinolite-rich bodies. Vertically focused potassic alteration zones cut the sodic-calcic alteration zones and grade laterally to chlorite-rich zones, which predominate in the structurally higher Sossego orebody (Monteiro et al., 2008a, 2008b). Similar potassic alteration overprinted by chlorite alteration was also identified in the Alvo 118 IOCG deposit, which may represent a shallow-emplaced deposit (Torresi et al., 2012).

A similar fluid evolution has been proposed for these distinct IOCG orebodies and deposits (Xavier et al., 2012). Fluid inclusion, stable (O, D, S, B and Cl) isotopes data and Cl/Br–Na/Cl systematics suggest that the main copper-gold precipitation mechanism was related to mixing of hot hypersaline metalliferous fluids with an important magmatic component and modified seawater (e.g., bittern fluids generated by seawater evaporation) and meteoric fluids within shear zones represents (Chiaradia et al., 2006; Xavier et al., 2008; Monteiro et al., 2008a, Carvalho, 2009; Xavier et al., 2009).

However, the available geochronological data are not sufficiently precise to support a genetic link between all IOCG orebodies. Dating of ore-related minerals has provided considerably different Archean (~2.75 or 2.57 Ga; Huhn et al., 1999a; Réquia et al., 2003; Tallarico et al., 2005; Villas et al., 2006; Neves, 2006; Grainger et al., 2008) or Paleoproterozoic (~1.88 Ga; Tallarico, 2003; Silva et al., 2005) ages, even in a single deposit. In the Sossego Mine, the existing geochronological data (Pb-Pb in chalcopyrite and Ar-Ar on amphibole; Marschik et al., 2003, Neves, 2006) were not able to accurately constrain the timing of copper mineralization. The Pb-Pb ages of 2530 ± 25 and 2608 ± 25 Ma for the Sequeirinho orebody (Neves, 2006) have been considered as related to resetting of the isotopic system, whereas the 1592 ± 45 Ma for the Sossego orebody (Neves, 2006) was interpreted as not having any geological meaning. Additionally, Ar-Ar on ore-related amphiboles suggested a minimum age of 2199 ± 13 Ma for the deposit (Marschik et al., 2003).

Considering the scarcity of precise geochronological data for the Sossego deposit, this paper presents results of Re-Os in molybdenite and SHRIMP IIe and LA–ICPMS U-Pb in monazite and zircon of mineralized samples of the Sossego deposits and their host rocks. These results provide new insights into the timing of IOCG formation at the Sossego deposit, revealing

the existence of at least two IOCG mineralizing events separated in time ca. 820 Ma. Additionally, these data allow a comparison to other IOCG deposits of the Carajás Province.

2. Geological Setting of the Carajás Province

The Carajás Province is located in the southeastern part of the Amazon Craton (Brazil), one of the largest cratonic areas in the world. It comprises two Archean domains, the northern Carajás Domain (Fig. 1) and the southern Rio Maria Domain, which corresponds to a typical granite-greenstone terrain. The Carajás Domain (Vasquez et al., 2008), previously known as the Itacaiúnas Shear Belt (Araújo et al., 1988), is divided into: (a) Carajás Basin, at north; and the (b) Transition Subdomain (Dall'Agnol et al., 2006, Feio et al., 2012a), at south. The contact between the Carajás Basin with its basement rocks is defined by a major transcurrent shear system (ca. 130 km) that hosts several world-class and smaller IOCG deposits (e.g., Sossego, Cristalino, Alvo 118, Bacaba, Castanha, Bacuri, Visconde, and Jatobá) of the Southern Carajás Copper Belt.

The basement rocks in the Carajás Domain comprise tonalitic to trondhjemite gneisses and migmatites of the Xingu Complex and mafic to felsic orthogranulites of the Pium Complex (Araújo and Maia, 1991) with protolith crystallization ages of ca. 3.0 Ga (Rodrigues et al., 1992, Pidgeon et al., 2000). The latter was renamed as Chicrim-Cateté Orthogranulites (Ricci and Carvalho, 2006; Vasquez et al., 2008) and separated from magmatic units encompassing norite and quartz gabbro (Oliveira et al., 2010), which were designated as Pium Diopside Norite (Vasquez et al., 2008). Migmatization that affected the Xingu Complex and the high-grade metamorphism of the Chicrim-Cateté Orthogranulites were coeval and took place at $2,859 \pm 2$ Ma (U-Pb zircon; Machado et al., 1991) and $2,859 \pm 9$ Ma (U-Pb SHRIMP zircon; Pidgeon et al., 2000), respectively.

Nonetheless, recent studies (Gomes, 2003; Moreto, 2010; Moreto et al., 2011; Feio et al., 2012a, Oliveira et al., 2010; Silva, 2011) have been endeavoring to individualize compositionally distinct units in the former Xingu Complex area. Such rocks correspond to: (a) ca. 3.0 Ga Bacaba Tonalite (Moreto et al., 2011); (b) ca. 2.96 Ga Canaã dos Carajás Granite and older rocks of the Rio Verde Thronthjemite (Feio et al., 2012a); (c) 2.87-2.83 Ga Serra Dourada and Cruzadão granites, and the Rio Verde Trondhjemite (Feio et al., 2012a; Moreto et al., 2011).

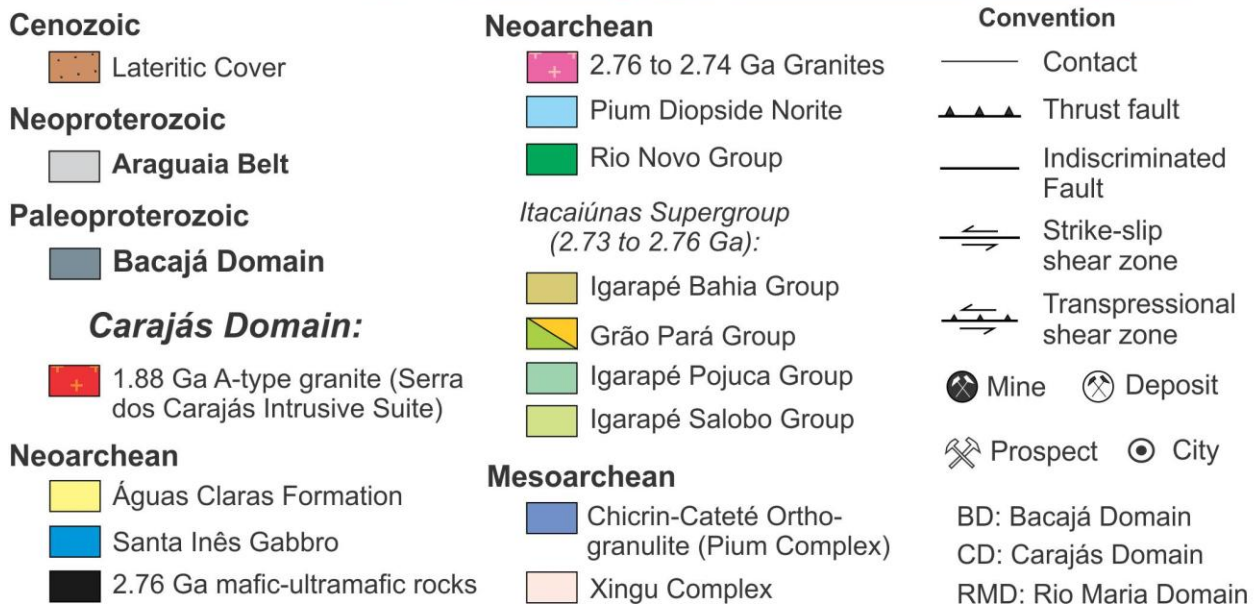
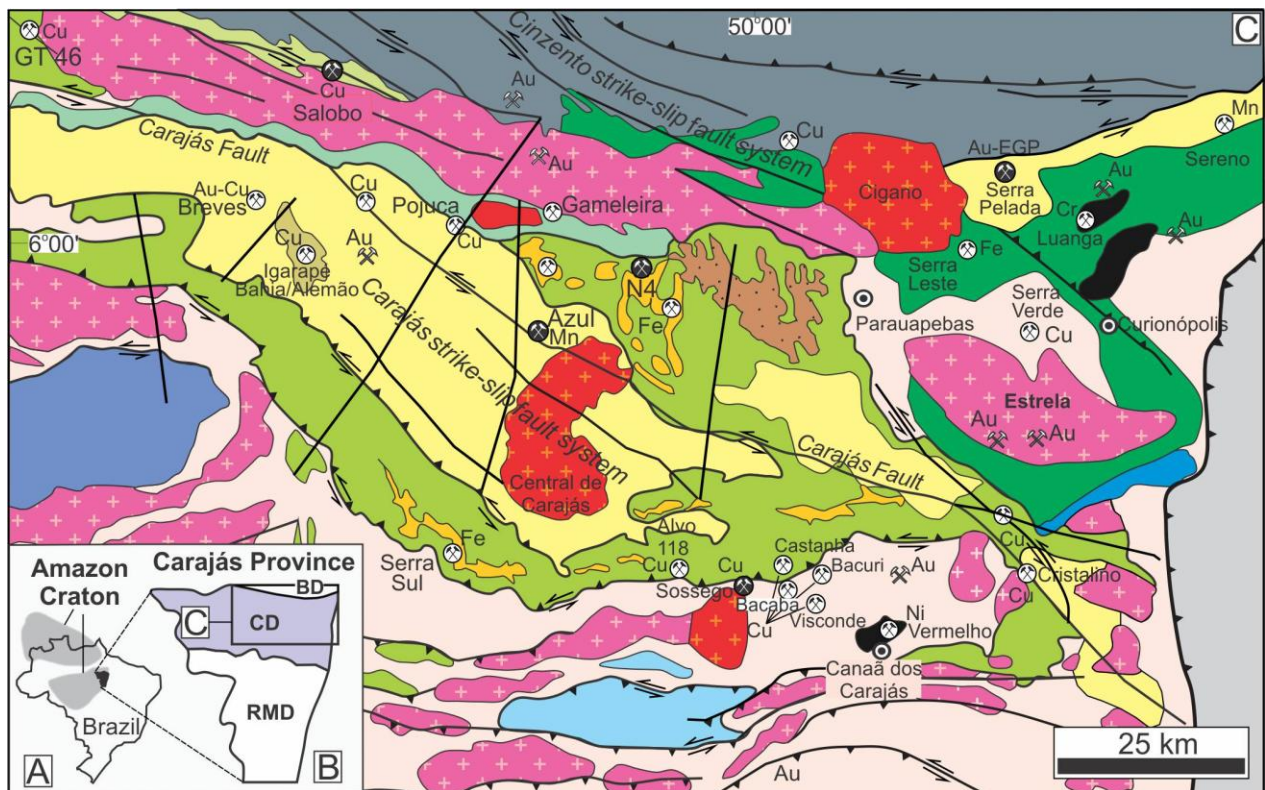


Fig. 1. Geological map of the Carajás Domain (Vasquez et al. 2008) A) Location in Brazil; B) Location of the Carajás Domain at the Carajás Province; C) Geological map of the Carajás Domain (Vasquez et al. 2008). Abbreviations: BD: Bacajá Domain; CD: Carajás Domain; RMD: Rio Maria Domain.

The Rio Novo Group (Hirata et al., 1982) and the Itacaiúnas Supergroup (Wirth et al., 1986; DOCEGEO, 1988; Machado et al., 1991) overlie the basement rocks and corresponds to ca. 2.76-2.74 Ga metavolcanic-sedimentary units that filled the Carajás Basin. The Rio Novo

Group includes amphibolite, schist, metagraywacke, tholeiitic metavolcanic rocks and gabbro (Hirata et al., 1982). The Itacaiúnas Supergroup is divided into the Igarapé Bahia, Grão Pará, Igarapé Pojuca, and Salobo groups, and mainly consist of metabasalt with associated intermediate and felsic metavolcanic rocks, metapyroclastic and metavolcaniclastic rocks, banded iron formations, amphibolite, and metasedimentary units.

The Itacaiúnas Supergroup and the Rio Novo Group are partially overlain by the Águas Claras Formation (Nogueira et al., 1994, 2000), a low-grade metasedimentary sequence deposited in fluvial to shallow marine environment. Dating of metagabbro sills ($2,645 \pm 12$ and $2,708 \pm 37$ Ma; Dias et al., 1996; Mougeot et al., 1996a) constrains the age of the Águas Claras Formation to the Archean.

The Luanga igneous layered complex and the Cateté Intrusive Suite (Serra da Onça, Serra do Puma, Serra do Jacaré-Jacarezinho, Vermelho and Igarapé Carapanã bodies; Macambira and Vale, 1997; Macambira and Ferreira Filho, 2002; Ferreira Filho et al., 2007) represent the mafic-ultramafic magmatism in the Carajás Domain. The Luanga complex intrudes the Rio Novo Group and hosts a Cr-PGE deposit. Machado et al. (1991) dated anorthositic gabbro from the Luanga complex in $2,763 \pm 6$ Ma (U-Pb zircon), whereas a gabbro from the Serra da Onça body was dated in $2,766 \pm 6$ Ma (U-Pb SHRIMP zircon; Lafon et al., 2000).

Neoarchean and Paleoproterozoic granitic episodes have been identified in the Carajás Domain. These granites intruded both supracrustal units of the Carajás Basin and the Mesoarchean basement rocks. The 2.75 to 2.74 Ga event is characterized by syntectonic foliated alkaline and metaluminous granites, similar to A-type granites, and correspond to the Plaquê, Planalto, Estrela, Serra do Rabo, Igarapé Gelado, and Pedra Branca suites (Huhn et al., 1999b; Avelar et al., 1999; Barbosa, 2004; Barros et al., 2004; 2009; Sardinha et al., 2006; Feio et al., 2012a,b). The 2.57 Ga granites are also alkaline, peralkaline to metaluminous and characterized by the Old Salobo and Itacaiúnas granites (Machado et al., 1991; Souza et al., 1996), located in the north part of the Carajás Domain, close to the Cinzento strike-slip fault system (Fig. 1). Finally, the 1.88 Ga granitic magmatism corresponds to A-type alkaline to sub-alkaline and metaluminous to slightly peraluminous granites, included in the Serra dos Carajás Intrusive Suite (Central de Carajás, Young Salobo, Cigano, Pojuca, Breves, and Rio Branco granites; Machado et al., 1991; Tallarico et al., 2004). This ca. 1.88 Ga anorogenic magmatism is extended to the southern Rio Maria Domain and to other tectonic provinces of the Amazon Craton.

Other magmatic events have locally been reported and comprise dacitic to rhyolitic porphyries dated at $2,645 \pm 9$ and $2,654 \pm 9$ Ma in the Alvo 118 deposit (Pb–Pb SHRIMP zircon; Tallarico, 2003). In the Gameleira deposit area, an alkali-rich leucogranite dike provided a U–Pb SHRIMP age of $1,583 + 9/-7$ Ma (Pimentel et al., 2003). Additionally, the Geladinho Granitic Stock, located close to the Salobo deposit, was dated in $2,688 \pm 11$ Ma (Pb-Pb zircon, Barbosa et al., 2001). The province was also affected by other magmatic events represented by late undeformed diabase, diorite, and gabbro dikes, whose ages are uncertain. The main regional structures in the Carajás Domain display E-W and WNW-ESE- trending. In terms of tectonic models for this domain, the transtensional-transpressional model from Araújo et al. (1988) suggested the Carajás sigmoidal structure would have formed during dextral transtension of the basement rocks that led to the formation of a pull-apart basin and the development of the Carajás, Cinzento, and Araraquara fault systems. This basin would have been filled with volcanic and sedimentary rocks of the Itacaiúnas Supergroup and the sediments of the Águas Claras Formation on top. After the deposition ended, sinistral transpression would lead to the basin tectonic inversion and creation of a positive flower structure in the Carajás shear system.

The tectonic reactivation model proposed by Pinheiro and Holdsworth (1997), Holdsworth and Pinheiro (2000), and Domingos (2009) suggest a different evolution in which the Itacaiúnas Supergroup and the Águas Claras Formation would have deposited in an intracratonic basin that overlain the basement rocks intensively deformed at ca. 2.85 Ga under high-temperature regional sinistral transpression. Under regional extension (brittle dextral transtension) around 2.8-2.7 Ga, the volcanic-sedimentary rocks would have accommodated by tectonic subsidence to the shape of the Carajás sigmoidal structure. The Carajás and Cinzento strike-slip fault systems were formed at this time. Domingos (2009) suggests a tectonic inversion of the basin initiating at about 2.7 Ga and lasting up to 2.6 Ga involving a regional phase of sinistral transpression. Furthermore, Pinheiro and Holdsworth (1997) argue that the Carajás and Cinzento strike-slip fault systems preserve direct and indirect evidence for several phases of dextral and sinistral movements since ca. 2.7 Ga. Indeed, the Carajás Fault (Fig. 1) would have formed during one of these reactivations phases, under brittle sinistral transpression. Domingos (2009) also suggests a later phase of crustal extension at about 1.8 Ga that allowed the emplacement of the Serra dos Carajás Intrusive Suite.

Wirth et al. (1986), Gibbs et al. (1986), DOCEGEO (1988), Olszewski et al. (1989), Macambira (2003) and Tallarico (2003) also suggest a continental rift setting for the establishment of the Carajás Basin. This model is based on the bimodal characteristic of the magmatism of the Itacaiúnas Supergroup with isotopic and chemical evidence for contamination of mantle-derived melts by significant continental crust (Gibbs et al., 1986). Tallarico (2003) suggests that rifting of the stabilized Carajás block resulted from the interaction with ascending mantle-plume. Mafic magma accumulated at the base of the crust ascended to shallower crustal levels, generating differentiated magma chambers (e.g., Luanga complex), or even erupted to the surface forming the volcanic-sedimentary units of the Itacaiúnas Supergroup (Tallarico, 2003).

On the other hand, Meirelles (1986), Dardenne et al. (1988), Meirelles and Dardenne (1991), Teixeira (1994), Lobato et al., (2005), Silva et al., (2005), and Teixeira et al. (2010), suggest that the Carajás Basin would have formed in a volcanic arc setting related to subduction processes, where high potassium calc-alkaline basalt of the Itacaiúnas Supergroup would have formed. Zucchetti (2007) proposes that the geochemical signatures of the metabasalt of the Grão Pará group (Itacaiúnas Supergroup) could reflect volcanism erupted on continental crust in a back-arc setting.

3. Timing of IOCG formation at the Carajás Province

Comprehensive review on the Carajás IOCG deposits is provided by Grainger et al. (2008) and Xavier et al. (2010; 2012). The geochronological data for these deposits and their host rocks are shown on Table 1. Most of the available data refer to the deposits located in the Northern Copper Belt. Distinct dating methods have been used to date ore-related minerals and their host rocks, and considerably different ages were obtained (Table 1) even in the same deposit (e.g., Igarapé Bahia/Alemão, Gameleira, Salobo, and Igarapé Cinzento deposits; Pimentel et al., 2003; Tassinari et al., 2003; Réquia et al., 2003; Marschik et al., 2005; Tallarico et al., 2005; Silva et al., 2005; Galarza et al., 2008). Re-Os in molybdenite (Salobo deposit, Réquia et al., 2003) and U-Pb SHRIMP in hydrothermal monazite (Igarapé Bahia deposit, Tallarico et al., 2005) point to an important metallogenetic event at 2.57 Ga in the Northern Copper Belt.

Table 1 Available geochronological data for IOCG deposits and their host rocks from the Carajás Domain

Rock/mineral	Age (Ma)	Method	Reference
Northern Copper Belt			
SALOBO			
Host Rocks			
iron formation (metamorphism)	2,551 ± 2	U-Pb, Mz	Machado et al. 1991
foliated amphibolite (metamorphism)	2,497 ± 5	U-Pb, Ti	Machado et al., 1991
	2,555 +4/-3	U-Pb, Zr	Machado et al., 1991
Old Salobo Granite	2,573 ± 2	U-Pb, Zr	Machado et al., 1991
granitic vein (metamorphism)	2,581 ± 5,	Pb-Pb, Zr	Machado et al., 1991
	2,584 ± 5		
	2,732	U-Pb, Ti	Machado et al., 1991
granitic vein	2,758	U-Pb, Zr	Machado et al., 1991
schist	2,700 ± 150	Rb-Sr, WR	Tassinari et al., 1982
foliated amphibolite (metamorphism)	2,761 ± 3	U-Pb, Zr	Machado et al., 1991
amphibolite and meta-andesite from Igarapé Pojuca group	2,812 ± 98	Sm-Nd, WR	Pimentel et al., 2003
Ore			
magnetite leachates	2,112 ± 12	Pb-Pb	Tassinari et al., 2003
chalcopyrite leachates	2,427 ± 130	Pb-Pb	Tassinari et al., 2003
molybdenite	2,562 ± 8	Re-Os	Réquia et al., 2003
	2,576 ± 8	Re-Os	Réquia et al., 2003
bornite–chalcopyrite leachates	2,579 ± 71	Pb-Pb	Réquia et al., 2003
tourmaline leachates	2,587 ± 150	Pb-Pb	Tassinari et al., 2003
chalcocite leachates	2,705 ± 42	Pb-Pb	Tassinari et al., 2003
IGARAPÉ CINZENTO/GT46			
Host Rocks			
gray granite	2,612.2 ± 1.5	U-Pb, Mz	Silva et al., 2005
pink and gray granites and garnet granites	2,652 ± 98	Sm-Nd, WR	Silva et al., 2005
pink and gray granites	2,668 ± 100	Sm-Nd, WR	Silva et al., 2005
basalts and gabbro	2,686 ± 87	Sm-Nd, WR	Silva et al., 2005
Ore			
ore breccia and hydrothermal sample from Salobo deposit	1,752 ± 77	Sm-Nd, WR	Silva et al., 2005
biotite (Potassic alteration)	1,810 ± 15	Ar-Ar	Silva et al., 2005
biotite (Potassic alteration)	1,858 ± 7	Ar-Ar	Silva et al., 2005
molybdenite from pegmatitic granite	2,554 ± 8	Re-Os	Silva et al., 2005
molybdenite from pegmatitic granite	2,557 ± 8	Re-Os	Silva et al., 2005
molybdenite from granite	2,600 ± 8	Re-Os	Silva et al., 2005
molybdenite from amphibolite	2,711 ± 9	Re-Os	Silva et al., 2005
IGARAPÉ BAHIA/ALEMÃO			
Host rocks			
dioritic dike	2,308 ± 10	Pb-Pb, WR	Santos, 2002
pyroclastic rock	2,360 ± 80	Rb-Sr, WR	Ferreira Filho, 1985
mafic metavolcanic rock	2,748 ± 34	U-Pb, Zr (*)	Tallarico et al., 2005
mafic metavolcanic rock	2,758 ± 75	Sm-Nd, WR	Galarza et al., 2003
	2,776 ± 12	Pb-Pb, WR	Galarza et al., 2003
	2,745 ± 1	Pb-Pb, Zr	Galarza and Macambira, 2002a

Table 1 (continued)

Rock/mineral	Age (Ma)	Method	Reference
IGARAPÉ BAHIA/ALEMÃO (cont.)			
Host rocks			
metapyroclastic rock	2,758 ± 36	Pb-Pb, WR	Galarza et al., 2003
	2,747 ± 1	Pb-Pb, Zr	Galarza and Macambira, 2002a
metavolcanic and metapyroclastic rocks	2,751 ± 81	Pb-Pb, WR	Santos, 2002
	2,759 ± 24	Sm-Nd, WR	Santos, 2002
gabbro	2,765 ± 36	Pb-Pb, WR	Galarza et al., 2003
Ore			
chalcocite leachates	2,385 ± 122	Pb-Pb	Galarza et al., 2008
chalcocite leachates	2,417 ± 120	Pb-Pb	Galarza et al., 2008
sulfides (ore breccia)	2,521±56	Pb-Pb	Santos, 2002
chalcocite + gold	2,539±26	Pb-Pb	Santos, 2002
monazite from ore breccia	2,575 ± 12	U-Pb (*)	Tallarico et al., 2005
gold (magnetite ore breccia)	2,575±86	Pb-Pb	Santos, 2002
fluorite (late carbonate vein)	2,580±79	Sm-Nd	Santos, 2002
gold	2,744 ± 12	Pb-Pb	Galarza et al., 2008
chalcocite (metapyroclastic rock)	2,754 ± 36	Pb-Pb	Galarza et al., 2008
chalcocite (mafic metavolcanic rock)	2,756 ± 24	Pb-Pb	Galarza et al., 2008
chalcocite (hydrothermal breccia)	2,772 ± 46	Pb-Pb	Galarza et al., 2008
chalcocite (mafic intrusive rock)	2,777 ± 22	Pb-Pb	Galarza et al., 2008
chalcocite	2,850 ± 65	Pb-Pb	Mougeot et al., 1996b
GAMELEIRA			
Host rocks			
mafic metavolcanic rocks	2,245 ± 29	Pb-Pb, WR	Galarza and Macambira, 2002b
meta-andesite	2,683 ± 80	Sm-Nd, WR	Lindenmayer et al., 2001
	2,719 ± 80	Sm-Nd, WR	Pimentel et al., 2003
metagabbro	2,696 ± 109	Sm-Nd, WR	Lindenmayer et al., 2001
quartz diorite	2,705 ± 2	Pb-Pb, Zr	Galarza and Macambira, 2002b
Amphibolite (metamorphism)	2,732 ± 2	U-Pb, Zr	Machado et al., 1991
metagabbro and cogenetic meta-andesite	2,757 ± 81	Sm-Nd, WR	Pimentel et al., 2003
Ore			
biotite–sulfide veins	1,700 ± 31	Sm-Nd, WR	Pimentel et al., 2003
	1,700 ± 60	Sm-Nd, WR	Lindenmayer et al., 2001
biotite (Potassic alteration) from meta-andesite	1,734 ± 8	Ar-Ar	Lindenmayer et al., 2001; Pimentel et al., 2003
quartz–grunerite–gold vein	1,837 ± 30	Sm-Nd, WR	Lindenmayer et al., 2001
	1,839 ± 15	Sm-Nd, WR	Pimentel et al., 2003
garnet-biotite schist	1,958 ± 230	Sm-Nd, WR	Pimentel et al., 2003
	2,668 ± 60	Sm-Nd, WR	Lindenmayer et al., 2001
chalcocite concentrates	2,180 ± 84, 2,217 ± 19	Pb-Pb	Galarza and Macambira, 2002b
chalcocite from quartz veins	2,419 ± 12	Pb-Pb	Galarza and Macambira, 2002b
molybdenite	2,614 ± 14	Re-Os	Marschik et al., 2005
Southern Copper Belt			
SOSSEGO			
Ore			
<i>Sossego Orebody</i>			
chalcocite from Ore breccia	1,592 ± 45	Pb-Pb	Neves, 2006

Table 1 (continued)

Rock/mineral	Age (Ma)	Method	Reference
SOSSEGO (cont.)			
<i>Sequeirinho Oreboby</i>			
ore-related amphibole	2,199 ± 13	Ar-Ar	Marschik et al., 2003
chalcopyrite from massive ore	2,530 ± 25	Pb-Pb	Neves, 2006
ore breccia	2,578 ± 29	Sm-Nd, WR	Neves, 2006
chalcopyrite from massive ore	2,608 ± 25	Pb-Pb	Neves, 2006
CRISTALINO			
<i>Host rocks</i>			
Cristalino Diorite	2,738 ± 6	Pb-Pb, Zr	Huhn et al., 1999b
Planalto Granite	2,747 ± 2	Pb-Pb, Zr	Huhn et al., 1999b
<i>Ore</i>			
Chalcopyrite and pyrite	2,700 ± 29* (*MSWD=656)	Pb-Pb	Soares et al., 2001
ALVO 118			
<i>Host rocks</i>			
dacitic dike	2,645 ± 9	U-Pb, Zr (*)	Tallarico, 2003
rhyolitic dike	2,654 ± 9	U-Pb, Zr (*)	Tallarico, 2003
Alvo 118 Tonalite	2,743 ± 3	U-Pb, Zr (*)	Tallarico, 2003
<i>Ore</i>			
xenotime	1,868 ± 7	U-Pb (*)	Tallarico, 2003
	1,869 ± 7	U-Pb (*)	Tallarico, 2003
VISCONDE			
<i>Host rocks</i>			
Serra Dourada Granite	2,860 ± 22	U-Pb, Zr	Moreto et al., 2011
<i>Ore</i>			
chalcopyrite concentrates	2,747 ± 140	Pb-Pb	Silva et al., 2012

Abbreviations : (*): SHRIMP; Mz: monazite; Ti: titanite; WR: whole rock; Zr: zircon.

In the Southern Copper Belt, U-Pb SHRIMP II in hydrothermal xenotime from the Alvo 118 deposit (Tallarico, 2003) suggests ore genesis at 1.88 Ga. Based on these different data in the literature, it is unlikely that a genetic link for all the IOCG deposits of the Carajás Province exists.

The genetic models for the IOCG deposits of the Carajás Province commonly associate ore formation with the emplacement of specific granites or granitic suites (e.g., 2.7 and 2.57 Ga; Huhn et al., 1999a; Réquia et al., 2003; Tallarico et al., 2005). Younger ages than 2.57 Ga were commonly interpreted as resetting of the isotopic systems due to the development and/or reactivation of the regional shear zones and/or due to Paleoproterozoic granite magmatism (Salobo deposit, Tassinari et al., 2003; Gameleira deposit, Galarza and Macambira, 2002b; Igarapé Bahia deposit, Galarza et al., 2008; Sossego deposit, Neves, 2006). For the Sossego deposit, Pb-Pb dating of chalcopyrite (total dissolution and leaching) provided ages of 2.53 Ga and 2.61 Ga for the Sequeirinho orebody, and 1.59 Ga for the Sossego orebody (Neves, 2006).

The Neoarchean ages were interpreted as isotopic resetting due to thermal/deformational events. Although speculative, the ore-formation event at both orebodies was associated (Neves, 2006) to the ca. 2.74 Ga magmatism at the province (e.g., Planalto Granite or Cristalino Diorite; Huhn et al., 1999b). Alternatively, ore formation could be attributed to metamorphic processes and the 2.53 Ga and 2.61 Ga ages would be intrinsically associated with a shearing event (Neves, 2006). No geological meaning was attributed to the Mesoproterozoic age of 1,592 Ma (Neves, 2006). Moreover, Ar-Ar dating of ore-related amphiboles of the Sequeirinho orebody suggested a minimum age of 2.2-2.3 Ga for the mineralization (Marschik et al. 2003).

4. Analytical Procedures

Characterization of the host rocks, hydrothermal alteration stages, and ore paragenesis of the Sossego deposit was previously reported by Monteiro et al. (2008a,b) and Carvalho (2009). However, additional observation of drill holes and detailed petrographic studies under transmitted and reflected light were performed in samples from the Sossego deposit. Geological mapping in the vicinity of the deposit has also been prioritized. These procedures were conducted in order to select the most appropriate rocks samples for the geochronological studies on host rock and ore-related minerals. All samples were selected from drill cores, except for samples SOS 39J (Sequeirinho orebody) and Min-Cp-SOS (Sossego orebody), which were collected from the high-grade ore pile in the Sossego mine.

4.1 U-Pb LA-ICPMS, zircon

In situ U-Pb LA-ICPMS zircon isotopic analyses were carried out at the James Cook University, Townsville, Australia. Zircon grains from the Sequeirinho Granite (SOS 259/177.4 and SOS 22/107.45) and the Sossego granophytic granite (SOS 35/406.88) were analyzed in thin sections. The data were acquired with a Varian 820 MS quadrupole ICPMS coupled with a 193 nm ArF GeoLas laser ablation sampling system. The Varian was operated in normal sensitivity mode. All analyses were undertaken on standard 30 micron thick petrographic thin sections, using a 21 micron beam diameter, 10 Hz laser repetition rate and a laser fluence of ~ 3 J/cm² (adjusted using an optical attenuator on the laser beam path and measured at the ablation site by an energy meter). Analysis involved 30 seconds of background measurement and 30 seconds of

ablation, although many zircons yielded signals of only 15-20 seconds duration before the laser fully penetrated the crystal. Data reduction was performed with GLITTER (Van Achterbergh et al. 2001), where isotope ratios were corrected for mass bias and laser induced Pb/U fractionation using FC1 (1099 Ma) as the primary standard. Zircon QGNG was used as a secondary monitor of data quality, and 18 analyses yield a mean $^{207}\text{Pb}/^{206}\text{Pb}$ age of 1856 ± 12 (2 standard deviations), identical to the accepted age of 1,852 Ma. U and Th concentrations were determined by standardization to NIST610 and assuming a stoichiometric silica content in zircon. Common lead corrections were not made, and 204 counts measured for sample zircons were generally very close to background levels.

4.2 U-Pb LA-MC-ICPMS, monazite

Monazite grains were selected from four distinct ore samples from the Sequeirinho (SOS 259/270), Sossego (Min-Cp-SOS and SOS 315/255.1) and Curral (SOS 106/84) orebodies. The monazite concentrates were extracted from ca. 400g to 2 kg rock using conventional gravity and magnetic techniques, at the mineral concentration facility at the University of Campinas. The conventional optical microscopy and BSE and CL images were performed at the Institute of Geosciences, University of Campinas. The mineral fractions were handpicked under a binocular microscope, mounted in epoxy blocks, and polished.

The *in situ* U-Pb monazite data was collected using laser ablation multi collector inductively coupled mass spectrometry (LA-MC-ICPMS) at the Radiogenic Isotope Facility of the University of Alberta, Edmonton, Canada. A full description of the analytical approach is reported in Simonetti et al. (2005). The analytical setup consists of a New Wave UP-213 laser ablation system interfaced with a Nu plasma MC-ICPMS equipped with three ion counters. The laser was operated at 4 Hz pulse rate and a beam diameter of 12 mm that yielded a fluence of ~ 3 J/cm². Ablations were conducted in a He atmosphere at a flow rate of 1 L/min through the cell. Output from the cell was joined to the output from a standard Nu plasma desolvating nebulizer (DSN). On peak gas + acid blanks (30s) were measured prior to a set of 10-20 analyses. Data was collected statically, consisting of 30 1s integrations. Before and after each set of analyses, an in house monazite reference material was repeatedly analyzed, which corresponded to the Western Australia (2.843 Ga, Simonetti et al., 2006; Heaman unpublished data), to monitor U-Pb fractionation, reproducibility, and instrument drift. Mass bias for Pb isotopes was corrected by

measuring $^{205}\text{Tl}/^{203}\text{Tl}$ from an aspirated Tl solution (NIST SRM 997) via the DSN using an exponential mass fractionation law and assuming a natural $^{205}\text{Tl}/^{203}\text{Tl}$ of 2.3871. All data were reduced offline using an Excel-based program. Unknowns were normalized to the in house monazite standard. The uncertainties reported are a quadratic combination of: 1) the standard error of the measured isotope ratio and 2) the standard deviation of the standards that bracket the unknowns. Reproducibility of the monazite standard is estimated to be ~1% for $^{207}\text{Pb}/^{206}\text{Pb}$ and 3% for $^{206}\text{Pb}/^{238}\text{U}$.

4.3 U-Pb SHRIMP IIe, zircon

A total of five samples of the host rocks and one sample of copper ore (Sequeirinho orebody; SOS 39J) were analyzed by the U-Pb SHRIMP IIe zircon method. The analyzed host rocks include the Sequeirinho Granite (SOS 450/13), gabbronorite (SOS 35 and SOS 35/30), and the Pista metavolcanic rock (SOS 364/138.35 and SOS 475/167). The U-Pb SHRIMP IIe zircon isotopic analyses were performed at the High-Resolution Geochronology Laboratory (HRGL) of the Geochronological Research Centre, University of São Paulo, Brazil.

The zircon concentrates were also extracted using conventional gravity and magnetic techniques at the mineral concentration facility at the University of Campinas. These concentrates were sent to the HRGL of the University of São Paulo for hand-picking and mounting. The crystals were mounted together with the TEMORA standard in epoxy and polished until attain quasi-central sections. After Au-coating, the polished mounts were comprehensively examined with a FEI-QUANTA 250 scanning electron microscope equipped with secondary-electron and CL detectors. The most common conditions used in CL analysis were as follows: 60 μA of emission current, 15.0 kV of accelerating voltage, 7 μm of beam diameter, 200 μs of acquisition time, and a resolution of 1024×884. The same mounts were afterwards analyzed by the U-Pb isotopic technique using a SHRIMP-IIe machine also at the HRGL following the analytical procedures presented in Williams (1998). Correction for common Pb was made based on the basis of the ^{204}Pb measured, and the typical error component for the $^{206}\text{Pb}/^{238}\text{U}$ ratio is less than 2%; uranium abundance and U/Pb ratios were calibrated against the TEMORA standard and the age calculations were performed with Isoplot© 3.0 (Ludwig, 2003).

4.4 Re-Os, molybdenite

Molybdenite crystals were selected from two hydrothermal altered and mineralized samples (SOS 364/76.84 and SOS 364/160.9) hosted by the Pista metavolcanic rock obtained from drill cores in the Pista orebody area. Methods used for molybdenite analysis at the Radiogenic Isotope Facility of the University of Alberta, Edmonton, Canada, are described in detail by Selby and Creaser (2004), and Markey et al. (2007). The ^{187}Re and ^{187}Os concentrations in molybdenite were determined by isotope dilution mass spectrometry using Carius-tube, solvent extraction, anion chromatography and negative thermal ionization mass spectrometry techniques. A mixed double spike containing known amounts of isotopically enriched ^{185}Re , ^{190}Os , and ^{188}Os analysis was used. Isotopic analyses were made using a ThermoScientific Triton mass spectrometer by Faraday collector. Total procedural blanks for Re and Os are less than <3 picograms and 2 picograms, respectively, which are insignificant for the Re and Os concentrations in molybdenite. The Chinese molybdenite powder HLP-5 (Markey et al., 1998), was analyzed as a standard. For this control sample over a period of two years, an average Re-Os date of 221.56 ± 0.40 Ma (1SD uncertainty, n=10) is obtained. This Re-Os age date is identical to that reported by Markey et al. (1998) of 221.0 ± 1.0 Ma.

5. Sossego deposit

The Sossego deposit (Fig. 2) comprises, from west to east, the Pista, Sequeirinho, Baiano, Curral, and Sossego orebodies. The Sequeirinho and Sossego orebodies represent the bulk of resources, with 85 and 15 percent of the ore reserves, respectively. The orebodies show distinct hydrothermal alteration assemblages, styles and intensity, which likely reflect different paleo-structural levels (Monteiro et al., 2008a,b). Intense hydrothermal alteration and mineralization is generally restricted to within several hundred meters of the main faults. Rocks in the immediate footwalls of the faults are intensely mylonitized and display biotite–tourmaline–scapolite alteration and silicification near the fault contacts (Monteiro et al., 2008a). A detailed description of the orebodies is provided below and in Table 2.

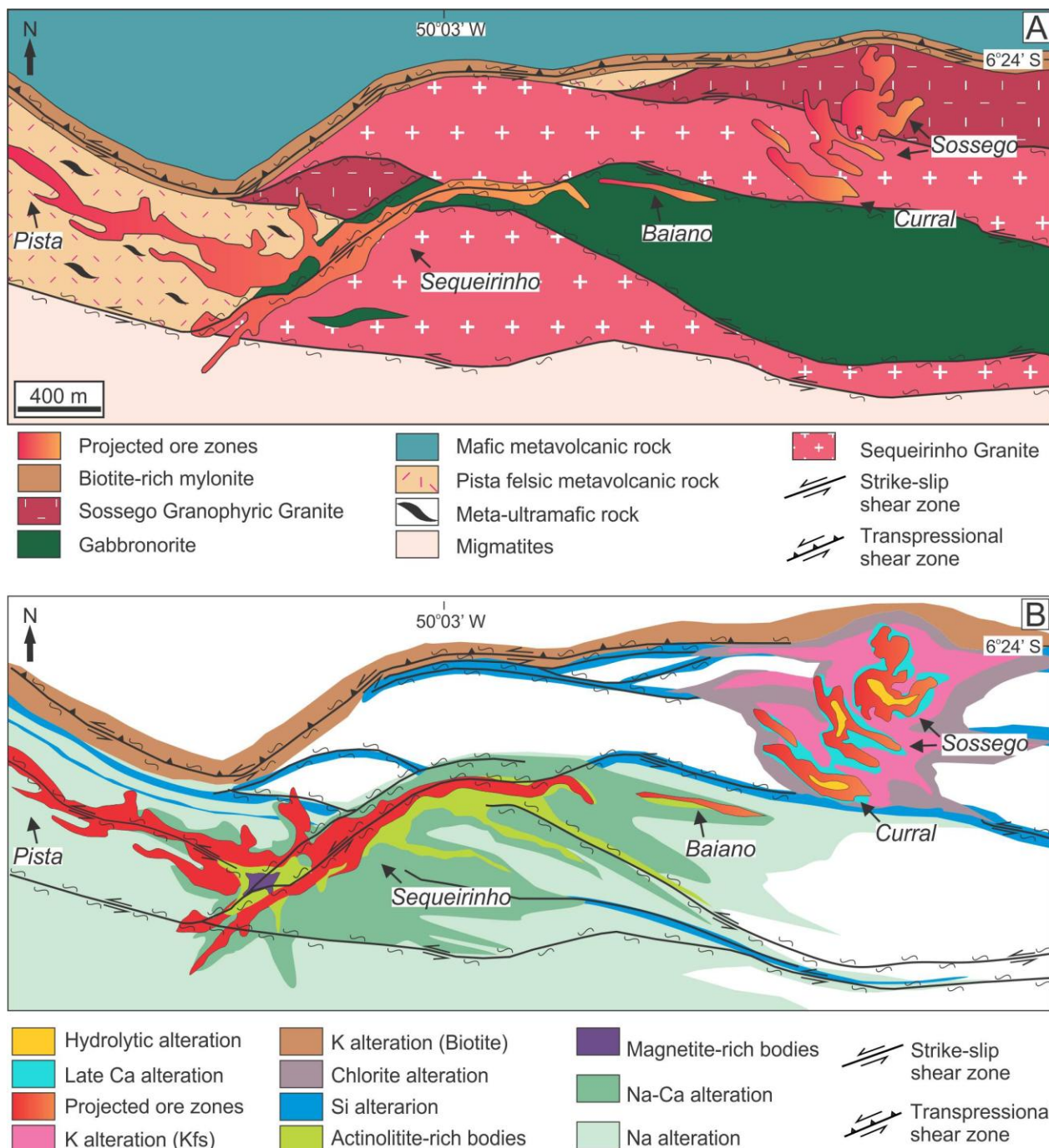


Fig. 2. A) Simplified geologic map of the Sossego deposit showing the location of the Sequeirinho, Pista, Baiano, Sossego and Curral, orebodies (Monteiro et al. 2008a modified from a VALE company figure); B) Schematic distribution of the hydrothermal alteration zones in the Sossego deposit (Monteiro et al. 2008a).

Table 2 Main characteristics of the Sequeirinho-Pista-Baiano and Sossego-Currall orebodies of the Sossego deposit

	Sequeirinho-Pista-Baiano	Sossego-Currall
Reserve	85% of 355 Mt @ 1.1% Cu, 0.28 g/t Au (1)	15% of 355 Mt @ 1.1% Cu, 0.28 g/t Au (1)
Host rocks	Sequeirinho Granite, gabbronorite, Pista felsic metavolcanic rock.	Sossego granophyric granite, gabbronorite.
Hydrothermal Alteration	Na- (albite-hematite) alteration. Na-Ca- (act-rich) associated with Mgt-(apt) formation. Poorly developed K and chlorite alteration. (2)	Well-developed K and chlorite alteration. Late hydrolytic alteration. Poorly developed Na- and Na-Ca- alteration. (2)
Ore Morphology	Breccia, disseminations along mylonitic foliation, veins and stockwork breccias. (2)	Subvertical breccia pipes, veins. (2)
Ore Mineralogy	Chalcopyrite, magnetite, pyrrhotite, pyrite, and minor molybdenite, sphalerite, siegenite, millerite, gold, Pd-melonite, galena, cassiterite, hessite. (2)	Chalcopyrite, magnetite, pyrite, and minor siegenite, millerite, hessite, Pd-melonite, molybdenite, gold and cassiterite. (2)
Geochemical signature	Cu- Fe- Au- Ni- Co- Pd- Se- V- P- LHEE, with low content of Ti and U. Relatively enriched in Co, Ni, Pd, V, and Se in comparison to Sossego-Currall orebodies. (3)	Cu- Fe- Au- Ni- Co- Pd- Se- V- P- LHEE. Relatively enriched in Au, Pb, Sn, Rb, Y, and Nb in comparison to Sequeirinho-Pista-Baiano orebodies. (3)
Fluid inclusion (T=°C; salinity =wt% eq. NaCl)	Na-Ca stage: Ti= -76 to -63 (L-V-S) and -63 to -53 (L-V); TH _{(s)LV-L} = 122 to 229 (LVS), and 116 to 250 (L-V); Salinity= 29 to 53 (L-V-S) and 3 to > 23 (LV). (3)	Ore stage: Ti= -65 (L-V-S) and -66 to -45 (L-V); TH _{(s)LV-L} = 102 to 312 (L-V); Salinity= 26 to 70 (L-V-S) and 0.2 to > 23 (LV). (3)
Stable isotopes: O in silicates and oxides (‰)	1) Early alteration stages: higher T fluids (> 550°C), and δ ¹⁸ O _{fluid} = 6.9; 2) Ore stage: lower T fluids (~300°C), and δ ¹⁸ O _{fluid} = 1.8. (2)	1) Early alteration stages: higher T fluids (400°C), and δ ¹⁸ O _{fluid} = 5.5 to 8.4; 2) Ore Stage: lower T fluids (~275°C), and δ ¹⁸ O _{fluid} = 0.4 to 1.9. (2)
Stable isotopes: O (SMOW) and C (PDB) in carbonates (‰)	Ore breccia: δ ¹³ C = -6.44 to -4.77; δ ¹⁸ O = 5.6 to 7.43; δ ¹⁸ O _{fluid} = -2.6 to 1.9; δ ¹³ C _{H2CO3} = -6.1 to -3.4 (T=230°C) (2)	Ore breccia: δ ¹³ C = -6.03 to -4.73; δ ¹⁸ O = 5.12 to 8.46; δ ¹⁸ O _{fluid} = -0.6 to 4.5; δ ¹³ C _{H2CO3} = -4.8 to -2.7 (T=275°C) (2)
Stable isotopes: H in silicates (‰)	Na-Ca stage: δD _{fluid} = -50 to -34 (T=550°C); Ore stage: δD _{fluid} = -47 to -37 (actinolite; T=400 °C) (2)	Ore stage: δD _{fluid} = -67 to -36 (actinolite; T=400°C); Post mineralization stage: -40 to -30 (chlorite; T=250°C) (2)
Stable isotopes: S (CDT) in sulfides (‰)	δ ³⁴ S: 2.2 to 6.1 (2)	δ ³⁴ S: 3.8 to 7.6 (2)
Stable isotopes: B in tourmaline (‰)	δ ¹¹ B: -8 to 11 (4)	Absent
Stable isotopes: Cl in quartz and calcite (‰)	δ ³⁷ Cl: 0.25 to 1.18 (5)	δ ³⁷ Cl: 0.78 to 1.53 (5)
Cl/Br systematics (mol)	742 to 932 (5)	748 to 1786 (5)

(1) Lancaster Oliveira et al., 2000; (2) Monteiro et al., 2008a; (3) Carvalho, 2009; (4) Xavier et al., 2008; (5) Chiaradia et al., 2006

5.1 Sequeirinho-Baiano-Pista Orebodies

The Sequeirinho-Baiano-Pista orebodies (Figs. 2 and 3) are located along a anastomosing NE-SW lineament related to regional WNW-ESE steeply dipping ductile shear zones, and

comprises an “S” shaped tabular sub-vertical orebody (Monteiro et al., 2008a,b; Domingos, 2009).

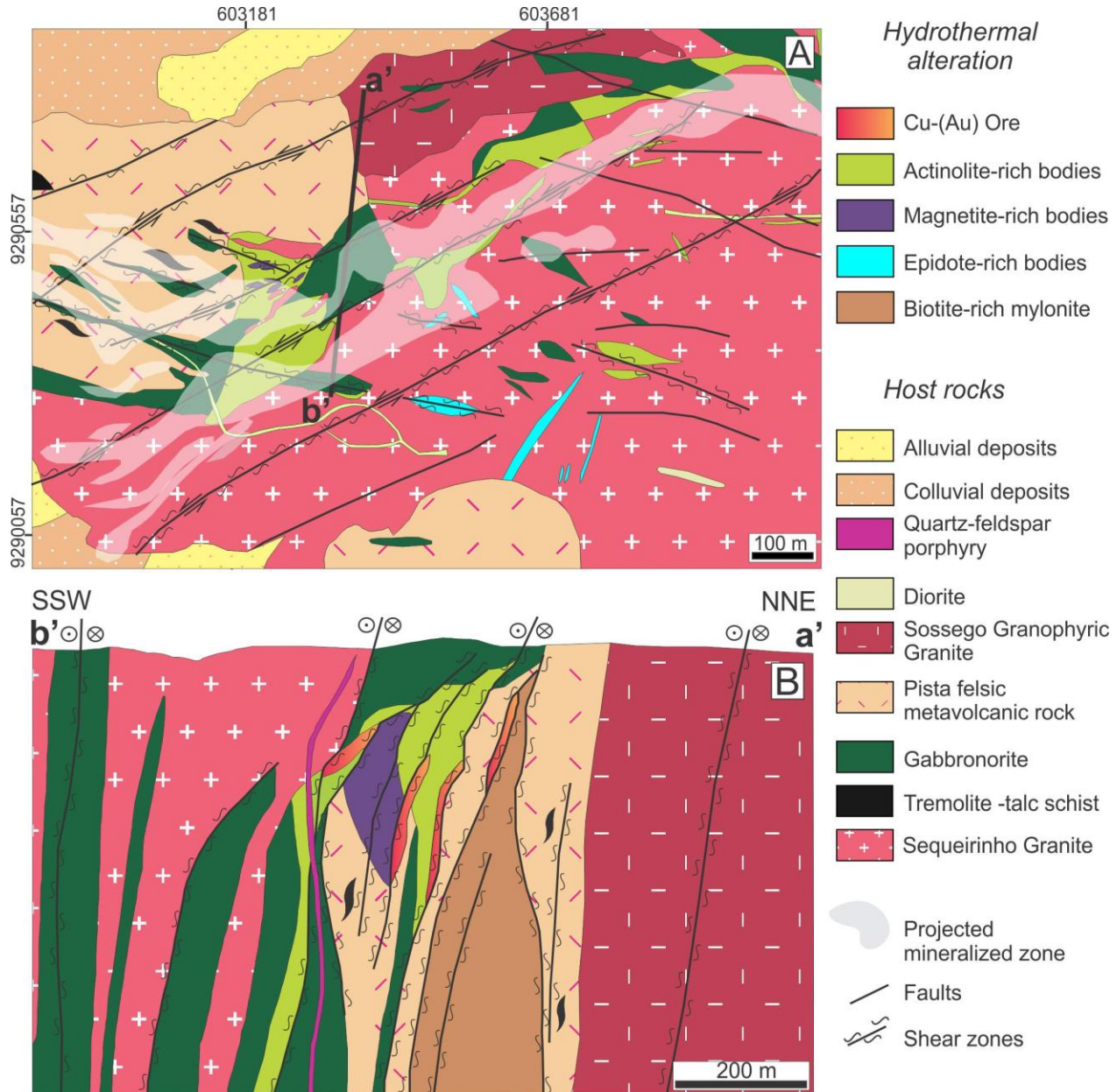


Fig. 3. A) Geological map and B) Simplified cross-section of the Sequeirinho orebody of the Sossego IOCG deposit (VALE company figure).

5.1.1 Host rocks

The Sequeirinho Granite (Figs. 4A, B and C) hosts the Sequeirinho orebody (Fig. 3), and corresponds to a WNW-ESE- trending body located along the regional ductile shear zone in

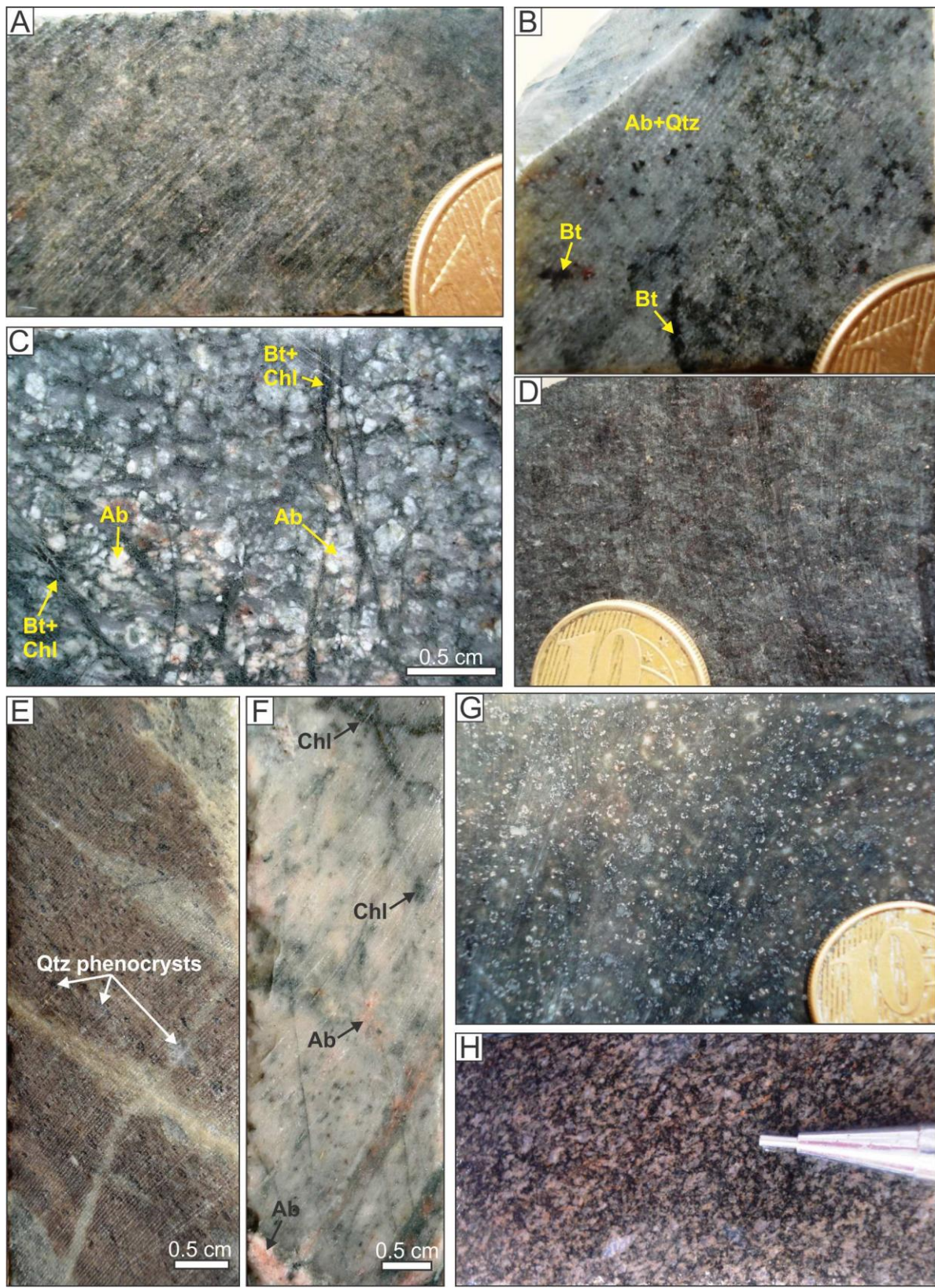
contact with mylonites and gneisses of the Xingú Complex. This granite is hydrothermally altered, deformed and shows mylonitic foliation with NW to E-W-trending with high dips to SW-S (Carvalho, 2009). The hydrothermal alteration is mainly structurally controlled by mylonitization, observed in several intervals and depths of drill holes.

Observation of weakly altered portions of the Sequeirinho Granite is difficult due to the conspicuous hydrothermal alteration, even in areas distal from the orebodies. When least altered this granite is gray, foliated (locally isotropic), fine- to medium-grained (0.4 to 4mm) with phaneritic texture, and is composed of subhedral crystals of quartz, plagioclase, alkali feldspar, biotite, and chlorite. Minor calcite, epidote, sericite and hematite can be also recognized.

Along the WNW-ESE-tending shear zone, the Sequeirinho granite shows blastomylonitic texture, with quartz ribbons and strong re-orientation of potassium feldspar. Along this crustal discontinuity, the granite is progressively affected by sodic alteration (albite). In initial stages of Na metasomatism, fractures and interstitial spaces are filled by albite, which also alters the rims of potassium feldspar grading to their completely substitution. Additionally, intense silicification accompanies the deformation, and the silicified and mylonitized granite becomes dark gray, and shows S-C structures. Epidote-rich fractures also containing albite-actinolite-magnetite-quartz-titanite-calcite cut the granite previous altered by albite and quartz. Magnetite occurs as large anhedral crystals, or in fractures associated with hematite and specularite. Late albite+magnetite veins cut the rock altered by the earlier stages of alteration (sodic).

Sampling of the Sequeirinho Granite for geochronology (U-Pb LA-ICPMS and SHRIMP IIe) was exclusively from drill cores. Least altered parts of the rock were selected, although sample SOS 22/107.45 (Fig. 4A) displays sodic (albite) and chlorite alteration, whereas samples SOS 259/177.40 (Fig. 4B) and SOS 450/13 (Fig. 4C) show sodic (albite) and potassic (biotite) alteration, respectively.

Sample SOS 22/107.45 (Fig. 4A) is gray, isotropic, medium-grained (0.2 to 5mm), inequigranular, and does not have the igneous texture recognizable due to alteration. It is composed of quartz, saussuritized plagioclase and alkali feldspar, chlorite, and hydrothermal albite with chessboard texture. Zircon occurs as an accessory phase. The sodic alteration is characterized by the replacement of igneous microcline by hydrothermal albite, which has chessboard texture in binocular microscope. Chlorite occurs as veins, filling mineral interstices, altering feldspars rims and along cleavage, and comprise approximately 30% of the granite.



« Fig. 4. Characteristic features of the host rocks of the Sequeirinho-Pista-Baiano (A-F) and Sossego-Currall orebodies (G-H). A) Sequeirinho Granite with sodic alteration (albite) and chlorite alteration (SOS 22/107.45); B) Sequeirinho Granite with sodic alteration (albite-hematite) and incipient potassic alteration (biotite) (SOS 259/177.40); C) Sequeirinho Granite with silicification and fissure-style chlorite alteration (SOS 450/13); D) clinopyroxene norite from the Sequeirinho orebody with sodic-calcic alteration (hastingsite) (SOS 35); E) Pista Metavolcanic rock with sodic alteration (albite) and silicification defining the mylonitic foliation (SOS 364/138.35); F) Pista Metavolcanic rock with pervasive albite-quartz alteration and chlorite alteration in veins (SOS 475/167); G) Sossego granophyric granite with hydrolytic alteration consisting of muscovite-chlorite-hematite-epidote (SOS 35/406); H) gabbro from the Currall orebody with silicification and sodic alteration defining the mylonitic foliation (SOS 35/30). Mineral abbreviations: Ab: albite, Bt: biotite, Chl: chlorite, Qtz: quartz.

Sample SOS 259/177.40 (Fig. 4B) is more preserved from hydrothermal alteration than sample SOS 22/107.45, and has its igneous texture recognizable. It is light gray, isotropic, equigranular and medium-grained (0.8 to 4mm). The rock is composed of quartz, intensively saussuritized alkali feldspar and plagioclase, hydrothermal biotite, and minor chlorite, epidote, allanite, titanite, clinozoisite and zircon. The biotite (10%) alters the feldspar rims, occurs in internal fractures and cleavages, and in mineral interstice. The feldspar are also altered by a late chlorite-epidote-titanite alteration.

Sample SOS 450/13 (Fig. 4C) is light gray, foliated, medium-grained, and composed of quartz, alkali feldspar and plagioclase, and hydrothermal biotite and chlorite. These two latter minerals occur as veinlets, surrounding the quartz and feldspar grains, or along the mylonitic foliation. This sample is also silicified.

Mafic intrusive rocks, mainly gabbronorites, are one of the host rocks of the Sequeirinho-Baiano orebodies as well as the Currall orebody (Fig. 2). The gabbronorite (Fig. 4D) occurs as an elongated to anastomosed body with NW-SE to E-W –trending. It is isotropic to foliated (weak to mylonitic), dark gray, phaneritic, medium- to coarse-grained (0.3 to 8 mm), and has subophitic to locally ophitic texture. It is composed of relicts of igneous pyroxene (clino- and orthopyroxene), plagioclase (labradorite and bytonite), ilmenite, magnetite, quartz, clinozoisite and hydrothermal biotite and hastingsite. Plagioclase is commonly saussuritized and/or altered to biotite. The igneous texture is identifiable even with the replacement of part of the pyroxene and plagioclase by hydrothermal biotite, hastingsite, clinozoisite and sericite.

Sample SOS 35 (Fig. 4D), classified as a clinopyroxene norite, was selected for U-Pb SHRIMP IIe geochronology. It is coarse-grained, dark gray to green and consist of pyroxene (orthopyroxene > clinopyroxene), plagioclase, hastingsite, quartz, ilmenite, epidote and apatite. It has protomylonitic foliation, and deformation was synchronous with hydrothermal alteration,

because hastingsite is deformed along the foliation and shows sigmoidal shape. Hastingsite replaces the pyroxene rims, and fills fractures that cut this mineral and plagioclase.

The Pista felsic metavolcanic rock (Figs. 4E and F) represents the main host rock of the Pista orebody, and shows anastomosed to sigmoidal shapes (Carvalho, 2009). The contact between this rock and the Sequeirinho Granite is along a NE-SW ductile shear zone. Additionally, the Pista metavolcanic rock is cut by several minor shear zones formed synchronously to the development of early stages of hydrothermal alteration, such as sodic alteration (Monteiro et al., 2008a). When least altered, this rock is isotropic to foliated, brown-pinkish, fine-grained, with porphyritic texture and aphanitic matrix (< 0.1 mm). The matrix is composed of quartz, extremely saussuritized feldspar (apparently both plagioclase and alkali feldspar), and hydrothermal biotite, sericite, and calcite. The megacrysts (0.5 to 2mm) correspond to quartz, microcline and plagioclase, and depending on the intensity of deformation, they can be euhedral to elongate along the mylonitic foliation. In some samples, the microcline megacrysts are altered to hydrothermal albite with chessboard texture. The feldspar crystals are commonly altered by biotite, which occurs initially in crystals rims but also along fractures and veinlets that cut the feldspar. In some areas, pervasive silicification controlled by the mylonitic fabric produces an alteration product of the metavolcanic rock mainly consisting of more than 85% of hydrothermal quartz.

Two samples of the Pista felsic metavolcanic rock were selected for U-Pb SHRIMP IIe geochronology. Sample SOS 364/138.35 (Fig. 4E) is foliated, brown-pinkish, and has porphyritic texture in an aphanitic matrix (< 0.1 mm). The latter is mainly composed of hydrothermal quartz (60%) and sericite (40%) with subordinate epidote. No feldspar was identified, indicating that matrix minerals are related to silicification and sericite alteration, along the mylonitic foliation. The megacrysts (0.5 to 1.5 mm) correspond to deformed quartz (weak sigmoidal shape) with undulose extinction, shadow pressure, and subgrain boundary in some crystals. Sample SOS 475/167 (Fig. 4F) is light pink, foliated, with quartz megacrysts in a fine-grained aphanitic matrix. It is composed of quartz, albite, alkali feldspar and minor chlorite. This sample is altered by pervasive albite and quartz alteration, which is cut by millimeter- to centimeter-scale veins of chlorite and albite with minor hematite.

Meter-scale lenses of meta-ultramafic rocks (tremolite-talc schist with relicts of forsterite) are found in the drill holes imbricated in the metavolcanic rock. The meta-ultramafic rock is dark

gray, fine-grained (<1 mm), with lepidoblastic texture defined by the parallel array of very fine-grained talc crystals. It is composed of talc (~ 50%), serpentine, calcite, magnetite, and tremolite. Very fine-grained talc crystals (< 0.01 mm) may show a radial texture. Millimeter-wide (0.3 to 1 mm) veinlets of tremolite or serpentine with minor magnetite and tremolite cut the rock, and locally display comb texture. Late calcite or calcite+magnetite veinlets are also recognized.

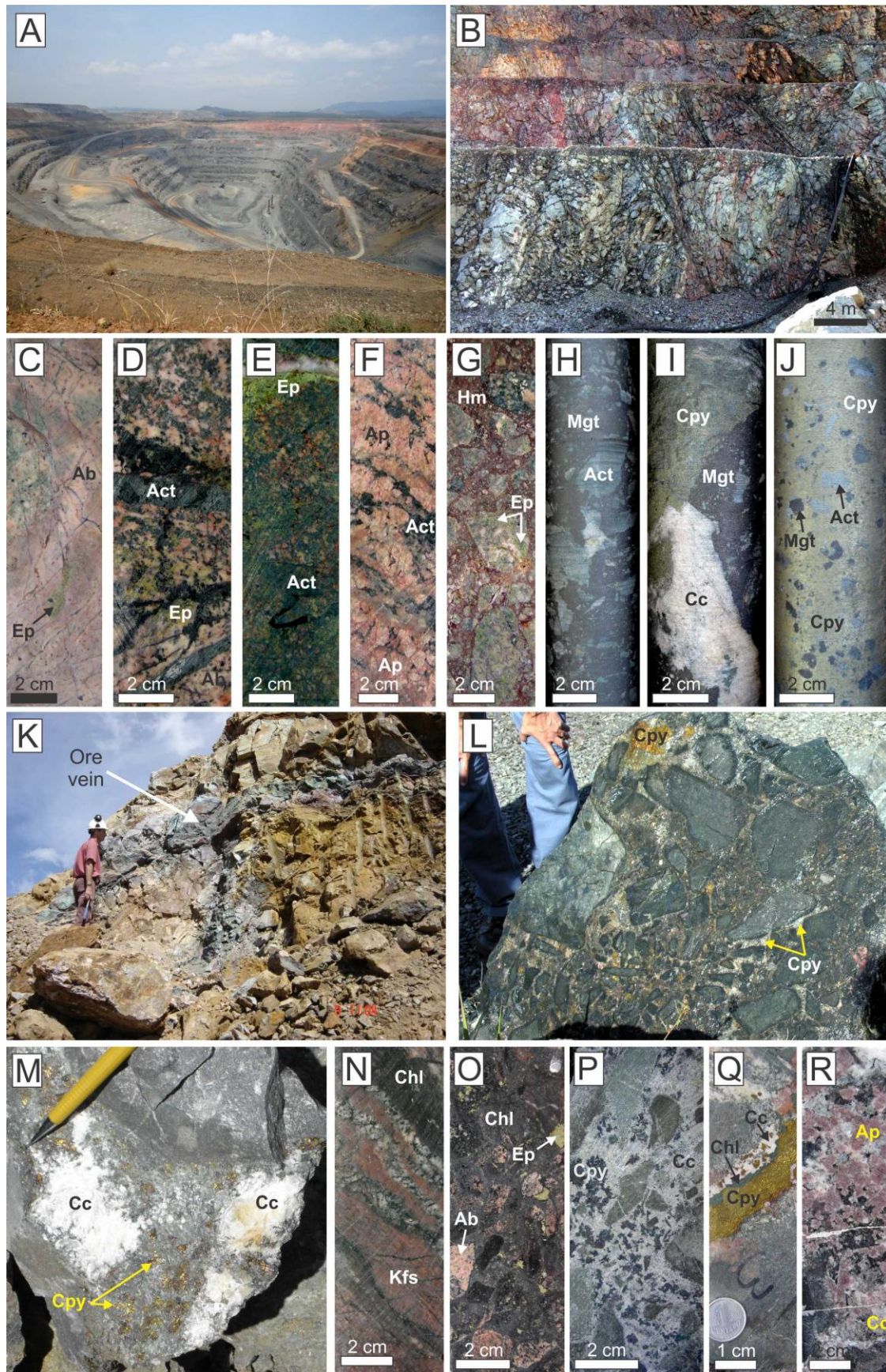
Late dacite porphyry dikes and the Paleoproterozoic Rio Branco Granite (Serra dos Carajás Intrusive Suite) crosscut the intrusive host rocks in the deposit area. Field relationship, together with the lack of hydrothermal alteration and mineralization in the dikes and in the Rio Branco Granite, indicate that they were emplaced after the copper-gold mineralization at the Sossego deposit.

5.1.2 Hydrothermal alteration

The Sequeirinho orebody (Figs. 5A-J) has undergone regional sodic (albite-hematite) (Fig. 5C) and sodic-calcic (actinolite-hastingsite-albite) alteration (Figs. 5D and E). The latter is commonly associated with massive magnetite bodies enveloped by apatite- and actinolite-rich bodies (Figs. 5F and H). These magnetite bodies are cut by relatively narrow and spatially restricted zones of potassic (biotite and potassic feldspar) alteration that form the locus for later structurally controlled, subvertical, breccia-hosted copper– gold mineralization (Monteiro et al., 2008a). The potassic alteration grades outward to also spatially restricted chlorite-rich zones.

5.1.3 Ore stage

The majority of the copper-gold mineralization in the Sequeirinho orebody was concentrated within steeply dipping bodies that contain fragments of magnetitite and actinolite-rich bodies (actinolite) within a matrix of chalcopyrite (Fig. 5J) and other hydrothermal minerals, such as actinolite, Cl-apatite, magnetite, epidote, chlorite, quartz, calcite and other sulfides (Monteiro et al., 2008a) (Fig. 5I). Chalcopyrite is the main ore mineral (>85% of the ore) and occurs associated with pyrite, gold, siegenite, millerite, Pd-melonite, hessite, cassiterite, sphalerite, and galena (Monteiro et al., 2008a,b). Sulfide mineralization is associated with a paragenetically late epidote–allanite–calcite–quartz–chlorite–(hematite–thorianite–monazite) assemblage (Monteiro et al., 2008a).



«Fig. 5. Characteristic features of hydrothermal alteration and ore, according to Monteiro et al. (in press). A-J) Sequeirinho orebody and the K-R) Sossego orebody; A) Open pit of the Sequeirinho orebody in 2009; B) View of the benches, in which the rocks are cut by shear zones and affected by sodic alteration; C) Pervasive Na-alteration characterized mainly by pinkish albite; D) Na-altered rock affected by Na-Ca alteration represented by actinolite, epidote, and albite; E) Na-Ca altered rock cut by actinolite-rich areas; F) Coarse-grained apatite crystals associated with actinolite; G) Breccia with matrix filled by hematite and fragments of Na-Ca altered rock; H) Breccia with matrix filled by magnetite and clasts of actinolite-rich rock; I) Ore containing chalcopyrite, magnetite and calcite; J) High-grade ore breccia containing clasts of magnetite and actinolite in a chalcopyrite-rich matrix; K) Wall rock of the Sossego orebody(2004) cut by chalcopyrite veins, replaced by malachite; L) Ore breccia with matrix filled by chalcopyrite and fragments of intensively chlorite- and biotite-altered rock; M) Chalcopyrite disseminations associated with calcite; N) Potassically altered rock with red potassium feldspar cut by later veins of chlorite; O) Chlorite alteration overprinting albite-rich zones from early Na alteration; P) Mineralized breccia with calcite-rich matrix (+ chalcopyrite, quartz, apatite, actinolite, chlorite) enclosing fragments of previously altered rocks (potassic alteration); Q) Chalcopyrite veins with subordinate chlorite and calcite; R) Coarse-grained apatite crystals with associated calcite. Mineral abbreviations: Ab: albite, Act: actinolite, Ap: apatite, Bt: biotite, Cc: calcite, Chl: chlorite, Cpy: chalcopyrite, Ep: epidote, Hm: hematite, Kfs: potassium feldspar, Mgt: magnetite, Qtz: quartz.

In the mineralized samples, monazite crystals are mainly included in hydrothermal apatite (Figs. 6A, B and D) and less frequently in actinolite crystals (Fig. 6B), found in the matrix of hydrothermal ore breccias. Cathodoluminescence (CL) images of apatite inclusions in chalcopyrite (Figs. 6C and D) revealed CL patterns ranging from darker green to greenish-yellow. The dark green areas have higher contents of REE³⁺ in comparison to the greenish-yellow, which are commonly recognized along the crystals edges and fractures. These lighter areas suggest apatite alteration due to the interaction with the mineralizing hydrothermal fluids, which cause remobilization of REE³⁺ and monazite precipitation. For this reason, monazite crystals are found in the most altered portions of the apatite crystals (greenish-yellow areas). Chalcopyrite involves and infills fractures in apatite crystals suggesting that apatite alteration, and monazite and chalcopyrite formation were coeval.

In the Pista orebody, sulfide mineralization occurred after a late calcic alteration that formed veins of actinolite-magnetite-epidote-apatite-calcite-(pyrrhotite). Sulfide minerals occur as disseminations along mylonitic fabric and within steeply dipping veins and stockwork breccias (Monteiro et al., 2008a). Both veins and the matrix of ore breccias contain an assemblage of chalcopyrite- (pyrrhotite-pyrite-molybdenite), but minor sphalerite, siegenite, and millerite are also recognized. In the Baiano orebody, calcite-chlorite-epidote-chalcopyrite-(albite) veins crosscutting the chlorite-altered gabbronorite form the majority of the potentially economic mineralization (Monteiro et al., 2008a).

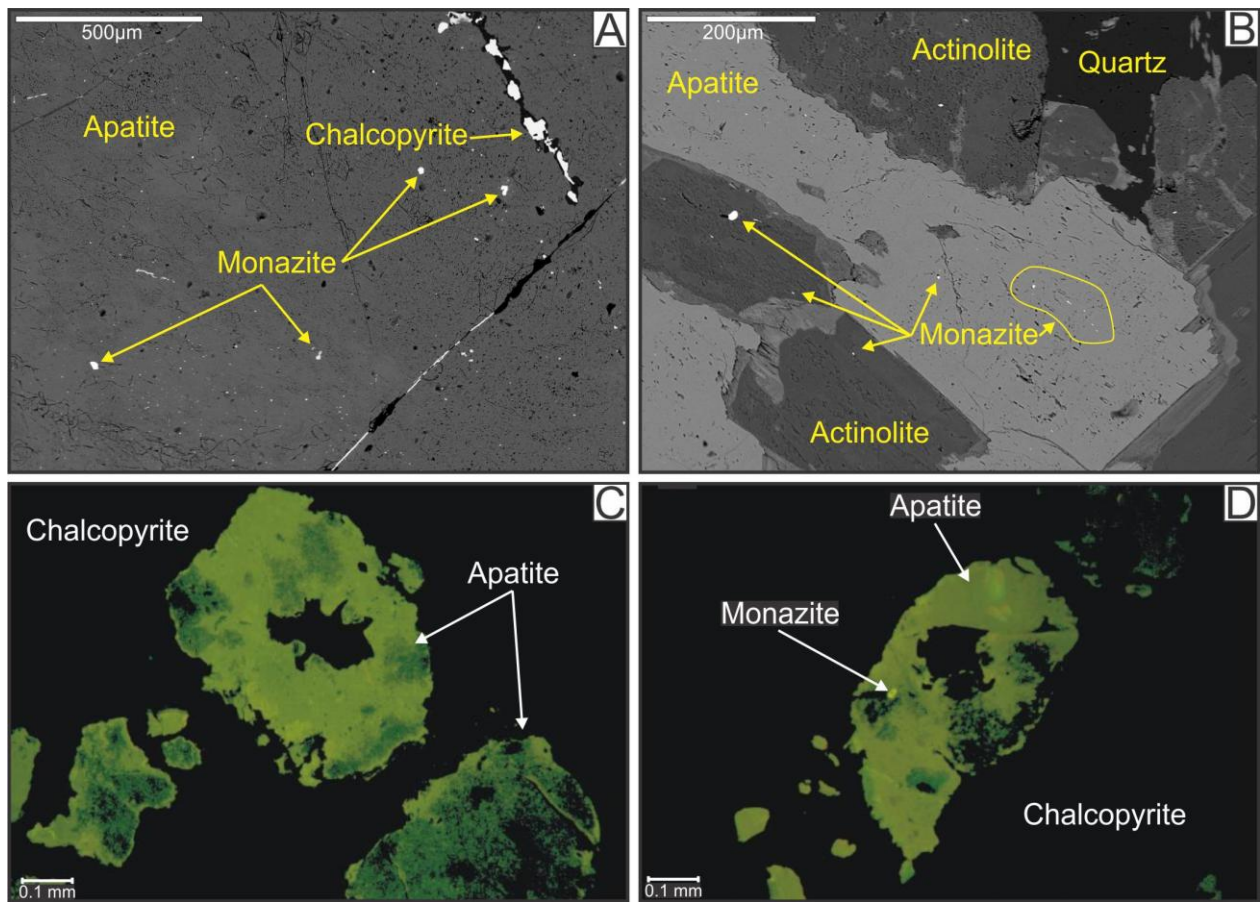


Fig. 6. BSE (A and B) and CL (C and D) images of high-grade ore breccia from the Sequeirinho orebody. A) Monazite inclusions in apatite grains; B) Monazite inclusions in apatite and actinolite crystals; C) Apatite crystals in the matrix of ore breccia; and D) Monazite inclusions in apatite crystals. Greenish-yellow areas in CL images show hydrothermally altered parts of the apatite, in which REE was removed and formed monazite crystals. Darker green areas correspond to more preserved parts of the apatite grain and black areas represent chalcopyrite.

Zircon crystals from a hydrothermal ore breccia from the Sequeirinho orebody (sample SOS 39J; Fig. 7A) was selected for U-Pb SHRIMP IIe dating. This breccia has a matrix filled by chalcopyrite with minor sulfides (e.g., pyrite, millerite and pyrrhotite), and has centimeter-scale fragments of magnetitite and actinolite rocks, formed at earlier stages of hydrothermal alteration in relation to mineralization. The intensity of the hydrothermal alteration is so extreme that all igneous features, such as mineralogy, texture and composition were completely modified.

Hydrothermal monazite from a different ore sample from the Sequeirinho orebody was chosen for U-Pb LA-MC-ICPMS geochronology. Sample SOS 259/270 (Fig. 7B) correspond to a matrix-supported ore breccia, with millimeter- to centimeter-scale fragments of actinolite, magnetite and apatite in a matrix mainly composed of chalcopyrite with subordinate quartz, epidote, calcite, allanite, and actinolite.

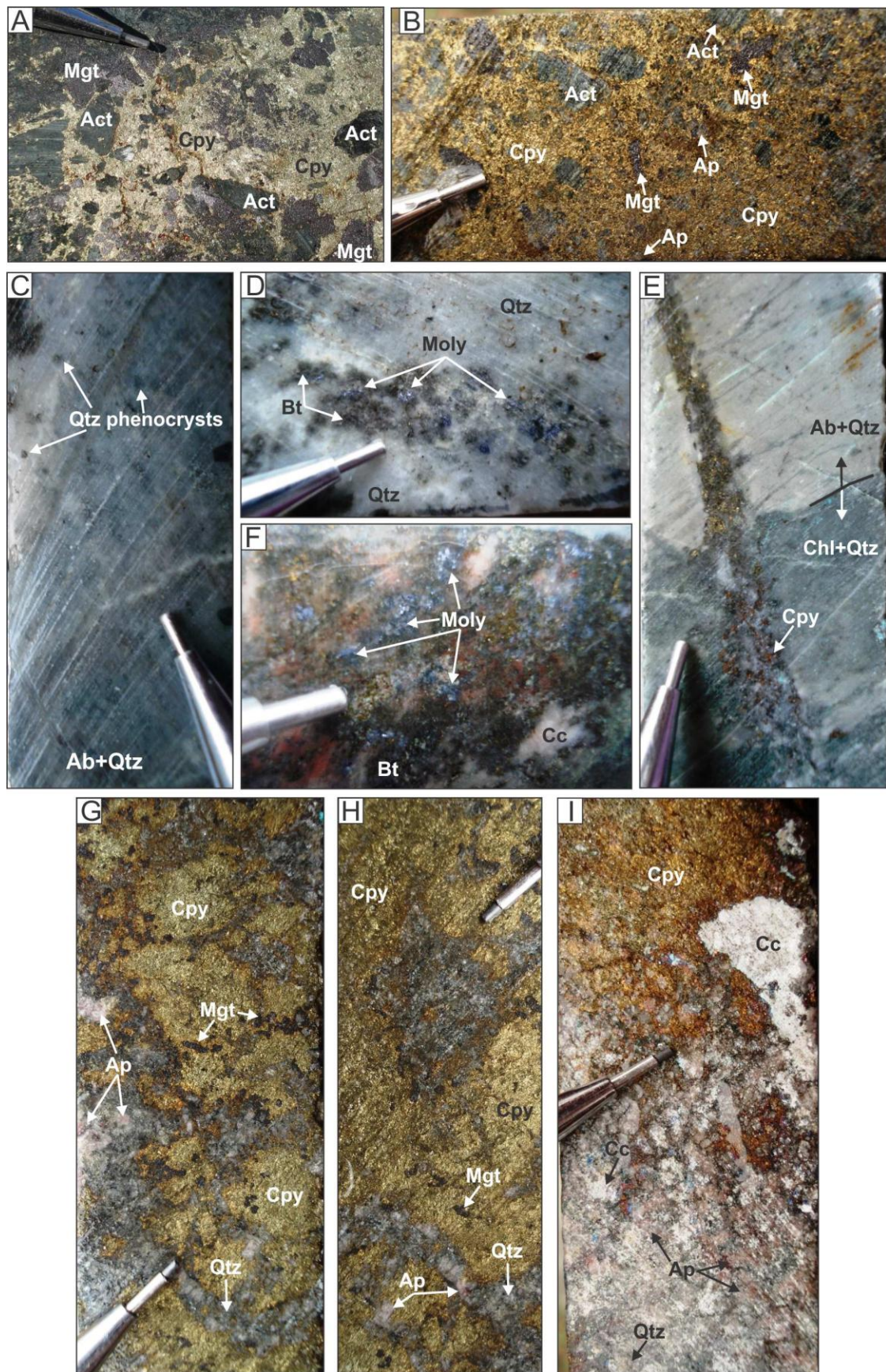
In the Pista orebody, molybdenite grains from two mineralized samples (SOS 364/76.84 and SOS 364/160.9) were selected for Re-Os NTIMS geochronology. Sample SOS 364/76.84 (Figs. 7C and D) corresponds to the Pista felsic metavolcanic rock intensively altered by pervasive sodic alteration (albite) (Fig. 7C). The igneous texture is almost completely obliterated, except for millimeter-scale quartz megacrysts that remain unaltered. Fine-grained chlorite-rich zones with subordinate quartz cut the previously altered rock (sodic alteration) and grade towards intense silicified areas, which predominates in the sample. Disseminated chalcopyrite and tourmaline are associated with chlorite and/or quartz. Fine-grained (~ 1 mm) molybdenite crystals occur with quartz from pervasive silicification and chalcopyrite disseminations.

Sample SOS 364/160.9 (Figs. 7E and F) also represents the Pista metavolcanic rock altered by albite and sericite alteration defining the mylonitic foliation, then cut by chlorite-rich zones (Fig. 7E). Silicification is not as pervasive as in the other ore sample, and rather occurs as vein and veinlets with associated chalcopyrite, albite and fine-grained disseminated molybdenite. Late millimeter-wide (<4 mm) malachite veins cut the early stages of hydrothermal alteration.

5.1.4 Nature of the hydrothermal fluids and isotopic signatures

In terms of whole rock geochemistry, ore from the Sequeirinho-Pista-Baiano is enriched in Cu–Fe–Au–Ni–Co–Pd–Se–V–P–LHEE, with low content of Ti and U. In comparison to the Sossego-Currall orebodies, Sequeirinho is relatively enriched in Co, Ni, Pd, V, and Se (Carvalho, 2009).

Stable isotope studies conducted by Monteiro et al. (2008a) concluded that the sodic-calcic alteration and the actinolitite and magnetitite bodies from the Sequeirinho orebody were formed by high-temperature hydrothermal fluids ($> 550^{\circ}\text{C}$) with oxygen isotopic composition ($\delta^{18}\text{O}_{\text{fluid}} = 6.9 \pm 0.9\text{\textperthousand}$ SMOW) (Table 2) similar to magmatic or formation/metamorphic fluids. On the other hand, the mineralization stage was associated with lower temperatures ($\sim 300^{\circ}\text{C}$) and the introduction of meteoric fluids ($\delta^{18}\text{O}_{\text{fluid}} = -1.8 \pm -3.4\text{\textperthousand}$ SMOW) (Table 2). The Baiano orebody shows a similar trend of decreasing $\delta^{18}\text{O}_{\text{fluid}}$ from early veins with magnetite $\delta^{18}\text{O}_{\text{fluid}} = 6.0 \pm 0.8\text{\textperthousand}$ to late epidote-bearing veins ($-4.2 \pm 1.2\text{\textperthousand}$, at $200 \pm 25^{\circ}\text{C}$). According to Monteiro et al. (2008a), the influx of such fluids could be related to episodic fluid overpressure, resulting in dilution and cooling of the metalliferous fluid, causing deposition of metals transported as metal chloride complexes.



«Fig. 7. Characteristic features of ore samples from the Sequeirinho-Pista-Baiano (A-F) and Sossego-Currall orebodies (G-I). A) Cu-Au ore from the Sequeirinho orebody (SOS 39J); B) Cu-Au ore from the Sequeirinho orebody (SOS 259/270); C) Pista felsic metavolcanic rock with sodic alteration (albite), chlorite alteration and silicification (SOS 364/76.84). This sample (SOS 364/76.84) contains D) molybdenite crystals associated with silicified zones; E) Pista felsic metavolcanic rock with sodic alteration (albite) cut by chlorite-rich zones (SOS 364/160.9) Sulfide veins containing F) molybdenite crystals cut the rock (SOS 364/160.9). G) Cu-Au ore from the Sossego orebody (Min-Cp-SOS); H) Cu-Au ore from the Sossego orebody (SOS 315/255.1); I) Cu-Au ore from the Currall orebody (SOS 106/84). Mineral abbreviations: Ab: albite, Act: actinolite, Ap: apatite, Bt: biotite, Cc: calcite, Chl: chlorite, Cpy: chalcopyrite, Mgt: magnetite, Moly: molybdenite, Qtz: quartz.

Sulfur isotopic compositions for the Sequeirinho ($4.6 \pm 1.6\text{\textperthousand}$; n = 15), Pista ($2.5 \pm 0.3\text{\textperthousand}$; n = 5), and Baiano ($5.6 \pm 0.5\text{\textperthousand}$; n = 2) orebodies (Table 2), determined by Monteiro et al. (2008a), are different from those of magmatic origin ($\delta^{34}\text{S} = 0 \pm 1\text{\textperthousand}$), and possibly point to a sulfur source from surface reservoirs, such as sulfate or leaching from host rocks (Monteiro et al., 2008a).

Tourmaline from the Pista orebody showed $\delta^{11}\text{B}$ (-8‰ to 11‰) consistent with mixed sources, including light boron with magmatic signature likely leached from felsic intrusive rocks, and heavy boron derived from marine evaporates (Xavier et al., 2008). Fluid origin based on $\delta^{37}\text{Cl}$ and Cl/Br isotopic data from Chiaradia et al. (2006) (Table 2) also indicate mixing of a high $\delta^{37}\text{Cl}$ magmatic fluid with $\delta^{37}\text{Cl}$ near 0‰, typical of basinal brines both in Sossego and Sequeirinho orebodies.

5.2 Sossego- Currall Orebodies

The Sossego-Currall orebodies (Figs. 2 and 8) comprise a sub-circular, vertical pipe-like orebody with a central breccia body surrounded by a stockwork array of sulfide veins, faults and shear zones (Morais and Alkmim, 2005; Monteiro et al., 2008a, Carvalho, 2009; Domingos, 2009). Unlike the Sequeirinho-Pista-Baiano orebodies, the Sossego-Currall orebodies do not show any evident link to major structures.

5.2.1 Host rock

The Sossego granophytic granite (Fig. 4G) is the main host rock of the Sossego orebody, and corresponds to a W-E –trending elongated body mainly located between the Sequeirinho Granite, at south, and mafic metavolcanic rocks of the Itacaiúnas Supergroup, at north (Fig. 2). The rock is light gray, isotropic to foliated and fine-grained (<0.1 to 2 mm). It has granophytic to

locally micrographic texture, with radial intergrowth of bluish quartz and feldspar. The granophytic granite shows euhedral megacrysts (ca. 1 mm) of quartz and feldspar in a matrix composed by quartz, alkali feldspar (microcline), plagioclase, calcite, biotite, muscovite, chlorite, hematite, epidote, allanite, and zircon. Even in more preserved samples, the feldspar megacrysts correspond to albite with chessboard texture, evidencing sodic alteration. Weak fissure-style potassic (biotite) and incipient hydrolytic (muscovite-calcite-chlorite-hematite-epidote) alteration are commonly observed altering the matrix minerals.

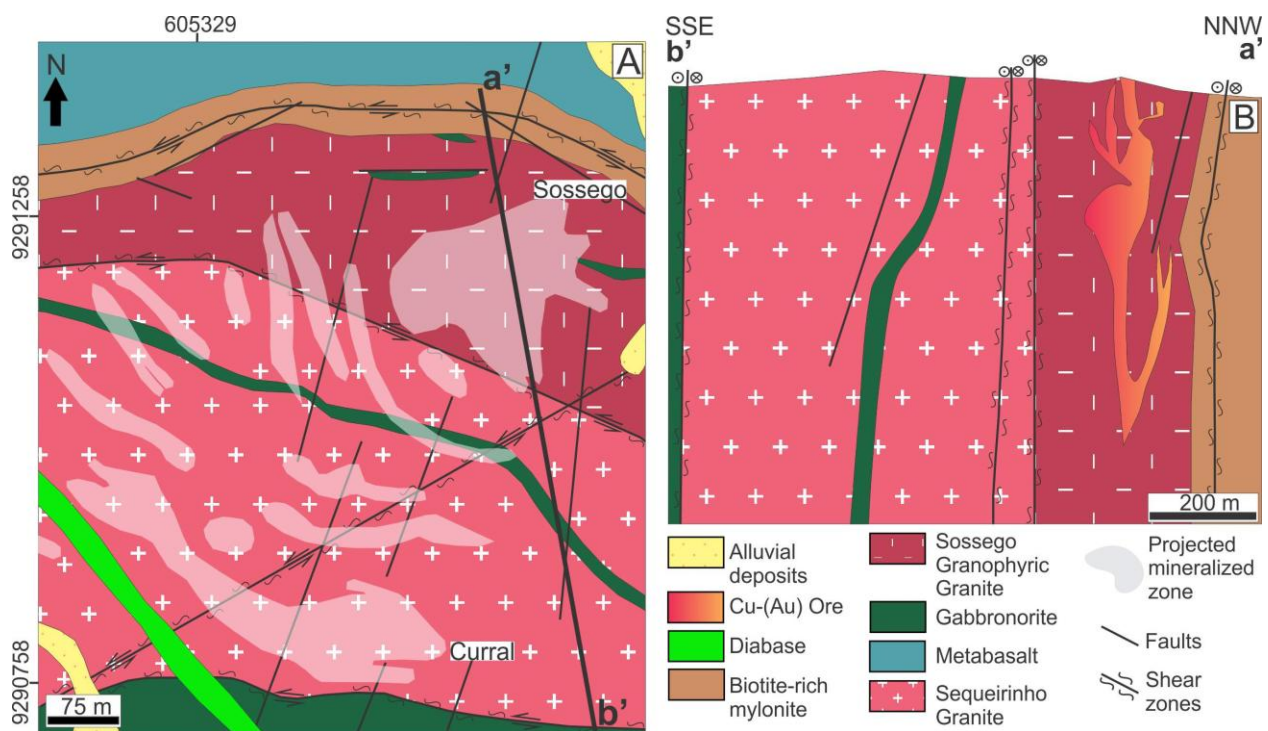


Fig. 8. A) Geological map and B) Simplified cross-section of the Sossego orebody of the Sossego IOCG deposit (modified from a VALE company figure).

The granophytic granite (sample SOS 35/406.88) (Fig. 4G) was selected for U-Pb LA-ICPMS geochronology. It is light gray, fine-grained (0.1 to 2 mm), isotropic, inequigranular, and composed of quartz, microcline, hydrothermal albite, plagioclase, chlorite, rutile, calcite, allanite, hematite, and epidote. The microcline crystals have been replaced by albite showing chessboard texture that comprises ca. 25% of total volume of the rock. Quartz crystals are anhedral, show undulose extinction, and subgrain boundaries. Smaller recrystallized grains are euhedral (0.1 mm) with uniform extinction.

As in the Sequeirinho orebody, mafic intrusive rocks (gabbro to gabbronorite) are also found in drill holes that intercept the Sossego and Curral orebodies. Sample SOS35/30 (Fig. 4H) of a hydrothermally altered gabbro from the Curral orebody, likely correlated to the gabbronorite (Fig. 4D) from the Sequeirinho orebody, was selected for U-Pb SHRIMP IIe geochronology. Sample SOS35/30 is gray, inequigranular, fine- to medium-grained (0.3 to 2 mm) and has a protomylonitic foliation. The rock is composed of quartz, plagioclase and biotite, with minor magnetite and zircon. Igneous pyroxene is not observed in thin sections, suggesting complete modification to hydrothermal biotite. The latter is also seen in the interstices of the minerals and cutting and altering the plagioclase crystals. Small euhedral hydrothermal quartz crystals (0.3 mm) and quartz ribbon along the protomylonitic foliation are also described.

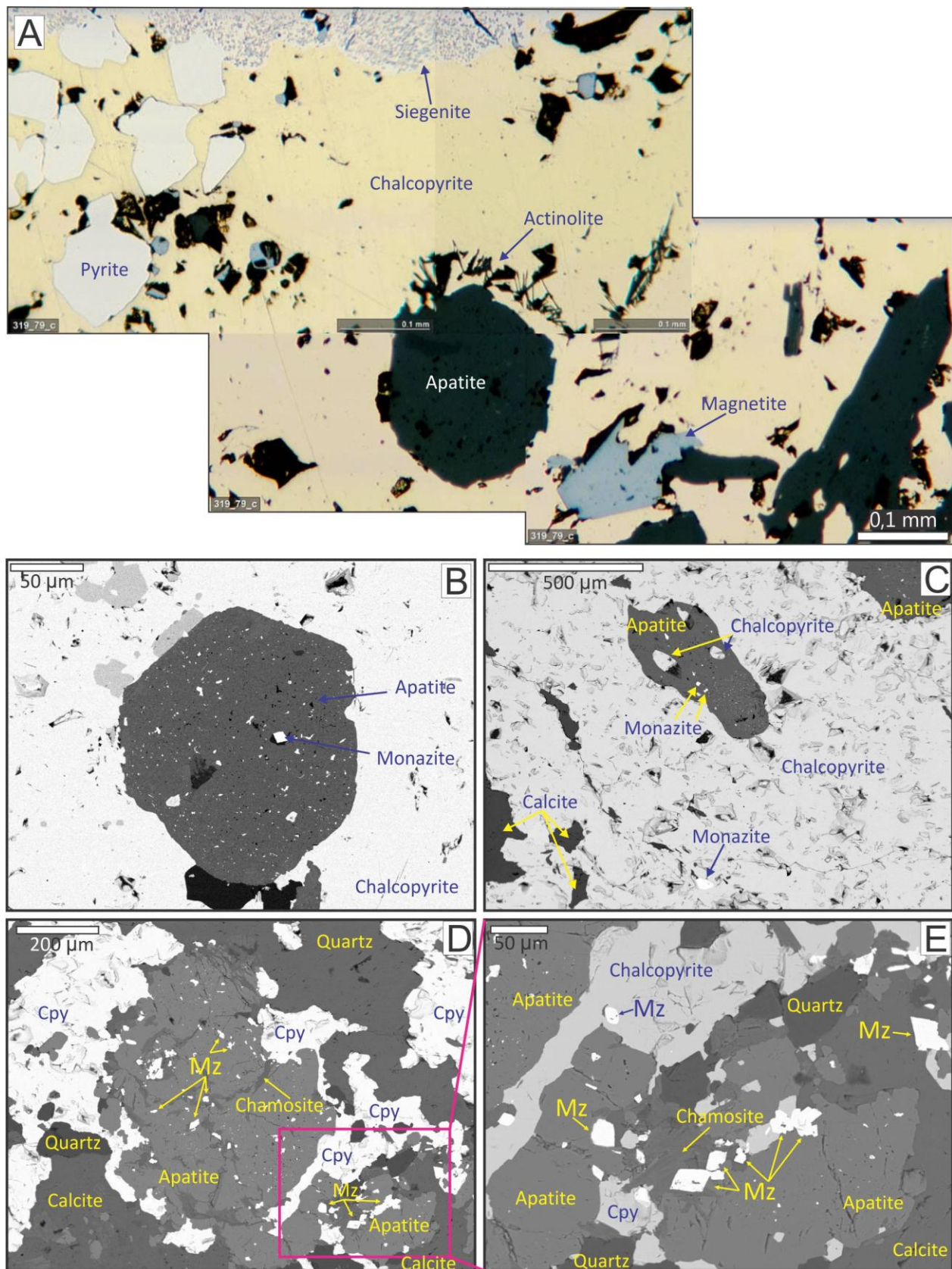
5.2.2 *Hydrothermal alteration*

In the Sossego-Curral orebodies (Figs. 5K-R), early sodic and successive sodic-calcic alteration are poorly developed, whereas potassic alteration (Fig. 5N) assemblages marks the onset of the mineralization and grades laterally outward to a widespread zone of chlorite (Fig. 5O) and late hydrolytic (sericite – hematite – quartz – chlorite – calcite) assemblages (Figs. 5M and P) (Carvalho et al., 2005; Carvalho, 2009; Monteiro et al., 2008a).

Sulfides at Sossego-Curral are largely restricted to subvertical breccia that contains open vugs. The dominance of potassic and chlorite alteration (Fig. 5Q) and the presence of hydrolytic alteration assemblages, together with the evidence for open space filling of porosity in the ore breccias, suggest that Sossego– Curral was formed at structurally higher levels in comparison to the Sequeirinho orebody (Monteiro et al., 2008a).

5.2.3 *Ore stage*

Mineralization at Sossego–Curral occurs within vein and breccia bodies (Fig. 5L). In plan view (Fig. 8), the breccia bodies (Fig. 9) are circular in shape and their contacts with host rocks are sharp, although marked by occurrence of mineralized vein networks related to radiating fracture patterns (Monteiro et al., 2008a). Sulfides consist of chalcopyrite and pyrite, with lesser siegenite, millerite, hessite, Pd–melonite, molybdenite, and galena. Magnetite, Cl-apatite (Fig. 5R), actinolite, and minor cassiterite, ilmenite and monazite are also recognized (Fig. 9). Gold occurs as inclusions within chalcopyrite.



«Fig. 9. Characteristic features of the Sossego (A and B) and Curral (C to E) high-grade ore breccia. A) Ore and ore-related minerals, such as chalcopyrite, pyrite, magnetite, actinolite, apatite and siegenite. Reflected light; B) Euhedral inclusions of monazite inside an apatite crystal; C) D) and E) Monazite inclusions in apatite and chalcopyrite crystals within the matrix of ore breccia. Photos B to E are backscattered electron (BSE) images. Mineral abbreviations: Cpy: chalcopyrite, Mz: monazite.

Magnetite, apatite and actinolite formed earlier than chalcopyrite show intense alteration patterns. Like in Sequeirinho ore, intensively altered portions of the Cl-apatite crystals contain inclusions of monazite (Fig. 9), amorphous silica, and iron oxides/hydroxides. During the alteration of Cl-rich apatite by the mineralizing fluids, REE³⁺ is remobilized and reprecipitated to form monazite crystals. Excesses of REE and Si are incorporated in epidote and quartz, respectively, formed in the borders of apatite. Monazite may also occur as inclusions in chalcopyrite (Figs. 9C and E) that fills the matrix of copper breccia.

Monazite from two samples of high-grade copper ore from the Sossego orebody (Min-Cp-SOS and SOS315/255.1) were selected for U-Pb LA-MC-ICPMS geochronology. Sample Min-Cp-SOS (Fig. 7G) is a matrix-supported breccia, with a chalcopyrite-rich matrix, which comprises approximately 80 to 85 percent of the rock. Angular to sub-rounded centimeter-wide fragments of the host granophytic granite are observed. Most of the rock fragments were affected by potassic alteration (mainly with biotite) before brecciation. Sample SOS315/255.1 (Fig. 7H) is a predominant clast-supported breccia, with centimeter-wide apatite crystals up to 1 cm in length. The matrix is composed of fine-grained angular hydrothermal apatite-quartz-actinolite assemblage. The sulfide, mainly chalcopyrite, partially fills the breccia matrix.

For the Curral orebody, monazite grains from a high-grade copper ore were also selected for U-Pb LA-MC-ICPMS geochronology. Sample SOS106/84 (Fig. 7I) corresponds to a matrix-supported ore breccia mainly composed of small fragments (> 0.4 cm) of apatite, albite, quartz, and calcite. Chalcopyrite in equilibrium with calcite infills the breccia matrix.

The ore breccias from the Sossego-Curral bodies have a geochemistry signature showing enrichment in Cu–Fe–Au–Ni–Co–Pd–Se–V–P–LHEE (Carvalho, 2009). In comparison to the Sequeirinho orebody, Sossego-Curral is relatively enriched in Au, Pb, Sn, Rb, Y, and Nb.

5.2.4 Nature of the hydrothermal fluids and isotopic signatures

The oxygen isotopic composition and temperatures of the hydrothermal fluids (Table 2) responsible for the genesis of the Sossego-Curral orebodies are similar to those of the

Sequeirinho-Pista-Baiano orebodies (Monteiro et al., 2008a). Minerals formed in the early stages of hydrothermal alteration (e.g., magnetite and actinolite) show $\delta^{18}\text{O}_{\text{fluid}}$ ($8.4 \pm 0.9\text{\textperthousand}$ and $5.5 \pm 1.3\text{\textperthousand}$ SMOW, respectively; 400°C) consistent with magmatic origin (Monteiro et al., 2008a). Lower temperature fluids ($\sim 275^\circ\text{C}$) with also lower $\delta^{18}\text{O}_{\text{fluid}}$ ($1.9 \pm 1.7\text{\textperthousand}$ and $0.4 \pm 1.0\text{\textperthousand}$ SMOW) are associated with the ore stage and related to the introduction of meteoric waters in the systems. This caused dilution and cooling of the metalliferous fluid, leading to metal deposition (Monteiro et al., 2008a).

Sulfur isotopic compositions for the Sossego-Currall orebodies ($^{34}\text{S} = 5.7 \pm 1.9\text{\textperthousand}$; $n = 25$) (Table 2) are heavier to those of the Sequeirinho-Pista-Baiano orebodies (Monteiro et al., 2008a) and could reflect a major sulfur input from surface reservoirs, rather than from magmatic sources (Monteiro et al., 2008a).

Fluid inclusion studies in quartz from ore breccia from Sequeirinho, Pista, and Sossego orebodies (Carvalho, 2009), point to involvement of: (1) high-temperature ($> 500^\circ\text{C}$) hypersaline brines (35 to 70% NaCl equiv.; $T_{\text{ht}} = 570$ a 250°C); (2) low-temperature ($\sim 150^\circ\text{C}$) CaCl_2 -rich saline brines (11 a 31% NaCl equiv.); and (3) low temperature ($< 250^\circ\text{C}$), and low- salinity ($< 11\%$ NaCl equiv.) aqueous fluids (Rosa, 2006; Carvalho, 2009). The CaCl_2 -rich saline brines could reflect the evolution of hypersaline magmatic or basin fluids (Carvalho, 2009), or metamorphic fluids that interacted with metaevaporites or metaexhalites becoming more saline (Rosa, 2006). The low salinity fluids could evidence the input of meteoric fluids in the hydrothermal system.

6. U-Pb and Re-Os Results

The isotopic data obtained in this study by different methods is summarized in Table 3.

Table 3 Synthesis of geochronological data for the Sequeirinho, Pista, Sossego and Curral orebodies

<i>Rock</i>	<i>Mineral</i>	<i>Method</i>	<i>Age (Ma)</i>	<i>MSWD</i>
<i>Sequeirinho Orebody</i>				
<i>Host rocks</i>				
Sequeirinho Granite (SOS 259/177.4)	zircon	U-Pb LA-ICPMS	$3,010 \pm 21$	0.81
Sequeirinho Granite (SOS 22/107.45)	zircon	U-Pb LA-ICPMS	$3,014 \pm 22$	2.5
Sequeirinho Granite (SOS 450/13)	zircon	U-Pb SHRIMP IIe	$2,989 \pm 5.2$	3.5
gabbronorite (SOS 35)	zircon	U-Pb SHRIMP IIe	$2,739 \pm 5.9$	1.4
<i>Ore</i>				
Ore breccia (SOS 39J)	zircon	U-Pb SHRIMP IIe	$3,076 \pm 5.3$	1.5
Ore breccia (SOS 259/270)	monazite	U-Pb LA-MC-ICPMS	$2,712.3 \pm 4.7$	1.6
<i>Pista Orebody</i>				
<i>Host rocks</i>				
Pista felsic metavolcanic rock (SOS 364/138.35)	zircon	U-Pb SHRIMP IIe	$2,968 \pm 15$	10.7
Pista felsic metavolcanic rock (SOS 475/167)	zircon	U-Pb SHRIMP IIe	$2,979 \pm 5.3$	0.28
<i>Ore</i>				
silicified Pista metavolcanic rock (SOS 364/76.84)	molybdenite	Re-Os NTIMS	$2,685 \pm 11$	
Na altered Pista metavolcanic rock (SOS 364/160.9)	molybdenite	Re-Os NTIMS	$2,710 \pm 11$	
<i>Sossego Orebody</i>				
<i>Host rocks</i>				
Sossego granophyric granite (SOS 35/406.88)	zircon	U-Pb LA-ICPMS	$2,740 \pm 26$	11.4
<i>Ore</i>				
Ore breccia (Min-Cp-SOS)	monazite	U-Pb LA-MC-ICPMS	$1,878.9 \pm 4.1$	1.3
Ore breccia (SOS 315/255.1)	monazite	U-Pb LA-MC-ICPMS	$1,904 \pm 5.2$	1.2
<i>Curral Orebody</i>				
<i>Host rocks</i>				
gabbro (SOS 35/30)	zircon	U-Pb SHRIMP IIe	$2,739.1 \pm 4.2$	2.1
<i>Ore</i>				
Ore breccia (SOS 106/84)	monazite	U-Pb LA-MC-ICPMS	$1,889.8 \pm 8.5$	2.7

6.1 Sequeirinho orebody

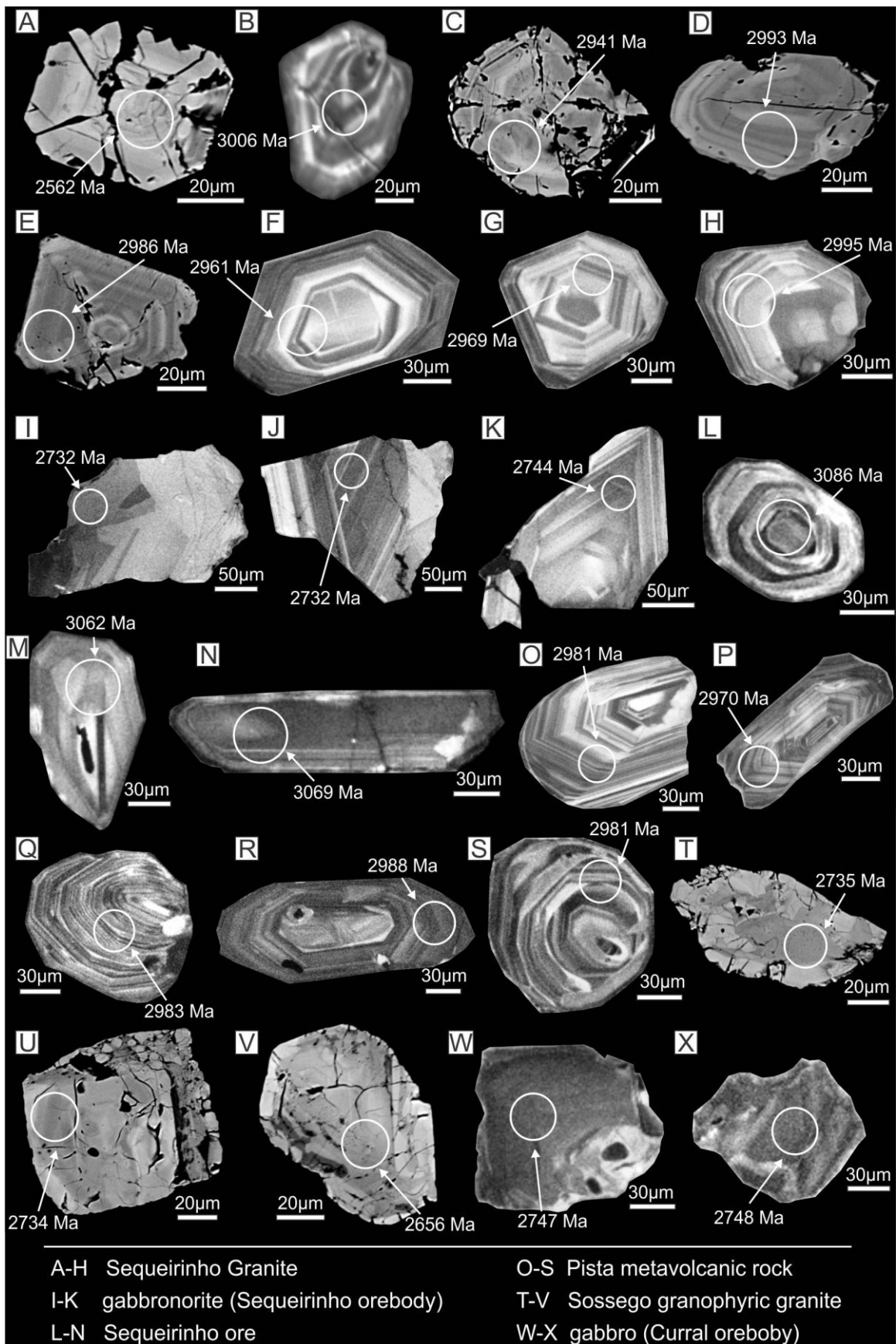
6.1.1 Host rocks

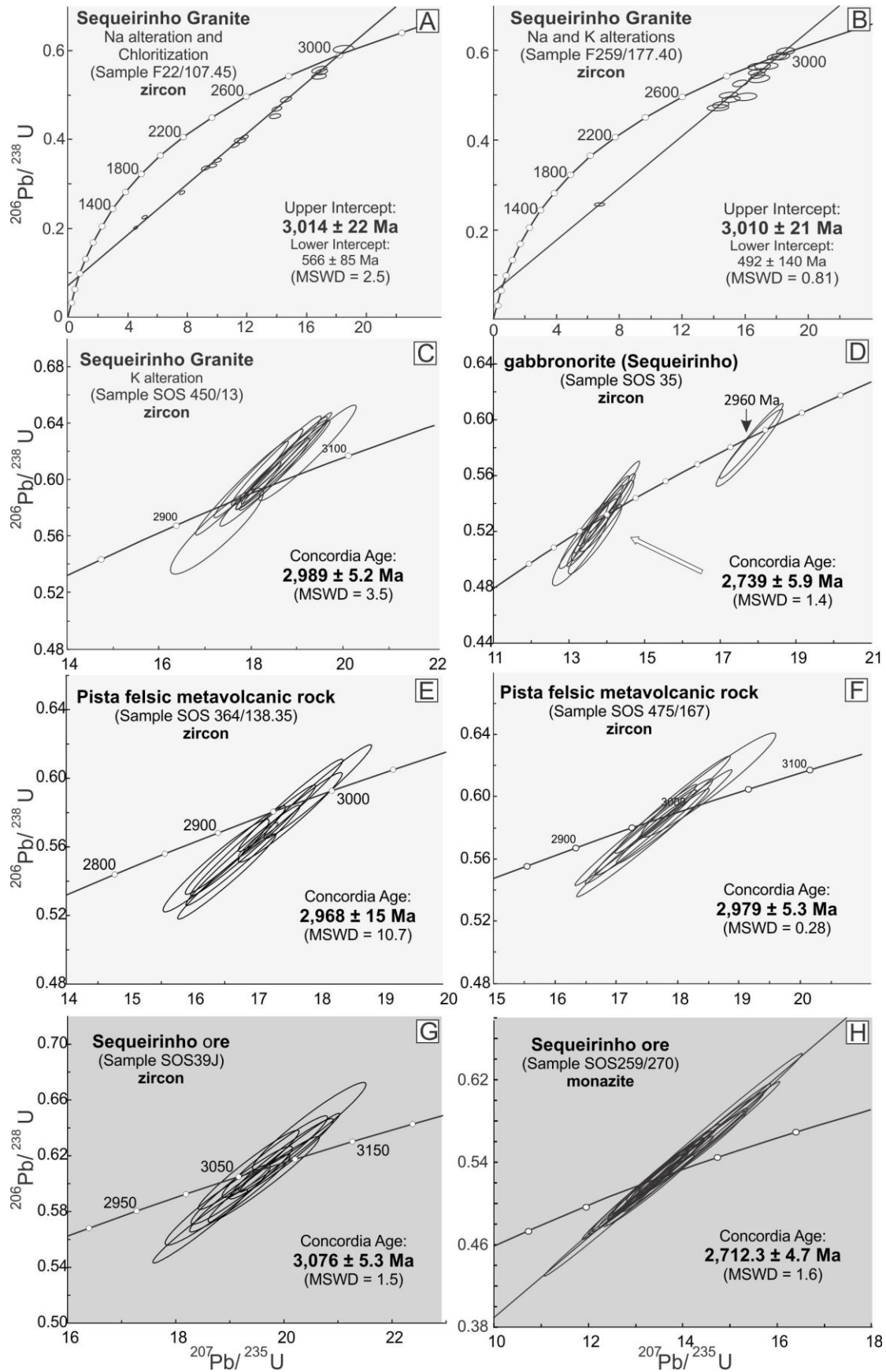
Zircon grains from the Sequeirinho Granite (samples SOS 22/107.45, SOS 259/177.40 and SOS 450/13; Figs. 4A, B and C, respectively) are dark pink, with crystal lengths ranging from 60 to 180 μm , and aspect ratios (length/width) from 1:1 to 4:1. The CL and BSE images (Figs. 10A-H) show that the zircon grains are more pyramidal than prismatic, with some rounded terminations. Some grains display prominent oscillatory zoning (Figs. 10B, D and F-H)

commonly attributed to magmatic crystallization (Vavra, 1990), although other grains show weakly – to blurred - oscillatory zoning (Figs. 10A and C), which could evidence potential physical and chemical disturbance. Partial to total metamict character is evidenced by abundant inclusions and internal fractures (Figs. 10A, C and E). Th/U ratios range from 0.31 to 0.54 with a mean value of 0.42 (SOS 22/107.45), 0.19 to 0.58 with a mean value of 0.36 (SOS 259/177.40), and 0.28 to 0.76 with a mean value of 0.42 (SOS 450/13). In sample SOS 22/107.45, sixteen spot U-Pb LA-ICPMS analyses yielded a discordant result with a projected upper intercept age of $3,014 \pm 22$ Ma and a projected lower intercept age of 566 ± 85 Ma (MSWD = 2.5; Fig. 11A, Supplementary Table 1). The fifteen U-Pb LA-ICPMS spot analyses from sample SOS 259/177.40 yielded an upper intercept age of $3,010 \pm 21$ Ma, and a projected lower intercept age of 492 ± 140 Ma (MSWD = 0.81; Fig. 11B, Supplementary Table 1). In sample SOS 450/13, ten U-Pb SHRIMP IIe spot analyses provided the concordia age of $2,989 \pm 5.2$ Ma (MSWD= 3.5; Fig. 11C, Supplementary Table 2).

Zircon grains from the gabbro (sample SOS 35; Fig. 6D) are intensely pink, euhedral, with aspect ratios (length/width) around 1.5:1, and crystal lengths ranging from 50 to 150 μm . CL images (Figs. 10I-K) show that the grains are more pyramidal than prismatic, and have sector zoning (Fig. 10I) and concentric oscillatory zoning in some zircon fragments (Figs. 10J and K). In some grains, textureless areas with brighter colors due to smaller U contents overprint areas with complex zoning patterns. This could indicate modification of zircon in a post magmatic stage. Th/U ratios vary from 0.22 a 0.63 with a mean value of 0.40. Ten concordant U-Pb SHRIMP IIe analyses rendered a concordia age of $2,739 \pm 5.9$ Ma (MSWD = 1.4; Fig. 11D, Supplementary Table 2). Moreover, two inherited grains were analyzed and provided the concordia age of 2,960 Ma.

»Fig. 10. BSE and CL images of zircon of the host rocks and ore samples of the Sequeirinho-Pista-Baiano orebodies (A-S) and host rocks of the Sossego-Currall (T-X) orebodies. $^{207}\text{Pb}/^{206}\text{Pb}$ ages are indicated in the image where analyses were done. A and C) BSE and B) CL images of zircon from the Sequeirinho Granite (SOS 22/107.45); D-E) BSE images of zircon from the Sequeirinho Granite (SOS 259/177.40); F-H) CL images of zircon from the Sequeirinho Granite (SOS 450/13); I-K) CL images of zircon from gabbro from the Sequeirinho orebody (SOS 35); L-N) CL images of zircon from Sequeirinho ore (SOS 39J); O-P) CL images of zircon from the Pista Metavolcanic rock (SOS 475/167); Q-S) CL images of zircon from the Pista Metavolcanic rock (SOS 364/138.35); T-V) BSE images of zircon from the Sossego granophytic granite (SOS 35/406); W-X) CL images of zircon from gabbro from the Currall orebody (SOS 35/30).





«Fig. 11. $^{206}\text{Pb} / ^{238}\text{U}$ vs. $^{207}\text{Pb} / ^{235}\text{U}$ diagrams for the Sequeirinho-Pista-Baiano host rocks (A-F; gray diagrams) and ore (G-H; yellow diagrams). A) Sequeirinho Granite with sodic and chlorite alterations (SOS 22/107.45); B) Sequeirinho Granite with sodic and potassic alterations (SOS 259/177.40); C) Sequeirinho Granite with potassic alteration (SOS 450/13); D) gabbronorite from the Sequeirinho orebody (SOS 35); E) Pista Metavolcanic rock (SOS 364/138.35); F) Pista Metavolcanic rock (SOS 475/167); G) Sequeirinho ore (SOS39J); H) Sequeirinho ore (SOS 259/270). In all the host rocks (A-F) and ore sample SOS 39 J (G) zircon was the analyzed mineral. In the Sequeirinho ore sample SOS 259/270 (H) monazite was analyzed.

6.1.2 Ore samples

Zircon grains from the ore breccia of the Sequeirinho orebody (sample SOS 39J; Fig. 7A) are light pink, euhedral and have pyramidal to prismatic forms with round terminations in a few cases. The aspect ratios (length/width) of the crystals are around 1:1 to 5:1, with crystal lengths ranging from 40 to 200 μm . The common zoning patterns are the concentric oscillatory and the sector zoning (Figs. 10L and M), although textureless areas are also recognize in CL images (Fig. 10N). The Th/U ratios of zircon grains from breccia sample SOS 39J range from 0.51 to 0.94, with a mean value of 0.72. The zircon grains were analyzed by the U-Pb SHRIMP IIe, and produced ten analyses, resulting in a concordia age of $3,076 \pm 5.3$ Ma (MSWD = 1.5; Fig. 11G, Supplementary Table 2).

Monazite grains from the other ore breccia from the Sequeirinho orebody (sample SOS 259/270; Fig. 7B) are light yellow with only minor inclusions. Crystals tend to be more rounded and range from 30 to 150 μm , with aspect ratios (length/width) around 1:1 to 1.5:1. Twenty nine U-Pb LA-MC-ICPMS spot analyses in nineteen grains provided a concordia age of $2,712.3 \pm 4.7$ Ma (MSWD=1.6; Fig. 11H, Supplementary Table 3).

6.2 Pista orebody

6.2.1 Host rocks

The zircon grains from the Pista Metavolcanic rock (samples SOS 364/138.35 and SOS 475/167; Figs. 4E and F, respectively) are pink, euhedral, some are prismatic with pyramidal terminations, whereas others are ovoid with rounded or flat terminations. The concentric oscillatory zoning is well-defined (Figs. 10O-S). The crystal lengths vary from 60 to 200 μm , and aspect ratios (length/width) from 1:1 to 3:1. The Th/U ratios vary from 0.39 to 0.84 with a mean value of 0.61. Zircon grains from both samples were analyzed by U-Pb SHRIMP IIe. In sample SOS 364/138.35, nine analyses yielded a concordia age of $2,968 \pm 15$ Ma (MSWD = 10.7; Fig.

11E, Supplementary Table 2), whereas ten spot analyses in zircon grains from sample SOS 475/167 provided the $2,979 \pm 5.3$ Ma age (MSWD = 0.28; Fig. 11F, Supplementary Table 2).

6.2.2 Ore samples

In the two molybdenite samples (SOS 364/76.84, Figs. 7C and D; SOS 364/160.9, Figs. 7E and F) from the Pista orebody, the Re abundances vary significantly, and is considerably lower in sample SOS 364/160.9 (7.8 ppm), in comparison to the 107.6 ppm measured from sample SOS 364/76.84. One analysis of molybdenite grains from sample SOS 364/76.84 yielded a Re-Os age of $2,685 \pm 11$ Ma, whereas sample SOS 364/160.9 yielded a Re-Os age of $2,710 \pm 11$ Ma (Table 4).

Table 4 Summary of Re-Os molybdenite data from the Pista orebody

Re (ppm)	$\pm 2\sigma$	^{187}Re (ppb)	$\pm 2\sigma$	^{187}Os (ppb)	$\pm 2\sigma$	Total common Os (pg)	Age (Ma)	$\pm 2\sigma$ with λ (Ma)
<i>Molybdenite from silicified Pista felsic metavolcanic rock (SOS364/76.84)</i>								
107.6	0.3	67,650	174	3,095	2	2.2	2,685	11
<i>Molybdenite from Na altered Pista felsic metavolcanic rock (SOS364/160.9)</i>								
7.831	0.02	4,922	13	227.3	0.2	10.1	2,710	11

6.3 Sossego-Curral orebodies

6.3.1 Host rocks

Zircon grains from the Sossego granophyric granite (sample SOS 35/406.88; Fig. 4G) are pink and have many fractures and inclusions, evidencing partial to total metamictization. Zircon grains are subhedral, with crystal lengths ranging from 40 to 100 μm , and aspect ratios (length/width) around 2:1. Oscillatory zoning patterns are weak to blurred (Figs. 10T-V), similar to those of the Sequeirinho Granite. Xenocrystic cores can be identified in some zircon grains, and they appear darker than the surrounding rim in CL images (Fig. 10T), indicating larger U content. Th/U ratios range from 0.16 to 0.97 with a mean value of 0.43. The zircon grains produced thirteen U-Pb LA-ICPMS analyses, resulting in an upper intercept age of $2,740 \pm 26$ Ma and a projected lower intercept age of 444 ± 67 Ma (MSWD = 11.4; Fig. 12A, Supplementary Table 1).

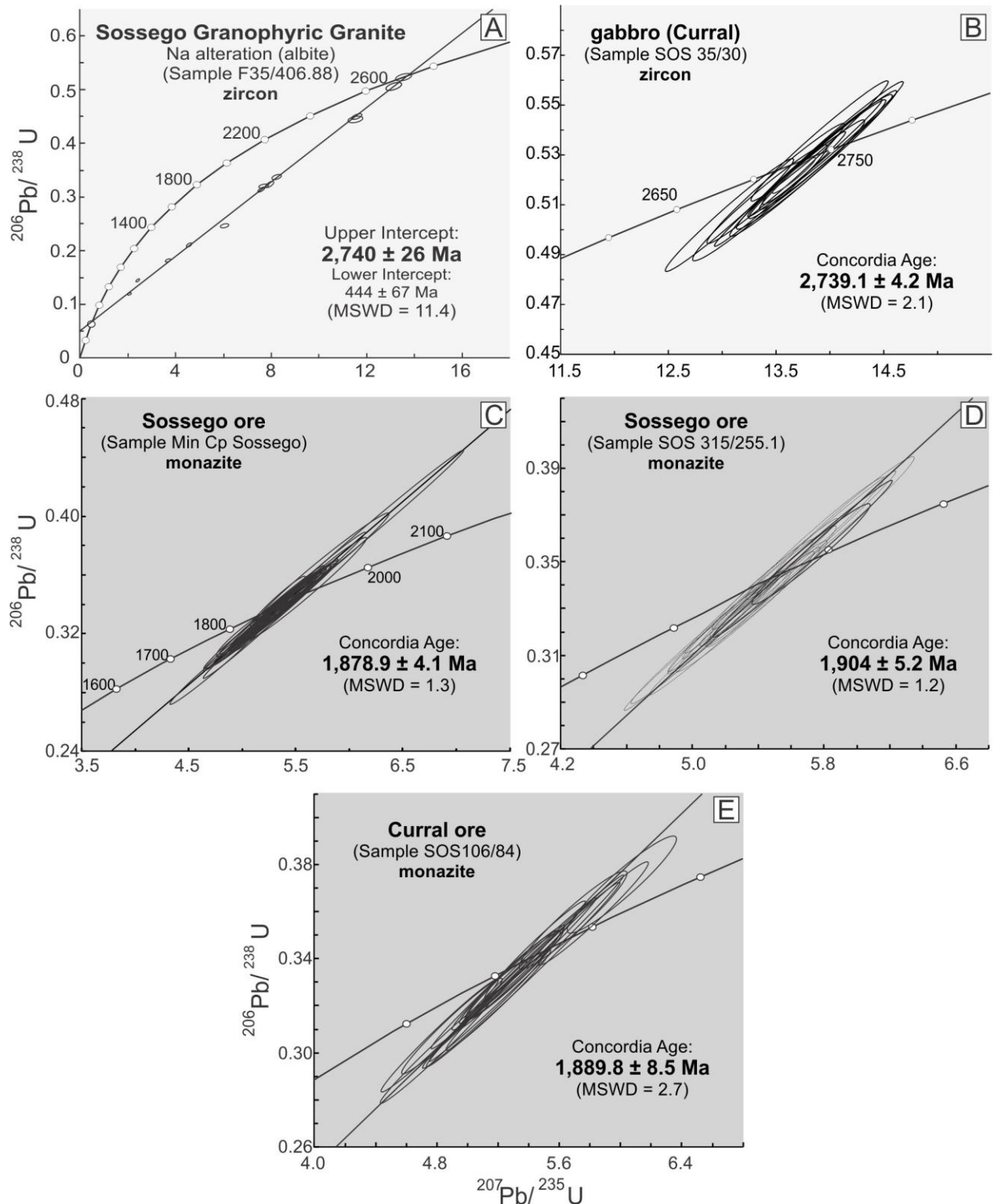


Fig. 12. $^{206}\text{Pb}/^{238}\text{U}$ vs. $^{207}\text{Pb}/^{235}\text{U}$ diagrams for the Sossego-Curral host rocks (A and B; gray diagrams) and ore (C-E; yellow diagrams). A) Sossego granophytic granite with sodic alteration (SOS 35/406.88); B) gabbro from the Curral orebody (SOS 35/30); C) Sossego ore (Min-Cp-SOS); D) Sossego ore (SOS 315/255.1); E) Curral ore (SOS 106/84). In both host rocks (A and B), zircon was the analyzed mineral, whereas in the ore samples (C-E) monazite was analyzed

Zircon grains from the gabbro from the Curral orebody (sample SOS35/30; Fig. 4H) are pinky brown, euhedral to subhedral, pyramidal with irregular terminations in some cases. Crystal lengths range from 40 to 170 µm, with aspect ratios (length/width) from 1:1 to 2:1. Some grains have poorly developed oscillatory zoning (Figs. 10W and X), whereas others have a sector and complex zoning patterns. Th/U ratios range from 0.26 to 1.32 with a mean value of 0.77. Eleven U-Pb SHRIMP IIe spot analyses in zircon from sample SOS 35/30 provided a concordia age of $2,739.1 \pm 4.2$ Ma (MSWD = 2.1; Fig. 12B, Supplementary Table 2). This age is identical to the one obtained for the gabbronorite from the Sequeirinho orebody (sample SOS 35; Fig. 11D), and confirms their correlation.

6.3.2 Ore samples

In both samples of the Sossego ore (Min-Cp-SOS and SOS315/255.1; Figs. 7G and H, respectively), monazite grains vary from 20 to 200 µm, are predominantly yellow, although dark yellow to brown areas are observed close to iron oxide-rich inclusion and fractures. Grain morphology varies from prismatic with slightly rounded terminations and triangular morphology, and aspect ratios from 1:1 to 1.8:1. Internal textures are absent in CL and BSE images. Thirty U-Pb LA-MC-ICPMS spot analyses in twenty grains from samples Min-Cp-SOS, and eighteen spot analyses in ten grains from sample SOS315/255.1 provided a concordia ages of $1,878.9 \pm 4.1$ Ma (MSWD=1.3; Fig. 12C, Supplementary Table 3) and $1,904 \pm 5.2$ (MSWD=1.2; Fig. 12D, Supplementary Table 3), respectively.

Monazite grains from ore of the Curral orebody (SOS106/84; Fig. 7I) are light to medium yellow, rounded to prismatic with triangular terminations. Some fractures and inclusions are observed in few grains. Monazite grains vary from 30 to 250 µm, and have aspect ratios from 1:1 to 1.5:1. The thirty six U-Pb LA-MC-ICPMS spot analyses in twenty one grains yielded a concordia age of $1,889.8 \pm 8.5$ Ma (MSWD = 2.7; Fig. 12E, Supplementary Table 3).

7. Discussions

7.1 Meso- and Neoarchean magmatism in the Sossego deposit area

The geochronological data presented in this contribution (Table 3) indicate that the magmatism in the Sossego deposit area took place during the Mesoarchean and Neoarchean. Rocks with different geochemical nature have been characterized, such as the Sequeirinho

Granite, gabbro to gabbronorite, granophyric granite, the Pista felsic metavolcanic rock, and meta-ultramafic lenses.

The $3,010 \pm 21$, $3,014 \pm 22$ and $2,989 \pm 5.2$ Ma ages (zircon U-Pb SHRIMP IIe and LA-ICPMS; Figs. 11A-C) acquired for the Sequeirinho Granite are interpreted as the timing of igneous crystallization for this unit. Ages of ca. 3.0 Ga represent the oldest magmatism registered at the Carajás Province. Similar ages were obtained for the Bacaba Tonalite ($3,001.2 \pm 3.6$ Ma, zircon U-Pb LA-MC-ICPMS; Moreto et al. 2011), which host the Bacaba deposit, and for the igneous protolith of enderbites and charnockites of the Chicrim-Cateté Orthogranulites (Rodrigues et al., 1992; Pidgeon et al., 2000; Vasquez et al. 2008).

Dating of the Pista metavolcanic rock suggests that this unit was crystallized at ca. 2.97 Ga ($2,968 \pm 15$ Ma and $2,979 \pm 5.3$ Ma; zircon U-Pb SHRIMP IIe; Figs. 11E and F). This is not only the oldest record for (meta-) volcanic rocks in the Carajás Domain, but also the first evidence for such rocks older than 2.76 Ga, since the widespread volcanism associated with the filling of the Carajás Basin (Itacaiúnas Supergroup) is Neoarchean (ca. 2.76-2.74 Ga; Gibbs et al., 1986; DOCEGEO, 1988; Machado et al., 1991; Trendall et al., 1998; Galarza and Macambira, 2002a). However, such old volcanic rocks are recognized at the Rio Maria Domain, and correspond to 2.97 Ga felsic metavolcanic rocks ($2,979 \pm 5$ Ma; Pimentel and Machado, 1994) and metagraywacke ($2,971 \pm 18$ Ma; Macambira and Lancelot, 1996) from the Lagoa Seca greenstone belt sequence.

Moreover, various drill cores from the Pista orebody intercepted several intervals of meta-ultramafic rocks intercalated with the Pista metavolcanic rock. Although speculative, this evidence and the geochronological results may suggest that the Pista metavolcanic could share similarities with those felsic metavolcanic rocks from the greenstone sequences of the Rio Maria Domain (e.g., 3.0 to 2.97 Ga Gradaús and Lagoa Seca greenstone belts; Macambira and Lancelot, 1991; Pimentel and Machado, 1994; Tassinari et al., 2005), and may be interpreted as allochthonous in origin. Tectonic transport could be related to the collision (?) between the two domains (Carajás and Rio Maria) in the Archean.

Neoarchean ages of ca. 2.74 Ga are attributed to the crystallization of the Sossego granophyric granite ($2,740 \pm 26$ Ma; zircon U-Pb LA-ICPMS; Fig. 12A) and to the gabbro to gabbronorite found in the Sequeirinho and Curral orebodies ($2,739 \pm 5.9$ and $2,739.1 \pm 4.2$ Ma; zircon U-Pb SHRIMP IIe; Figs. 11D and 12B). In sample SOS 35 (Fig. 11D) from the

gabbronorite, two inherited zircon grains were dated in 2.96 Ga, which are similar to the age of the Pista metavolcanic rock. Possibly, the gabbronorite assimilated these inherited grains during its emplacement into the crust.

The ca. 2.74 Ga ages are slightly younger than the predominant ca. 2.76 Ga felsic and mafic volcanic magmatism of the Itacaiúnas Supergroup (Gibbs et al., 1986; Machado et al., 1991; Trendall et al., 1998; Galarza and Macambira, 2002a) that filled the Carajás Basin. However, the obtained Neoarchean ages are quite similar to the ages of several syntectonic A-type granites that intruded the Carajás Basin and its basement (e.g., Estrela, Serra do Rabo, Igarapé Gelado granites; Barbosa, 2004; Barros et al., 2004, 2009; Sardinha et al., 2006).

Coeval mafic (gabbronorite) and felsic (granophyric granite) rocks represent the 2.74 Ga magmatism at the Sossego deposit area, revealing its bimodal character. Similar Neoarchean bimodal magmatism in the Transition Subdomain is also evidenced by the Pedra Branca Granite ($2,750 \pm 5$ Ma, Feio et al., 2012a), Planalto Granite ($2,747 \pm 2$ and $2,733 \pm 2$ Ma; Huhn et al. 1999b; Feio et al., 2012b, respectively), Pium diopside Norite ($2,735 \pm 5$ Ma, Feio et al., 2012b), and the Cristalino Diorite ($2,738 \pm 5$ Ma, Huhn et al., 1999b). The extensive magmatism at ca. 2.74 Ga has been related to emplacement of high-temperature magmas under active regional stress near the borders of Precambrian domains with different ages and tectonic evolution or in their zone of interaction (Feio et al., 2012b).

7.2 Metallogenetic evolution of the Sossego deposit

A common and synchronous evolutionary history was previously proposed for the hydrothermal paleo-system associated with the formation of the Sequeirinho-Pista-Baiano and Sossego-Currall orebodies based on similarities of paragenetic evolution, stable isotopic signatures and fluid inclusion data (Monteiro et al., 2008a, Xavier et al., 2010). According to these authors, the two sets of orebodies would have formed at the same time, but at distinct crustal levels. These differences in structural levels jointly with variations in fluid-rock interaction were mainly responsible for differences in the types and distribution of hydrothermal alteration zones.

The Sequeirinho-Pista-Baiano orebodies show hydrothermal alteration patterns (sodic, sodic-calcic alterations and magnetite-apatite formation) compatible with those of IOCG deposits formed at deeper crustal levels (Monteiro et al., 2008a), according to the model proposed by

Hitzman et al. (1992) and Hitzman (2000). On the other hand, hydrothermal alteration assemblages at Sossego-Currall (potassic, chlorite and hydrolytic alterations) imply that these orebodies were formed at structurally higher levels than Sequeirinho-Pista-Baiano (Monteiro et al., 2008a). The new geochronological data presented in this study (Table 3) suggest, however, a more complex evolutional history for the Sossego deposit, in which the two sets of orebodies (Sequeirinho-Pista-Baiano and Sossego-Currall) would have formed during distinct IOCG mineralizing events.

In terms of the Sequeirinho orebody, an age of $3,076 \pm 5.3$ Ma was obtained from zircon crystals (U-Pb SHRIMP IIe; Fig. 11G) of an ore breccia. This age is quite similar to those obtained for the host Sequeirinho Granite. Furthermore, the zircon features (e.g., internal oscillatory zoning and external morphologies) from both ore and host samples are similar and typical of igneous rocks. Thus, the analyzed zircon grains from this ore sample are interpreted as igneous rather hydrothermal. The Neoarchean age of $2,712.3 \pm 4.7$ Ma (U-Pb LA-MC-ICPMS; Fig 11H) was obtained for monazite from high-grade ore interpreted as coeval with alteration of apatite and with chalcopyrite formation.

For the Pista orebody, ages of $2,685 \pm 11$ and $2,710 \pm 11$ Ma (Re-Os in molybdenite; Table 4) were acquired and also interpreted as related to the mineralizing event (s) responsible for IOCG formation. As previously suggested (Monteiro et al., 2008a), the Sequeirinho and Pista orebodies are cogenetic, mainly because they share the same hydrothermal alteration patterns and similar isotopic data, which pointed to a common evolution. The same age of 2.71 Ga was obtained in both orebodies and by different methods, indicating its reliability. The 2.68 Ga age for molybdenite from the Pista orebody is, however, ca. 25 Ma younger and not similar, within error, to the older 2.71 Ga age.

For the Sossego-Currall system, monazite from Sossego ore provided the U-Pb ages of $1,878.9 \pm 4.1$ Ma and $1,904 \pm 5.2$ Ma (Figs. 12C and D, respectively). For the Currall ore, a U-Pb monazite age of 1889.8 ± 8.5 Ma was obtained (Fig. 12E), and can overlap, within error, either the older (1,904 Ma) or younger (1,878.9 Ma) ages obtained for Sossego ore. However, the 1904 Ma and 1879 Ma ages do not overlap in time even considering the analytical error. The significance of the Paleoproterozoic ages should be carefully examined. Monazite from Sossego ore breccia is spatially and temporally related to alteration zones in apatite. A hydrothermal Paleoproterozoic overprint unrelated to IOCG mineralization could have been responsible by this

alteration pattern in early-formed (Neoarchean) apatite crystals. However, similar paragenetic evolution was also reported for the Sequeirinho ore, where Paleoproterozoic ages have not been obtained in monazite grains.

Vertical zonation recognized in the Sossego deposit may be best explained if shallow-emplaced mineralized zones (Sossego-Currall) have developed after exhumation of IOCG systems formed at deeper crustal levels (Sequeirinho-Pista-Baiano). This assumption is more coherent if geochronological data for the Alvo 118 deposit (U-Pb SHRIMP II age of $1,868 \pm 7$ Ma in hydrothermal xenotime; Tallarico, 2003) is also considered, since this deposit also reveals predominance of potassic and chlorite alteration zones, typical of IOCG systems developed in shallow crustal levels. Thus, the new isotopic data present here point to a distinct and much younger IOCG-forming event in the Sossego-Currall orebodies than at the Sequeirinho-Pista-Baiano orebodies, revealing the superposition of IOCG systems in the same deposit area.

The 25 Ma interval found in ore ages from both Sequeirinho-Pista-Baiano and Sossego-Currall systems must be appraised. Several studies (Cathles et al., 1997; Stein and Cathles 1997; Marsh et al., 1997; Ballard et al., 2001; Quadt et al., 2005) showed that the duration and episodicity of ore-forming activity in intrusive, diagenetic and metamorphic environment encompasses a few million years, but the actual duration of ore-forming pulses is on the scale of only tens to hundreds of thousands of years. For example, Marsh et al. (1997) pointed that for the Potrerillos district (Chile), hydrothermal activity in porphyry-related systems lasted less than 40,000 years. Cathles et al. (1997) demonstrated that near-surface hydrothermal systems can be sustained by a single intrusion for as long as $\sim 800,000$ years. In the Panagyurishte region of the Apuseni-Banat-Timok-Srednogorie belt (Bulgaria), magmatism and ore formation (Cu-Au porphyry and high-sulfidation Au-As-Cu ore) in individual magmatic-hydrothermal systems occurred within a time span of about 1 million years (Quadt et al., 2005). All these examples sustain the idea that a 25 Ma time interval for a single IOCG event is implausible. Lead loss being responsible for the 1879 Ma age at the Sossego ore also does not seem a viable explanation, mostly because this age is very concordant. A reasonable justification would be that multiple discrete IOCG mineralizing events took place in the Neoarchean, during 2.71 to 2.68 Ga, and at the Paleoproterozoic, during the 1.90 Ga to 1.88 Ga interval.

Several temporally discrete IOCG events over a larger range in time (500 Ma) were proposed for Cu deposits from the Selwyn-Mount Dore corridor (e.g., Starra, Mount Elliot,

SWAN, Mount Dore and Lady Ella), Mount Isa Inlier, Australia (Duncan et al., 2011). Geochronological data from these deposits suggest that they were formed at different moments, and mineralization was associated with distinct sources of hydrothermal fluids and metal (e.g., igneous activity, metamorphic processes) (Duncan et al., 2011).

In the Sossego deposit, previous studies provided detailed information regarding the distribution and style of hydrothermal alteration, geochemistry of the altered rocks, stable isotopes, fluid inclusion and structural geology (Rosa, 2006; Chiaradia et al., 2006; Monteiro et al., 2008a,b; Xavier et al., 2008; Domingos, 2009; Carvalho, 2009). However, reliable geochronology studies on this deposit were scarce. The existing geochronological results (Neves, 2006) for the Sequeirinho (2.53 and 2.61 Ga; Pb-Pb in chalcopyrite) and Sossego (1.59 Ga) orebodies could represent isotopic resetting due to subsequent thermal/deformational events (Neves, 2006). However, these data already pointed out that the Sequeirinho and the Sossego orebodies were possibly not formed simultaneously.

High-temperature ($>500^{\circ}\text{C}$), high-salinity and deep-seated fluids, which may represent bittern brines involving magmatic components, were responsible for early sodic (albite-scapolite-iron oxide) and sodic-calcic (actinolite-hastingsite-albite -apatite) alteration, well developed in the Sequeirinho orebody (Monteiro et al., 2008a; Xavier et al., 2008) and in the country rocks of the Southern Copper Belt. These high-salinity and hot fluids possibly played a major role in leaching metals and other elements from the host rocks. As a consequence, the type of hydrothermal alteration and the ore chemical signature are strongly controlled by the geochemical nature of the host and country rocks, and by the intensity of fluid–rock interaction at different fluid/rock ratios.

Globally, IOCG deposits are genetically diverse and can apparently be formed by magmatic, non-magmatic and hybrid fluids and metal reservoirs (Barton and Johnson, 1996; 2000, 2004; Pollard, 2001, 2006; Hunt et al., 2007; Groves et al., 2010). Moreto et al. (2011) showed that the host rocks (ca. 2.84 Ga Serra Dourada Granite and ca. 3.0 Ga Bacaba Tonalite) of the Bacaba deposit were not responsible for the establishment of the hydrothermal system related to ore genesis. However, these feldspar-rich reactive host rocks were completely altered by the subsequent IOCG-forming event.

The ca. 2.71-2.68 Ga IOCG mineralizing event do not overlap in time with any magmatism registered in the Carajás Province. The closest ages correspond to the widespread

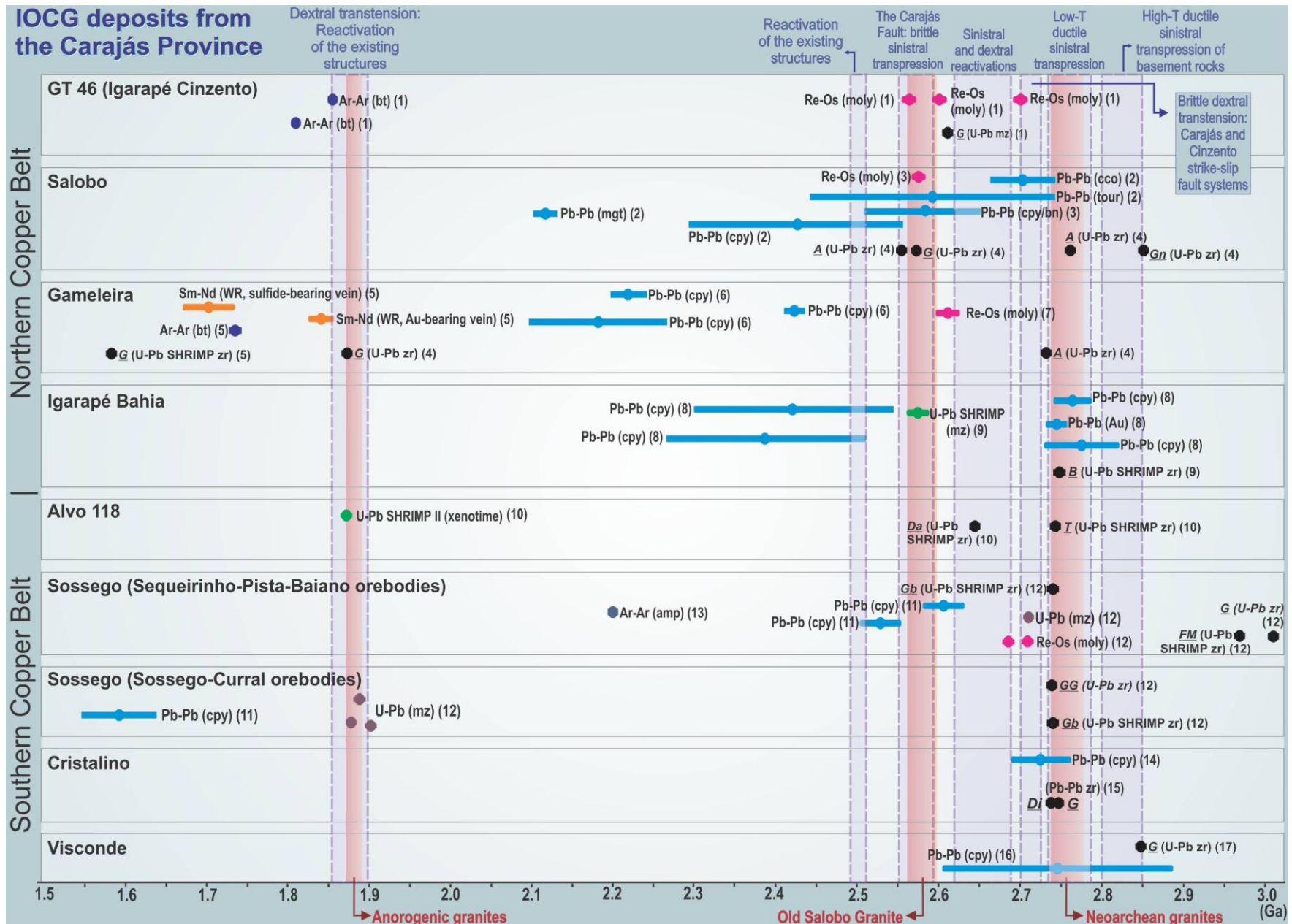
2.74 Ga magmatism that shows bimodal geochemical nature (e.g., Planalto and Pedra Branca granites, Cristalino Diorite, and mafic rocks from the Pium diopside Norite), including the host rocks of the Sossego deposit (e.g., granophyric granite and gabbronorite). But as discussed above, a 30 Ma interval is too long for duration of an ore-forming activity. A time gap is also observed between the mineralization interval and the deposition of the thick (~4-6 km; Gibbs et al., 1986) 2.76-2.74 Ga metavolcanic (-sedimentary) sequence that filled the Carajás Basin.

It is likely that alternative sources of heat, different to those from magmatism, caused the circulation of hydrothermal fluids in regional scale through major crustal discontinuities, leading to metal leaching from the country rocks (basement and sedimentary-volcanic sequence of the Itacaiúnas Supergroup) and subsequent ore deposition at ca. 2.7 Ga. A reasonable interpretation could be related to reactivation of regional shear zones, especially those in the southern contact between the Carajás Basin and its basement, where the Sossego and other IOCG deposits are located. The rocks that comprise the basement of the Carajás Basin were affected by high-grade and intense mylonitic deformation at ca. 2.85 Ga, and experience several events of ductile-brittle transcurrent reactivations in the Archean and Paleoproterozoic (Pinheiro and Holdsworth, 1997). For instance, the Carajás and Cinzento strike-slip fault systems were developed during regional extension (under brittle dextral transtension) that formed the sigmoidal shape of the Carajás Basin by tectonic subsidence (Pinheiro and Holdsworth, 1997). Figure 13 integrates the existing geochronological data for the IOCG deposits, the main tectonic events and granite magmatism registered in the Carajás Domain.

According to Domingos (2009), the tectonic inversion of the Carajás Basin and consequent reactivation of the previously formed major crustal discontinuities (e.g., Carajás and Cinzento strike-slip fault systems) initiated at about 2.7 Ga and involved a regional phase of sinistral transpression controlled by a NNE-directed oblique shortening. During this reactivation, E-W to WNE-ESE trending foliations were formed. As deformation progressed, rocks locally reached their limit of mechanical plasticity promoting nucleation and propagation of NE-SW sinistral brittle-ductile shear zones and faults (Domingos, 2009). The mineralizing ore breccia of the Sequeirinho-Pista-Baiano orebodies would have formed along these NE-SW structures (Fig. 14A), close to the interception with the major WNE-ESE shear zone in the southern contact between the Carajás Basin and its basement. Microstructural observations of quartz and feldspar by Domingos (2009) suggest that the sinistral transpressive deformation at the Sequeirinho

orebody took place under middle-to-upper (400–500°C) greenschist facies. These temperatures are consistent with those (> 550°C) from the hydrothermal fluids associated with development of the early alteration stages at the Sequeirinho-Pista-Baiano orebodies (Monteiro et al., 2008a).

The sources of heat and fluids for the development of the Paleoproterozoic IOCG-forming interval at the Carajás Province should also be evaluated. The 1.88 Ga age is similar to those of the widespread suite of non-deformed alkaline Paleoproterozoic granites, which have been related to A-type granite magmatism (Dall'Agnol et al., 1999a,b, 2005; Dall'Agnol and Oliveira, 2007). These granites are included in the Serra dos Carajás Intrusive Suite (Central Carajás, Cigano, Pojuca, Breves, Young Salobo, and Rio Branco granites) in the Carajás Domain, and in the Jamon Intrusive Suite (Jamon, Musa, Redenção, Seringa and Bannach granites) in the Rio Maria Domain. A-type granites are originally defined as alkaline granites mainly characterized by low water and oxygen fugacity, low CaO and Al₂O₃ contents, and formed along rift zones and within stable continental blocks (Loiselle and Wones, 1979; Eby, 1990). However, the Paleoproterozoic granites from the Carajás Province were apparently formed at various redox conditions, varying from intermediate reduced states (e.g., Serra dos Carajás Suite) to oxidized conditions (e.g., Jamon Suite; Dall'Agnol et al., 2005). Moreover, the 1.88 Ga granites have water contents higher than normally suggested (Loiselle and Wones, 1979; Collins et al., 1982; Rämö and Haapala, 1995; Frost and Frost, 1997) for typical A-type granite magmas (Dall'Agnol et al., 2005). Some of the 1.88 Ga granites from the Carajás Province (e.g., Jamon Suite) were attributed to the oxidized, magnetite-series, rapakivi-type group of A-type granites defined by Anderson and Bender (1989), that do not strictly follow the original definition of A-type granites, and approach calc-alkaline and I-type granites in some aspects (Dall'Agnol et al., 2005; Dall'Agnol and Oliveira, 2007).



«Fig. 13. Summary of geochronological data for IOCG deposits and their host rocks and main tectonic and magmatic events recorded in the province. The data obtained in this study is included. Data source: (1) Silva et al. (2005); (2) Tassinari et al. (2003); (3) Réquia et al. (2003); (4) Machado et al. (1991); (5) Pimentel et al. (2003); (6) Galarza and Macambira (2002b); (7) Marshick et al. (2005); (8) Galarza et al. (2008); (9) Tallarico et al. (2005); (10) Tallarico (2003); (11) Neves (2006); (12) Moreto et al., this study; (13) Marschik et al. (2003); (14) Soares et al., 2001; (15) Huhn et al. (1999b); (16) Silva et al. (2012); (17) Moreto et al. (2011). A amphibolite; amp amphibole; Au gold; B basalt; bn bornite; bt biotite; cco chalcocite; cpy chalcopyrite; Da dacite; Di diorite; FM felsic metavolcanic rock; G granite; GG granophyric granite; Gb gabbro; Gn gneiss; mz monazite; mgt magnetite; moly molybdenite; T tonalite; tour tourmaline; WR whole rock; zr zircon.

In terms of metallogenetic specialization, the classical reduced, low water content, within plate A-type granite magmatism is intrinsically associated with tin, tungsten and fluorite deposits. In the Carajás Province, the Pedra Preta wolframite deposit (508.300 ton of ore; 1.01% de WO₃; Cordeiro et al., 1988) has been associated with the emplacement of the 1.88 Ga Musa Granite. Occurrences of cassiterite and copper-molybdenum sulfides are described associated with pegmatites and veins formed in the final phases of crystallization of the 1.88 Ga Serra dos Carajás Granite (Javier Rios et al., 1995a,b).

Additionally, several 1.88 Ga mineral deposits from the Carajás Domain have their genesis related to the emplacement of the 1.88 Ga Paleoproterozoic granites (Xavier et al., 2003; Tallarico et al., 2004; Lindenmayer et al., 2005; Volp et al., 2006; Grainger et al., 2008). Examples of these deposits are the polymetallic Cu-Au (W, Bi, Sn ± Mo), including the Estrela ($1,839 \pm 14$ Ma, EPMA in hydrothermal monazite; Volp et al., 2006; $1,857 \pm 98$ Ma, Sm-Nd in mineralized veins, Lindenmayer et al., 2005), Breves ($1,872 \pm 7$ Ma, U-Pb SHRIMP II in monazite and xenotime; Tallarico et al., 2004), and the Águas Claras (Silva and Villas, 1998) deposits. Additionally, the Au-Pt-Pd mineralization at the Serra Pelada deposit ($1,861 \pm 45$ Ma, U-Pb SHRIMP in hydrothermal monazite; and $1,882 \pm 3$ Ma, Ar-Ar in biotite; Grainger et al., 2008) was also related to the emplacement of the Cigano Granite ($1,883 \pm 2$ Ma, U-Pb in zircon; Machado et al., 1991).

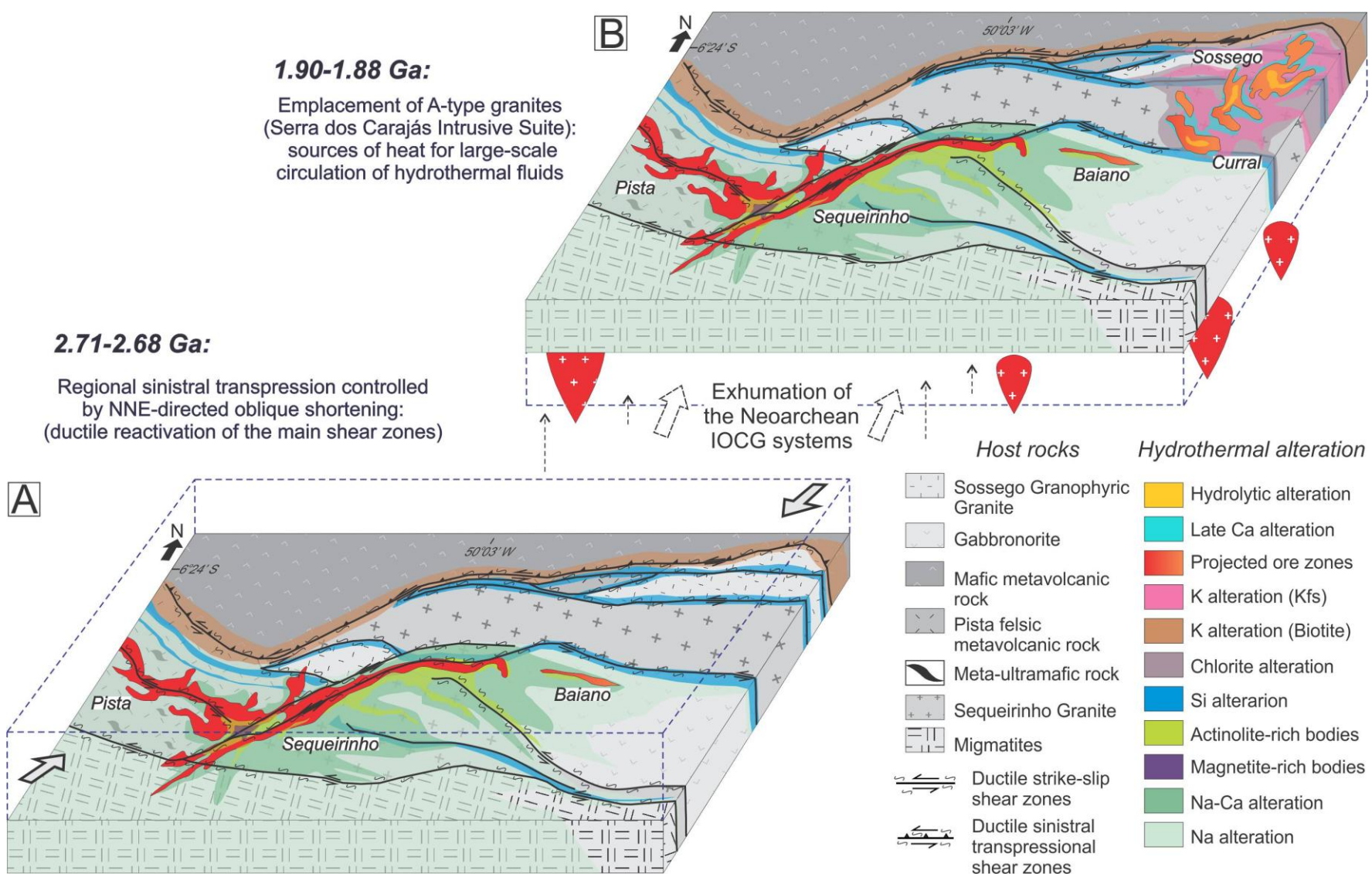


Fig. 14. Schematic diagram showing the metallogenetic evolution of the Sossego deposit in time. A) Formation of the Sequeirinho-Pista-Baiano orebodies at 2.71-2.68 Ga in the interception of WNW-ESE and NE-SW ductile shear zones; B) Formation of the vertical pipe-like Sossego-Currall orebodies at 1.90-1.88 Ga after exhumation of the Neoarchean IOCG systems.

The diversity in the metallogenetic specialization of the Paleoproterozoic deposits from the Carajás Province is notable and may require significative variation in geochemical affinity and oxidation state of the source magma. Alternatively, intense metal leaching promoted by large scale circulation of oxidized hydrothermal fluids (Monteiro et al., *in press*) may have contributed to the evolution of these hydrothermal systems. In this case, the heat released during the emplacement of the Paleoproterozoic granites would be crucial to the establishment of the hybrid hydrothermal systems. These systems would involve, in addition to magmatic fluids, externally-derived, basin fluids derived from the paleo-aquifer associated with the Águas Claras Formation, which overlain the Itacaiúnas Supergroup (Monteiro et al., *in press*).

With respect to the 1.88 Ga Sossego-Currall IOCG orebodies, it is unlikely to affirm if their genesis is directly related to the 1.88 Ga magmatism registered in the province. One possibility is that the 1.88 Ga magmatism would have acted as sources of heat that caused the circulation of hydrothermal fluids in regional scale, including the areas where the Neoarchean IOCG orebodies (Sequeirinho-Pista-Baiano) were located. The hydrothermal fluids may have interacted with the metasomatized country rocks, previously hydrothermally altered during the Neoarchean IOCG event. The fluids may have caused metal (Cu, Fe, Au) leaching from the ca. 2.71-2.68 Ga IOCG deposits and reconcentration in the 1.90-1.88 Ga deposits (Fig 14B).

On the other hand, genetic models proposed for IOCG deposits worldwide (Groves and Bierlin, 2007; Pollard, 2001, 2006; Pirajno et al., 2008; Groves et al., 2010) suggest spatially and temporally relation of IOCG deposits to widespread anorogenic alkaline or A-type magmatism in intracratonic settings. According to Groves and Bierlin (2007) and Groves et al. (2010), Precambrian IOCG deposits would be associated with magmatism and related hydrothermal activity driven by mantle underplating and/or plumes. Plume-induced partial melting of subcontinental lithospheric mantle previously metasomatized during earlier subduction probably produced basic to ultrabasic magmas that melted overlying continental crust and mixed with resultant felsic melts to produce the IOCG deposits (Groves et al., 2010).

The vertical pipe-like Sossego-Currall orebodies were formed at higher structural levels in comparison to the Sequeirinho-Pista-Baiano orebodies after exhumation of these Neoarchean IOCG systems. Although there are differences in the crustal depths in which these two sets of orebodies were formed, the poorly-developed early sodic and sodic-calcic alteration stages at Sossego-Currall orebodies are also related to high-temperature (<400°C; against >500°C at

Sequeirinho orebody; Monteiro et al., 2008a) and high-salinity fluids. Like the fluids responsible for the early alteration stages in the ~2.7 Ga orebodies (e.g., Sequeirinho), these reactive fluids (hot and saline) may also have played an important role in leaching metals and other elements from the country rocks. As the paleo-hydrothermal system evolved, the fluid-rock interaction, especially in rocks intensively altered by the Neoarchean IOCG event, caused significant chemical modification of the hydrothermal fluids. This may have been responsible for the formation of wide zones containing potassic and chlorite alteration at Sossego-Currall, which cut the early (sodic and sodic calcic) alteration stages. This overprint of potassic and chlorite zones over sodic altered areas is also commonly recognized in the country rocks. The superimposed mineral assemblage due to evolution of the hydrothermal system is similar to the models described by Hitzman (2000) and may imply in telescoping of hydrothermal zones.

7.3 IOCG Metallogenesis in the Carajás Province

The new geochronological data on the IOCG-forming systems from this study provided a better understanding of the evolution of the Sossego deposit. Moreover, they allow a comparison to other IOCG systems from the Southern Copper Belt (e.g., Cristalino, Visconde and Alvo 118 deposits), and to those from the Northern Copper Belt, such as the world-class Salobo, Igarapé-Bahia, Igarapé-Cinzento/GT4 and Gameleira.

In the Southern Copper Belt, ore sulfides from the Cristalino (chalcopyrite and pyrite) and Visconde (chalcopyrite) deposits, yielded Pb-Pb ages of $2,700 \pm 29$ Ma (MSWD= 656; Soares et al., 2001) and $2,747 \pm 140$ Ma (MSWD=12; Silva et al., 2012), respectively, which were interpreted as related to the hydrothermal event responsible for copper ore formation. Although there are large errors associated with these imprecise ages, these data strongly suggest that the timing of IOCG formation in these deposits is likely related to the Neoarchean, and could overlap the 2.71-2.68 Ga age interval of IOCG formation at the Sequeirinho-Pista-Baiano orebodies.

Although the Alvo 118 deposit had been attributed to the Cu-Au (W, Bi, Sn \pm Mo) class (Tallarico, 2003; Grainger et al., 2008), Torresi et al. (2012) provided a detailed description on the styles and distribution of the hydrothermal alteration, as well as stable isotope data, which ascribed the Alvo 118 deposit to the IOCG class. The similarities of the Alvo 118 deposit with the world-class IOCG deposits from Carajás included the spatial association with shear zones, intense hydrothermal alteration (including major K– Fe metasomatism), an ore-related late stage

of chlorite alteration, and quartz and carbonate infill of the ore breccia (Torresi et al., 2012). In terms of geochronological data for the Alvo 118 deposit, an U-Pb SHRIMP II age of $1,868 \pm 7$ Ma was obtained in hydrothermal xenotime from copper ore (Tallarico, 2003). This data indicates that the Alvo 118 deposit was also formed during the Paleoproterozoic, possibly during the IOCG event responsible for the genesis of the Sossego and Curral orebodies.

Dating of molybdenite (Re-Os) and monazite (U-Pb SHRIMP II) revealed an important IOCG event at $2.57 - 2.56$ Ga at the Northern Copper Belt. In the Salobo deposit, molybdenite ages of $2,576 \pm 8$ and $2,562 \pm 8$ Ma (Réquia et al., 2003) are similar to the $2,575 \pm 12$ Ma age in monazite from ore breccia at the Igarapé Bahia deposit (Tallarico et al., 2005). For the Gameleira deposit, the slightly older $2,614 \pm 14$ Ma age was acquired for molybdenite (Re-Os; Marschik et al., 2005). Silva et al. (2005) interpreted the Igarapé-Cinzento/GT46 deposit as Paleoproterozoic in age (1.88 Ga), based on a whole rock Sm-Nd isochron for ore breccia (1.75 Ga) and Ar-Ar ages for biotite (1.86 – 1.81 Ga). However, the authors also obtained a 2.56 Ga Re-Os ages on molybdenite from the host pegmatitic granite, which was considered as unrelated to the mineralization event. All in all, the isotopic data indicate that the IOCG genesis at the Northern Copper Belt apparently had an evolutional history different from the Sossego, Alvo 118, Cristalino and Visconde deposits, at the Southern Copper Belt.

According to several authors (Réquia et al., 2003; Tallarico et al., 2005; Marschik et al., 2005), the timing of formation of the ca. 2.57 Ga deposits of the Northern Copper Belt is intrinsically associated with the emplacement of peralkaline to meta-aluminous 2.57 Ga granites, which correspond to the small Itacaiúnas and Old Salobo granites (mainly found in drill holes). Alternatively, this IOCG event could be related to reactivation under brittle sinistral transpression of the Carajás and Cinzento strike-slip fault systems at ca. 2.6 Ga, which was responsible for the nucleation of the Carajás Fault (Pinheiro and Holdsworth, 1997). Machado et al. (1991) also suggest regional basement reactivations between 2,573 and 2,551 Ma, based on metamorphic monazite from a banded iron formation of the Salobo Group, and zircon overgrowths on igneous cores in amphiboles from the Salobo Group.

In the Southern Copper Belt, no evidence for the 2.57 Ga IOCG event exist in the literature. Moreover, the analyzed minerals grains from host rocks and ore did not provide lead loss towards the 2.57 Ga age or new mineral growing at this time. This evidence implies that the Southern Copper Belt was probably not affected by the hydrothermal fluid circulation associated

with the younger Neoarchean IOCG event (2.57 Ga) in the province. Possibly, fluid circulation was restricted to the northern main fault systems (Carajás and Cinzento strike-slip fault systems) rather than the one in the southern contact of the basin with its basement rocks.

8. Conclusions

The new geochronological data on host rocks and ore from the Sossego deposit, including Re-Os in molybdenite and U-Pb in zircon and hydrothermal monazite, provide new insights into the evolution of the Sossego deposit and in the metallogeny of the Carajás Province, as listed below:

- The Sossego deposit is hosted by Mesoarchean and Neoarchean rocks, including the 3.0 Ga Sequeirinho Granite (Sequeirinho orebody), which represents the oldest magmatism registered at the Carajás Province. The 2.97 Ga Pista felsic metavolcanic rock, which hosts the Pista orebody, corresponds to the oldest volcanic unit of the Carajás Domain. This rock contains intensively deformed meta-ultramafic lenses. Although speculative, the Pista metavolcanic rock could be interpreted as allochthonous in origin and similar to 2.97 Ga greenstone belts of the Rio Maria Domain. Finally, the Neoarchean 2.74 Ga Sossego granophyric granite (Sossego orebody), and gabbronorite (Curral and Sequeirinho orebodies) are consistent with a widespread bimodal magmatism at 2.74 Ga. This magmatism is also evidenced by the ca. 2.74 Ga Planalto and Pedra Branca granites, Cristalino Diorite and Pium diopside Norite.
- The evolutionary history for the Sossego deposit was complex, with multiple IOCG-mineralizing events responsible for ore genesis and hydrothermal alteration. In this sense, recurrence of hydrothermal systems within the same area is suggested for the Sossego deposit. The older IOCG-forming interval took place at ca. 2.71-2.68 Ga and was responsible for the genesis of the NE-SW-trending Sequeirinho, Pista, and possibly the Baiano orebodies. These Neoarchean systems were also possibly responsible for IOCG ore genesis at the Cristalino and Visconde deposits. The younger interval for IOCG mineralization occurred at ca. 1.90-1.88 Ga and was responsible for the development of the Sossego and Curral orebodies, and the Alvo 118 deposit. The Paleoproterozoic systems were installed after the progressive exhumation of the Neoarchean deposits.

- Alternative sources of heat, different to those from magmatism, possibly caused at ca. 2.71-2.68 Ga the circulation of hot and saline hydrothermal fluids in regional scale along major crustal discontinuities. These fluids caused metal leaching from the country rocks (basement and supracrustal sequence) and subsequent hydrothermal alteration development and copper ore deposition. The heat sources could be related to the ca. 2.70 Ga tectonic inversion of the Carajás Basin under ductile sinistral transpression, controlled by a NNE-directed oblique shortening. As deformation progressed, rocks reached their limit of mechanical plasticity promoting nucleation and propagation of NE-SW sinistral ductile shear zones. The Sequeirinho-Pista-Baino deposits were installed along one of the interceptions between WNW-ESE and NE-SW ductile structures in the southern contact between the Carajás Basin and its basement.
- The hot ($> 500^{\circ}\text{C}$) and saline fluids (bittern brines with magmatic-derived contribution), responsible for the early stages of hydrothermal alteration at the Sequeirinho-Pista-Baiano orebodies, possibly enhanced metal leaching from the country rocks. The chemical signature of the ore and hydrothermal alteration zones is strongly dependent upon the composition of the host rocks and intensity of fluid-rock interaction.
- Regarding the ca. 1.9-1.88 Ga IOCG forming interval, it is likely that the widespread 1.88 Ga anorogenic magmatism in the Carajás Province acted as a source of heat that caused the circulation of hydrothermal fluids in regional scale, including the crustal discontinuities where the ca. 2.71-2.68 Ga IOCG orebodies (Sequeirinho-Pista-Baiano) are located. The hot ($> 400^{\circ}\text{C}$) and saline hydrothermal fluids may have caused reworking of the Neoarchean IOCG deposits, with leaching of metal (Cu, Fe, Au) and other elements. Remobilization could have been followed by the development of new hydrothermal alteration zones and ore reconcentration in the Paleoproterozoic IOCG deposits.
- The heat released during the multiple emplacements of igneous bodies that host the Sossego deposit may have caused regional circulation of high-temperature and high-salinity hydrothermal fluids. These fluids were possibly related to hybrid magmatic-hydrothermal systems, with the contribution of magmatic and with non-magmatic components. Although these systems were developed before the establishment of the

Neoarchean orebodies, the hot and hypersaline fluids possibly enhanced metal leaching, and other elements from the country rocks.

- The Southern Copper Belt, in which Neoarchean (ca. 2.7 Ga) and Paleoproterozoic (ca. 1.88 Ga) IOCG events are registered, differs in terms of IOCG metallogenetic evolution from the Northern Copper Belt, which host the Salobo, Igarapé Bahia and other deposits. In the northern area, a 2.57 Ga IOCG event is well constrained by reliable geochronological data. Fluid circulation at 2.57 Ga was possibly restricted to the northern crustal structures (Carajás and Cinzento strike-slip fault systems), since no evidence for such event is found in the Southern Copper Belt.

Acknowledgments

We are very grateful to Vale company for the continuous support provided to the researchers and students of the Institute of Geosciences, UNICAMP, during their activities in the Carajás region. We are particularly indebted to Márcio Godoy, Benevides Aires and Cleive Ribeiro for their invaluable support. We would also like to thank Erica Tonetto for her assistance with the SEM imaging. This research was funded by CNPq (grants 555065/2006-5, 472549/2009-0), FAPESP (grants 03/09584-3, 03/07453-9, 03-11163-603/01159-1), FAPESPA /VALE, and INCT/GEOCIAM (CNPq/MCT/FAPESPA). Carolina P. N. Moreto also thanks FAPESP for the PhD scholarship (grant 2009/18371-0).

REFERENCES

- Alves, C.A.S., Bernardelli, A.L., and Beisiegel, V.R, 1986, A jazida de níquel laterítico do Vermelho, Serra dos Carajás, Pará. In: Schobbenhaus, C., Coelho, C.E.S. (Coord.). Principais depósitos minerais do Brasil: ferro e metais da indústria do aço. DNPM/CVRD, v. 2, p. 325-334.
- Anderson, J.L., and Bender, E.E., 1989, Nature and origin of Proterozoic A-type granitic magmatism in the southwestern United States of America. *Lithos* 23, 19– 52.
- Araújo O.J.B., Maia R.G.N., Jorge-João, X.S. Costa, and J.B.S., 1988, A megaestruturação da folha Serra dos Carajás. In: Congresso Latino Americano de Geologia., 7, pp. 324–333.
- Araújo, O.J.B. and Maia, R.G.N., 1991 - Serra dos Carajás, folha SB.22-ZA, Estado do Pará. Programa Levantamentos Geológicos Básicos do Brasil. Companhia de Pesquisa de Recursos Minerais. 136 p.
- Avelar, V.G., Lafon, J.M., Correia JR, F.C., and Macambira, E.M.B., 1999, O Magmatismo arqueano da região de Tucumã-Província Mineral de Carajás: novos resultados geocronológicos. *Revista Brasileira de Geociências*. 29(4): 453-460

- Ballard, J.R., Palin, J.M., Williams, I.S., and Campbell, I.H., 2001, Two age of porphyry intrusion resolved for the super-giant Chuquicamata copper deposit of northern Chile by ELA-ICP-MS and SHRIMP. *Geology* 29 (5): 383–386
- Barbosa, J.P.O., 2004, Geologia estrutural, geoquímica, petrografia e geocronologia de granitóides da região do Igarapé Gelado, norte da Província Mineral de Carajás. Unpublished Master Thesis, Universidade Federal do Pará, Belém, 112 p.
- Barbosa, J.P.O., Barros, C.E.M., Macambira, M.J.B., and Vale, A.G., 2001, Geologia e Geocronologia do Stock Granítico Geladinho, região de Parauapebas, Província Mineral de Carajás. In: Simpósio de Geologia da Amazônia, 7, Belém. SBG-NO. CD-ROM.
- Barros, C.E.M., Macambira, M.J.B., Barbey P., and Scheller, T., 2004, Dados isotópicos Pb–Pb em zircão (evaporação) e Sm–Nd do Complexo Granítico Estrela, Província Mineral de Carajás, Brasil: implicações petrológicas e tectônicas. *Rev. Brasil. Geoci.* 34, 531–538.
- Barros, C.E.M., Sardinha, A.S., Barbosa, J.P.O., and Macambira, M.J.B., 2009, Structure, Petrology, Geochemistry and zircon U/Pb and Pb/Pb geochronology of the synkinematic Archean (2.7 Ga) A-type granites from the Carajás Metallogenic Province, northern Brazil, *The Canadian Mineralogist*. 47: 1423-1440
- Barton, M. D., and Johnson D. A., 2000, Alternative brine sources for Fe oxide (-Cu-Au) systems: implication for hydrothermal alteration and metals. In: Porter, T. M. (ed) *Hydrothermal iron oxide copper-gold and related deposits: A global perspective*. Adelaide, Australian Mineral Foundation, vol. 1. p43-60
- Barton M.D., and Johnson D.A., 1996, Evaporitic source model for igneous-related Fe oxide-(REE-Cu-Au-U) mineralization. *Geology* 24, 259–262.
- Barton, M.D. and Johnson, D.A., 2004, Footprints of Fe-oxide(-Cu-Au) systems. SEG 2004: Predictive Mineral Discovery Under Cover. Centre for Global Metallogeny, Spec. Pub. 33, The University of Western Australia, 112-116.
- Cabral, A.R., Lehmann, B., Kwitko-Ribeiro, R. and Costa, C.H.C., 2002a, Palladium and platinum minerals from the Serra Pelada Au-Pd-Pt Deposit, Carajás Mineral Province, Northern Brazil. *The Canadian Mineralogist*, 40: 1451-1463.
- Cabral, A.R., Lehmann, B., Kwitko-Ribeiro, R., and Costa, C.H.C., 2002b, The Serra Pelada Au-Pd-Pt Deposit, Carajás Mineral Province, Northern Brazil: reconnaissance mineralogy and chemistry of very high grade palladian gold mineralization. *Economic Geology*. 97: 1127–1138.
- Carvalho, E.R., Xavier, R.P., Monteiro, L.V.S., and Souza Filho, C.R., 2005, Geology and hydrothermal alteration of the Sossego iron oxide-copper-gold deposit, Carajás Mineral Province, Brazil. In: Simpósio Brasileiro de Metalogenia, 1, [CD-ROM]
- Carvalho, E.R., 2009, Caracterização geológica e gênese das mineralizações de óxido de Fe-Cu-Au e metais associados na Província Mineral de Carajás: estudo de caso do depósito de Sossego: Unpublished Ph.D Dissertation, Universidade Estadual de Campinas, 141 p.
- Cathles, L.M., Erendi, A.H.J., and Barrie, T., 1997, How long can a hydrothermal system be sustained by a single intrusive event? *Economic Geology*, v. 92, p. 766–771.
- Chiaradia, M., Banks, D., Cliff R., Marschik, R., and de Haller, A., 2006, Origin of fluids in iron oxide-copper-gold deposits: constraints from $\delta^{37}\text{Cl}$, $^{87}\text{Sr}/^{86}\text{Sr}$ and Cl/Br. *Mineralium Deposita* 41, 565–573.
- Collins, W.J., Beams, S.D., White, A.J., and Chappell, B.W., 1982, Nature and origin of A-type Granites with particular reference to southeastern Australia. *Contributions to Mineralogy and Petrology* 80, 189– 200.
- Cordeiro, A.A.C., Alves, C.A., Biagini, D.O., Fonseca, L.R., de Nascimento, J.A.S., Azevedo, L.L., and Santos, F.F., 1988, Depósito de wolframita de Pedra Preta, sul do Pará. In: Cong. Bras. Geol., 35, Belém, 1988. Província Mineral de Carajás: Litoestratigrafia e principais depósitos minerais. Anexo aos anais, CVRD/SBG.p.161-165.
- Dall'Agnol, R., Costi, H.T., Leite, A.A., Magalhães, M.S., and Teixeira, N.P., 1999a, Rapakivi granites from Brazil and adjacent areas. *Precambrian Research* 95, 9–39.

- Dall'Agnol, R., and Oliveira, D.C., 2007, Oxidized, magnetite-series, rapakivi-type granites of Carajás, Brazil: implications for classification and petrogenesis of A-type granites. *Lithos* 93, 215–233.
- Dall'Agnol, R., Rämö, O.T., Magalhães, M.S., and Macambira, M.J.B., 1999b, Petrology of the anorogenic, oxidised Jamon and Musa granites, Amazonian craton: implications for the genesis of Proterozoic A-type granites. *Lithos* 46, 431–462.
- Dall'Agnol, R., Oliveira, M.A., Almeida, J.A.C., Althoff, F.J., Leite, A.A.S., Oliveira, D.C., and Barros, C.E.M., 2006, Archean and paleoproterozoic granitoids of the Carajás Metallogenic Province, eastern Amazonian craton. In: Symposium on magmatism, crustal evolution and metallogenesis of the Amazoniam Craton, Belém, Excursion Guide, p.: 99-150.
- Dall'Agnol, R., Teixeira, N.P., Rämö, O.T., Moura, C.A.V., Macambira, M.J.B., and Oliveira, D.C., 2005, Petrogenesis of the Paleoproterozoic, rapakivi, A-type granites of the Archean Carajás Metallogenic Province, Brazil. *Lithos* 80: 101–129.
- Dardenne, M.A., and Schobbenhaus, C.S., 2001, Metalogênese do Brasil. Editora Universidade de Brasília/CNPq, Brasília, 392 p.
- Dardenne, M.A., Ferreira Filho, C.F. and Meirelles, M.R., 1988, The role of shoshonitic and calc-alkaline suites in the tectonic evolution of the Carajás district, Brazil. *Journal of South American Earth Sciences*, 1: 363–372.
- Dias, G.S., Macambira, M.B., Dall'Ágnol, R., Soares, A.D.V., and Barros, C.E.M., 1996, Datações de zircões de sill de metagabro: comprovação de idade arqueana da Formação Águas Claras, Carajás, Pará. In: Simpósio de Geologia da Amazônia, 5, SBG, Belém, pp. 376-378.
- Diella, V., Ferrario, A., and Girardi, V.A.V., 1995, PGE and PGM in the Luanga mafic-ultramafic intrusion in Serra dos Carajás (Pará State, Brazil). *Ore Geology Reviews*, 9: 445—453.
- DOCEGEO, 1988, Revisão litoestratigráfica da Província Mineral de Carajás – Litoestratigrafia e principais depósitos minerais. 35o Congresso Brasileiro de Geologia, Belém, SBG, Proceedings, 11–54.
- Domingos, F., 2009, The structural setting of the Canaã dos Carajás region and Sossego-Sequeirinho deposits, Carajás, Brazil: Unpublished Ph.D. Dissertation, Durham University, 483 p. Available at Durham E-Theses Online: <http://etheses.dur.ac.uk/144/>.
- Duncan, R., Stein, H., Evans, K., Hitzman, M., Nelson, and Kirwin, D. 2011, A new geochronological framework for mineralization and alteration in the Selwyn-Mount Dore corridor, eastern fold belt, Mt. Isa Inlier, Australia: Genetic implications for iron oxide-copper-gold deposits: *Econ. Geol.*, 106: 169-192.
- Eby, G.N., 1990, The A-type granitoids; a review on their occurrence and chemical characteristics and speculation on their genesis. *Lithos* 26, 115-134.
- Feio, G.R.L., Dall'Agnol, R., Dantas, E.L., Macambira, M.J.B., Gomes, A.C.B., Sardinha, A.S., Oliveira, D.C., Santos, R.D., and Santos, P.A., 2012b, Geochemistry, geochronology, and origin of the Neoarchean Planalto Granite suite, Carajás, Amazonian craton: A-type or hydrated charnockitic granites?. *Lithos*, 151: 57-73
- Feio, G.R.L., Dall'Agnol R., Dantas E.L., Macambira M.J.B., Santos J.O.S., Althoff F.J., and Soares J.E.B., 2012a, Archean granitoid magmatism in the Canaã dos Carajás area: Implications for crustal evolution of the Carajás province, Amazonian craton, Brazil. *Precambrian Research* in press, Corrected Proof.
- Fernandes, C.M.D., Juliani, C., Monteiro, L.V.S., Lagler, B., and Misas, C.M.E. 2011, High-K calc-alkaline to A-type fissure-controlled volcano-plutonism of the São Félix do Xingu region, Amazonian Craton, Brazil: Exclusively crustal sources or mixed Nd model ages? *Journal of South American Earth Sciences*, 32: 351–368. DOI: 10.1016/j.jsames.2011.03.004.
- Ferreira Filho, C.F., 1985, Geologia e mineralizações sulfetadas do Prospecto Bahia, Província Mineral de Carajás, PA. Unpublished Master Thesis, Universidade de Brasília, 112p
- Ferreira Filho, C.F., Cançado, F., Correa, C., Macambira, E.M.B., Junqueira-Brod, T.C., and Siepierski, L. 2007, Mineralizações estratiformes de PGE-Ni associadas a complexos acamados em Carajás:

- os exemplos de Luanga e Serra da Onça. In: Rosa-Costa, L. T., Klein, E.L., Viglio, E.P. (Ed.). Contribuições à geologia da Amazônia. Belém: SBG-Núcleo Norte, v. 5, p. 1-14.
- Frost, C.D., and Frost, B.R., 1997, Reduced rapakivi type granites: the tholeiitic connection. *Geology* 25, 647–650.
- Galarza, M.A., Macambira, M.J.B. and Moura, C.A.V., 2003, Geocronologia Pb–Pb e Sm–Nd das rochas maficas do depósito Igarapé Bahia, Província Mineral de Carajás (PA). VII Simpósio de Geologia da Amazônia, SBG, [CD-ROM]
- Galarza, M.A., Macambira, M.J.B., and Villas, R.N., 2008, Dating and isotopic characteristics (Pb and S) of the Fe oxide–Cu–Au–U–REE Igarapé Bahia ore deposit, Carajás mineral province, Pará state, Brazil. *Journal of South American Earth Sciences*. 25:377-397.
- Galarza, M.A., and Macambira, M.J.B., 2002a, Petrologia e geocronologia das rochas encaixantes do depósito de Cu–Au Igarapé Bahia, Província Mineral de Carajás, Pará, Brasil, in: Kein, E.L., Vasquez, M.L., Rosa-Costa, L.T., Contribuições à Geologia da Amazônia, v. 3, SBG/NN, Belém, p. 153–168.
- Galarza, M.A., and Macambira, M.J.B., 2002b, Geocronologia e Evolução Crustal da Área do Depósito de Cu–Au Gameleira, Província Mineral de Carajás (Pará), Brasil: *Geologia USP Série Científica* v. 2, p. 143–159.
- Gibbs, A.K., Wirth, K.R., Hirata, W.K., and Olszewski Jr., W.J., 1986, Age and composition of the Grão Pará Group volcanics, Serra dos Carajás. *Revista Brasileira de Geociências*, 16: 201–211.
- Gomes, A.C.B., 2003, Geologia, petrografia e geoquímica dos granitóides de Canaã dos Carajás, SE do Estado do Pará. Belém. Unpublished Master Thesis, UFPA, 160p.
- Grainger, C.J., Groves, D.I., Tallarico, F.H.B., and Fletcher, I.R. 2008, Metallogenesis of the Carajás Mineral Province, Southern Amazon Craton, Brazil: Varying styles of Archean through Paleoproterozoic to Neoproterozoic base- and precious-metal mineralization. *Ore Geology Reviews*, 33: 451-489.
- Groves, D.I., and Bierlein, F.K., 2007, Geodynamic settings of mineral deposit systems. *Journal of the Geological Society, London*, 164, 19–30.
- Groves, D.I., Bierlein, F.P., Meinert, L.D., and Hitzman, M.W., 2010, Iron Oxide Copper-Gold (IOCG) Deposits through Earth History: Implications for Origin, Lithospheric Setting, and Distinction from Other Epigenetic Iron Oxide Deposits: *Economic Geology*, v. 105, p. 641-654.
- Hirata, W.K., Rigon, J.C., Kadekaru, K., Cordeiro, A.A.C., and Meireles, E.A., 1982, Geologia Regional da Província Mineral de Carajás. In: Simpósio de Geologia da Amazônia, 1, Belém, SBG/NO, p. 100–110.
- Hitzman, M.W., 2000, Iron oxide–Cu–au deposits: what, where, when, and why. In: Porter TM (ed) Hydrothermal iron oxide cooper-gold and related deposits: a global perspective. Australian Miner. Fund, Adelaide, Vol 1, p. 9–25.
- Hitzman, M.W., Oreskes N., Einaudi M.T., 1992, Geological characteristics and tectonic setting of Proterozoic iron oxide (Cu–U–Au–REE) deposits. *Precambrian Research*, 58, 241-287.
- Holdsworth, R. and Pinheiro, R., 2000, The anatomy of shallow-crustal transpressional structures: insights from the Archean Carajás fault zone, Amazon, Brazil. *Journal of Structural Geology* 22: 1105–1123.
- Huhn, S.B., Macambira, M.J.B., and Dall’Agnol, R., 1999b, Geologia e geocronologia Pb-Pb do Granito Alcalino Planalto, Região da Serra do Rabo, Carajás-PA. In: SBG, Simpósio de Geologia da Amazônia, 6, Boletim de Resumos, p. 463-466.
- Huhn, S.R.B., Souza, C.I.J., Albuquerque, M.C., Leal, E.D., Brustolin, V., 1999a, Descoberta do depósito Cu(Au) Cristalino: Geologia e mineralização associada região da Serra do Rabo - Carajás – PA. SBG/NO, Simpósio de Geologia da Amazônia, 6, pp 140–143.
- Hunt, J.A., Baker, T., and Thorkelson, D.J., 2007, A review of iron oxide copper- gold deposits, with focus on the Wernecke Breccias, Yukon, Canada, as an example of a non-magmatic end member and implications for IOCG genesis and classification: *Exploration and Mining Geology*, v. 16, p. 209–232.

- Javier Rios, F.; Villas, R.N.N; and Dall’Agnol, R. 1995a, O Granito Serra dos Carajás, Pará: I. Fácies petrográficas e avaliação do potencial metalogenético para estanho no setor norte. Revista Brasileira de Geociências, v. 25, n. 1, p. 20-31.
- Javier Rios, F.; Villas, R.N.N; and Fuzikawa, K. 1995b, O Granito Serra dos Carajás, Pará: II. Caracterização dos fluidos aquosos e alteração hidrotermal. Revista Brasileira de Geociências, v. 25, n. 1, p. 32-40.
- Klein, E.L., and Carvalho, J.M. de A., 2008, Recursos Minerais. In: M.L Vasquez, L.T. Rosa-Costa. (Orgs) Geologia e Recursos Minerais do Estado do Pará: SIG: Texto explicativo dos Mapas Geológico e Tectônico e de Recursos Minerais do Estado do Pará. Escala 1:1.000.000. Belém: CPRM.
- Lafon, J.M., Macambira, M.J.B., and Pidgeon, R.T. 2000, Zircon U-Pb SHRIMP dating of Neoarchean magmatism in the southwestern part of the Carajás Province (eastern Amazonian Craton, Brazil). In: International Geological Congress, 31., Abstracts, Rio de Janeiro, [CD-ROM].
- Lancaster Oliveira, J., Fanton, J., Almeida, A.J., Leveille, R.A., and Vieira, S., 2000, Discovery and geology of the Sossego copper-gold deposit, Carajás District, Pará State, Brazil: International Geology Congress, 31st, Proceedings, International Union of Geological Sciences, [CD-ROM].
- Lindenmayer, Z.G., Pimentel, M.M., Ronchi, L.H., Althoff, F.J., Laux, J.H., Araújo, J.C., Fleck A., Bortowski, D.C., Nowatzki, A.C., 2001. Geologia do depósito de Cu–Au do Gameleira, Serra dos Carajás, Pará. In: Jost H, Brod JA, Quieroz ET (eds) Caracterizacão de Depósitos Auríferos Brasileiros, ADIMB–DNPM, Brasília, pp. 79–139
- Lindenmayer, Z. G., Fleck, A., Gomes, C.H., Santos, A.B.S., Caron, R., Paula, F.C., Laux, J.H., Pimentel, M.M., and Sardinha, A.S. 2005, Caracterização geológica do alvo estrela (Cu-Au), Serra dos Carajás, Pará In: Caracterização de Depósitos Minerais em Distritos Mineiros da Amazônia. DNPM, CT-Mineral / FINEP, ADIMB, CD-ROM, 2005, cap. IV, 1, 137-205.
- Lobato, L.M., Roaière, C.A., Silva, R.C.F., Zucchetti, M., Baars, F.J., Seoane, J.C.S., Rios, F.J., Pimentel, M., Mendes, G.E. and Monteiro, A.M., 2005, A mineralização hidrotermal de ferro da Província Mineral de Carajás - controle estrutural e contexto na evolução metalogenética da Província. In: Marini, J.O.; Queiróz, E.T.; Ramos, W.B. (eds.), Caracterização de distritos mineiros da Amazônia. DNPM-CT-Mineral-ADIMB, 25–92.
- Loiselle, M.C., and Wones, D.R., 1979, Characteristics and origin of anorogenic granites. Abstracts with programs-Geological Society of America 11, 468.
- Ludwig K.R. 2003. User’s Manual for Isoplot/Ex v. 3.00. A Geochronological Toolkit for Microsoft Excel. BGC Special Publication 4, Berkeley, 71 pp.
- Macambira, E.M.B., and Vale, A.G., 1997, São Félix do Xingu: folha SB.22-Y-B, Estado do Pará, escala 1:250.000. Texto Explicativo. Brasília: CPRM. 344 p., il. Programa Levantamentos Geológicos Básicos do Brasil (PLGB).
- Macambira, E.M.B., and Ferreira Filho, C.F., 2002, Fracionamento magmático dos corpos máfico-ultramáficos da Suíte Intrusiva Cateté – sudeste do Pará. In: Klein, E.L., Vasquez, M.L., Rosa-Costa, L.T. (Ed.). Contribuições à geologia da Amazônia. Belém: SBG-Núcleo Norte. v. 3, p. 105-114.
- Macambira, E.M.B., and Tassinari, C.C.G., 1998, Estudos Sm-Nd no complexo máfico-ultramáfico da Serra da Onça, sul do Pará: implicações geocronológicas e geotectônicas. In: Cong. Bras. Geol., 40., 1998, Belo Horizonte. Anais... Belo Horizonte: SBG Núcleo Minas Gerais, p. 463.
- Macambira, M.J.B., and Lancelot, J., 1996, Time constraints of Archean Rio Maria crust, Southeastern Amazonian Craton, Brazil. International Geology Review, 38 (12): 1134–1142.
- Macambira, J.B., 2003, O ambiente deposicional da Formação Carajás e uma proposta de modelo evolutivo para a Bacia Grão Pará. Tese de Doutorado, IG-UNICAMP, 217p.
- Machado, N., Lindenmayer, D.H., Krough, T.E., and Lindenmayer, Z.G., 1991, U-Pb geochronology of Archean magmatism and basement reactivation in the Carajás area, Amazon Shield, Brazil. Precambrian Research, 49:329-354

- Markey, R.J., Stein, H.J., and Morgan, J.W., 1998, Highly precise Re-Os dating for molybdenite using alkaline fusion and NTIMS. *Talanta* 45, 935–946.
- Markey, R.J., Stein, H.J., Hannah, J.L., Selby, D. and Creaser, R.A., 2007, Standardizing Re-Os geochronology: A new molybdenite Reference Material (Henderson, USA) and the stoichiometry of Os salts". *Chemical Geology*, 244, 74-87.
- Marschik, R., Mathur, R., Ruiz, J., Leveille, R., and Almeida, A.J. de, 2005, Late Archean Cu-Au-Mo mineralization at Gameleira and Serra Verde, Carajás Mineral Province, Brazil: constraints from Re-Os molybdenite ages. *Mineralium Deposita* 39:983–991
- Marschik, R., Spangenberg, J.E., Leveille, R.A., and de Almeida, A.J., 2003, The Sossego iron oxide-Cu-Au deposit, Carajás, Brazil. In: Eliopoulos D et al (eds) *Mineral Exploration and Sustainable Development v 1*. Millpress, Rotterdam, p. 331–334
- Marsh, T.M., Einaudi, M.T., and McWilliams, M., 1997, $^{40}\text{Ar}/^{39}\text{Ar}$ geochronology of Cu-Au and Au-Ag mineralization in the Potrerillos district, Chile: Economic Geology, v. 92, p. 784–806
- Meirelles, M.R., 1986, Geoquímica e petrologia dos jaspilitos e rochas vulcânicas associadas, Grupo Grão-Pará, Serra dos Carajás. Unpublished Master Thesis, UnB, pp.
- Meirelles, M.R., and Dardenne, M.A., 1991, Vulcanismo basáltico de afinidade shoshonítica em ambiente de arco arqueano, Grupo Grão Pará, Serra dos Carajás, Pa. *Revista Brasileira de Geociências*, 21: 41-50.
- Monteiro, L.V.S., Xavier, R.P., Carvalho, E.R., Hitzman, M.W., Johnson, C.A., Souza Filho, C.R., and Torresi, I., 2008a, Spatial and temporal zoning of hydrothermal alteration and mineralization in the Sossego iron oxide–copper–gold deposit, Carajás Mineral Province, Brazil: paragenesis and stable isotope constraints. *Mineralium Deposita*, 43:129–159.
- Monteiro, L.V.S., Xavier, R.P., Hitzman, M.W., Juliani, C., Souza Filho, C.R., and Carvalho, E.R., 2008b, Mineral chemistry of ore and hydrothermal alteration at the Sossego iron oxide–copper–gold deposit, Carajás Mineral Province, Brazil. *Ore Geology Reviews*, 34:317-336.
- Monteiro, L.V.S., Xavier, R.P., Souza Filho, C.R., Moreto, C.P.N. (in press). Metalogenia da Província Carajás. In: "Metalogenia das Províncias Tectônicas Brasileiras". Serviço geológico do Brasil-CPRM. 1 ed, 50p.
- Morais, R.P.S., and Alkmim, F.F., 2005, O controle litoestrutural da mineralização de cobre do Depósito Sequeirinho, Canaã dos Carajás, PA. In: I Simpósio Brasileiro de Metalogenia, Gramado, [CD-ROM]
- Moreto, C.P.N., 2010, O depósito de óxido de ferro-cobre-ouro Bacaba, Província Mineral de Carajás: Geocronologia U-Pb das rochas hospedeiras. Unpublished Master Thesis. UNICAMP. 85p.
- Moreto, C.P.N., Monteiro L.V.S., Xavier R.P., Amaral W.S., Santos T.J.S., Juliani C., and Souza Filho C.R., 2011, Mesoarchean (3.0 and 2.86 Ga) host rocks of the iron oxide-Cu-Au Bacaba deposit, Carajás Mineral Province: U-Pb geochronology and metallogenetic implications. *Mineralium Deposita* V. 46, pps. 789-811. DOI: 10.1007/s00126-011-0352-9.
- Moroni, M., Girardi, V.A.V., and Ferrario, A., 2001, The Serra Pelada Au–PGE deposit, Serra dos Carajás (Pará State, Brazil): geological and geochemical indications for a composite mineralising process: *Mineralium Deposita*, v. 36, p. 768-785.
- Mougeot, R., Respaut, J.P., Briquel, L., Ledru, P., Milesi, J.P., Macambira, M.J.B., and Huhn S.B. 1996a, Geochronological constrains for the age of the Águas Claras Formation (Carajás Province, Pará, Brazil). In: Congresso Brasileiro de Geologia, 39, Salvador, 1996. Anais., Salvador, SBG. 6:579-581.
- Mougeot, R., Respaut, J.P., Briquel, L., Ledru, P., Milesi J.P., Lerouge, C., Marcoux, E., Huhn, and S.B., Macambira, M.J.B, 1996b, Isotope geochemistry constrains for Cu, Au mineralizations and evolution of the Carajás Province (Para, Brazil). In: SBG, Congresso Brasileiro de Geologia, 39, Salvador, Anais, 7, 321-324 (in Portuguese).
- NCL Brasil, 2005, Revision de La Estimación de Recursos del Proyecto Cristalino. Vale S.A Internal Report, 1-103.

- Neves, M.P., 2006, Estudos isotópicos (Pb-Pb, Sm-Nd, C e O) do depósito Cu-Au do Sossego, Província Mineral de Carajás. Unpublished Master Thesis. Universidade Federal do Pará. 116 p.
- Nogueira, A.C.R., Truckenbrod, W., Costa, J.B.S., and Pinheiro, R.V.L., 1994, Análise faciológica e estrutural da Formação Águas Claras, Pré-Cambriano da Serra dos Carajás. 4 Simpósio de Geologia da Amazônia, pp. 363–364.
- Nogueira, A.C.R., Truckenbrod, W., Pinheiro, R.V.L., 2000, Storm and tide-dominated siliciclastic deposits of the Archean Águas Claras Formation, Serra dos Carajás, Brazil. 31st International Geological Congress, Rio de Janeiro. Sociedade Brasileira de Geologia. Abstract volume CD-ROM.
- Oliveira, C.G., and Leonardos, O.H., 1990, Gold mineralization in the Diadema shear belt, northern Brazil. *Economic Geology*, 85: 1034-1043.
- Oliveira, D.C., Santos, P.J.L., Gabriel, E.O., Rodrigues, D.S., Faresin, A.C., Silva, M.L.T., Sousa, S.D., Santos, R.V., Silva, A.C., Souza, M.C., Santos, R.D., and Macambira, M.J.B., 2010, Aspectos geológicos e geocronológicos das rochas magmáticas e metamórficas da região entre os municípios de Água Azul do Norte e Canaã dos Carajás – Província Mineral de Carajás, In: SBG, Congresso Brasileiro de Geologia, 45, CDrom (in Portuguese).
- Olszewski, W.J., Wirth, K.R., Gibbs, A.K., and Gaudette, H.E., 1989, The age, origin, and tectonics of the Grão Pará Group and associated rocks, Serra dos Carajás, Brazil: Archean continental volcanism and rifting. *Precambrian Research*, 42, 229-254.
- Pidgeon, R.T., Macambira, M.J.B., and Lafon, J.M. 2000, Th–U–Pb isotopic systems and internal structures of complex zircons from an enderbite from the Pium Complex, Carajás Province, Brazil: evidence for the ages of granulite facies metamorphism and the protolith of the enderbite. *Chemical Geology* 166, 159–171.
- Pimentel, M.M., Lindenmayer, Z.G., Laux, J.H., Armstrong, R. and Araújo, J.C., 2003, Geochronology and Nd geochemistry of the Gameleira Cu-Au deposit, Serra dos Carajás, Brazil: 1.8–1.7 Ga hydrothermal alteration and mineralization. *Journal of South American Earth Sciences*, 15: 803-813.
- Pimentel, M.M., and Machado, N., 1994, Geocronologia U–Pb dos terrenos granito-greenstone de Rio Maria, Pará. In: Cong. Bras. Geol., Anais, Sociedade Brasileira de Geologia, vol. 2, pp. 390–391.
- Pinheiro, R.V.L., and Holdsworth, R.E., 1997, Reactivation of Archaean strike-slip fault systems, Amazon region, Brazil. *Journal of the Geological Society of London* 154, 99–103.
- Pirajno, F., Mao, J., Zhang, Z., Zhang, Z., and Chai, F., 2008, The association of mafic-ultramafic intrusions and A-type magmatism in the Tian Shan and Altay orogens, NW China: Implications for geodynamic evolution and potential for the discovery of new ore deposits. *Journal Asian Earth Sciences*, 32: 165-183
- Pollard, P.J., 2001, Sodic–(calcic) alteration in Fe-oxide–Cu–Au districts: an origin via unmixing of magmatic H₂O–CO₂–NaCl + CaCl₂–KCl fluids. *Mineralium Deposita* 36: 93–100.
- Pollard, P.J. 2006, An intrusion-related origin for Cu–Au mineralization in iron oxide–copper–gold (IOCG) provinces. *Mineralium Deposita*, 41: 179-187.
- Quadt, A. v., Moritz, R., Peytcheva, I., and Heinrich, C. A., 2005, Geochronology and geodynamics of Late Cretaceous magmatism and Cu-Au mineralization in the Panagyurishte region of the Apuseni-Banat-Timok-Srednogorie belt, Bulgaria. *Ore Geology Reviews*, 27 (2005) 95-126.
- Rämö, O.T., Haapala, I., Vaasjoki, M., Yu, J.H., and Fu, H.Q., 1995, 1700 Ma Sachang complex, northeast China: Proterozoic rapakivi granite not associated with Paleoproterozoic orogenic crust. *Geology* 23, 815–818.
- Réquia, K., Stein, H., Fontboté, L., and Chiaradia, M., 2003, Re-Os and Pb-Pb geochronology of the Archean Salobo iron oxide copper–gold deposit, Carajás Mineral Province, northern Brazil: *Mineralium Deposita*, v. 38, p. 727-738.
- Ricci, P.S.F., Carvalho, M.A., 2006, Rocks of the Pium-Area, Carajás Block, Brazil – A Deep seated High-T Gabbroic Pluton (Charnockitoid-Like) with Xenoliths of Enderbitic Gneisses Dated at

- 3002 Ma – The Basement Problem Revisited. In: Simpósio de Geologia da Amazônia, 8, [CD-ROM]
- Rigon, J.C., Munaro, P., Santos, L.A., Nascimento, J.A.S. and Barreira, C.F., 2000, Alvo 118 copper–gold deposit: geology and mineralization, Serra dos Carajás, Pará, Brazil. 31st International Geological Congress, Rio de Janeiro. SBG, Abstract Volume, [CD-ROM].
- Rios, F.J., Villas, R.N., Fuzikawa, K., Sial, A.N., and Mariano, G., 1998, Isótopos de oxigênio e temperatura de formação dos veios mineralizados com wolframita da jazida Pedra Preta, sul do Pará. Revista Brasileira de Geociências 28(3):253–256
- Rios, F.J., Villas, R.N., and Fuzikawa, K., 2003, Fluid Evolution in the Pedra Preta wolframite ore deposit, Paleoproterozoic Musa Granite, eastern Amazon craton, Brazil. Journal of South American Earth Sciences, 15: 787-802.
- Rodrigues, E.S., Lafon, J.M., and Scheller, T., 1992, Geocronologia Pb-Pb da Província Mineral de Carajás: primeiros resultados. In: Congresso Brasileiro de Geologia, 37, Boletim Resumos Expandidos, SBG, São Paulo, vol. 2, pp. 183-184.
- Rosa, A.G.N., 2006, Rochas encaixantes, alteração hidrotermal e caracterização dos fluidos relacionados à formação do Corpo Sequeirinho do Depósito Cu-Au do Sossego, região de Carajás: Unpublished Master Thesis, Universidade Federal do Pará.
- Santos, M.G.S., 2002, Estudo dos isótopos de Pb e Nd do depósito de Cu– Au (U-Etr) Alemão, Província Mineral de Carajás (PA). Unpublished Master Thesis, Universidade Federal do Pará, 126p.
- Sardinha, A.S., Barros, C.E. de M., Krymsky, M., 2006, Geology, geochemistry and U–Pb geochronology of the Archean (2.74Ga) Serra do Rabo granite stocks, Carajás Metallogenetic Province, northern Brazil. Journal of South American Earth Sciences 20, 327–339.
- Selby, D, and Creaser, R.A., 2004, Macroscale NTIMS and microscale LA-MC-ICP-MS Re-Os isotopic analysis of molybdenite: Testing spatial restrictions for reliable Re-Os age determinations, and implications for the decoupling of Re and Os within molybdenite. *Geochimica et Cosmochimica Acta* (2004), 68, 3897-3908.
- Silva, M.A.D, 2011, O Domínio de Transição da Província Mineral de Carajás: Contexto geológico e litoquímica das unidades hospedeiras de mineralizações cúpro-auríferas. Trabalho de Conclusão de Curso. UNICAMP. 74p.
- Silva, C.M.G., and Villas, N.R., 1998, The Águas Claras Cu-sulfide ± Au deposit, Carajás region, Pará, Brazil: geological setting, wall-rock alterationand mineralizing fluids: Revista Brasileira de Geociências, v. 28, p. 315-326.
- Silva, J.L. 1988, Mina de manganês do Azul. In: Cong. Bras. Geol., 35, Anexo aos anais. SBG, p. 73-94.
- Silva, M.G., Teixeira, J.B.G., Pimentel, M.M., Vasconcelos, P.M., Arielo, A. and Rocha, W.J.S.F., 2005, Geologia e mineralizações de Fe-Cu-Au do Alvo GT46 (Igarapé Cinzento, Carajás). In: Marini, O.J., Queiroz, E.T., Ramos, B.W. (eds.), Caracterização de Depósitos Minerais em Distritos Mineiros da Amazônia, 94-151.
- Silva, A.R.C., Villas, R.N.N., Lafon, J.M., and Craveiro, G.S., 2012, Idade da alteração e mineralização do depósito de Cu-Au Visconde, Província Mineral de Carajás (Pará), Brasil. 46º Congresso Brasileiro de Geologia, Santos. (CD-ROM).
- Simonetti, A., Heaman ,L.M., Hartlaub, R.P., Creaser, R.A., Machattie, T.G., and Bohm, C. 2005, U-Pb zircon dating by laser ablation MC-ICP-MS using a new multiple ion counting Faraday collector array. *Journal of Analytical Atomic Spectrometry* 20: 677-686.
- Simonetti, A., Heaman, L.M., Chacko, T. and Banerjee, N.R., 2006, In situ petrographic thin section U-Pb dating of zircon, monazite, and titanite using laser ablation-MC-ICP-MS. *International Journal of Mass Spectrometry*, 253(1-2): 87-97.
- Soares, A.D.V., Macambira, M.J.B., Santos, M.G.S., Vieira, E.A.P., Massoti, F.S., Souza, C.I.J., Padilha, J.L., and Magni, M.C.V., 2001, Depósito Cu-(Au) Cristalino, Serra dos Carajás, PA: Idade da mineralização com base em análises Pb-Pb em sulfetos (dados preliminares): Simpósio de Geologia da Amazônia, VII, Belém, Sociedade Brasileira de Geologia, [CD-ROM].

- Souza, S.R.B., Macambira, M.J.B., Sheller, T., 1996, Novos dados geocronológicos para os granitos deformados do Rio Itacaiúnas (Serra dos Carajás, PA); implicações estratigráficas. V Simpósio de Geologia da Amazônia, Belém, Anais, 380–383.
- Stein, H.J., and Cathles, L.M., 1997, Preface: A special issue on the timing and duration of hydrothermal events: *Economic Geology*, v. 92, p. 763–765.
- Tallarico, F.H.B., 2003, O cinturão cupro-aurífero de Carajás, Brasil. Unpublished Ph.D. Dissertation, Universidade Estadual de Campinas, 229p
- Tallarico, F.H.B., Figueiredo B.R., Groves D.I., Kositcin N., McNaughton N.J., Fletcher I.R., and Rego J.L., 2005, Geology and SHRIMP U–Pb geochronology of the Igarapé Bahia deposit, Carajás copper–gold belt, Brazil: an Archean (2.57 Ga) example of iron–oxideCu–Au–(U– REE) mineralization. *Economic Geology* 100:7–28.
- Tallarico, F.H.B., McNaughton, N.J., Groves, D.I., Fletcher, I.R., Figueiredo, B.R., Carvalho, J.B., Rego, J.L., Nunes, A.R., 2004, Geological and SHRIMP II U-Pb constraints on the age and origin of the Breves Cu-Au-(W-Bi-Sn) deposit, Carajás, Brazil. *Mineralium Deposita*. 39, 68-86.
- Tassinari, C.C.G., 1996, O mapa geocronológico do Cráton Amazônico no Brasil: revisão dos dados isotópicos. Tese de Livre Docência, IG-USP, 139p.
- Tassinari, C.C.G., and Macambira, M.J.B., 1999, Geochronological Provinces of the Amazonian Craton. *Episodes*, 22 (3):174-182.
- Tassinari C.C.G., and Macambira M.J.B., 2004, A evolução tectônica do Cráton Amazônico. In: Mantesso-Neto, V., Bartorelli, A., Carneiro, C.D.R., Brito-Neves, B.B. (eds.). *Geologia do continente Sul-Americano: Evolução da obra de Fernando Flávio Marques de Almeida*. São Paulo, Beca, 2004. p. 471-485.
- Tassinari, C.C.G., Tachibana, J., Tulio, M., Livio, R., and Gaia, C., 2005, Geologia isotópica aplicada nas mineralizações de Cu-Au do greenstone belt da Serra dos Gradaús, Província Mineral de Carajás, Cráton Amazônico: exemplo de mineralizações policíclicas. In: *Simpósio Brasileiro de Metalogenia*, 1, [CD-ROM]
- Tassinari, C.C.G., Mellito, M.K. and Babinski, M., 2003, Age and origin of the Cu (Au–Mo–Ag) Salobo 3A ore deposit, Carajás Mineral Province, Amazonian Craton, Northern Brazil. *Episodes* 26 (1), 2–9.
- Tassinari, C. C. G., Hirata, W. K., and Kawashita, K., 1982, Geologic evolution of the Serra dos Carajás, Pará, Brazil: *Revista Brasileira de Geociências*, v. 12, nos. 1-3, pp. 263-267
- Tavaza, E., 1999, Mineralização de Au-Cu-(ETR-U) associada às brechas hidrotermais do depósito de Iagarapé Bahia, província Mineral de Carajás, PA. Unpublished Master Thesis, Ouro Preto, Brazil, Universidade Federal de Ouro Preto. 81p.
- Teixeira, J.B.G., 1994, Geochemistry, petrology, and tectonic setting of archean basaltic and dioritic rocks from the N4 Iron deposit, Serra dos Carajás, Pará, Brazil. 1994. 161 f. Unpublished Ph.D. Dissertation.
- Teixeira, J.B.G., Lindenmayer, Z.G., and Silva, M.G., 2010, Depósitos de Óxido de Fe, Cu-Au de Carajás. In: R.S.C. Brito, M.G. Silva, R.M. Kuyumjian. (Org.). *Modelos de depósitos de cobre do Brasil e sua resposta ao intemperismo*. 1 ed. Brasilia: CPRM, p. 15-48.
- Teixeira, W., Tassinari, C.C.G., Cordani, U.G., and Kawashita, K., 1989, A review of the geochronological of the Amazonian Craton: tectonic implications. *Precambrian Research*, 42: 213-227.
- Tolbert, G.E., Tremaine, J.W., Melcher, G.C., Gomes, C.B., 1971, The recently discovered Serra dos Carajás iron deposits, Northern Brazil. *Economic Geology*, 66: 985-994
- Torresi, I., Bortholoto, D.F.A., Xavier, R.P., and Monteiro, L.V.S., 2012, Hydrothermal alteration, fluid inclusions and stable isotope systematics of the Alvo 118 iron oxide–copper–gold deposit, Carajás Mineral Province (Brazil): implications for ore genesis. *Mineralium Deposita*, 47: 299-323.
- Trendall, A.F., Basei, M.A.S., De Laeter, J.R., and Nelson, D.R., 1998, SHRIMP U-Pb constraints on the age of the Carajás formation, Grão Pará Group, Amazon Craton. *Journal of South American Earth Sciences* 11, 265-277.

- Vale. 2012. Vale obtains operation license for Salobo. <http://saladeimprensa.vale.com/en/release/interna.asp?id=22000>. Accessed in february 04, 2013.
- Van Achterbergh, E., Ryan, C.G., Jackson, S.E., and Griffin, W.L., 2001. Data reduction software for LA-ICP-MS: appendix. In: Syl-vester, P.J. (Ed.), Laser Ablation-ICP-Mass Spectrometry in the Earth Sciences: Principles and Applications, Mineralog. Assoc. Canada (MAC) Short Course Series, Ottawa, Ontario, Canada, vol. 29, pp. 239 – 243.
- Vasquez, L.V., Rosa-Costa, L.R., Silva, C.G., Ricci, P.F., Barbosa, J.O., Klein, E.L., Lopes, E.S., Macambira, E.B., Chaves, C.L., Carvalho, J.M., Oliveira, J.G., Anjos, G.C., and Silva, H.R., 2008, Geologia e Recursos Minerais do Estado do Pará: Sistema de Informações Geográficas – SIG: Texto Explicativo dos Mapas Geológico e Tectônico e de Recursos Minerais do Estado do Pará. Organizadores: M.L Vasquez, L.T. Rosa-Costa. Escala 1:1.000.000. Belém: CPRM.
- Vavra, G., 1990, On the kinematics of zircon growth and its petrogenetic significance: A cathodoluminescence study. Contributions to Mineralogy and Petrology 106:90-99.
- Villas, R.N., and Santos, M.D., 2001, Gold deposits of the Carajás Mineral Province: deposit types and metallogenesis. Mineralium Deposita, 36:300–331
- Villas, R.N., Neves, M.P., Moura, C.V., Toro, M.A.G., Aires, B. and Maurity, C., 2006, Estudos isotópicos (Pb, C e O) no depósito Cu-Au do Sossego, Província Mineral de Carajás. IX Simpósio de Geologia da Amazônia, SBG/Núcleo Norte, [CD-ROM].
- Volp, K., Evins, P., and Maffre, S., 2006, EPMA and LA-ICPMsdating of hydrothermal REE-minerals from the Estrela Copper Deposit, Carajás, Brazil. Goldschmidt Conference, Abstract.
- Williams I.S., 1998, U-Th-Pb geochronology by ion microprobe. In: McKibben, M.A. Shanks, W.C. and Ridley W.I. (eds) Applications of Microanalytical Techniques to Understanding Mineralizing Processes. Reviews in Economic Geology 7: 1-35.
- Wirth, K.R., Gibbs, A.K., and Olszewski, W.J.Jr., 1986, U-Pb ages of zircons from the Grão Pará Group and Serra dos Carajás granite, Pará, Brasil. Revista Brasileira de Geociências 16: 195–200.
- Xavier, R.P., Monteiro, L.V.S., Souza Filho, C.R., Torresi, I., Carvalho, E.R., Dreher, A.M., Wiedenbeck, M., Trumbull, R.B., Pestilho, A.L.S., and Moreto, C.P.N., 2010, The iron oxide copper– gold deposits of the Carajás Mineral Province, Brazil: an updated and critical review. In: Porter TM (ed) Hydrothermal Iron Oxide Copper-Gold & Related Deposits: A Global Perspective. Australian Miner. Fund, Adelaide, Vol 3, pp. 285-306.
- Xavier, R.P., Monteiro, L.V.S., Moreto, C.P.N., Pestilho, A.L.S., Melo, G.H.C., Silva, M.A.D., Aires, B., Ribeiro, C., and Silva, F.H.F., 2012, The The Iron Oxide Copper-Gold Systems of the Carajás Mineral Province, Brazil. In: “Geology and Genesis of Major Copper Deposits and Districts of the World: A Tribute To Richard Sillitoe”. Special publication of the Society of Economic Geologists.
- Xavier, R.P., Wiedenbeck, M., Trumbull, R.B., Dreher, A.M., Monteiro, L.V.S., Rhede, D., Araújo, C.E.G., and Torresi, I., 2008, Tourmaline B-isotopes fingerprint marine evaporites as the source of high-salinity ore fluids in iron oxide-copper-gold deposits, Carajás Mineral Province (Brazil): Geology 36: 743-746.
- Xavier, R.P., Araújo, C.E.G., Dreher, A.M., Nunes, and A.R., Rêgo, J.L, 2003, Fluid evolution in the Paleoproterozoic Intrusion-related Breves Cu-Au (Mo-W-Bi) deposit, Carajás Mineral Province, Northern Brazil. In VIII Simpósio de Geologia da Amazônia. Manaus, Amazonas.
- Xavier, R.P., Rusk, B., Emsbo, P., and Monteiro, L.V.S., 2009, Composition and source of salinity of ore-bearing fluids in Cu-Au systems of the Carajás Mineral Province, Brazil: In: 10th Biennial Meeting of the SGA, Townsville (Australia), Proceedings, p. 272-274.
- Zuchetti, M., 2007, Rochas maficas do grupo Grão Pará e sua relação com a mineralização de ferro dos depósitos N4 E N5, Carajás, PA: Unpublished Ph.D. Dissertation, Universidade Federal de Minas Gerais, 165p.

Appendix

Supplementary Table 1 Summary of U-Pb LA-ICPMS zircon data from the host rocks of the Sequeirinho and Sossego orebodies

Isotopic ratios										Ages								
Zircon Grain	Th/U	Th (ppm)	U (ppm)	$^{204}\text{Pb}/^{206}\text{Pb}$	$^{207}\text{Pb}/^{206}\text{Pb}$	\pm	$^{207}\text{Pb}/^{235}\text{U}$	\pm	$^{206}\text{Pb}/^{238}\text{U}$	\pm	$^{207}\text{Pb}/^{206}\text{Pb}$	\pm	$^{207}\text{Pb}/^{235}\text{U}$	\pm	$^{206}\text{Pb}/^{238}\text{U}$	\pm	% disc	
Sequeirinho Granite (F259/177.4)																		
ZR3-1	0.32	59	182	0.00026	0.2217	0.0024	18.14	0.30	0.5878	0.0050	2993	17	2997	16	2981	20	-0.4	
ZR6-2	0.38	62	163	0.00052	0.2192	0.0029	15.99	0.48	0.4975	0.0051	2975	21	2876	28	2603	22	-12.5	
ZR4	0.51	112	221	0.00022	0.2203	0.0024	16.81	0.27	0.5461	0.0046	2983	17	2924	16	2809	19	-5.8	
ZR6-1	0.42	74	174	0.00036	0.2204	0.0027	14.43	0.35	0.4795	0.0046	2983	19	2779	23	2525	20	-15.4	
ZR5b-1	0.45	56	124	0.00007	0.2187	0.0026	16.87	0.43	0.5379	0.0049	2971	19	2927	24	2775	21	-6.6	
ZR1-2	0.33	43	130	0.00007	0.2199	0.0025	18.54	0.39	0.5994	0.0053	2980	18	3018	20	3027	21	1.6	
ZR7a-1	0.31	68	216	0.00029	0.2170	0.0027	15.66	0.30	0.5267	0.0045	2959	20	2856	18	2728	19	-7.8	
ZR7a-2	0.42	80	190	0.00031	0.2213	0.0028	16.75	0.36	0.5537	0.0048	2991	20	2921	20	2840	20	-5.0	
ZR7b-1	0.54	73	134	0.00015	0.2207	0.0032	16.90	0.48	0.5646	0.0053	2986	23	2929	27	2886	22	-3.3	
ZR7b-2	0.49	84	172	0.00031	0.2140	0.0035	14.24	0.46	0.4735	0.0048	2936	27	2766	31	2499	21	-14.9	
ZR7b-2a	0.42	72	170	0.00024	0.1926	0.0031	6.72	0.19	0.2572	0.0022	2765	26	2076	25	1476	11	-46.6	
ZR6-1	0.43	48	112	0.00060	0.2218	0.0030	18.12	0.47	0.5865	0.0053	2993	22	2996	25	2975	21	-0.6	
ZR5a-1	0.47	147	312	0.00014	0.2177	0.0033	14.90	0.37	0.5017	0.0046	2964	24	2809	23	2621	20	-11.6	
ZR5a-2	0.36	62	172	0.00021	0.2158	0.0033	15.09	0.40	0.4920	0.0044	2950	24	2821	25	2579	19	-12.6	
ZR1-1	0.38	49	129	0.00040	0.2185	0.0033	17.32	0.48	0.5655	0.0049	2970	24	2953	27	2889	20	-2.7	
Sequeirinho Granite (F22/107.45)																		
ZR11b	0.46	408	882	0.00004	0.2038	0.0026	9.20	0.17	0.3367	0.0030	2857	20	2358	17	1871	15	-34.5	
ZR11b2	0.58	225	390	0.00012	0.2099	0.0023	11.23	0.16	0.3896	0.0031	2905	18	2543	13	2121	14	-27.0	
ZR11A	0.48	333	698	0.00019	0.2002	0.0022	7.64	0.10	0.2814	0.0022	2828	18	2189	11	1598	11	-43.5	
ZR12A	0.48	155	323	0.00015	0.2202	0.0024	17.01	0.25	0.5532	0.0043	2982	18	2935	14	2839	18	-4.8	
ZR8	0.30	162	537	0.00019	0.2192	0.0026	14.61	0.25	0.4908	0.0041	2975	19	2790	16	2574	18	-13.5	
ZR6	0.31	165	526	0.00019	0.2068	0.0023	10.05	0.14	0.3545	0.0028	2881	18	2439	13	1956	13	-32.1	
ZR7B	0.25	304	1227	0.00017	0.1661	0.0019	4.52	0.06	0.2019	0.0016	2518	19	1736	11	1185	8	-52.9	
ZR7a	0.19	247	1282	0.00011	0.1705	0.0021	5.11	0.08	0.2255	0.0020	2562	21	1837	14	1311	10	-48.8	
ZR20	0.43	188	433	0.00011	0.2137	0.0024	14.01	0.21	0.4697	0.0037	2934	18	2750	14	2482	16	-15.4	
ZR10A	0.43	77	180	0.00036	0.2234	0.0026	16.86	0.33	0.5582	0.0046	3006	19	2927	19	2859	19	-4.9	
ZR10B	0.35	81	232	0.00057	0.2147	0.0025	13.91	0.24	0.4529	0.0036	2941	19	2744	17	2408	16	-18.1	
ZR9	0.22	138	623	0.00017	0.2083	0.0025	9.67	0.15	0.3419	0.0028	2892	19	2404	15	1896	13	-34.5	
ZR5C	0.31	66	215	0.00026	0.2218	0.0027	16.85	0.33	0.5436	0.0045	2994	19	2927	19	2799	19	-6.5	
ZR10	0.28	25	90	0.00054	0.2179	0.0027	18.45	0.45	0.6055	0.0048	2965	19	3013	24	3052	19	2.9	
ZR10	0.31	150	485	0.00013	0.2092	0.0028	11.53	0.24	0.3991	0.0035	2899	22	2567	20	2165	16	-25.3	
ZR1	0.42	225	530	0.00021	0.2113	0.0024	11.84	0.17	0.4058	0.0031	2916	18	2592	13	2196	14	-24.7	

Supplementary Table 1 (continued)

Isotopic ratios											Ages						
Zircon Grain	Th/U	Th (ppm)	U (ppm)	$^{204}\text{Pb}/^{206}\text{Pb}$	$^{207}\text{Pb}/^{206}\text{Pb}$	\pm	$^{207}\text{Pb}/^{235}\text{U}$	\pm	$^{206}\text{Pb}/^{238}\text{U}$	\pm	$^{207}\text{Pb}/^{206}\text{Pb}$	\pm	$^{207}\text{Pb}/^{235}\text{U}$	\pm	$^{206}\text{Pb}/^{238}\text{U}$	\pm	% disc
<i>Sossego granophyric granite (F35/406.88)</i>																	
ZR5B-1	0.63	147	235	0.00029	0.1883	0.0021	13.12	0.21	0.5067	0.0041	2728	18	2643	18	2688	15	-3.1
ZR5B-2	0.45	139	308	0.00018	0.1861	0.0020	11.57	0.17	0.4497	0.0036	2708	18	2394	16	2570	13	-11.6
ZR51	0.16	262	1643	0.00029	0.1288	0.0015	2.06	0.03	0.1190	0.0009	2082	20	725	5	1135	9	-65.2
ZR5	0.18	74	407	0.00016	0.1891	0.0021	13.56	0.22	0.5227	0.0046	2735	18	2711	19	2720	16	-0.9
ZR6a-1	0.36	126	349	0.00013	0.1777	0.0020	7.93	0.12	0.3242	0.0027	2632	18	1810	13	2223	13	-31.2
ZR6a-2	0.44	113	255	0.00023	0.1891	0.0021	11.51	0.19	0.4448	0.0037	2734	18	2372	16	2565	15	-13.2
ZR6B-1	0.45	257	576	0.00026	0.1803	0.0021	7.69	0.13	0.3208	0.0025	2655	19	1794	12	2196	15	-32.4
ZR6B-2	0.39	230	594	0.00018	0.1803	0.0020	8.23	0.12	0.3368	0.0027	2656	19	1871	13	2257	13	-29.5
ZR2A-1	0.44	483	1090	0.00015	0.1510	0.0017	3.67	0.05	0.1822	0.0015	2357	19	1079	8	1565	11	-54.2
ZR2A-2	0.53	453	852	0.00017	0.1579	0.0018	4.56	0.06	0.2115	0.0017	2433	19	1237	9	1742	11	-49.2
ZR2C-1	0.97	731	756	0.00016	0.1772	0.0019	7.60	0.09	0.3143	0.0025	2627	18	1762	12	2185	11	-32.9
ZR6d-1	0.36	342	951	0.00012	0.1824	0.0024	6.05	0.12	0.2464	0.0023	2675	21	1420	12	1983	17	-46.9
ZR6e-1	0.18	252	1366	0.00023	0.1277	0.0015	2.42	0.03	0.1448	0.0011	2066	20	872	6	1248	10	-57.8

Supplementary Table 2 Summary of U-Pb SHRIMP IIe zircon data from the host rocks of the Sequeirinho, Pista and Sossego orebodies, and an ore sample from the Sequeirinho orebody

Zircon Grain	Isotopic ratios								Ages (204 corr)					
	% 206 comm	U (ppm)	Th (ppm)	$^{232}\text{Th}/$ ^{238}U	$^{207}\text{Pb}/$ ^{235}U	1s	$^{206}\text{Pb}/$ ^{238}U	1s	err corr	$^{206}\text{Pb}/$ ^{238}U	1s	$^{207}\text{Pb}/$ ^{206}Pb	1s	% disc
Gabbronorite from the Sequeirinho orebody (SOS 35)														
Zr-1.1	0.17	128	21	0.17	13.72	3.2	0.5231	3.1	0.959	2712.5	67.8	2744	15	1
Zr-2.1	0.20	76	23	0.32	14.00	3.3	0.5310	3.2	0.946	2745.8	70.9	2753	18	0
Zr-4.1	0.17	115	38	0.34	14.07	3.2	0.5365	3.1	0.963	2768.9	69.2	2744	14	-1
Zr-5.1	0.15	128	63	0.51	13.92	3.2	0.5348	3.1	0.964	2761.6	69.4	2732	14	-1
Zr-6.1	0.15	52	18	0.35	13.29	3.6	0.5065	3.3	0.910	2641.5	71.4	2745	25	4
Zr-7.1	0.06	195	54	0.29	13.79	3.1	0.5288	3.0	0.976	2736.4	67.6	2735	11	0
Zr-8.1	0.19	65	17	0.28	13.69	3.4	0.5145	3.2	0.937	2675.7	70.0	2768	19	3
Zr-9.1	0.18	124	46	0.39	13.61	3.2	0.5191	3.1	0.962	2695.5	68.1	2744	14	2
Zr-10.1	-0.04	139	30	0.22	13.40	3.2	0.5172	3.0	0.950	2687.5	67.0	2723	17	1
Zr-12.1	-0.07	191	117	0.63	14.18	3.2	0.5448	3.1	0.973	2803.4	70.6	2732	12	-3
Sequeirinho Granite (SOS 450/13)														
Zr-1.1	0.10	112	43	0.40	18.65	3.6	0.6104	3.5	0.974	3071.7	85.5	2993	13	-3
Zr-2.1	0.00	155	44	0.30	18.73	3.5	0.6103	3.5	0.981	3071.3	84.8	3000	11	-2
Zr-3.1	0.07	128	52	0.42	18.67	3.6	0.6116	3.5	0.979	3076.2	85.7	2991	12	-3
Zr-4.1	0.29	109	43	0.40	18.27	3.6	0.5972	3.5	0.968	3018.6	84.4	2995	15	-1
Zr-5.1	0.20	121	45	0.38	17.78	3.7	0.5934	3.6	0.976	3003.1	87.0	2961	13	-1
Zr-7.1	0.21	150	111	0.76	17.25	3.9	0.5632	3.5	0.908	2879.8	81.6	2996	26	4
Zr-8.1	0.00	63	27	0.45	19.25	3.7	0.6188	3.6	0.966	3105.3	88.2	3021	15	-3
Zr-10.1	0.01	216	80	0.38	18.75	3.5	0.6146	3.5	0.988	3088.2	84.9	2990	9	-3
Zr-11.1	0.00	141	59	0.44	18.17	3.5	0.6043	3.5	0.980	3047.3	84.2	2966	11	-3
Zr-12.1	0.00	135	36	0.28	18.56	3.5	0.6135	3.5	0.979	3083.8	85.0	2977	12	-3
Sequeirinho ore (SOS 39J)														
Zr-1.1	0.25	77	38	0.51	20.44	3.4	0.6403	3.2	0.955	3190.3	81.4	3062	16	-4
Zr-2.1	-0.26	230	209	0.94	20.10	3.0	0.6220	3.0	0.984	3118.0	74.1	3082	9	-1
Zr-3.1	-0.80	119	85	0.74	19.33	3.2	0.6092	3.1	0.966	3066.9	75.2	3053	13	0
Zr-4.1	0.06	76	45	0.61	18.75	3.4	0.5840	3.3	0.950	2965.1	77.5	3072	17	4
Zr-5.1	-0.01	111	74	0.69	19.17	3.2	0.5925	3.1	0.964	2999.7	74.2	3084	14	3
Zr-6.1	-0.23	114	98	0.89	19.21	3.2	0.5986	3.1	0.957	3024.1	74.4	3071	15	2
Zr-7.1	-0.08	178	134	0.78	18.44	3.1	0.5690	3.1	0.974	2903.8	71.4	3086	11	6
Zr-8.1	0.03	95	54	0.59	19.61	3.5	0.6026	3.4	0.969	3040.4	81.3	3093	14	2
Zr-10.1	-0.09	116	91	0.81	19.93	3.2	0.6173	3.1	0.967	3099.1	75.8	3081	13	-1
Zr-12.1	0.17	90	49	0.56	19.81	3.2	0.6188	3.1	0.961	3105.3	77.0	3067	14	-1

Supplementary Table 2 (continued)

Zircon Grain	$\frac{\%}{206}$ comm	Isotopic ratios								Ages (204 corr)					
		U (ppm)	Th (ppm)	$^{232}\text{Th}/^{238}\text{U}$	$^{207}\text{Pb}/^{235}\text{U}$	1s	$^{206}\text{Pb}/^{238}\text{U}$	1s	err corr	$^{206}\text{Pb}/^{238}\text{U}$	1s	$^{207}\text{Pb}/^{206}\text{Pb}$	1s	% disc	
Pista metavolcanic rock (SOS 364/138.35)															
Zr-1.1	0.02	167	81	0.50	17.96	3.1	0.5917	3.1	0.976	2996.5	73.2	2981	11	-1	
Zr-3.1	-0.09	224	107	0.49	17.53	3.1	0.5769	3.0	0.970	2936.0	70.6	2983	12	2	
Zr-4.1	0.00	213	113	0.55	16.03	3.1	0.5446	3.0	0.979	2802.9	68.2	2932	10	5	
Zr-5.1	0.04	182	115	0.65	17.53	3.1	0.5839	3.0	0.978	2964.5	72.3	2964	11	0	
Zr-6.1	0.07	168	63	0.39	16.78	3.5	0.5548	3.5	0.982	2845.1	80.2	2976	11	5	
Zr-8.1	-0.17	191	92	0.50	16.94	3.8	0.5635	3.8	0.984	2881.2	88.0	2966	11	3	
Zr-9.1	0.25	147	120	0.85	16.35	3.4	0.5485	3.2	0.960	2819.0	74.2	2952	15	5	
Zr-10.1	-0.43	251	209	0.86	16.66	3.1	0.5579	3.1	0.972	2858.1	70.6	2956	12	3	
Zr-11.1	-0.04	209	97	0.48	16.53	3.1	0.5424	3.0	0.976	2793.4	68.5	2988	11	7	
Pista metavolcanic rock (SOS 475/167)															
Zr-1.1	0.07	174	29	0.17	17.60	3.6	0.5803	3.5	0.973	2949.8	82.2	2981	13	1	
Zr-2.1	0.13	252	205	0.84	18.97	3.5	0.5930	3.5	0.989	3001.6	83.1	3066	8	2	
Zr-3.1	0.05	200	77	0.40	17.92	3.5	0.5945	3.5	0.985	3007.5	83.5	2970	10	-1	
Zr-4.1	0.32	65	31	0.49	19.33	3.7	0.6074	3.6	0.956	3059.4	87.1	3057	17	0	
Zr-5.1	0.08	325	148	0.47	17.38	3.5	0.5502	3.4	0.977	2825.9	78.7	3046	12	8	
Zr-7.1	0.16	65	24	0.38	18.49	3.8	0.6075	3.6	0.949	3060.1	88.6	2986	19	-2	
Zr-8.1	0.11	187	81	0.45	17.38	3.5	0.5734	3.5	0.983	2921.8	81.4	2980	10	2	
Zr-9.1	0.10	219	56	0.27	17.93	3.5	0.5870	3.5	0.987	2977.3	82.3	2992	9	0	
Zr-11.1	0.09	235	111	0.49	17.30	3.8	0.5754	3.8	0.989	2930.1	89.4	2967	9	1	
Zr-12.1	0.08	148	22	0.15	17.42	4.1	0.5692	4.0	0.984	2904.6	94.4	2995	12	3	
Gabbro from the Curral orebody (SOS 35/30)															
Zr-1.1	-0.07	193	247	1.32	13.35	3.1	0.5108	3.0	0.973	2660.0	65.6	2738	12	3	
Zr-2.1	-0.13	346	188	0.56	13.90	3.0	0.5356	3.0	0.983	2765.1	67.0	2727	9	-1	
Zr-3.1	-0.10	507	464	0.95	13.86	3.0	0.5288	2.9	0.990	2736.3	65.7	2743	7	0	
Zr-4.1	0.01	260	164	0.65	13.86	3.4	0.5272	3.4	0.983	2729.8	75.4	2747	11	1	
Zr-5.1	4.40	381	279	0.76	13.70	3.0	0.5207	3.0	0.982	2702.1	65.6	2749	9	2	
Zr-6.1	0.01	354	345	1.01	14.03	3.1	0.5348	3.0	0.986	2761.6	68.4	2744	9	-1	
Zr-7.1	0.06	501	128	0.26	13.54	3.0	0.5164	2.9	0.991	2683.7	64.6	2743	7	2	
Zr-8.1	-0.14	318	194	0.63	13.88	3.0	0.5283	3.0	0.985	2734.3	66.5	2747	9	0	
Zr-9.1	0.31	234	229	1.01	13.50	3.1	0.5186	3.1	0.981	2693.0	67.6	2732	10	1	
Zr-11.1	0.00	335	202	0.62	13.98	3.0	0.5320	3.0	0.985	2749.7	66.4	2748	8	0	
Zr-12.1	2.82	429	264	0.64	13.07	3.0	0.5059	3.0	0.981	2639.0	64.0	2719	10	3	

Supplementary Table 3 Summary of U-Pb LA-MC-ICPMS monazite data from ore samples of the Sequeirinho, Sossego and Curral orebodies

Zircon Grain	Isotopic ratios						Ages											
	^{206}Pb	^{204}Pb	$^{207}\text{Pb}/^{206}\text{Pb}$	2σ	$^{207}\text{Pb}/^{235}\text{U}$	2σ	$^{206}\text{Pb}/^{238}\text{U}$	2σ	$^{207}\text{Pb}/^{206}\text{Pb}$	2σ	$^{207}\text{Pb}/^{235}\text{U}$	2σ	$^{206}\text{Pb}/^{238}\text{U}$	2σ	% disc	r		
Sequeirinho ore breccia (SOS259/270)																		
M4A	198903	64	0.17703	0.00163	11.9224	0.7147	0.4884	0.0289	2625	15	2598	55	2564	124	2.8	0.988		
M17A	175277	56	0.17991	0.00215	12.3137	0.6176	0.4964	0.0242	2652	20	2629	46	2598	103	2.5	0.971		
M7B	144709	51	0.18028	0.00175	12.3906	0.6319	0.4985	0.0250	2655	16	2634	47	2607	106	2.2	0.982		
M7A	242792	51	0.18042	0.00168	13.0268	0.7591	0.5237	0.0301	2657	15	2682	54	2715	126	-2.7	0.987		
M1B	288572	149	0.18156	0.00168	12.2725	0.6702	0.4902	0.0264	2667	15	2625	50	2572	113	4.3	0.985		
M1A	286997	150	0.18246	0.00175	12.4170	0.6995	0.4936	0.0274	2675	16	2636	52	2586	117	4.1	0.985		
M2B	183476	92	0.18445	0.00176	12.9666	1.1378	0.5099	0.0445	2693	16	2677	80	2656	187	1.7	0.994		
M14A	89001	47	0.18466	0.00194	12.9574	0.7205	0.5089	0.0278	2695	17	2677	51	2652	118	2.0	0.982		
M20A	234835	57	0.18509	0.00172	12.6878	0.6992	0.4972	0.0270	2699	15	2657	51	2602	115	4.4	0.986		
M16A	164844	60	0.18521	0.00180	12.9998	0.9472	0.5091	0.0368	2700	16	2680	66	2653	155	2.1	0.991		
M6A	131923	44	0.18530	0.00197	13.2699	0.6137	0.5194	0.0234	2701	17	2699	43	2697	98	0.2	0.973		
M13A	235655	49	0.18545	0.00173	14.4638	1.6834	0.5657	0.0656	2702	15	2781	105	2890	265	-8.6	0.997		
M9B	148324	57	0.18548	0.00174	13.6259	0.6496	0.5328	0.0249	2703	15	2724	44	2753	104	-2.3	0.980		
M5B	113412	25	0.18555	0.00175	13.1161	0.9177	0.5127	0.0355	2703	16	2688	64	2668	150	1.6	0.991		
M2A	225830	147	0.18559	0.00174	13.0299	0.7944	0.5092	0.0307	2703	15	2682	56	2653	130	2.3	0.988		
M6B	250312	44	0.18582	0.00174	13.2548	0.6318	0.5173	0.0242	2706	15	2698	44	2688	102	0.8	0.980		
M9A	163439	74	0.18592	0.00183	13.8462	0.7891	0.5401	0.0303	2706	16	2739	53	2784	126	-3.5	0.985		
M3B	231396	74	0.18605	0.00173	13.4290	0.9974	0.5235	0.0386	2708	15	2710	68	2714	161	-0.3	0.992		
M3A	168509	98	0.18612	0.00172	13.2589	0.6948	0.5167	0.0266	2708	15	2698	48	2685	112	1.0	0.984		
M4B	213966	76	0.18624	0.00172	13.7563	0.5749	0.5357	0.0218	2709	15	2733	39	2765	91	-2.5	0.975		
M5A	118891	56	0.18651	0.00185	13.5087	0.6888	0.5253	0.0263	2712	16	2716	47	2722	110	-0.4	0.981		
M21A	307723	69	0.18727	0.00194	12.2727	0.9977	0.4753	0.0383	2718	17	2625	74	2507	165	9.4	0.992		
M8B	209876	45	0.18727	0.00183	14.5342	1.1071	0.5629	0.0425	2718	16	2785	70	2879	173	-7.3	0.992		
M10A	268806	83	0.18729	0.00186	14.8242	0.7375	0.5741	0.0280	2718	16	2804	46	2924	114	-9.4	0.980		
M12A	199185	42	0.18780	0.00177	13.4862	0.9669	0.5208	0.0370	2723	15	2714	66	2703	155	0.9	0.991		
M19A	582949	71	0.18801	0.00173	14.0415	1.1112	0.5417	0.0426	2725	15	2753	72	2790	176	-3.0	0.993		
M10B	277729	68	0.18820	0.00187	14.6419	1.1441	0.5643	0.0437	2726	16	2792	72	2884	178	-7.2	0.992		
M15A	305792	35	0.18841	0.00181	13.3119	0.7576	0.5124	0.0287	2728	16	2702	52	2667	121	2.7	0.986		
M8A	437887	54	0.18860	0.00185	14.5115	0.6913	0.5580	0.0260	2730	16	2784	44	2858	107	-5.8	0.979		
Sossego ore breccia (Min Cp SOS)																		
M1A	265071	66	0.11612	0.00111	5.0508	0.3489	0.3155	0.0216	1897	17	1828	57	1768	105	7.8	0.990		
M1B	295219	45	0.11560	0.00110	4.7570	0.3544	0.2985	0.0221	1889	17	1777	61	1684	109	12.4	0.992		
M2A	210782	51	0.11495	0.00113	5.3306	0.3544	0.3363	0.0221	1879	18	1874	55	1869	106	0.6	0.989		
M2B	222516	43	0.11542	0.00113	5.2456	0.2319	0.3296	0.0142	1887	18	1860	37	1836	69	3.0	0.975		
M3A	133948	50	0.11469	0.00119	5.3191	0.3008	0.3364	0.0187	1875	19	1872	47	1869	90	0.4	0.983		
M3B	143850	44	0.11489	0.00108	5.2939	0.3187	0.3342	0.0199	1878	17	1868	50	1859	95	1.2	0.988		
M4A	392075	80	0.11527	0.00110	5.5238	0.2500	0.3476	0.0154	1884	17	1904	38	1923	73	-2.4	0.977		
M4B	183718	63	0.11481	0.00108	5.3143	0.2874	0.3357	0.0179	1877	17	1871	45	1866	86	0.7	0.985		
M5A	51264	91	0.11526	0.00134	5.5121	0.3063	0.3468	0.0188	1884	21	1902	47	1920	90	-2.2	0.978		
M5B	74134	115	0.11609	0.00165	5.6050	0.4329	0.3502	0.0266	1897	25	1917	64	1935	126	-2.4	0.983		
M6A	357565	130	0.11576	0.00110	5.4363	0.2704	0.3406	0.0166	1892	17	1891	42	1890	79	0.1	0.982		
M6B	132821	119	0.11521	0.00119	5.4902	0.2900	0.3456	0.0179	1883	18	1899	44	1914	85	-1.9	0.981		
M7A	122399	117	0.11516	0.00121	5.2764	0.3411	0.3323	0.0212	1882	19	1865	54	1849	102	2.0	0.987		
M7B	271031	140	0.11554	0.00111	5.4790	0.3368	0.3439	0.0209	1888	17	1897	51	1906	99	-1.1	0.988		
M8A	168679	135	0.11478	0.00112	5.2278	0.3329	0.3303	0.0208	1876	17	1857	53	1840	100	2.2	0.988		
M8B	253651	105	0.11569	0.00111	5.4075	0.4079	0.3390	0.0254	1891	17	1886	63	1882	121	0.5	0.992		
M9A	185938	104	0.11543	0.00114	6.3014	0.6791	0.3959	0.0425	1887	18	2019	90	2150	193	-16.5	0.996		

Supplementary Table 3 (continued)

Zircon Grain	Isotopic ratios						Ages									
	^{206}Pb	^{204}Pb	$^{207}\text{Pb}/^{206}\text{Pb}$	2σ	$^{207}\text{Pb}/^{235}\text{U}$	2σ	$^{206}\text{Pb}/^{238}\text{U}$	2σ	$^{207}\text{Pb}/^{206}\text{Pb}$	2σ	$^{207}\text{Pb}/^{235}\text{U}$	2σ	$^{206}\text{Pb}/^{238}\text{U}$	2σ	% disc	r
<i>Sossego ore breccia (Min Cp SOS)</i>																
M9B	306964	137	0.11487	0.00112	5.4306	0.3093	0.3429	0.0192	1878	17	1890	48	1901	92	-1.4	0.985
M10A	248174	121	0.11547	0.00109	5.1653	0.3152	0.3244	0.0196	1887	17	1847	51	1811	95	4.6	0.988
M10B	286178	134	0.11505	0.00108	5.0441	0.2558	0.3180	0.0158	1881	17	1827	42	1780	77	6.1	0.983
M11A	220983	141	0.11463	0.00109	5.6757	0.3886	0.3591	0.0243	1874	17	1928	57	1978	114	-6.4	0.990
M12A	458314	105	0.11411	0.00109	4.9759	0.2663	0.3163	0.0167	1866	17	1815	44	1771	81	5.8	0.984
M13A	539467	120	0.11446	0.00108	5.4287	0.2949	0.3440	0.0184	1871	17	1889	46	1906	88	-2.1	0.985
M14A	435798	109	0.11413	0.00109	5.2235	0.3547	0.3319	0.0223	1866	17	1856	56	1848	107	1.1	0.990
M15A	58143	141	0.11312	0.00126	5.3263	0.2199	0.3415	0.0136	1850	20	1873	35	1894	65	-2.7	0.963
M16A	420738	121	0.11400	0.00107	5.2597	0.4254	0.3346	0.0269	1864	17	1862	67	1861	129	0.2	0.993
M17A	172604	136	0.11441	0.00110	5.3193	0.3413	0.3372	0.0214	1871	17	1872	53	1873	102	-0.2	0.989
M18A	79525	303	0.11436	0.00198	5.7475	0.5066	0.3645	0.0315	1870	31	1939	74	2004	147	-8.3	0.981
M19A	40185	125	0.11396	0.00162	5.0551	0.2449	0.3217	0.0149	1864	25	1829	40	1798	72	4.0	0.956
M20A	524070	102	0.11476	0.00109	4.9485	0.2486	0.3128	0.0154	1876	17	1811	42	1754	75	7.4	0.982
<i>Sossego ore breccia (SOS 315/255.1)</i>																
M1A	522768	53	0.11541	0.00112	5.1339	0.3892	0.3226	0.0243	1886	17	1842	62	1803	117	5.1	0.992
M2A	83970	51	0.11570	0.00120	5.4269	0.2479	0.3402	0.0151	1891	19	1889	38	1888	72	0.2	0.974
M2B	70214	21	0.11572	0.00109	5.4191	0.3828	0.3396	0.0238	1891	17	1888	59	1885	113	0.4	0.991
M10B	40717	37	0.11576	0.00139	5.7451	0.3464	0.3599	0.0213	1892	21	1938	51	1982	100	-5.5	0.980
M4A	57329	47	0.11621	0.00131	5.0491	0.3522	0.3151	0.0217	1899	20	1828	57	1766	105	8.0	0.987
M7A	79139	49	0.11627	0.00117	5.5862	0.5354	0.3485	0.0332	1900	18	1914	79	1927	157	-1.7	0.994
M3A	72360	28	0.11629	0.00124	5.2017	0.2904	0.3244	0.0178	1900	19	1853	46	1811	86	5.4	0.982
M4B	59548	41	0.11639	0.00131	5.0054	0.3462	0.3119	0.0213	1902	20	1820	57	1750	104	9.1	0.987
M8A	51113	33	0.11642	0.00119	5.1987	0.2906	0.3239	0.0178	1902	18	1852	47	1809	86	5.6	0.983
M9A	50890	30	0.11649	0.00147	5.9177	0.3592	0.3684	0.0219	1903	22	1964	51	2022	102	-7.3	0.978
M8B	77432	29	0.11667	0.00118	5.4917	0.3176	0.3414	0.0194	1906	18	1899	48	1893	93	0.8	0.985
M6A	87617	34	0.11677	0.00116	5.3207	0.2254	0.3305	0.0136	1907	18	1872	36	1841	66	4.0	0.972
M7B	82077	54	0.11715	0.00121	5.6753	0.4507	0.3514	0.0277	1913	18	1928	66	1941	131	-1.7	0.991
M5A	96628	37	0.11740	0.00123	5.4077	0.2779	0.3341	0.0168	1917	19	1886	43	1858	81	3.5	0.979
M3B	61450	38	0.11744	0.00113	5.1699	0.3557	0.3193	0.0218	1918	17	1848	57	1786	105	7.8	0.990
M10A	68990	52	0.11750	0.00151	5.7210	0.2998	0.3531	0.0179	1919	23	1935	44	1949	85	-1.9	0.969
M6B	116308	30	0.11752	0.00114	5.3605	0.3677	0.3308	0.0225	1919	17	1879	57	1842	108	4.6	0.990
M9B	52908	47	0.11766	0.00123	5.4352	0.2903	0.3350	0.0175	1921	19	1890	45	1863	84	3.5	0.981
<i>Curral ore breccia (SOS 106/84)</i>																
M3A	11523	79	0.10738	0.00263	5.0116	0.3237	0.3385	0.0202	1756	44	1821	53	1879	97	-8.1	0.925
M8A	23085	93	0.10790	0.00173	4.2843	0.2960	0.2880	0.0194	1764	29	1690	55	1631	96	8.5	0.973
M15A	28647	100	0.10937	0.00149	4.7043	0.2632	0.3120	0.0169	1789	25	1768	46	1750	83	2.5	0.970
M15B	15321	123	0.10978	0.00267	5.1781	0.3552	0.3421	0.0219	1796	44	1849	57	1897	105	-6.5	0.935
M18B	12102	111	0.10992	0.00250	5.1659	0.2582	0.3409	0.0152	1798	41	1847	42	1891	73	-6.0	0.890
M3B	9709	101	0.11041	0.00273	5.3922	0.4265	0.3542	0.0266	1806	44	1884	66	1955	125	-9.5	0.950
M9B	73747	145	0.11095	0.00122	4.9583	0.2723	0.3241	0.0174	1815	20	1812	45	1810	84	0.3	0.980
M12A	20649	120	0.11103	0.00183	4.7910	0.4572	0.3130	0.0294	1816	30	1783	77	1755	143	3.8	0.985
M12B	16260	101	0.11133	0.00226	5.4318	0.3185	0.3538	0.0195	1821	36	1890	49	1953	92	-8.4	0.938
M16B	28825	127	0.11153	0.00158	4.6606	0.2952	0.3031	0.0187	1825	26	1760	52	1706	92	7.4	0.975
M9A	22537	143	0.11189	0.00308	4.6120	0.5698	0.2989	0.0360	1830	49	1751	98	1686	176	9.0	0.975
M8B	31470	124	0.11232	0.00160	4.8834	0.3080	0.3153	0.0194	1837	26	1799	52	1767	94	4.4	0.974
M22B	725168	155	0.11371	0.00119	4.8168	0.3158	0.3072	0.0199	1860	19	1788	54	1727	97	8.1	0.987
M4A	24887	133	0.11418	0.00151	4.8995	0.2730	0.3112	0.0168	1867	24	1802	46	1747	82	7.4	0.971
M5A	655610	128	0.11477	0.00105	5.1650	0.3317	0.3264	0.0207	1876	16	1847	53	1821	100	3.4	0.990

Supplementary Table 3 (continued)

Zircon Grain	Isotopic ratios						Ages									
	^{206}Pb	^{204}Pb	$^{207}\text{Pb}/^{206}\text{Pb}$	2σ	$^{207}\text{Pb}/^{235}\text{U}$	2σ	$^{206}\text{Pb}/^{238}\text{U}$	2σ	$^{207}\text{Pb}/^{206}\text{Pb}$	2σ	$^{207}\text{Pb}/^{235}\text{U}$	2σ	$^{206}\text{Pb}/^{238}\text{U}$	2σ	% disc	r
<i>Curral ore breccia (SOS 106/84)</i>																
M19C	87828	108	0.11488	0.00135	5.4416	0.2768	0.3435	0.0170	1878	21	1891	43	1904	81	-1.6	0.973
M6A	556764	105	0.11495	0.00107	5.1432	0.2039	0.3245	0.0125	1879	17	1843	33	1812	61	4.1	0.972
M11B	253235	99	0.11524	0.00114	5.2931	0.2789	0.3331	0.0172	1884	18	1868	44	1854	83	1.8	0.982
M21B	58903	141	0.11540	0.00146	5.2949	0.2579	0.3328	0.0157	1886	23	1868	41	1852	75	2.1	0.966
M21A	91302	136	0.11554	0.00129	5.3067	0.2622	0.3331	0.0160	1888	20	1870	41	1853	77	2.1	0.974
M19B	208489	113	0.11555	0.00112	4.7941	0.2972	0.3009	0.0184	1889	17	1784	51	1696	91	11.6	0.988
M22A	339373	138	0.11572	0.00110	5.3903	0.3755	0.3378	0.0233	1891	17	1883	58	1876	111	0.9	0.991
M14A	18076	123	0.11588	0.00207	5.6938	0.2926	0.3564	0.0172	1894	32	1930	43	1965	81	-4.4	0.938
M13B	137145	86	0.11635	0.00121	5.3892	0.5250	0.3359	0.0325	1901	19	1883	80	1867	155	2.0	0.994
M11A	180814	139	0.11672	0.00121	5.1000	0.3257	0.3169	0.0200	1907	19	1836	53	1775	97	7.9	0.987
M13A	109499	127	0.11683	0.00147	5.3662	0.5182	0.3331	0.0319	1908	22	1879	79	1853	152	3.3	0.991
M19A	119177	132	0.11710	0.00116	5.2036	0.2876	0.3223	0.0175	1912	18	1853	46	1801	85	6.7	0.984
M17A	15197	127	0.11733	0.00211	6.0075	0.2975	0.3713	0.0171	1916	32	1977	42	2036	80	-7.3	0.932
M1B	37661	159	0.11764	0.00147	5.8192	0.2980	0.3588	0.0178	1921	22	1949	43	1976	84	-3.4	0.970
M18A	8483	127	0.11801	0.00418	5.7867	0.3635	0.3556	0.0184	1926	62	1944	53	1961	87	-2.1	0.825
M2B	42099	124	0.11876	0.00233	4.9982	0.3926	0.3052	0.0232	1938	35	1819	64	1717	114	12.9	0.968
M1A	40497	158	0.11953	0.00185	5.7455	0.3250	0.3486	0.0190	1949	27	1938	48	1928	90	1.3	0.962
M10A	59917	185	0.12229	0.00250	5.4930	0.4032	0.3258	0.0230	1990	36	1900	61	1818	111	9.9	0.961
M16A	38142	150	0.12392	0.00340	6.0104	0.5115	0.3518	0.0283	2013	48	1977	72	1943	134	4.1	0.947
M7B	50013	132	0.12692	0.00199	5.8380	0.4468	0.3336	0.0250	2056	27	1952	64	1856	120	11.2	0.979
M17B	28885	155	0.12748	0.00238	5.8424	0.3251	0.3324	0.0174	2064	33	1953	47	1850	84	11.9	0.942

Anexo 02

Artigo:

Timing of multiple Iron oxide Cu-Au systems in the Southern Copper Belt, Carajás Province, Brazil: U-Pb zircon and monazite and Re-Os molybdenite geochronology

Carolina P. N. Moreto et al.

Abstract

The Southern Copper Belt of the Carajás Province, Brazil, hosts several iron oxide–copper–gold (IOCG) deposits, including the Sossego (Sequeirinho-Pista-Baiano and Sossego-Currall orebodies), Cristalino, Alvo 118, Bacuri, Bacaba, Castanha, Visconde, and Jatobá deposits, which are situated within a WNW–ESE shear zone. Geological mapping and geochronological studies (U-Pb SHRIMP IIe in zircon) allowed the characterization of distinct lithotypes in the central west part of the Southern Copper Belt, which encompass mainly Mesoarchean (ca. 3.0 Ga to 2.84 Ga) and Neoarchean (ca. 2.74 Ga) intrusive units. The host rocks of the IOCG deposits mainly comprise: (1) ca. 3.0 Ga Bacaba Tonalite and Sequeirinho Granite, (2) ca. 2.97 Ga Pista felsic metavolcanic rock with lenses of meta-ultramafic rocks; (3) the ca. 2.87 Ga Campina Verde Tonalite and the Rio Verde Trondhjemite; (4) 2.84 Ga Serra Dourada Granite; and (5) several 2.74 Ga plutonic and subvolcanic units, such as quartz feldspar porphyries, including the Castanha porphyry and the Sossego granophyric granite; gabbronorite (Sequeirinho and Currall orebodies), Planalto Granite, Cristalino Diorite, and the Pium diopside Norite. Meta-ultramafic lenses occur as mylonites tectonically imbricated along several shear zones that cut the entire area. All these rocks were variably modified by hydrothermal alteration, which comprehends regional Na (albite, scapolite and iron oxides), Na-Ca (actinolite-albite), potassic and chlorite alteration (K-feldspar, biotite, chlorite and quartz), silicification, and epidote-calcite-chlorite formation. U-Pb LA-MC-ICPMS in hydrothermal monazite and Re-Os NTIMS in molybdenite suggest multiple discrete Neoarchean and Paleoproterozoic hydrothermal episodes responsible for alteration and ore formation at the Bacaba and Bacuri deposits. These results, combined with available geochronological data from the IOCG deposits of the Southern Copper Belt, indicate recurrence of hydrothermal events. This episodicity was facilitated by major shear zones, which allowed regional circulation of hot and saline hydrothermal fluids. In this sense, metal and other elements were leached (e.g., Cl and Na from extensive scapolite zones) from previously altered and unaltered country rocks, leading to the overprinting of hydrothermal systems, and eventually new ore deposition. The multiple hydrothermal events registered in the Southern Copper Belt took place at: (1) 2.76 Ga (Bacuri deposit); (2) 2.71-2.68 Ga (Bacuri, Bacaba, Visconde and Cristalino deposits, Pista and Sequeirinho orebodies); (3) 2.05 Ga (Bacaba deposit); and (4) 1.90-1.88 Ga (Sossego and Currall orebodies and Alvo 118 deposit).

The 2.71-2.68 Ga and 1.90-1.88 Ga intervals are interpreted as the main episodes IOCG ore genesis. The former is apparently not directly related to a magmatic event, but coeval with the ca. 2.7 Ga reactivation of main shear zones as a consequence of tectonic inversion of the Carajás Basin. The Orosinian IOCG-forming event is possibly linked to heat sources associated with the emplacement of several A-type granites at the Carajás Province. In this case, reworking of the Neoarchean IOCG deposits and further ore deposition is suggested.

Keywords: IOCG deposits, Carajás Province, Southern Copper Belt, Bacaba deposit, Bacuri deposit, U-Pb geochronology, Re-Os geochronology

1. Introduction

The Archean Carajás Province corresponds to oldest and most preserved crustal nucleus of the Amazon Craton, NW Brazil (Teixeira et al., 1989; Tassinari, 1996; Tassinari and Macambira, 1999, 2004). This province is notable due to its remarkable metallogenetic diversity due to its high-grade iron, orogenic gold, tungsten, nickel- PGE, gold-PGE, polymetallic copper-gold, and lateritic gold, nickel and bauxite deposits (Oliveira and Leonardos, 1990; Rios et al., 1998, 2003; Dardenne and Schobbenhaus, 2001; Villas and Santos, 2001; Ferreira Filho et al., 2007; Klein and Carvalho, 2008). The Carajás Province is also host to the largest amount of world-class iron oxide-copper-gold (IOCG) deposits in the world. The economic relevance of the province has also increased after the opening of the Sossego and Salobo IOCG Mines, in 2004 and 2011, respectively, by VALE Company.

The IOCG deposits of the Carajás Province are mainly situated along or close to two distinct E-W and WNW-ESE- trending regional shear zones, located in the northern and southern contacts of the Carajás Basin with its basement. The Northern Copper Belt mainly hosts Archean deposits (ca. 2.57 Ga; Réquia et al., 2003; Tallarico et al., 2005), and encompasses the Salobo (1.112 Bt @ 0.69% Cu and 0.43 g/t Au; Vale, 2012), Igarapé Bahia-Alemão (219 Mt @ 1.4% Cu and 0.86 g/t Au; Tavaza, 1999; Tallarico et al., 2005), Gameleira, Pojuca, Paulo Alfonso, Furnas, Polo, and Igarapé Cinzento/Alvo GT46 deposits.

The Southern Copper Belt (Moreto et al., submitted), which is the aim of this study, includes Archean and Paleoproterozoic deposits (Tallarico, 2003; Moreto et al., submitted), such as Sossego (355 Mt @ 1.1% Cu e 0.28 g/t Au; Lancaster Oliveira et al., 2000), Cristalino (482 Mt @ 0.65% Cu and 0.06 g/t Au; NCL Brasil, 2005), and Alvo 118 (170 Mt @ Cu and 0.3 g/t Au; Rigon et al., 2000). Several smaller deposits, including the Bacaba, Castanha, Bacuri, Visconde, and Jatobá, are located from 8 to 15 km northeast of the world-class Sossego mine, in the Serra Dourada area. They are still in evaluation by VALE company, and the estimation on resources are unpublished. Additionally, diverse barren massive magnetite bodies have also been recognized in the area.

The IOCG deposits from the Southern Copper Belt are notable because they appear to contain mineralized zones similar to those recognized worldwide as formed at a range of depths. These features are sometimes recognized even in a single deposit, such as Sossego (Monteiro et al., 2008a,b). Interestingly, for the Sossego deposit, reliable isotopic data (Re-Os NTIMS in

molybdenite and U-Pb LA-MC-ICPMS in hydrothermal monazite) revealed that deeper-emplaced orebodies (Sequeirinho-Baiano-Pista), with typical sodic-calcic alteration (albite-actinolite) associated with massive magnetite-(apatite), were formed during Neoarchean (2.71-2.68 Ga; Moreto et al., submitted). Although spatially very close, the shallow-emplaced Sossego-Currall orebodies, which have characteristic potassic and chlorite alteration, were formed in the Paleoproterozoic (1.90-1.88 Ga; Moreto et al., submitted).

Several other IOCG deposits (e.g., Castanha, Bacaba, Bacuri, Jatobá, and Visconde) are related to extensive zones of scapolite alteration coeval with shear zone development. These deposits have been interpreted as representative of distal and deeper envelopes to major paleohydrothermal IOCG systems (Xavier et al., 2010; Moreto et al., 2011). Despite evidence of spatial zonation of hydrothermal alteration, the characterization of multiple IOCG events in Southern Copper Belt precludes the association of each deposit with a specific mineralization episode or with different portions of a large-scale hydrothermal system.

Additionally, fluid inclusion and stable isotope data suggest that the IOCG deposits from the Southern Copper Belt formed at a range of depths and represent hybrid systems with variable component sources, including magmatic and externally-derived fluids (Monteiro et al., 2008a; Ribeiro, 2008; Carvalho, 2009; Melo, 2010; Pestilho, 2011; Torresi et al., 2012; Craveiro et al., 2012b). However, the intensity of the hydrothermal alteration combined with the strong deformation along the shear zones where these deposits are located, frequently obliterated igneous features of the lithologies. This hampers precise characterization of host rock nature and its relationship with the establishment of magmatic-hydrothermal systems. Thus, a deeper comprehension and comparison between these IOCG systems is limited by the scarcity of geological and geochronological data for most deposits from the Southern Copper Belt.

This paper aims to present detailed characterization of the host rocks and the distribution of the hydrothermal alteration in the central west part of the Southern Copper Belt. Furthermore, the purpose is to constrain the timing of IOCG formation and emplacement of the intrusive host rocks (U-Pb SHRIMP IIe in zircon, Re-Os in molybdenite, and U-Pb LA-MC-ICPMS). These results provide new insights into the timing of hydrothermal alteration and IOCG formation at the Southern Copper Belt, with emphasis on the Bacaba and Bacuri deposits, revealing the existence of multiple discrete hydrothermal events in the considered area. This study not only contributes to a better understanding of the magmatic events at the Southern Copper Belt, but also improves

the comprehension on the metallogenesis of this part of the Carajás Province.

2. Geological Setting of the Carajás Province

The Carajás Province, situated in the southeastern part of the Amazon Craton (Brazil), is composed of two Archean domains: Rio Maria, at south, and Carajás (Fig. 1; Table 1), at north. The Rio Maria Domain is composed of 3.0 to 2.90 Ga greenstone belt sequences (e.g., Gradaús, Serra do Inajá, Babaçu, Lagoa Seca, and Sapucaia; Ianhez et al., 1980; Cordeiro and Saueressig, 1980; Macambira et al., 1986; DOCEGEO, 1988; Araújo and Maia, 1991; Vasquez et al., 2008a), ca. 2.97 Ga mafic-ultramafic complexes (Serra Azul and Guara-Pará; Macambira et al., 1986; DOCEGEO, 1988; Pimentel and Machado, 1994) and sensu lato granitoids with different ages and compositions. Briefly, the granitic rocks correspond to ca. 2.93-2.98-Ga and 2.86 Ga TTG suites (e.g., Arco Verde and Caracol tonalites, Mogno and Água Fria trondhjemites; DOCEGEO, 1988; Leite et al., 2004; Almeida et al., 2011), 2.87 Ga sanukitoid rocks (Rio Maria Granodiorite; Dall'Agnol et al. 2006; Oliveira et al. 2009, 2011), ca. 2.86-2.87-Ga potassic granites (e.g., Xinguara, Guarantã, Mata Surrão, Rancho de Deus Granites; Althoff et al., 2000; Leite et al., 2004; Almeida et al., 2010), and 1.88 Ga A-type granites (Jamon Intrusive Suite; Machado et al. 1991; Dall'Agnol et al. 1999a,b, 2005; Dall'Agnol and Oliveira, 2007).

The Carajás Domain (Fig. 1; Table 1) (Vasquez et al., 2008a) comprises the northern Carajás Basin and the southern Transition Subdomain (Dall'Agnol et al., 2006, Feio et al., 2012a), which is situated below a regional E-W- to WNW-ESE-trending shear zone in the contact of the Carajás Basin and its basement rocks.

The basement rocks of the Carajás Province were previously referred to as gneisses and migmatites of the Xingu Complex and orthogranulites of the Pium Complex, with protolith crystallization ages of ca. 3.0 Ga (Rodrigues et al., 1992, Pidgeon et al., 2000). Nevertheless, recent studies in the Transition Subdomain (Gomes, 2003; Moreto, 2010; Moreto et al., 2011; Feio et al., 2012a, Oliveira et al., 2010; Silva, 2011) have been endeavoring to individualize distinct Mesoarchean units in the former Xingu Complex area (Table 1). For instance, the oldest rocks from the entire Carajás Province were characterized in these areas (ca. 3.0 Ga; Bacaba Tonalite and Sequeirinho Granite; Moreto et al., 2011; Moreto et al., submitted). Moreover, the original orthogranulites belonging to the Pium Complex (Araújo and Maia, 1991) were reinterpreted as norite and quartz gabbro (Oliveira et al., 2010) and designated as Pium Diopside

Norite (Vasquez et al., 2008a). The orthogranulites were only maintained along the Cateté river, close to the Chicrim indigenous village, and renamed as Chicrim-Cateté Orthogranulite (Ricci and Carvalho, 2006; Vasquez et al., 2008a).

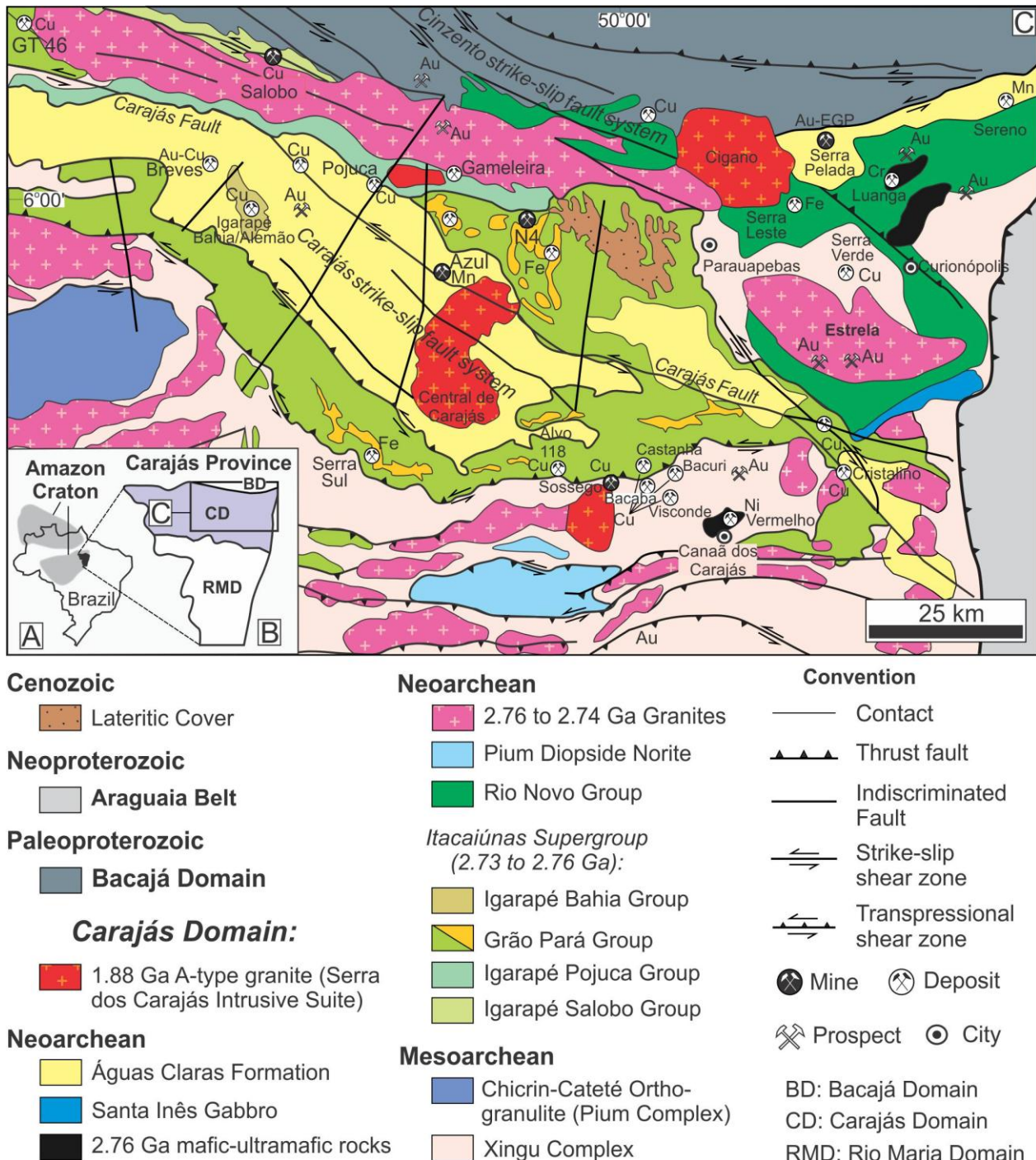


Fig. 1. Geological map of the Carajás Domain (Vasquez et al. 2008a) A) Location in Brazil; B) Location of the Carajás Domain at the Carajás Province; C) Geological map of the Carajás Domain (Vasquez et al. 2008a). Abbreviations: BD: Bacajá Domain; CD: Carajás Domain; RMD: Rio Maria Domain.

Table 1 Available geochronological data for the Carajás Domain.

Unit	Age (Ma)	Method	Reference
Meso- and Neoproterozoic granites			
Formiga Granite (lower intercept age)	ca. 600	U-Pb, Zr (*)	Grainger et al., 2008
Gameleira syenogranite	1,583.3 +8.5 / -6.8	U-Pb, Zr (*)	Pimentel et al., 2003
Paleoproterozoic granites			
Central de Carajás Granite	1,820 ± 49	U-Pb, Zr	Wirth et al., 1986
	1,880 ± 2	U-Pb, Zr	Machado et al., 1991
Pojuca Granite	1,874 ± 2	U-Pb, Zr	Machado et al., 1991
Breves Granite	1,879 ± 6	U-Pb, Zr (*)	Tallarico et al., 2004
	1,880 ± 9	U-Pb, Zr (*)	Tallarico et al., 2004
	1,878 ± 8	U-Pb, Zr (*)	Tallarico et al., 2004
Young Salobo Granite	1,880 ± 80	Rb-Sr, WR	Cordani, 1981
Cigano Granite	1,731 ± 28	Rb-Sr, WR	Gonçalez et al., 1988
	1,883 ± 2	U-Pb, Zr	Machado et al., 1991
Neoarchean granites			
Old Salobo Granite	2,573 ± 2	U-Pb, Zr	Machado et al., 1991
Itacaiúnas Granite	2,560 ± 37	Pb-Pb, Zr	Souza et al., 1996
	2,480 ± 40	Rb-Sr, WR	Montalvão et al., 1984
dacitic dike (Alvo 118 deposit)	2,645 ± 9	U-Pb, Zr (*)	Tallarico, 2003
rhyolitic dike (Alvo 118 deposit)	2,654 ± 9	U-Pb, Zr (*)	Tallarico, 2003
Geladinho Granitic Stock	2,688 ± 11	Pb-Pb, Zr	Barbosa et al., 2001
Igarapé Gelado Granite	2,731 ± 26	Pb-Pb, Zr	Barbosa, 2004
biotite-hornblende granite from Canaã dos Carajás area	2,734 ± 4	Pb-Pb, Zr	Sardinha et al., 2004
Plaquê Suite	2,736 ± 24	Pb-Pb, Zr	Avelar et al., 1999
Sossego granophyric granite	2,740 ± 26	U-Pb, Zr	Moreto et al., submitted
Castanha quartz-feldspar porphyry	2,744.8 ± 4	U-Pb, Zr (*)	Moreto et al., this work
Quartz-feldspar porphyry	2,740.9 ± 4.7	U-Pb, Zr (*)	Moreto et al., this work
Alvo 118 Tonalite	2,743 ± 3	U-Pb, Zr (*)	Tallarico, 2003
Serra do Rabo Granite	2,743 ± 1.6	U-Pb, Zr	Sardinha et al., 2006
Planalto Granite	2,747 ± 2	Pb-Pb, Zr	Huhn et al., 1999b
	2,733 ± 2, 2,731 ± 1	Pb-Pb, Zr	Feio et al., 2012b
	2,729 ± 17, 2,710 ± 10	U-Pb, Zr	Feio et al., 2012b
Pedra Branca Granite	2,750 ± 5	U-Pb, Zr	Feio et al., 2012a
Tonalite/Trondhjemite from Canaã dos Carajás area	2,750 ± 3	U-Pb, Zr	Sardinha et al., 2004
Estrela Granite	2,527 ± 34	Rb-Sr, WR	Barros et al., 1992
	2,763 ± 7	Pb-Pb, Zr	Barros et al., 2004
Trondhjemite from Canaã dos Carajás area	2,765 ± 39	U-Pb, Zr	Sardinha et al., 2004
Águas Claras Formation			
crosscutting gabbro dikes	2,645 ± 12	U-Pb, Zr	Dias et al., 1996
sandstone (with zircon derived from syndepositional volcanic rock)	2,681 ± 5	U-Pb, Zr (*)	Trendall et al., 1998
Detrital zircon grains from arenite and conglomerate	2,778 to 3,020	U-Pb, Zr	Mougeot et al., 1996a

Table 1 (continued)

Unit	Age (Ma)	Method	Reference
Mafic intrusive rocks			
metagabbro	2,708 ± 37	U-Pb, Zr	Mougeot et al., 1996b
gabbro (Pium diopside Norite)	2,735 ± 5	U-Pb, Zr	Feio et al., 2012b
Cristalino Diorite	2,738 ± 6	Pb-Pb, Zr	Huhn et al., 1999b
gabbronorite (Sequeirinho orebody)	2,739 ± 5.9	U-Pb, Zr (*)	Moreto et al., submitted
gabbro (Curral orebody)	2,739.1 ± 4.2	U-Pb, Zr (*)	Moreto et al., submitted
Itacaiúnas Supergroup			
<i>Igarapé Bahia Group</i>			
dioritic dike	2,308 ± 10	Pb-Pb, WR	Santos, 2002
pyroclastic rock	2,360 ± 80	Rb-Sr, WR	Ferreira Filho, 1985
basic granophyre	2,577 ± 72	Rb-Sr, WR	Ferreira Filho, 1985
	2,274 ± 67, 2,268 ± 41	K-Ar, Amp	Ferreira Filho, 1985
mafic metavolcanic rock	2,748 ± 34	U-Pb, Zr (*)	Tallarico et al. 2005
mafic metavolcanic rock	2,745 ± 1	Pb-Pb, Zr	Galarza and Macambira, 2002a
	2,758 ± 75	Sm-Nd, WR	Galarza et al., 2003
	2,776 ± 12	Pb-Pb, WR	Galarza et al., 2003
	2,747 ± 1	Pb-Pb, Zr	Galarza and Macambira, 2002a
metapyroclastic rock	2,758 ± 36	Pb-Pb, WR	Galarza et al., 2003
	2,751 ± 81	Pb-Pb, WR	Santos, 2002
metavolcanic and metapyroclastic rocks	2,759 ± 24	Sm-Nd, WR	Santos, 2002
	2,765 ± 36	Pb-Pb, WR	Galarza et al., 2003
gabbro	3,208 ± 10	Pb-Pb, WR	Santos, 2002
<i>Grão Pará Group</i>			
basalt and basaltic andesite	2,687 ± 54	Rb-Sr, WR	Gibbs et al., 1986; Olszewski et al., 1989
metarhyolite	2,497 ± 62	Rb-Sr, WR	Olszewski et al., 1989
porphyritic metarhyolite	2,760 ± 11	U-Pb, Zr (*)	Trendall et al., 1998
rhyolite	2,759 ± 2	U-Pb, Zr	Machado et al., 1991
	2,758 ± 39	U-Pb, Zr	Wirth et al., 1986; Olszewski et al., 1989
mylonitized metarhyolite	2,757 ± 7	U-Pb, Zr (*)	Trendall et al., 1998
rhyolite or probable tuff	2,757 ± 18	Pb-Pb, Zr	Macambira et al., 1996
probable tuff	2,743 ± 11	U-Pb, Zr (*)	Trendall et al., 1998
dolerite	2,740 ± 8	U-Pb, Zr (*)	Trendall et al., 1998
felsic volcanic rock	2,751 ± 4	Pb-Pb, Zr	Krymsky et al., 2002
rhyodacite	2,759 ± 2	Pb-Pb, Zr	Machado et al., 1991
<i>Igarapé Pojuca Group</i>			
Mafic metavolcanic rocks	2,245 ± 29	Pb-Pb, WR	Galarza and Macambira, 2002b
meta-andesite	2,683 ± 80	Sm-Nd, WR	Lindenmayer et al., 2001
	2,719 ± 80	Sm-Nd, WR	Pimentel et al., 2003
saprolith	2,683 ± 7	Pb-Pb, WR	Galarza and Macambira, 2002b
garnet-biotite schist	2,668 ± 60	Sm-Nd, WR	Lindenmayer et al., 2001
metagabbro	2,696 ± 109	Sm-Nd, WR	Lindenmayer et al., 2001
metagabbro and cogenetic meta-andesite	2,757 ± 81	Sm-Nd, WR	Pimentel et al., 2003
Quartz diorite	2,705 ± 2	Pb-Pb, Zr	Galarza and Macambira, 2002b
amphibolite (metamorphism)	2,732 ± 2	U-Pb, Zr	Machado et al., 1991

Table 1 (continued)

Unit	Age (Ma)	Method	Reference
<i>Salobo Group</i>			
biotite and muscovite from schist	1,950	K-Ar	Tassinari et al., 1982
foliated amphibolite (metamorphism)	2,497 ± 5	U-Pb, Ti	Machado et al., 1991
	2,555 +4/-3	U-Pb, Zr	Machado et al., 1991
iron formation (metamorphism)	2,551 ± 2	U-Pb, Mz	Machado et al., 1991
amphibolite (metamorphism)			
granitic vein (metamorphism)	2,581 ± 5, 2,584 ± 5	Pb-Pb, Ti	Machado et al., 1991
	2,732	U-Pb, Zr	Machado et al., 1991
granitic vein	2,758	U-Pb, Zr	Machado et al., 1991
schist	2,700 ± 150	Rb-Sr, WR	Tassinari et al., 1982
foliated amphibolite (metamorphism)	2,761 ± 3	U-Pb, Zr	Machado et al., 1991
amphibolite and meta-andesite from Igarapé Pojuca group	2,812 ± 98	Sm-Nd, WR	Pimentel et al., 2003
<i>Mafic-ultramafic complex</i>			
anorthositic gabbro (Luanga Complex)	2,763 ± 6	U-Pb, Zr	Machado et al., 1991
gabbro from Serra da Onça (Cateté Intrusive Suite)	2,766 ± 6	U-Pb, Zr (*)	Lafon et al., 2000
<i>Mesoarchean granites</i>			
Serra Dourada Granite	2,860 ± 22	U-Pb, Zr	Moreto et al., 2011
	2,831 ± 6	U-Pb, Zr	Feio et al., 2012a
	2,848 ± 5.5	U-Pb, Zr (*)	Moreto et al., this work
Campina Verde Tonalite	2,868 ± 2, 2,872 ± 1	Pb-Pb, Zr	Feio et al., 2012a
	2,850 ± 7, 2,851 ± 18	U-Pb, Zr	Feio et al., 2012a
	2,876 ± 6.8	U-Pb, Zr (*)	Moreto et al., this work
	2,876 ± 5.2	U-Pb, Zr (*)	Moreto et al., this work
Rio Verde Trondhjemite	2,868 ± 4, 2,923 ± 15	U-Pb, Zr	Feio et al., 2012a
Leucomonzogranite	2,928 ± 1	Pb-Pb, Zr	Sardinha et al., 2004
Canaã dos Carajás Granite	2,959 ± 6	U-Pb, Zr	Feio et al., 2012a
Pista felsic metavolcanic rock	2,968 ± 15, 2,979 ± 5.3	U-Pb, Zr (*)	Moreto et al., submitted
Sequeirinho Granite	3,014 ± 22, 3,010 ± 21	U-Pb, Zr	Moreto et al., submitted
	2,989 ± 5.2	U-Pb, Zr (*)	Moreto et al., submitted
Bacaba Tonalite	3,001.2 ± 3.6, 3,004.6 ± 9, 2,990.9 ± 5.9	U-Pb, Zr	Moreto et al., 2011
<i>Xingu Complex</i>			
Xingu migmatite	3,005 to 2,588	U-Pb, Zr	Feio et al., 2012a
Amphibolite (metamorphism)	2,519 ± 5	U-Pb, Ti	Machado et al., 1991
Amphibolite	2,856 ± 3	Pb-Pb, Zr	Machado et al., 1991
Lower Gneiss (metamorphism)	2,739, 2,742	Pb-Pb, Zr	Machado et al., 1991
Lower Gneiss	2,841	Pb-Pb, Zr	Machado et al., 1991
granitic leucosome - migmatization event	2,859 ± 2, 2,860 ± 2	U-Pb, Zr	Machado et al., 1991

Table 1 (continued)

Unit	Age (Ma)	Method	Reference
Xingu Complex			
mesocratic gneiss - migmatization event	2,851 ± 4	U-Pb, Zr	Machado et al., 1991
granodioritic orthogneiss	2,974 ± 15	Pb-Pb, Zr	Avelar et al., 1999
Chicrim- Cateté orthogranulites (former Pium Complex)			
granulite	3,050 ± 57	Pb-Pb, Zr	Rodrigues et al., 1992
protoliths of the enderbite	3,002 ± 14	U-Pb, Zr (*)	Pidgeon et al., 2000
granulitization event	2,859 ± 9	U-Pb, Zr (*)	Pidgeon et al., 2000

Abbreviations: (*): SHRIMP; Amp: amphibole; Zr: zircon; Ti: titanite; Mz: monazite; Opx: orthopyroxene; WR: whole rock.

The Neoarchean Carajás Basin comprises ca. 2.76-2.74 Ga metavolcanic-sedimentary units (e.g., banded iron formations, bimodal volcanic and volcaniclastic rocks), attributed to the Rio Novo Group (Hirata et al., 1982) and the Itacaiúnas Supergroup (Wirth et al., 1986; DOCEGEO, 1988; Machado et al., 1991). The Itacaiúnas Supergroup differs from the greenstone belts of the Rio Maria Domain due to the lack or very restricted volume of ultramafic rocks. Neoarchean low-grade metasedimentary sequence of the Águas Claras Formation (Nogueira et al., 1994, 2000) overlain the Itacaiúnas Supergroup and Rio Novo Group, and were deposited in fluvial to shallow marine environments.

The mafic-ultramafic magmatism in the Carajás Domain is represented by the Luanga igneous layered complex (2.76 Ga; U-Pb zircon; Machado et al., 1991), which was metamorphosed at greenschist facies (Ferreira Filho et al., 2007), and the Cateté Intrusive Suite (e.g., Serra da Onça, Serra do Puma, Serra do Jacaré-Jacarezinho, Vermelho and Igarapé Carapanã bodies) (Macambira and Vale, 1997; Macambira and Ferreira Filho, 2002; Ferreira Filho et al., 2007), which show evidence for neither metamorphism nor deformation (Macambira and Vale, 1997). Both the Luanga complex and Cateté Suite were crystallized at ca. 2.76 Ga (Machado et al., 1991; Lafon et al., 2000).

The felsic magmatism is represented by Neoarchean (2.75-2.74 Ga and 2.57 Ga) and Paleoproterozoic (1.88 Ga) granites. The older Neoarchean event is widespread through the Carajás Domain and characterized by syntectonic foliated alkaline granites (e.g., Estrela; Planalto, Serra do Rabo granites; Huhn et al., 1999b; Barros et al., 2004; 2009; Sardinha et al., 2006). The younger Neoarchean alkaline granites (e.g., Old Salobo and Itacaiúnas granites; Machado et al., 1991; Souza et al., 1996) are restricted to the north part of the Carajás Domain, close to the Cinzento strike-slip fault system (Fig. 1). Lastly, the Paleoproterozoic episode of A-

type alkaline granite formation corresponds to the Serra dos Carajás Intrusive Suite (e.g., Central de Carajás, Cigano, Rio Branco granites; Machado et al., 1991). It is widespread not only through the Carajás Domain, but also to the southern Rio Maria Domain and other tectonic provinces of the Amazon Craton. The province was also affected by other magmatic events represented by late undeformed diabase, diorite, and gabbro dikes, whose ages are uncertain.

In terms of tectonic models proposed for the Carajás Domain, Araújo et al. (1988) suggested that the Carajás Basin represents a pull-apart basin formed during dextral transtension, which was subsequently tectonically inverted to positive flower structures by sinistral transpression. However, the tectonic reactivation model of Pinheiro and Holdsworth (1997), Holdsworth and Pinheiro (2000), and Domingos (2009) argue that the sedimentary and volcanic units were deposited in an intracratonic basin over basement rocks intensively deformed at ca. 2.85 Ga by high-temperature regional sinistral transpression. Reactivations would have occurred at 2.8-2.7 Ga, related to brittle dextral transtension, at 2.7-2.6 Ga associated with tectonic inversion of the basin under regional sinistral transpression and at ca. 1.8 Ga, which allowed the emplacement of the Serra dos Carajás Intrusive Suite (Domingos, 2009). The Carajás and Cinzento strike-slip fault systems preserve direct and indirect evidence for several phases of dextral and sinistral movements since ca. 2.7 Ga (Pinheiro and Holdsworth, 1997). Furthermore, the evolutionary models proposed by Wirth et al. (1986), Gibbs et al. (1986), DOCEGEO (1988), Olszewski et al. (1989), Macambira (2003) and Tallarico (2003), supports the idea that the Carajás Basin formed in a continental rift setting related to mantle-plume activity (Tallarico, 2003). Mafic magma accumulated in the base of the crust would have ascended to shallow crustal levels, generating differentiated magma chambers (e.g., Luanga complex), or even erupted in the surface forming the volcanic-sedimentary units of the Itacaiúnas Supergroup (Tallarico, 2003).

However, Meirelles (1986), Dardenne et al. (1988), Meirelles and Dardenne (1991), Teixeira (1994), Lobato et al., (2005), Silva et al., (2005), and Teixeira et al. (2010), suggest that the Carajás Basin would have formed in a volcanic arc setting related to subduction processes, where high potassium calc-alkaline basalt of the Itacaiúnas Supergroup would have formed. Zucchetti (2007) proposes that the geochemical signatures of the metabasalt of the Grão Pará group (Itacaiúnas Supergroup) could reflect a volcanism erupted in a back-arc setting.

3. Iron oxide-copper-gold deposits from the Southern Copper Belt

The Southern Copper Belt of the Carajás Province hosts a large concentration of IOCG deposits, such as the world-class Sossego, Cristalino, and Alvo 118 and the smaller Bacaba, Castanha, Bacuri, Visconde, and Jatobá deposits. These deposits are located along a regional, 130 km-long, E-W- to WNW-ESE-trending shear zone in the contact of the Carajás Basin and its basement rocks. A synthesis of geological attributes and genetic parameters for these deposits is presented in Table 2 and geochronological data in Table 3.

The geochemical nature of the host rocks of these deposits is variable (e.g., quartz-feldspar porphyry, granophyric granite, granite and gabbro, metavolcanic-sedimentary rocks of the Itacaiúnas Supergroup and Mesoarchean basement) and relationship between emplacement of specific intrusive rocks and development of the hydrothermal system(s) in the area is poorly understood.

Extensive scapolite-rich zones, representative of distal and deeper sodic alteration, have been recognized in the vicinities of the Bacaba, Castanha, Visconde, Bacuri, and Jatobá deposits, in the Serra Dourada area. Within these zones, scapolite replaces granitic and gabbroic host rocks, but ore zones are spatially related to later potassic alteration (biotite-scapolite-tourmaline-hastingsite) developed synchronous to mylonitic foliation.

Alteration patterns typical of deeper portions of IOCG systems also corresponds to sodic-calcic alteration (albite-actinolite-hastingsite) controlled by ductile structures and associated with the formation of massive magnetite-rich bodies enveloped by apatite- and actinolite-rich rocks (Monteiro et al., 2008a,b). This alteration pattern has been recognized mainly in the Sequeirinho-Baiano-Pista orebodies (Sossego deposit) and at the Castanha deposit. Potassic alteration with potassium feldspar overprinted by chlorite alteration predominates in the Sossego- Curral orebodies (Sossego deposit) and in the Alvo 118 deposit, which may represent shallow-emplaced deposits (Monteiro et al., 2008a; Torresi et al., 2012).

Table 2 Main characteristics of the IOCG deposits from the Southern Copper Belt

	Sequeirinho-Pista-Baiano	Sossego-Currall	Cristalino
Reserve	85% of 355 Mt @ 1.1% Cu, 0.28 g/t Au. (1)	15% of 355 Mt @ 1.1% Cu, 0.28 g/t Au. (1)	482 Mt @ 0.65% Cu and 0.06 g/t Au. (5)
Host rocks	Sequeirinho Granite, gabbronorite, Pista felsic metavolcanic rock. (2) (3)	Sossego granophytic granite, gabbro. (2) (3)	Acid, intermediate and mafic metavolcanic rocks (Itacaiúnas Supergroup), BIF and the Cristalino Diorite. (6)
Hydrothermal alteration	Na (albite-hematite) alteration. Na-Ca (act-rich) associated with Mgt-(Ap) formation. Poorly developed K and chlorite alteration. (2)	Well-developed K and chlorite alteration. Late hydrolytic alteration. Poorly developed Na- and Na-Ca- alteration. (2)	K, Na (albite-scapolite), and chlorite alteration. Carbonate, apatite and magnetite formation. Minor sericite, tourmaline and allanite formation. (6)
Ore morphology	Breccia, disseminations along mylonitic foliation, veins and stockwork breccias. (2)	Subvertical breccia pipes, veins. (2)	Breccia, stockwork, fractures, along foliation and disseminations. (6)
Ore mineralogy	Chalcopyrite, magnetite, pyrrhotite, pyrite, and minor molybdenite, sphalerite, siegenite, millerite, gold, Pd-melonite, galena, cassiterite and hessite. (2)	Chalcopyrite, magnetite, pyrite, and minor siegenite, millerite, hessite, Pd-melonite, molybdenite, gold and cassiterite. (2)	Chalcopyrite, pyrite, magnetite, bravoite, cobaltite, millerite, vaesite and gold. (6)
Geochemical signature of ore	Cu- Fe- Au- Ni- Co- Pd- Se- V- P- LHEE, with low content of Ti and U. Relatively enriched in Co, Ni, Pd, V, and Se in comparison to Sossego-Currall. (4)	Cu- Fe- Au- Ni- Co- Pd- Se- V- P- LHEE. Relatively enriched in Au, Pb, Sn, Rb, Y, and Nb in comparison to Sequeirinho-Pista-Baiano. (4)	Cu- Fe- Co- Ni- Ba- Pb- K e P. (7)
Fluid inclusions (T=°C; salinity =wt% eq. NaCl)	Na-Ca stage: Ti= -76 to -63 (L-V-S) and -63 to -53 (L-V); TH _{(s)LV-L} = 122 to 229 (LVS), and 116 to 250 (L-V); Salinity= 29 to 53 (L-V-S) and 3 to > 23 (LV). (4)	Ore stage: Ti= -65 (L-V-S) and -66 to -45 (L-V); TH _{(s)LV-L} = 102 to 312 (L-V); Salinity= 26 to 70 (L-V-S) and 0.2 to > 23 (LV). (4)	Absent
Stable isotopes: O in silicates and oxides (‰)	Early alteration stages: higher T fluids (> 550°C), and δ ¹⁸ O _{fluid} = 6.9; Ore stage: lower T fluids (~300°C), and δ ¹⁸ O _{fluid} = 1.8. (2)	Early alteration stages: higher T fluids (400°C), and δ ¹⁸ O _{fluid} =5.5 to 8.4; Ore stage: lower T fluids (~275°C), and δ ¹⁸ O _{fluid} = 0.4 to 1.9. (2)	Absent
Stable isotopes: O (SMOW) and C (PDB) in carbonates (‰)	Ore breccia: δ ¹³ C = -6.44 to -4.77; δ ¹⁸ O = 5.6 to 7.43; δ ¹⁸ O _{fluid} = -2.6 to 1.9; δ ¹³ C _{H2CO3} = -6.1 to -3.4 (T=230°C). (2)	Ore breccia: δ ¹³ C = -6.03 to -4.73; δ ¹⁸ O = 5.12 to 8.46; δ ¹⁸ O _{fluid} = -0.6 to 4.5; δ ¹³ C _{H2CO3} = -4.8 to -2.7 (T=275°C). (2)	Ore breccia: δ ¹³ C = -7.2 to -4.8; δ ¹⁸ O = 8.2 to 9.3. (7)
Stable isotopes: H in silicates (‰)	Na-Ca stage: δD _{fluid} = -50 to -34 (T=550°C); Ore stage: δD _{fluid} = -47 to -37 (actinolite; T=400 °C). (2)	Ore stage: δD _{fluid} = -67 to -36 (actinolite; T=400°C); Post mineralization stage: -40 to -30 (chlorite; T=250°C). (2)	Absent
Stable isotopes: S (CDT) in sulfides (‰)	Ore zone: δ ³⁴ S= 2.2 to 6.1. (2)	Ore zone: δ ³⁴ S= 3.8 to 7.6. (2)	Ore zone: δ ³⁴ S= 0.6 to 1.5. (7)
Mineralization age (Ma)	2,710 ± 11, molybdenite (Re-Os TIMS); 2,712 ± 4.7, hydrothermal monazite (U-Pb LA-MC-ICPMS). (3)	1,878.9 ± 4.1; 1,889.8 ± 8.5 and 1,904 ± 5.2, hydrothermal monazite (U-Pb LA-MC-ICPMS). (3)	2,700 ± 29, chalcopyrite and pyrite (Pb-Pb leaching) (8)

Table 2 (continued)

	Alvo 118	Bacaba	Castanha
Reserve	170 Mt @ Cu e 0.3 g/t Au. (9)	Absent	Absent
Host rocks	Mafic and felsic metavolcanic rocks, tonalite and gabbro. (10) (11)	Serra Dourada Granite, Bacaba Tonalite, and gabbro (locally porphyritic). (13) (14)	Castanha quartz-feldspar porphyry and gabbro. (17)
Hydrothermal alteration	K, iron oxide and chlorite (well-developed) alteration, carbonate formation. Poorly developed Na alteration. (11)	Well-developed Na (albite and scapolite) alteration, iron oxide formation, K, chlorite and epidote alteration. (13) (14)	Na (albite and scapolite) alteration, well-developed Na-Ca and magnetite formation, K alteration, tourmaline, chlorite and carbonate formation. (17)
Ore morphology	Breccia, veins, stockwork. (11)	Veins and replacement zones related to mylonitic foliation. (13) (14)	Veins, veinlets, stockwork, and structurally controlled breccia. (17)
Ore mineralogy	Chalcopyrite, hematite > magnetite, bornite, pyrite. (11)	Chalcopyrite, bornite, covellite, chalcocite, magnetite, hematite, and minor melanite, hessite, altaite, uraninite, cassiterite, and ferberite. (13)	Chalcopyrite, pyrrhotite, pyrite, magnetite, pentlandite, sphalerite, molybdenite, and marcasite. (17)
Geochemical signature of ore	Fe- Cu- Au- Ag- Y- Ni- Sn- Be- Co- REE- Pb- U- Bi. (12)	Cu- Fe- Co- Ni- LREE- P- Y- Yb- U. (15)	Cu- Fe- Ni- Co- Zn- Mo. (17)
Fluid inclusions (T=°C; salinity =wt% eq. NaCl)	Ti= -61 to -40 (L-V-S) and -40 to -17 (L-V); TH _{(s)LV-L} = 219 to 330 (LVS), and 127 to 257 (L-V); Salinity= 33 to 40 (L-V-S) and 1 to 14 (LV). (11)	Post alt K: Ti= 1) -79 to -62, 2) -79 to -63, 3) -73 to -65; TH _{(s)LV-L} = 1) 162 to 210, 3) 145 to 175; Salinity= 1) 11 to 54, 2) 30 to 36, 3) 13 to 20. (16)	Early stage: TH _{(s)LV-L} = 179 to 278 (LVS); Late stage: Ti= -72 to -59 (L-V-S) and -65 to -45 (L-V); TH _{(s)LV-L} = 101 to 414 (LVS), and 66 to 257 (L-V); Salinity= 22 to 34. (19)
Stable isotopes: O in silicates and oxides (‰)	Absent	Carbonate alt: δ ¹⁸ O _{fluid} = 1.3 to 10.8 (T=225°C); K alt: δ ¹⁸ O _{fluid} = 4.8 to 7.2 (T=420-450°C); Sericite alt: δ ¹⁸ O _{fluid} = 2 to 7.8 (T=370°C). (17)	Carbonate alt: δ ¹⁸ O _{fluid} = 4.2 to 8.9 (T=400°C); Na-Ca alt: δ ¹⁸ O _{fluid} = 7.2 to 8.2 (T=345°C); K alt: δ ¹⁸ O _{fluid} = 4.9 to 8.4 (T=440-525°C); Sericite alt: δ ¹⁸ O _{fluid} = 3.9 to 9 (T=500-525°C). (17)
Stable isotopes: O (SMOW) and C (PDB) in carbonates (‰)	Ore breccia: δ ¹³ C = -8.1 to -5; δ ¹⁸ O = 4.9 to 16.5; Ore veins: δ ¹³ C = -7.3 to -4.3; δ ¹⁸ O = 6.2 to 7.9; barren samples: δ ¹³ C = -7.5 to -1.7; δ ¹⁸ O = 3.9 to 9; δ ¹⁸ O _{fluid} responsible for Cu-Au ore = -1 to 7.5. (11)	Carbonate alt: δ ¹³ C = -5.9 to -3.63; δ ¹⁸ O = 8.31 to 17.33; δ ¹³ C _{H2CO3} = -4.9 to -2.7 (T=225°C). (17)	Carbonate alt: δ ¹³ C = -7.01 to -3.34; δ ¹⁸ O = 8.07 to 10.88; δ ¹³ C _{H2CO3} = -4.6 to -0.9 (T=400°C). (17)
Stable isotopes: H in silicates (‰)	Absent	K alt: δD _{fluid} = -62 to -40 (T=420°C); Sericite alt: δD _{fluid} = -25 to -9 (T=370°C). (17)	Na-Ca alt: δD _{fluid} = -74 to -70 (T=345°C); K alt: δD _{fluid} = -62 to -52 (T=440-525°C); Sericite alt: δD _{fluid} = -57 to -53 (T=525°C). (17)
Stable isotopes: S (CDT) in sulfides (‰)	Ore zone: δ ³⁴ S= 5.1 to 6.3. (11)	Ore zone: δ ³⁴ S= 1.3 to 5.4. (17)	Ore zone: δ ³⁴ S= 0.1 to 3. (17)
Mineralization age (Ma)	1,868 ± 7; hydrothermal xenotime (U-Pb SHRIMP). (10)	2,716.4 ± 8.4; 2,681 ± 11, hydrothermal monazite (U-Pb LA-MC-ICPMS). (18)	Absent

Table 2 (continued)

	Bacuri	Visconde
Reserve	Absent	Absent
Host rocks	Serra Dourada Granite, Bacuri porphyry and gabbro. (20)	Serra Dourada Granite, felsic subvolcanic rock, mafic volcanic and intrusive rock, and meta-ultramafic rock. (21)
Hydrothermal alteration	Na (albite and scapolite), K alterations, tourmaline, chlorite (well developed) and sericite formation. (20)	Na, Na-Ca alteration (well-developed), magnetite formation, K and chlorite alteration, carbonate formation. (21)
Ore morphology	Disseminations, along mylonitic foliation, veins and veinlets. (20)	Breccia, veins and veinlets, disseminations. (21)
Ore mineralogy	Chalcopyrite, magnetite, pyrite, melonite, altaite, galene and cheralite. (20)	Chalcopyrite, bornite, pyrite, magnetite, chalcocite, digenite, molybdenite, magnesite. (21)
Geochemical signature of ore	Cu- Fe- Ni- Pb- Te- Th- P. (20)	Cu- Fe- REE- Ni- Co- Mo- Ca- P- Mg- Nb- Tb- Y- Zn- SE- Au. (21)
Fluid inclusions (T=°C; salinity =wt% eq. NaCl)	Absent	Na-Ca alt: TH _{(s)LV-L} = 160-480, salinity= 25-58; Late stage I: TH _{(s)LV-L} = 160-350, salinity= 8-30; Late stage II: TH _{(s)LV-L} = <300, salinity= 6-19. (22)
Stable isotopes: O in silicates and oxides (‰)	Absent	Absent
Stable isotopes: O (SMOW) and C (PDB) in carbonates (‰)	Absent	Absent
Stable isotopes: H in silicates (‰)	Absent	Absent
Stable isotopes: S (CDT) in sulfides (‰)	Ore zone: δ ³⁴ S= 0.8 to 1.1. (17)	Ore zone: δ ³⁴ S= 1.5. (17)
Mineralization age (Ma)	2,758 ± 11, molybdenite (Re-OS TIMS); 2,703.0 ± 5.8, hydrothermal monazite (U-Pb LA-MC-ICPMS). (18)	2,747 ± 140, chalcopyrite (Pb-Pb leaching). (23)
(1) Lancaster Oliveira et al., 2000; (2) Monteiro et al., 2008a; (3) Moreto et al., submitted; (4) Carvalho, 2009; (5) NCL Brasil, 2005; (6) Huhn et al., 1999a; (7) Ribeiro, 2008; (8) Soares et al., 2001; (9) Rigon et al., 2000; (10) Tallarico, 2003; (11) Torresi et al., 2012; (12) Moreto et al., 2009; (13) Augusto et al., 2008; (14) Moreto et al., 2011; (15) Roscito, 2009; (16) Melo, 2010; (17) Pestilho, 2011; (18) Moreto et al., this study; (19) Pestilho, 2008; (20) Melo et al., submitted; (21) Craveiro et al., 2012a; (22) Craveiro et al., 2012b; (23) Silva et al., 2012.		

Table 3 Available geochronological data for the IOCG deposits and their host rocks from the Southern Copper Belt

Rock/mineral	Age (Ma)	Method	Reference
Sossego			
Sequeirinho-Pista-Curral orebodies			
Host rocks			
Sequeirinho Granite	3,014 ± 22, 3,010 ± 21	U-Pb, Zr	Moreto et al., submitted
	2,989 ± 5.2	U-Pb, Zr (*)	Moreto et al., submitted
gabbronorite	2,739 ± 5.9	U-Pb, Zr (*)	Moreto et al., submitted
Pista felsic metavolcanic rock	2,968 ± 15, 2,979 ± 5.3	U-Pb, Zr (*)	Moreto et al., submitted
Ore			
ore-related amphibole	2,199 ± 13	Ar-Ar	Marschik et al., 2003
chalcopyrite from massive ore	2,530 ± 25; 2,608 ± 25	Pb-Pb	Neves, 2006
ore breccia	2,578 ± 29	Sm-Nd, WR	Neves, 2006
ore breccia (Sequeirinho orebody)	2,712.3 ± 4.7	U-Pb, Mz	Moreto et al., submitted
Molybdenite from silicified Pista metavolcanic rock (Pista orebody)	2,685 ± 11	Re-Os, Moly	Moreto et al., submitted
Molybdenite from Na altered Pista metavolcanic rock (Pista orebody)	2,710 ± 11	Re-Os, Moly	Moreto et al., submitted
Sossego-Curral orebodies			
Host rocks			
Sossego granophytic granite	2,740 ± 26	U-Pb, Zr	Moreto et al., submitted
gabbro	2,739.1 ± 4.2	U-Pb, Zr (*)	Moreto et al., submitted
Ore			
chalcopyrite from ore breccia	1,592 ± 45	Pb-Pb	Neves, 2006
Ore breccia (Sossego orebody)	1,878.9 ± 4.1	U-Pb, Mz	Moreto et al., submitted
Ore breccia (Sossego orebody)	1,904 ± 5.2	U-Pb, Mz	Moreto et al., submitted
Ore breccia (Curral orebody)	1,889.8 ± 8.5	U-Pb, Mz	Moreto et al., submitted
Cristalino			
Host rocks			
Cristalino Diorite	2,738 ± 6	Pb-Pb, Zr	Huhn et al., 1999b
Planalto Granite	2,747 ± 2	Pb-Pb, Zr	Huhn et al., 1999b
Ore			
chalcopyrite and pyrite	2,700 ± 29* (*MSWD=656)	Pb-Pb	Soares et al., 2001
Alvo 118			
Host rocks			
dacitic dike	2,645 ± 9	U-Pb, Zr (*)	Tallarico, 2003
rhyolitic dike	2,654 ± 9	U-Pb, Zr (*)	Tallarico, 2003
Alvo 118 Tonalite	2,743 ± 3	U-Pb, Zr (*)	Tallarico, 2003
Ore			
xenotime	1,868 ± 7, 1,869 ± 7	U-Pb (*)	Tallarico, 2003
Visconde			
Host rocks			
Serra Dourada Granite	2,860 ± 22	U-Pb, Zr	Moreto et al., 2011
Ore			
chalcopyrite concentrates	2,747 ± 140	Pb-Pb	Silva et al., 2012

Abbreviations: (*) SHRIMP; Moly: molybdenite; Mz: monazite; WR: whole rock; Zr: zircon.

Geochemical ore signatures defined by the Fe-Cu-Au-REE-(U-Y-Ni-Co-Pd-Sn-Bi-Pb-Ag-Te) association are variably present at the IOCG deposits from the Carajás Province, and strongly dependent upon the chemistry of the leached host rocks (Xavier et al., 2010). Contribution of magmatic fluids with limited input of surface-derived fluids in deeper parts of the hydrothermal paleo-system (e.g., Castanha deposit) is supported by fluid inclusions and stable isotopes data (Table 2). Oppositely, in shallow-emplaced deposits (Sossego-Currall orebodies and Alvo 118), Cu-Au mineralization is characterized by significant influx of surface-derived fluids for ore deposition. Variable mixing between hypersaline hot fluids and meteoric waters is strongly suggested for most of the deposits (Table 2).

Isotopic data (Re-Os NTIMS in molybdenite and U-Pb LA-MC-ICPMS in hydrothermal monazite; Table 3) for the Sossego deposit revealed that the two sets of orebodies (Sequeirinho-Baiano-Pista and Sossego-Currall), although spatially very close, were formed during distinct IOCG-forming intervals in the Neoarchean (2.71-2.68 Ga; Sequeirinho-Pista-Baiano) and Paleoproterozoic (1.90-1.88 Ga; Sossego-Currall) (Moreto et al., submitted; Table 3). These data, combined with the U-Pb SHRIMP age for the Alvo 118 deposit ($1,868 \pm 7$ Ma; hydrothermal xenotime; Tallarico, 2003), suggest that shallow-emplaced deposits were formed during the Paleoproterozoic after progressive exhumation of Neoarchean IOCG systems. However, the available data are not sufficient to prove whether the scapolite-rich IOCG deposits (Castanha, Bacaba, Bacuri and Jatobá) represent different portions of these hydrothermal systems, or have a distinct evolutionary history in the Southern Copper Belt.

4. Analytical Procedures

Fieldwork was performed in the vicinities of the Bacaba, Bacuri, Castanha and Visconde IOCG deposits (coordinates 601900 and 627300E, and 9285600 and 9296000N), which comprise the central west part of the Southern Copper Belt. Characterization of the host rocks, hydrothermal alteration stages and ore paragenesis of the Bacaba, Bacuri and Castanha deposit was previously reported in the literature (Augusto et al., 2008; Moreto et al., 2011; Pestilho, 2011; Melo et al., submitted). However, additional observation of drill holes and detailed petrographic studies under transmitted and reflected light were performed in samples from these deposits.

Least altered samples of the host rocks were collected in the field for U-Pb geochronology. Monazite concentrates were extracted from ore and hydrothermally altered samples of the IOCG deposits, which were selected from drill cores, kindly given by VALE company. The main host rock of the Castanha deposit (quartz-feldspar porphyry) was also selected from drill cores.

4.1 U-Pb SHRIMP, zircon

The U-Pb SHRIMP IIe zircon isotopic analyses were performed at the High-Resolution Geochronology Laboratory (HRGL) of the Geochronological Research Centre, University of São Paulo, Brazil. The zircon concentrates were extracted using conventional gravity and magnetic techniques at the mineral concentration facility at the University of Campinas. The concentrates were sent to the HRGL of the University of São Paulo for hand-picking and mounting. The crystals were mounted together with the TEMORA standard in epoxy and polished until attain quasi-central sections. After Au-coating, the polished mounts were comprehensively examined with a FEI-QUANTA 250 scanning electron microscope equipped with secondary-electron and cathodoluminescence (CL) detectors. The most common conditions used in CL analysis were as follows: 60 μ A of emission current, 15.0 kV of accelerating voltage, 7 μ m of beam diameter, 200 μ s of acquisition time, and a resolution of 1024 \times 884. The same mounts were afterwards analyzed by the U-Pb isotopic technique using a SHRIMP-IIe machine also at the HRGL following the analytical procedures presented in Williams (1998). Correction for common Pb was made based on the basis of the ^{204}Pb measured, and the typical error component for the $^{206}\text{Pb}/^{238}\text{U}$ ratio is less than 2%; uranium abundance and U/Pb ratios were calibrated against the TEMORA standard and the age calculations were performed with Isoplot \circledcirc 3.0 (Ludwig, 2003).

4.2 U-Pb LA-MC-ICPMS, monazite

The monazite concentrates were extracted from ca. 400g to 1 kg of rock also using conventional gravity and magnetic techniques, at the mineral concentration facility at the University of Campinas. Conventional optical microscopy, backscattered electron (BSE) and CL images were also performed at the Institute of Geosciences, University of Campinas. The mineral fractions were handpicked under a binocular microscope, mounted in epoxy blocks, and polished.

The *in situ* U-Pb monazite data was collected using laser ablation multi collector inductively coupled mass spectrometry (LA-MC-ICPMS) at the Radiogenic Isotope Facility of the University of Alberta. A full description of the analytical approach is reported in Simonetti et al. (2005). The analytical setup consists of a New Wave UP-213 laser ablation system interfaced with a Nu plasma MC-ICPMS equipped with three ion counters. The laser was operated at 4 Hz pulse rate and a beam diameter of 12 mm that yielded a fluency of ~3 J/cm². Ablations were conducted in a He atmosphere at a flow rate of 1 L/min through the cell. Output from the cell was joined to the output from a standard Nu plasma desolvating nebulizer (DSN). On peak gas + acid blanks (30s) were measured prior to a set of 10-20 analyses. Data was collected statically, consisting of 30 1s integrations. Before and after each set of analyses, an in house monazite reference material was repeatedly analyzed, which corresponded to the Western Australia (2.843 Ga, Simonetti et al., 2006; Heaman unpublished data), to monitor U-Pb fractionation, reproducibility, and instrument drift. Mass bias for Pb isotopes was corrected by measuring ²⁰⁵Tl/²⁰³Tl from an aspirated Tl solution (NIST SRM 997) via the DSN using an exponential mass fractionation law and assuming a natural ²⁰⁵Tl/²⁰³Tl of 2.3871. All data were reduced offline using an Excel-based program. Unknowns were normalized to the in house monazite standard. The uncertainties reported are a quadratic combination of: 1) the standard error of the measured isotope ratio and 2) the standard deviation of the standards that bracket the unknowns. Reproducibility of the monazite standard is estimated to be ~1% for ²⁰⁷Pb/²⁰⁶Pb and 3% for ²⁰⁶Pb/²³⁸U.

4.3 Re-Os, molybdenite

Methods used for molybdenite analysis at the Radiogenic Isotope Facility of the University of Alberta, Edmonton, Canada, are described in detail by Selby and Creaser (2004), and Markey et al. (2007). The ¹⁸⁷Re and ¹⁸⁷Os concentrations in molybdenite were determined by isotope dilution mass spectrometry using Carius-tube, solvent extraction, anion chromatography and negative thermal ionization mass spectrometry techniques. A mixed double spike containing known amounts of isotopically enriched ¹⁸⁵Re, ¹⁹⁰Os, and ¹⁸⁸Os analysis was used. Isotopic analyses were made using a ThermoScientific Triton mass spectrometer by Faraday collector. Total procedural blanks for Re and Os are less than <3 picograms and 2 picograms, respectively, which are insignificant for the Re and Os concentrations in molybdenite. The Chinese

molybdenite powder HLP-5 (Markey et al., 1998), was analyzed as a standard. For this control sample over a period of two years, an average Re-Os date of 221.56 ± 0.40 Ma (1SD uncertainty, n=10) is obtained. This Re-Os age date is identical to that reported by Markey et al. (1998) of 221.0 ± 1.0 Ma.

5. The host rocks of the IOCG deposits from the Southern Copper Belt

The central west part of the Southern Copper Belt (Fig. 2), in the surroundings of the Bacaba, Bacuri, Castanha, and Visconde deposits (Serra Dourada area), mainly comprises the Serra Dourada Granite and mafic intrusive rocks variably obliterated by hydrothermal process. Other important host rocks correspond to felsic subvolcanic rocks, meta-ultramafic rocks, granites (*sensu lato*), and migmatites, as described below.

5.1 Felsic subvolcanic rocks

The felsic subvolcanic rocks (Figs. 2 and 3A-G) comprise centimeter- to meter-wide dikes of quartz porphyry that cut all the country rocks (Fig. 3A), and subcircular bodies (< 4 m in diameter) of quartz-feldspar porphyries (Figs. 3B and C), which intrude the Serra Dourada Granite and mafic intrusive rocks. The intensity and types of the hydrothermal alteration vary among the quartz-feldspar porphyries.

The quartz porphyry dikes (Fig. 3A) are isotropic, pink, inequigranular, and show porphyritic texture with a fine-grained phaneritic matrix. The rock is composed of millimeter-size phenocrysts (1 to 4 mm) of quartz, potassium feldspar, plagioclase, biotite, and minor magnetite and chalcopyrite. The composition varies from rhyodacite to rhyolite. These dikes cut intensively hydrothermally altered portions of the Serra Dourada Granite. The same pristine porphyry dikes also crosscut extremely altered rocks from the Sossego and Alvo 118 IOCG deposits.

The quartz-feldspar porphyries (Fig. 3B) are black or dark gray and predominantly isotropic, although mylonitic fabrics are locally observed along several shear zones that cut the entire area. The porphyries have a fine- to very fine-grained matrix (> 0.1 mm), and millimeter-scale (0.2 to 4 mm) euhedral blue quartz megacrysts with bi-pyramidal terminations and undulose extinction. Locally, millimeter-scale (1 to 3 mm) subhedral plagioclase crystals are also recognized. Potassic alteration with biotite (Fig. 3C) commonly alters the feldspar grains from the matrix, and is related to mylonitic foliation in more deformed rocks.

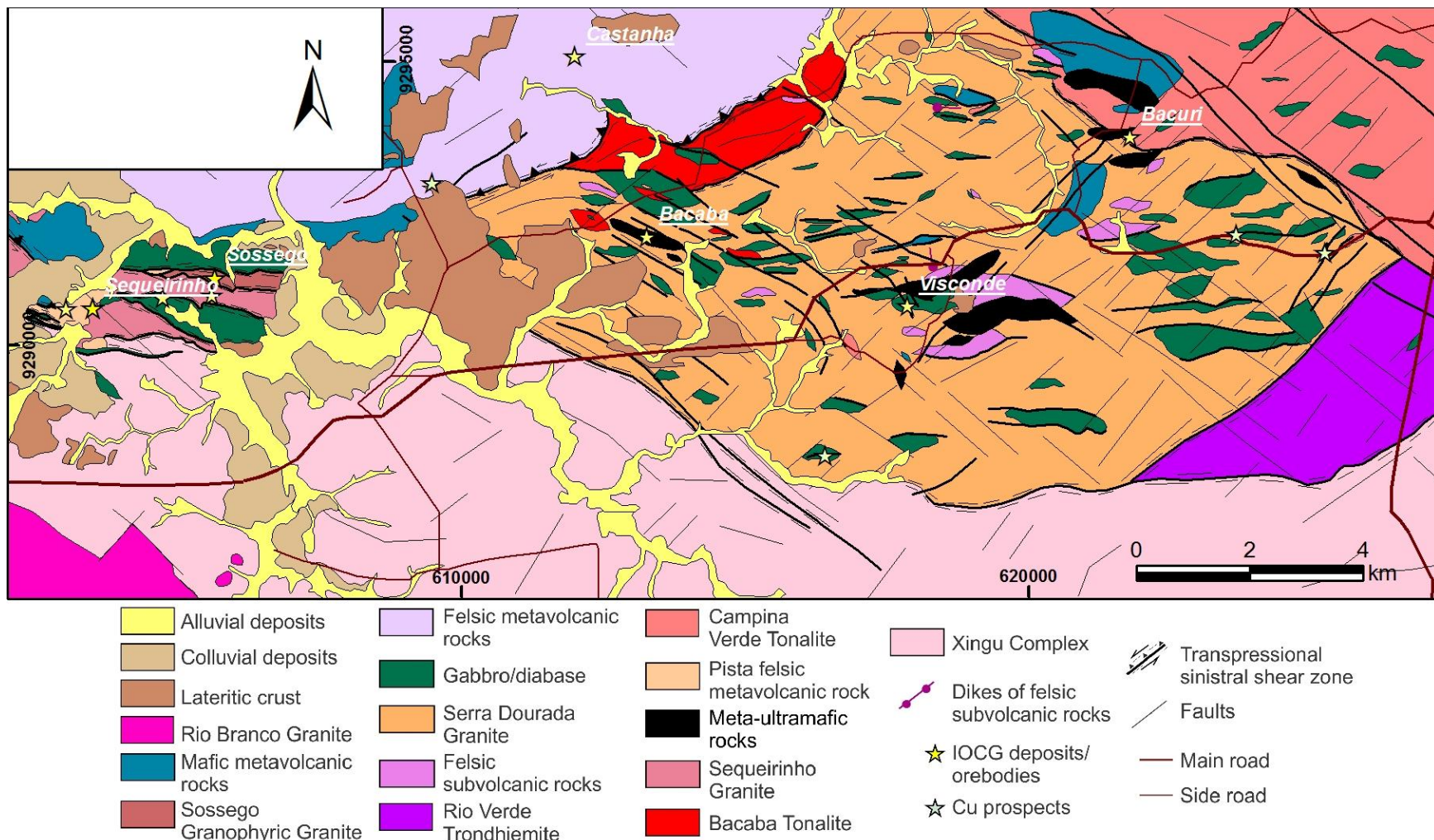


Fig. 2. Geological map of the central west part of the Southern Copper Belt (modified from VALE company).



«Fig. 3. Characteristic features, field aspects, and photomicrographs of the felsic subvolcanic, mafic volcanic and intrusive, and meta-ultramafic rocks from the area. A) Late quartz-feldspar porphyry dikes; B) Quartz-feldspar porphyry with blue quartz megacrysts. Zircon grains from this sample (GMCL 54) were analyzed by U-Pb SHRIMP IIe; C) Outcrop of the quartz-feldspar porphyry altered by potassic alteration (biotite), scapolite and quartz alterations; D) Castanha quartz-feldspar porphyry with millimeter-scale megacrysts of blue quartz and feldspar; E) Castanha quartz-feldspar porphyry. Zircon grains from this sample (CASD 02/424.9) were analyzed by U-Pb SHRIMP IIe; F) Castanha quartz-feldspar porphyry with euhedral bipyramidal quartz megacrysts. Note the feldspar megacrysts in the center, which correspond to hydrothermal albite with chessboard texture; G) Castanha quartz-feldspar porphyry (CASD 02/424.9) with scapolite and biotite (sodic and potassic alterations, respectively) altering the feldspar in the fine-grained matrix; H) An outcrop of gabbronorite; I) Fine- to medium-grained gabbro sample with preserved subophitic texture; J) Porphyritic diabase with up to 3 centimeter-long plagioclase phenocrysts; K) Diopside norite with recognizable subophitic texture; L) Amphibolite with hydrothermal hastingsite; M) A basalt outcrop. Fractures with random directions are filled by fine-grained amphibole; N) Basalt; O) Abandoned copper (malachite) prospect, in which the orebody were hosted by a granite (Serra Dourada Granite) and a meta-ultramafic lens along a shear zone; P) S-C structures in the granite (Serra Dourada Granite) along the shear zone where the copper prospect from Fig. 3O is located; Q) Chlorite-tremolite mylonite. Note the centimeter-scale tremolite crystals; R) Meta-ultramafic rock with chlorite, talc and tremolite. Mineral abbreviations: Chl: chlorite, Di: diopside, Hs: hastingsite, Mgt: magnetite, Tlc: talc, Tr: tremolite.

The quartz-feldspar porphyries found in the area are very similar to those found in drill cores from the Castanha deposit. The Castanha quartz-feldspar porphyry (Figs. 3D-G), firstly described by Pestilho et al. (submitted), is one of the host rocks of the Castanha deposit. The drill holes intercept several meters of this lithotype, which is intensely hydrothermally altered by actinolite- and magnetite-rich alteration.

The Castanha porphyry (Fig. 3D and E) is also gray, isotropic to foliated, inequigranular with porphyritic texture. The matrix has dacite composition and shows very fine-grained (<0.1 to 0.2 mm) texture. The megacrysts (0.5 to 5 mm) comprise euhedral to subhedral quartz and plagioclase (Fig. 3F and G). The former shows undulose extinction, bipyramidal terminations, and are blue due to tiny ilmenite inclusions identified using SEM (Pestilho, 2011). In more deformed samples, higher content of hydrothermal biotite is observed along the mylonitic foliation, and is accompanied by crystal stretching and comminuting of quartz and other mineral phases, including scapolite (Pestilho and Monteiro, 2008).

Two samples of the quartz-feldspar porphyries, including one of the Castanha porphyry, were selected for U-Pb SHRIMP IIe zircon geochronology in this study. Sample GMCL 54A (Fig. 3B) correspond to one of the subcircular subvolcanic bodies with meter-wide diameter mapped in the field. This sample is isotropic, dark gray, fine-grained (> 0.1 mm) and has a very fine-grained matrix composed of quartz, alkali feldspar, plagioclase, biotite, chlorite, muscovite,

epidote, and zircon. Millimeter-scale (0.3 to 3 mm) euhedral blue quartz megacrysts, some with bipyramidal terminations are present. Pervasive hydrothermal alteration in this sample corresponds to fine-grained biotite and chlorite that replace the feldspar in the matrix, or occurs filling grain interstice. Quartz and quartz+epidote millimeter-wide veins (0.1 mm) cut the rock and may be aligned filling fractures.

The other sample chosen for geochronology is the Castanha quartz-feldspar porphyry (sample CASD 02/424.90) (Fig. 3E and G). It is foliated, gray, with a fine-grained (0.1 to 0.5 mm) matrix composed of quartz, alkali feldspar, plagioclase, zircon, and hydrothermal biotite, scapolite, and chlorite. Euhedral to subhedral blue quartz and plagioclase megacrysts with 0.8 to 3 mm in length are also present. Hydrothermal alteration in this sample consists of fine-grained scapolite and biotite altering the feldspar in the matrix, or along the foliation. Biotite is partially altered to chlorite.

5.2 Mafic intrusive rocks

The mafic intrusive rocks (Figs. 2 and 3H-L) are isotropic or preferentially oriented along E-W and NW-SE-trending, and consist of either intrusions (e.g., 800 m²), or dikes that cut the Serra Dourada Granite and the tonalitic rocks (e.g., Campina Verde and Bacaba tonalites). Although the E-W- and NW-SE-trendings are the main directions for the mafic dikes, other directions are also recognized. In some cases, the dikes are oriented along shear zones. Foliation around N085/70SE and mineral lineation of N320/85SE were measured in a porphyritic diabase close to the Bacaba deposit.

These mafic rocks vary in composition and in terms of clinopyroxene and orthopyroxene content, from norite to gabbro (or diabase). Some samples also show a few grains of olivine. Nonetheless, hydrothermally altered mafic rocks (Fig. 3L) with amphibole, biotite, and scapolite are the predominant lithotype characterized.

The preserved mafic intrusive rocks (Figs. 3H, I, and K) are isotropic to foliated, dark-gray, fine- to medium-grained, usually with recognizable subophitic to ophitic textures (Figs. 3I and K). Diopside norite occurs as an irregular intrusion, is dark gray, medium-grained (0.3 to 3.5 mm), isotropic, has subophitic texture, and is composed of plagioclase (50%, bytownite), enstatite (30%), diopside (10%), hastingsite (7%), biotite (3%) and ilmenite (<1%). The hydrothermal hastingsite and biotite replace euhedral plagioclase along the rims and cleavage

planes. The diabase occurs as dikes that cut the granitic rocks, show E-W to NE-SW-trending, are dark gray, fine-grained, phaneritic and show preserved subophitic textures. It is composed of plagioclase, clinopyroxene, and minor orthopyroxene, ilmenite, and magnetite. Hydrothermal minerals, such as interstitial hastingsite, epidote, and titanite around plagioclase laths replaced by albite and scapolite are also recognized under the microscope. Additionally, in some outcrops (one of them close to the Bacaba deposit) 4-5 centimeter-long euhedral plagioclase crystals were observed in a diabase (Fig. 3J). Sulfides and magnetite are disseminated in this rock.

Commonly, the mafic rocks are hydrothermally altered, so that the igneous mineralogy and texture have been completely modified. Some samples contain a great quantity of hydrothermal amphibole (Fig. 3L), and are isotropic to foliated, medium-grained (0.3 to 3 mm), phaneritic, and composed of hornblende and hastingsite (up to 60%), plagioclase (25%), chlorite (Fe- and Mg-rich; 9%), quartz (5%), and subordinate (2%) epidote, clinozoisite, ilmenite, rutile, and calcite. Other rocks are foliated, fine-grained (<0.1 to 0.5 mm), and composed of hydrothermal biotite (50%), scapolite (30%) and quartz (20%) along the mylonitic foliation.

The ages for the mafic intrusive rocks are unknown, but the contact relations with the Serra Dourada Granite ($2,860 \pm 22$ Ma, Moreto et al., 2011), suggest that they are younger than 2.86 Ga. If these rocks are related to gabbro and gabbronorites from the Sossego deposit (less than 10 km distant), ages of ca. 2.74 Ga are suggested ($2,739 \pm 5.9$ and $2,739 \pm 4.2$ Ma; U-Pb SHRIMP IIe in zircon; Moreto et al., submitted).

5.3 Mafic metavolcanic rocks

Mafic metavolcanic rocks (Figs. 2 and 3M and N) occur as lenses inside the Serra Dourada Granite and the Campina Verde Tonalite. They are intensively hydrothermally and/or weatherly altered. When more preserved, the metabasites are foliated, dark-green to black, with nematoblastic textures, and are composed of amphibole, chlorite, biotite, quartz, epidote, and titanite. Hydrothermal chlorite also alters the amphibole crystals. In some outcrops several millimeter-wide families of fractures with different directions are recognized (Fig. 3M). These fractures are mainly filled by amphibole.

Deformation can be extremely intense among these rocks, in which mylonitic foliation is developed along the meter-wide shear zones that cut the unit. Foliation is anastomosed, and the most frequent measured direction was NW-SE with low to high angle dip (5 to 80°) to SW. E-W

striking foliation with dips around 85° to south and NE-SW trending foliation with high angle dips ($>80^\circ$) to NW were also identified.

5.4 Meta-ultramafic rocks

The meta-ultramafic rocks (Figs. 2 and 3O-R) occur as intensively deformed lenses along shear zones inside the Serra Dourada Granite (Figs. 3O and P), mafic intrusive and volcanic rocks. The meta-ultramafic rocks have mylonitic foliation, nematoblastic texture, are fine- to medium-grained, and dark-green to dark-gray. They are composed of tremolite, talc, and Mg-chlorite in different proportions, and minor calcite and serpentine (Fig. 3R). In some areas, up to two centimeter-long tremolite crystals (Fig. 3Q) and sulfide disseminations are identified. The meta-ultramafic rocks can be completely weathered, although tremolite pseudomorphs are still recognizable.

The meta-ultramafic rocks are invariably mylonitized along shear zones (Figs. 3O and P) that cut the entire area. Several Cu prospects and deposits occur along or close to the regional and local shear zones where the meta-ultramafic rocks are found. Additionally, these rocks are also found in drill holes from the Sossego, Bacaba and Visconde deposits. The Bacaba deposit, in which an active malachite prospect exists, is hosted by talc-tremolite mylonite with foliation of N298/60SW.

In an abandoned malachite prospect hosted by tremolite-chlorite mylonite, two shear systems were identified. The first was NNW-SSE (N350)-striking with high angle dip (70°) to NE, whereas the other was NNE-SSW (N15)-striking with lower angle dip (30°) to SE. In a second abandoned malachite prospect (Figs. 3O and P), the orebody was located in the contact of the Serra Dourada Granite and talc-chlorite mylonite lenses. S/C structures were observed, and the shear foliation (C) corresponded to E-W with high angle (86°) to SE, whereas the S foliation corresponded to NW-SE with low angle dip (35°) to SW. In a different location, a tremolite-talc mylonite was formed along a N-S-trending transcurrent shear zone with foliation dip around 80° .

5.5 Granitic rocks

5.5.1 Serra Dourada Granite

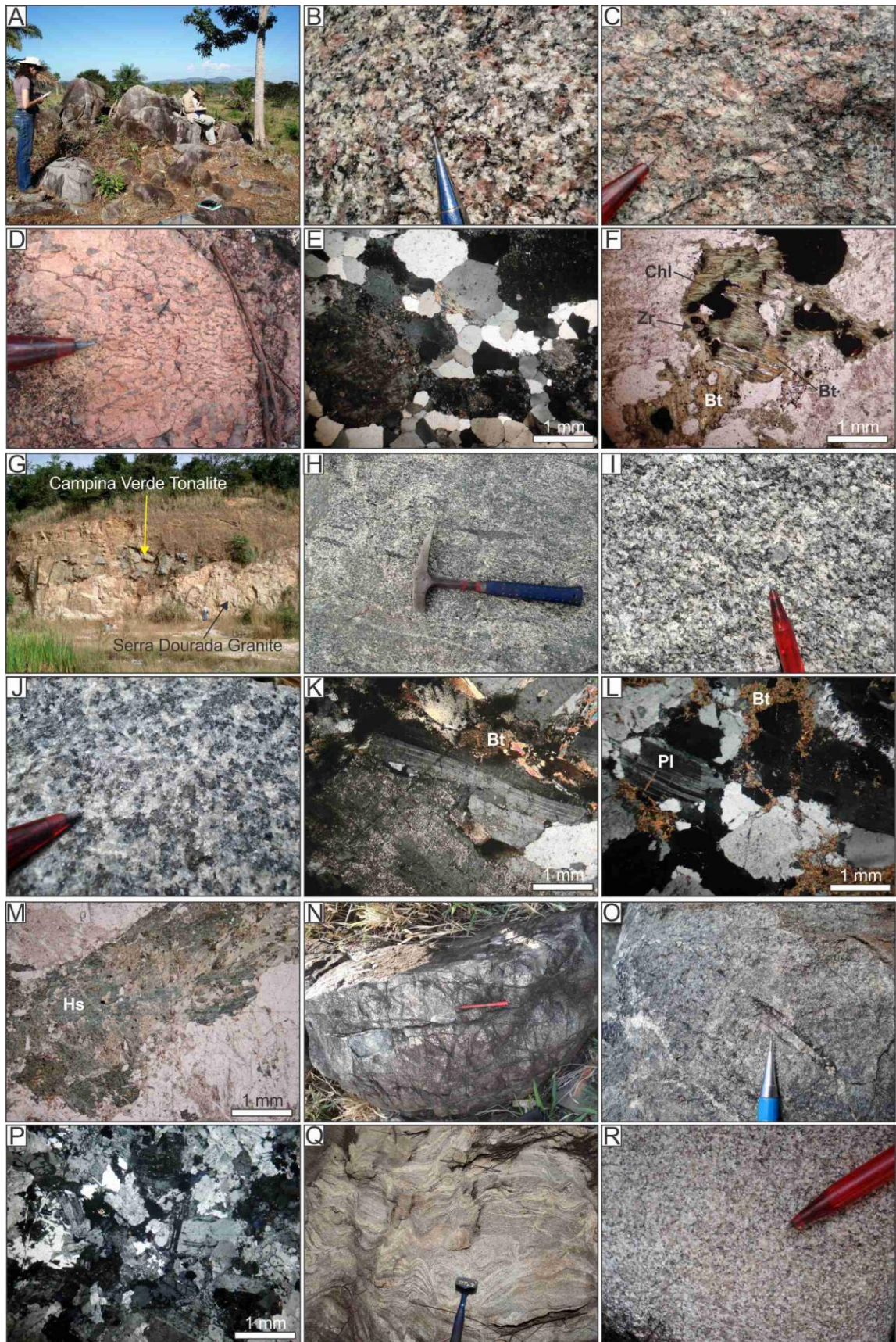
The Serra Dourada Granite (Moreto et al., 2011; Feio et al., 2012a; Figs. 2, 4A-G) occurs as a stock (100 km^2) at east of the Sossego deposit. There are several outcrops of the granite,

which usually have boulder shapes (Fig. 4A). It also occurs as small hills, which were preserved from erosion and weathering. The Serra Dourada Granite is one of the main host rocks of the Bacaba, Bacuri, and Visconde deposits and several Cu prospects located along shear zones in the contact between the granite and mylonitized meta-ultramafic lenses. Hydrothermal alteration is especially conspicuous in rocks found in or close to the shear zones and gets more intense westwards, close to the Sossego deposit.

The Serra Dourada Granite is isotropic to foliated, pink to light grayish pink, and medium- (0.3 to 4 mm) to coarse-grained (2 to 6 mm) with phaneritic texture (Fig. 4B) and syenogranite composition. It is mainly composed of quartz, alkali feldspar (orthoclase and microcline) and plagioclase, with minor mafic minerals, such as biotite and chlorite. Accessory minerals such as epidote, allanite, zircon, pyrite, magnetite, and hematite are also observed. Quartz crystals are subhedral with undulose extinction, whereas subhedral feldspar crystals are commonly saussuritized.

In addition to the phaneritic facies described above (Fig. 4B), other facies, with similar mineralogy have been described in the field, such as: i) porphyritic facies (Figs. 4C and E); ii) pegmatitic facies; and iii) graphic to micrographic facies (Fig. 4D). In the porphyritic facies (Figs. 4C and E), large potassium feldspar crystals (up to 3-4 cm in diameter) in a medium-grained matrix are characterized. In the pegmatitic facies, the feldspar and quartz crystals can be as large as ~5 cm in diameter. The graphic facies (Figs. 4D), which is frequently described, is characterized by a macroscopic intergrowth of potassium feldspar and quartz (up to ~3 cm long).

The Serra Dourada Granite can be isotropic or locally have mylonitic foliation. Foliation varies around WNW-ESE with dips showing variable angles to SSW (N274/87SW, N284/25SW, N280/40SW, N310/80SW). NE-SW-trending foliations with dips around 50° to 70° to SE (N050/50SE, N040/70SE) were also described. S/C structures were recognized in an abandoned malachite prospect (Figs. 3O and P), in which the orebody was hosted within a shear zone in the contact of the Serra Dourada Granite and a lens of a talc-chlorite mylonite. The shear foliation (C) was measured in N080/86SE and the S foliation in N296/35SW.



«Fig. 4. Characteristic features, field aspects, and photomicrographs of the felsic intrusive rocks from the area. A) Typical outcrop of the Serra Dourada Granite; B) Serra Dourada Granite with medium-grained phaneritic facies; C) Serra Dourada Granite with porphyritic facies. Zircon grains from this sample (GMCL 40) were analyzed by U-Pb SHRIMP IIe; D) Serra Dourada Granite with micrographic facies, consisting of the intergrowth of alkali feldspar and quartz; E) Serra Dourada Granite (sample GMCL 40) in thin section. Feldspar crystals are saussuritized. F) Serra Dourada Granite (sample GMCL 40) with biotite partially altered to chlorite; G) Exposure of Serra Dourada Granite and the Campina Verde Tonalite in an abandoned quarry for grit; H) The Campina Verde Tonalite with elongated mafic enclaves due to deformation; I) Foliated and medium-grained Campina Verde Tonalite. Zircon grains from this sample (GMCL 01) were analyzed by U-Pb SHRIMP IIe; J) Isotropic and medium-grained Campina Verde Tonalite. Zircon grains from this sample (GMCL 66) were analyzed by U-Pb SHRIMP IIe; K) Campina Verde Tonalite (sample GMCL 01). Plagioclase crystals is slightly deformed and with irregular polysynthetic twinning; L) Campina Verde Tonalite (sample GMCL 66) partially altered by potassic alteration. Biotite alters the plagioclase rims and in fractures; M) Hydrothermal hastingsite in the Campina Verde Tonalite; N) Outcrop of the Bacaba Tonalite altered by potassic and chlorite alteration along fractures; O) and P) Fine-grained Bacaba Tonalite; Q) Xingu Complex; R) Rio Verde Trondhjemite. Mineral abbreviations: Bt: biotite, Chl: chlorite, Hs: hastingsite, Pl: plagioclase, Zr: zircon.

The Serra Dourada Granite was dated at $2,860 \pm 22$ Ma (U-Pb LA-MC-ICPMS; Moreto et al., 2011), and at $2,831 \pm 6$ Ma (U-Pb LA-ICPMS; Feio et al., 2012a). In this study, another sample was selected for U-Pb SHRIMP IIe zircon geochronology. Sample GMCL 40A (Figs. 4C, E and F) correspond to the porphyritic facies, and is isotropic, light pink, with a medium-grained matrix (0.4 to 2 mm) composed of quartz, alkali feldspar, plagioclase, biotite, chlorite, and zircon. Euhedral orthoclase and microcline (2 to 5 mm) occurs as megacrysts.

5.5.2 Campina Verde Tonalite

The Campina Verde Tonalite (Figs. 2, 4G-M) occurs in the northeast portion of the area, north of the Rio Verde Trondhjemite and northeast of the Serra Dourada Granite. Its best outcrop exposure is in an abandoned quarry for grit in the vicinities of the Planalto village (Fig. 4G). The Campina Verde tonalite also occurs as meter-scale lenses inside the Serra Dourada Granite.

The Campina Verde Tonalite is isotropic to weakly foliated, although intense deformation can be observed in the contact with the Serra Dourada Granite. The tonalite (Figs. 4H-J) is gray, phaneritic, medium-grained (0.5 to 4 mm) to locally coarse-grained, and composed of quartz, plagioclase, alkali feldspar, amphibole (hydrothermal hastingsite; Fig. 4M), biotite, with subordinate titanite, ilmenite, pyrite, and chalcopyrite. Quartz crystals are anhedral and show undulose extinction and subgrain boundary. Feldspar crystals are subhedral and variably deformed (Fig. 4K). The composition of the Campina Verde Tonalite varies from tonalite to granodiorite. The general foliation is WNE-ESE-trending with 20-40° dips to SSW. Elongated

mafic enclaves of dioritic composition and with a large amount of hydrothermal biotite are found in the tonalite. Aplitic dikes cutting the tonalite were also observed. The former has granodioritic composition, are fine-grained, beige and consist of quartz, plagioclase and alkali feldspar.

The intensity of deformation increases close to the contact of the Campina Verde Tonalite with the Serra Dourada Granite, where meter-wide shear zones and S-C structures are recognized. The mylonitic foliation in these areas is predominantly WNW-ESSE with low angle dips (20 to 40°) to SW, whereas the lineation has a strike-slip displacement. The contact relationship and structural elements indicate that the Campina Verde Tonalite is older than, and intruded by, the Serra Dourada Granite (Fig. 4G). This is evidenced by the granite apophysis in the Campina Verde Tonalite and by the tonalitic lenses inside the Serra Dourada Granite, indicating that part of the tonalite was assimilated during the granite emplacement.

The Campina Verde Tonalite was dated in $2,872 \pm 1$ Ma (Pb-Pb zircon evaporation), and $2,850 \pm 7$ Ma (zircon U-Pb LA-ICPMS) (Feio et al., 2012a). Two samples of the Campina Verde Tonalite were selected for U-Pb SHRIMP IIe geochronology in this study. Sample GMCL 01 (Figs. 4I and K) is gray, foliated, phaneritic, medium-to coarse-grained (1 to 4.5 mm), and composed of quartz, plagioclase, hastingsite, alkali feldspar, biotite, titanite and zircon. It has tonalitic composition. Sample GMCL 66 (Figs. 4J and L) is gray, isotropic, medium-grained (0.4 to 3 mm), phaneritic, and composed of quartz, plagioclase, alkali feldspar, hydrothermal biotite, epidote and zircon. It has a granodioritic composition. Potassic alteration (biotite; 15%) occurs in mineral interstice, along fractures and altering the feldspar.

5.5.3 Bacaba Tonalite

The occurrence of the Bacaba Tonalite (Figs. 2, 4N-P) is restricted to the northwest part of Southern Copper Belt. Its southern contact is with the Serra Dourada Granite, whereas the northern contact is with the metavolcanic rocks of the Itacaiúnas Supergroup. The tonalite also occurs as meter-scale lenses within the Serra Dourada Granite. The Bacaba Tonalite, which corresponds to one of the host rocks of the Bacaba deposit, was firstly described and dated in $3,001 \pm 3.6$ Ma by Moreto et al. (2011).

The tonalite is gray, isotropic to foliated, fine- to medium- grained (0.2 to 3 mm), phaneritic (Figs. 4O and P), and composed of quartz, plagioclase, alkali feldspar, biotite, amphibole, chlorite, and minor calcite, epidote and hematite. Its composition varies from granodiorite to tonalite. Deformed amphibolite enclaves partially altered by hydrothermal biotite

are commonly identified. Subhedral to euhedral plagioclase is normally saussuritized.

Outcrops of the tonalite are not abundant and are small in size (Fig. 4N). However, drill holes in the Bacaba deposit area intercepts the Bacaba Tonalite in several intervals and depths. Although the hydrothermal alteration varies in intensity, style and type (e.g., silicification, scapolite and biotite alteration) it is almost always present regardless the depth that the tonalite is intercepted. The potassic alteration with biotite and scapolite is frequently controlled by mylonitic foliation.

5.5.4 Other units

The Xingu Complex (Figs. 2, 4Q) outcrops south of the Serra Dourada Granite. This unit comprises metatexite to diatexite migmatite, which is pink to gray, medium- to coarse-grained and banded. It has NE-SW- to W-E- trending foliation with low angle dips to south, excepting along shear zones, in which high angle foliations are recognized. The mesosome is composed of biotite, actinolite, plagioclase, quartz, and minor magnetite. The leucosome has phaneritic texture, is coarse-grained and consists of megacrysts of potassium feldspar, quartz, plagioclase, and magnetite. Melanosome comprises biotite and hornblende and suggests in situ partial melting. The leucosome and mesosome, which are both folded, are cut by granite and pegmatite injections with graphic textures, evidenced by the intergrowth of quartz and potassium feldspar. In these injections, quartz, biotite and magnetite are also present. Potassium feldspar is also observed along fractures and surrounding plagioclase crystals, evidencing discrete potassic alteration. U-Pb zircon dating (LA-ICPMS and SHRIMP) of the Bom Jesus Granite (Feio et al., 2012a), which has the same spatial distribution of the Xingu migmatite, revealed considerably different ages ranging from 3.0 to 2.6 Ga. The wide age interval could reflect dating of both leucosome and mesosome in the same sample.

The Rio Verde Trondhjemite (Figs. 2, 4R) is located in the southeast part of the area, in contact at east with the Serra Dourada Granite and at north with the Campina Verde Tonalite. The Rio Verde Trondhjemite is gray to beige, fine-grained, isotropic to foliated close to the contact with the Serra Dourada Granite, and composed of quartz, plagioclase and minor alkali feldspar and biotite. It was dated in $2,868 \pm 4$ Ma (Pb-Pb zircon evaporation) although an older age of $2,923 \pm 15$ Ma (zircon U-Pb LA-ICPMS) was also obtained in a different sample (Feio et al., 2012a).

6. IOCG deposits and hydrothermal alteration in the Southern Copper Belt

Hydrothermal alteration is often recognized in the lithotypes of the Southern Copper Belt. The metasomatism is not restricted to the deposit area, but extends to up to 20 km in distance. The alteration is more intense along the controlling regional structures, which have WNW-ESE-trending foliation. These structures correspond to penetrative sub-vertical to vertical fabrics related to transcurrent ductile shear zones, which act as the main mechanism for interaction of hydrothermal fluids with the country rocks.

Detailed description of the types, styles and distribution of hydrothermal alteration in the central west part of the Southern Copper Belt is presented below. These field observations were integrated with carefully examination of the drill cores from the Bacaba, Castanha and Bacuri IOCG deposits (Fig. 5), reported by Augusto et al. (2008), Moreto et al. (2011), Pestilho (2011), and Melo et al. (submitted).

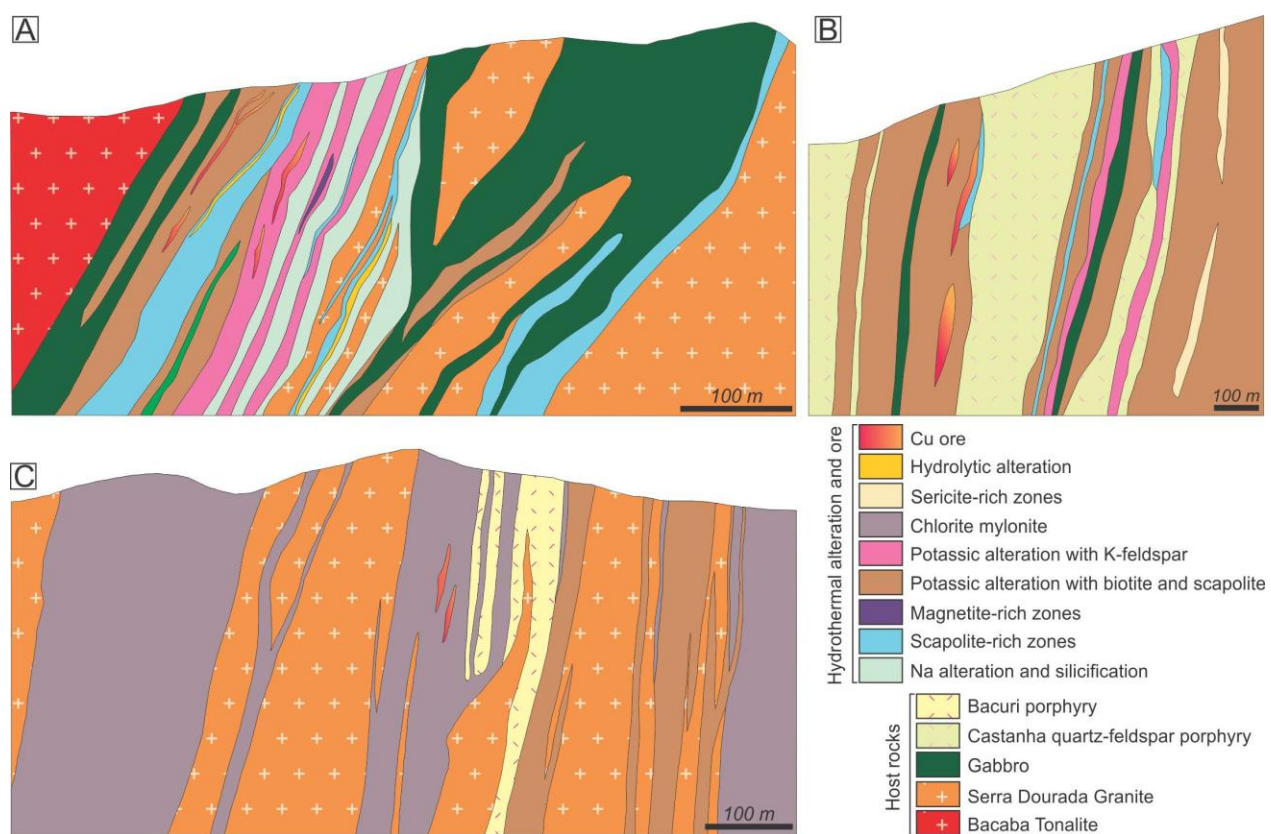


Fig. 5. Simplified cross sections of the A) Bacaba; B) Castanha; and C) Bacuri deposits (modified from VALE company).

The temporal sequence of hydrothermal alteration corresponds to well-developed sodic alteration (albite-scapolite-magnetite; Figs. 6A-G and L), followed by sodic-calcic alteration and Fe metasomatism (poorly developed in the country rocks) (Figs. 3L, 4M and 6H), potassic and chlorite alteration (Figs. 3F and G, 4F and L, 6I-N), tourmaline formation, silicification (Fig. 6O), epidote-calcite-chlorite formation (Fig. 6P-R), and finally copper (-gold) mineralization.

6.1 Host rocks of the Bacaba, Castanha and Bacuri IOCG deposits

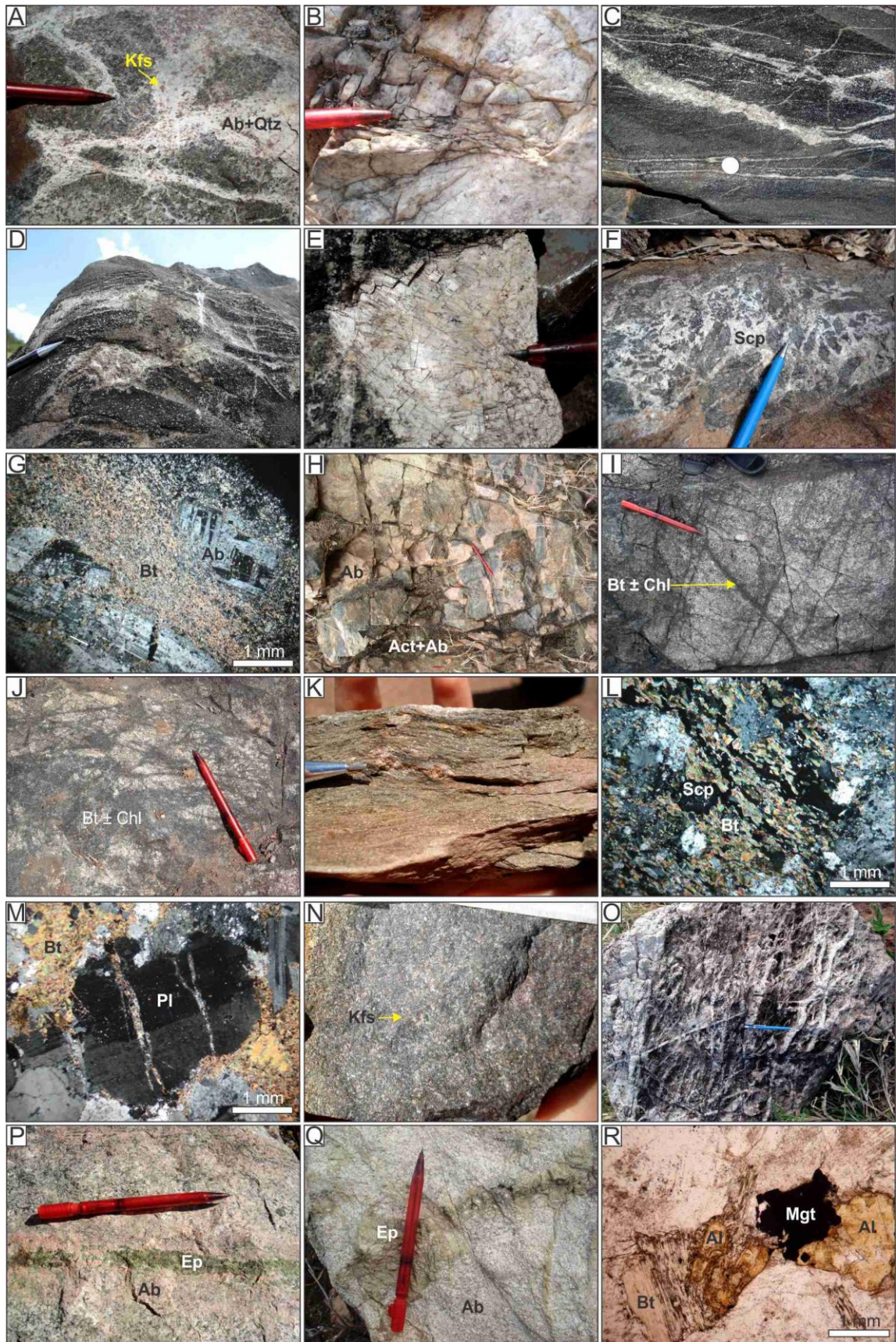
The Bacaba deposit, firstly described by Augusto et al. (2008), is mainly hosted by the Serra Dourada Granite (Moreto et al., 2011; Feio et al., 2012a) and the Bacaba Tonalite (Moreto et al., 2011). Additionally, in the vicinities of the deposit, quartz-feldspar porphyries, lenses of tremolite-talc mylonite, and porphyritic gabbro were identified. The Castanha deposit is mainly hosted by hydrothermally altered subvolcanic acid rocks of rhyolitic to rhyodacitic composition, named as the Castanha quartz-feldspar porphyry (Pestilho, 2011). Crosscutting gabbro is also described in drill holes from both deposits. The Bacuri deposit is also hosted by the Serra Dourada Granite, and by subvolcanic dacitic rocks, named as the Bacuri porphyry (Melo et al., submitted).

6.2 Sodic alteration

The sodic alteration (Figs. 3F, 6A-G, and L) is the most developed and widespread type of alteration, and corresponds to formation of albite, scapolite and minor iron oxide (magnetite). This alteration affects different rock types, and shows different intensities and styles that vary from structurally controlled to pervasive.

6.2.1 Albite alteration

Hydrothermal albite occurs in veins and veinlets (Fig. 6A), and as selective and pervasive alteration (Fig. 6B). Albite crystals can be white to beige, or be pink to reddish due to tiny microscopic inclusions of hematite. Structurally controlled alteration, represented by albite veins, veinlets and filling of fractures and open spaces is observed in all types of rocks, especially in the Serra Dourada granite, where millimeter-scale albite and albite+quartz veinlets are common. A late generation of albite occurs in paragenesis with chalcopyrite in veins that cut some rocks. Albite and scapolite can be altered to sericite and/or chlorite, which provide a light green color to the rocks.



«Fig. 6. Characteristic features, field aspects, and photomicrographs of the hydrothermal alteration in the rocks from the area. A-B), G), and P-Q) Sodic alteration with albite formation; C-F) and L) Sodic alteration with scapolite formation; H) Sodic-calcic alteration; I-M) Potassic alteration with biotite –(chlorite-quartz); N) Potassic alteration with potassium feldspar; O) Silicification; P-R) Epidote alteration. A) Albite-quartz –(potassium feldspar) veins altering the Serra Dourada Granite; B) Pervasive albite alteration in the Serra Dourada Granite; C-D) Scapolite disseminations and in veins and veinlets altering a diabase; E) Scapolite crystal with radial texture filling a fracture plane of the Serra Dourada Granite; F) Scapolite filling the matrix of a hydrothermal breccia with fragments of the Bacaba Tonalite; G) Sodic alteration altering the microcline megacrysts of the Castanha quartz-feldspar porphyry, and forming and albite crustal with chessboard texture. Biotite alteration overprint the albite alteration; H) Actinolite-albite (sodic-calcic alteration) overprinting a sodic alteration (albite) in the Serra Dourada Granite; I) Biotite –(chlorite) filling fractures on the Bacaba Tonalite; J) Intense biotite and chlorite alteration on the Serra Dourada Granite. The igneous mineralogy and texture is completely modified, except for small areas preserved from alteration; K) Mylonite consisting of biotite, chlorite and quartz; L) Biotite, scapolite and quartz altering the matrix of the Castanha quartz-feldspar mylonite along the protomylonitic foliation; M) Biotite altering the plagioclase rim and along a fracture of the feldspar in the Campina Verde Tonalite; N) Diabase with selective potassic alteration, in which the igneous plagioclase are replaced by potassium feldspar; O) Quartz stockwork; P) Epidote vein surrounded by albite alteration cutting the Campina Verde Tonalite; Q) Epidote veins cutting the albite altered Rio Verde Trondhjemite; R) Allanite formed during a late epidote-chlorite-calcite alteration in the Serra Dourada Granite. Mineral abbreviations: Ab: albite, Act: actinolite, Al: allanite, Bt: biotite, Chl: chlorite, Ep: epidote, Kfs: potassium feldspar, Mgt: magnetite. Qtz: quartz, Scp: scapolite.

Pervasive selective alteration, in which the igneous texture is frequently recognizable, corresponds to the replacement of igneous microcline by albite (Figs. 3F and 6G), particularly in the granites (e.g., Serra Dourada Granite and Rio Verde Trondhjemite) and felsic subvolcanic rocks. In the quartz-feldspar porphyries and Bacaba Tonalite, several samples show euhedral microcline megacrysts completed replaced by albite, which has chessboard texture in thin sections. Meter-size parts of the rocks, especially the Serra Dourada Granite, can be completely altered to albite and scapolite. Locally, in an outcrop of the Rio Verde Trondhjemite, approximately 80% of the rock was replaced by hydrothermal albite and cut by epidote veins.

6.2.2 Scapolite alteration

Disseminated scapolite crystals (> 1mm) are commonly observed in the metamafic rocks, such as the diabase dikes and mafic intrusions (Figs. 6C and D), and corresponds to pseudomorphs after plagioclase. Scapolite with fibro-radial texture (Fig. 6E) filling fracture planes is also common, and can be altered to late chlorite and/or epidote. Scapolite and minor magnetite also occurs in millimeter- to centimeter-wide veins and veinlets (Figs. 6C and D) crosscutting the quartz-feldspar porphyries, metamafic rocks, the Bacaba Tonalite, and the Serra Dourada Granite. In such veins, coarse-grained fibrous marialite crystals typically have undulose

extinction and subgrain boundaries. Additionally, scapolite in dense millimeter- to centimeter-wide veinlet network (stockwork) obliterates almost completely the igneous texture in some part of the felsic rocks. In the Bacaba, Castanha and Bacuri deposits, the fissure-controlled to pervasive marialitic scapolite alteration is increasingly intense towards the mineralized zones. It can also pervasively occur in large veins (> 10 m) containing marialitic scapolite (+ quartz, magnetite and fluorite), especially in the Bacaba deposit.

Replacement of igneous feldspar by scapolite (selective alteration) is more frequently observed in the Castanha quartz-feldspar porphyry (Fig. 6L) and mafic intrusive rocks, although is also seen in the granitic rocks. In the large halos of scapolite alteration in the Bacaba deposit, scapolite not only replaces the igneous feldspar but also hydrothermal albite. In thin sections, scapolite is also observed along fractures and cleavages.

The matrix of hydrothermal breccias may be filled by scapolite with subordinated euhedral magnetite. These breccias, identified in the Bacaba Tonalite (Fig. 6F) and in the mafic intrusive rock, had centimeter-wide angled fragments of the host rocks, indicating that fluid pressure was locally high enough to cause the brecciation.

Mylonites composed of fine-grained hydrothermal scapolite, biotite, quartz and minor tourmaline along the mylonitic fabric are observed in the area. The protolith rocks of these mylonites are uncertain since fluid/rock interaction is so intense that rocks with completely distinct geochemical nature can develop the same mineralogy.

In the Castanha deposit, scapolite is commonly associated with biotite-rich altered zones, occurring along the foliation as deformed crystals with pressure shadows.

6.3 Na-Ca alteration and Fe metasomatism

Sodic-calcic alteration is less expressive in the country rocks than the sodic and potassic alterations. The styles of alteration vary from structurally-controlled (veins) to pervasive. Centimeter-wide veins of actinolite with minor albite were identified in the Campina Verde Tonalite. Additionally, millimeter-scale crystals of amphibole, albite, and quartz occur disseminated in one outcrop of the Serra Dourada Granite, previously altered by pervasive sodic (albite) alteration (Fig. 6H).

On the other hand, hydrothermal amphibole (mainly hastingsite) is frequently recognized in thin sections of different lithotypes (Figs. 3L and 4M) (e.g., Campina Verde and Bacaba

tonalites, mafic intrusive and volcanic rocks). In the mafic rocks, hastingsite completely replaces pyroxene crystals, and may alter the feldspar rims or occur along cleavage and fractures inside the grain. This last feature is also observed in the felsic intrusions.

In the IOCG deposits, however, the sodic-calcic alteration and iron oxide formation were responsible for the development of expressive and massive actinolite- and magnetite-rich bodies, known as actinolitite and magnetitite, respectively. These rocks are notably present in the Castanha deposit (Pestilho, 2011). In the magnetitites, which are also present at the Bacaba deposit, up to 85% of magnetite occurs associated with apatite + monazite ± actinolite ± chlorite ± calcite ± biotite ± pyrite ± chalcopyrite.

6.4 Potassic alteration (biotite) and chlorite formation

In the country rocks, potassic alteration with biotite (Figs. 3F and G, 4L, 6I-M) is commonly followed by chlorite alteration and silicification. This type of alteration affects both mafic and felsic rocks. The biotite-chlorite-quartz association occurs filling fractures (Fig. 6I) or as millimeter- to centimeter-wide veins and veinlets. The latter can evolve to a dense network with stockwork texture that becomes pervasive through the rock (Fig. 6J), and obliterate all the igneous features. In some areas is possible to observe the transition from predominant fissure-style to pervasive alteration. Locally, centimeter-wide veins with coarse-grained biotite cut the Bacaba Tonalite.

Biotite alteration is identified in thin section of several samples of the felsic subvolcanic (Figs. 3F and G, 6G) and intrusive rocks. Fine-grained biotite is found altering the rims and fractures of feldspar (Fig. 6M), in grain interstice (Figs. 4K and L), and in veins and veinlets. In some areas, all feldspar are destroyed and altered to biotite, and only the quartz grains remain unaltered. Biotite is commonly partially to totally altered to chlorite in all these rocks (Fig. 4F).

Fine-grained biotite, with subordinate scapolite and quartz are observed pervasively in the matrix of the quartz-feldspar porphyries (Fig. 6L) and in the mafic volcanic rocks. This alteration is more intense towards mylonitic zones, in which the rocks show S-C structures accompanied by crystal stretching and comminuting of quartz, scapolite and biotite.

In the Bacaba, Castanha and Bacuri deposits, the biotite-rich alteration is ubiquitous and occurs in wide zones (> 300 m) crosscut by late alteration stages. Altered rocks are fine-grained, foliated, murky-brown and composed of biotite with subordinate scapolite, quartz, magnetite, and

potassium feldspar. Biotite is deformed and oriented along the mylonitic fabrics and scapolite occurs as zoned and rotated megacrysts exhibiting pressure shadows of quartz. These features suggest that biotite and scapolite crystallization was pre- to syn-kinematic in relation to shearing.

6.5 Tourmaline formation

Tourmaline is identified along the mylonitic foliation in the Bacaba, Castanha and Bacuri deposits, especially in biotite-rich zones with associated scapolite. The subhedral dark greenish-blue tourmaline reveals mutual replacement by biotite. The highest tourmaline content (up to 30% molar volume) is observed in the Bacaba deposit (Augusto et al., 2008).

6.6 Potassic alteration (potassium feldspar)

In the country rocks, potassic alteration with potassium feldspar is not as well developed as the alteration with biotite. Potassium feldspar can occur as millimeter- to centimeter-wide veins and veinlets that cut the rocks with the previous alterations. Alternatively, it replaces igneous plagioclase (selective alteration), as recognized in a diabase dike (Fig. 6N) and in the Campina Verde Tonalite. Additionally, potassium feldspar occurs as disseminations in the rock, or filling microfractures. Locally in the Serra Dourada Granite, initially structurally-controlled potassic alteration becomes more intense, that eventually assimilates parts of the previously altered rock.

In the Bacaba and Castanha deposits, potassium feldspar-bearing alteration zones are also narrower (< 20 m) than biotite-rich zones, are structurally-controlled to pervasive, and defined by replacement of hydrothermal chessboard albite and scapolite by red cloudy orthoclase containing tiny hematite inclusions (Augusto et al., 2008, Pestilho, 2011). Veins and veinlets with alkali feldspar crosscut zones with albite, scapolite and some magnetite veins, and commonly precede the main stage of ore formation. The alkali feldspar veins are associated with mylonitic foliation and temporally related to rutile or with calcite ± musketovite (hematite replaced by magnetite) ± hematite ± chalcopyrite. In both Bacaba and Castanha deposits, late veins (up to 1 cm thick) of potassium feldspar are very common in mineralized zones crosscutting biotite- and chlorite-rich rocks. In the Bacuri deposit, potassium feldspar alteration occurs both pervasively and structurally-controlled, and is more developed than at the Bacaba and Castanha deposits (Melo et al., submitted).

6.7 Silicification

Silicification, a very common alteration in the area, occurs as quartz veins, stockwork zones (Fig. 6O), or pervasively through the rock. It is more frequently seen along or close to shear zones, where crystal stretching and comminuting is particularly observed in thin sections.

Hydrothermal breccia with matrix filled by quartz and fragments of the host rocks are recognized in some areas, especially in the Rio Verde Trondhjemite and the Campina Verde Tonalite.

In the Bacaba, Castanha and Bacuri deposits, pervasive and fissure-style quartz alteration overprint early albite alteration zones. In the Castanha deposit, pervasive silicified zones are associated with biotite, or with disseminated chalcopyrite in the magnetite- and actinolite-rich bodies (Pestilho, 2011). Among the three deposits, silicification is more typically observed in the Bacuri deposit, either as veins and fractures filling, or as disseminations cut by chalcopyrite veins (Melo et al., submitted).

6.8 Epidote, calcite and chlorite formation

Millimeter-scale epidote veins cut different rock, such as the mafic and felsic intrusive rocks (Fig. 6P and Q). In the Campina Verde Tonalite, epidote may be associated with chalcopyrite or malachite in centimeter-wide veins, whereas in the Serra Dourada Granite epidote veinlets also contain quartz. The Rio Verde Trondhjemite is the lithotype mostly affected by epidote alteration. In one outcrop, up to ten centimeter-wide epidote veins cut the rock previously replaced by albite alteration (Fig. 6Q).

Scapolite crystals, particularly those along plane fractures, are easily altered to chlorite and/or epidote. Hydrothermal assemblage consisting of chlorite, epidote, calcite, clinozoisite, allanite and iron oxide (Fig. 6R) is commonly present in the matrix of the felsic subvolcanic and intrusive rocks altering the feldspar or in the minerals interstices. It is also possible to observe chlorite crystals along fractures, or in quartz veins cutting the rock.

Particularly at the Bacaba and Bacuri deposits, chlorite and epidote alteration are strongly correlated to the mineralizing stage (Augusto et al., 2008, Melo et al., submitted). They are both structurally-controlled and concordant with the mylonitic foliation. These alteration zones replace potassic alteration zones, especially those with biotite and magnetite. In the Bacuri deposit,

chlorite alteration is the most developed type of hydrothermal alteration, and locally, responsible for the formation of massive chlorite-rich bodies (Melo et al., submitted).

Carbonate alteration is more developed at Castanha, followed by the Bacuri and Bacaba deposits. In the former, calcite veins and veinlets are associated with sulfides ± epidote ± chlorite and occur crosscutting all the previous mineral assemblages. Pervasive carbonate alteration is closely related to pyrrhotite-rich copper orebodies at the Castanha deposit.

6.9 Ore stage

6.9.1 Bacaba deposit

At the Bacaba deposit (Fig. 5A), the IOCG mineralization is spatially related to late potassium feldspar veins, which crosscut chlorite- and epidote-bearing zones. Ore occurs as veins and replacement zones relayed to mylonitic foliation, and comprises chalcopyrite, bornite, covellite, chalcocite, magnetite and hematite, with subordinate melonite, hessite, altaite, uraninite, cassiterite, and ferberite. The gangue minerals consist in chlorite, calcite, epidote, clinozoisite, allanite, apatite, monazite, and rutile. The late stage of hydrothermal alteration is characterized by sericitic and hydrolytic associations, the latter typified by a hematite-muscovite-kaolinite–illite association (Pestilho, 2011).

Two hydrothermally altered samples from the Bacaba deposit, including an ore sample, were selected for U-Pb LA-MC-ICPMS monazite geochronology. Ore sample BACD 25/229.25 (Fig. 7A) corresponds to the Bacaba Tonalite intensively altered by pervasive potassic alteration (potassium feldspar and minor biotite) associated with silicification. Chalcopyrite veins and veinlets cut these previous alteration stages and may be related to silicification. Hydrothermal monazite occurs as inclusions in apatite crystals (Figs. 8A and B). Igneous zircon grains from this ore sample and have been dated using U-Pb LA-MC-ICPMS method and yielded the $2,990.9 \pm 5.8$ Ma age (Moreto et al., 2011).

Sample BACD 15/237.4 (Fig. 7B) is not mineralized and corresponds to the Serra Dourada Granite pervasively affected by silicification and albite alteration, consistent with the early stages of evolution of the hydrothermal system. The igneous texture of the granite is still preserved in sample BACD 15/237.4. Monazite crystals are included in hydrothermal albite (Fig. 8C). Igneous zircon crystals from this sample were also analyzed by the U-Pb LA-MC-ICPMS systematic by Moreto et al. (2011) and yielded a $2,860 \pm 22$ Ma age, which was interpreted as the

igneous crystallization of the Serra Dourada Granite.

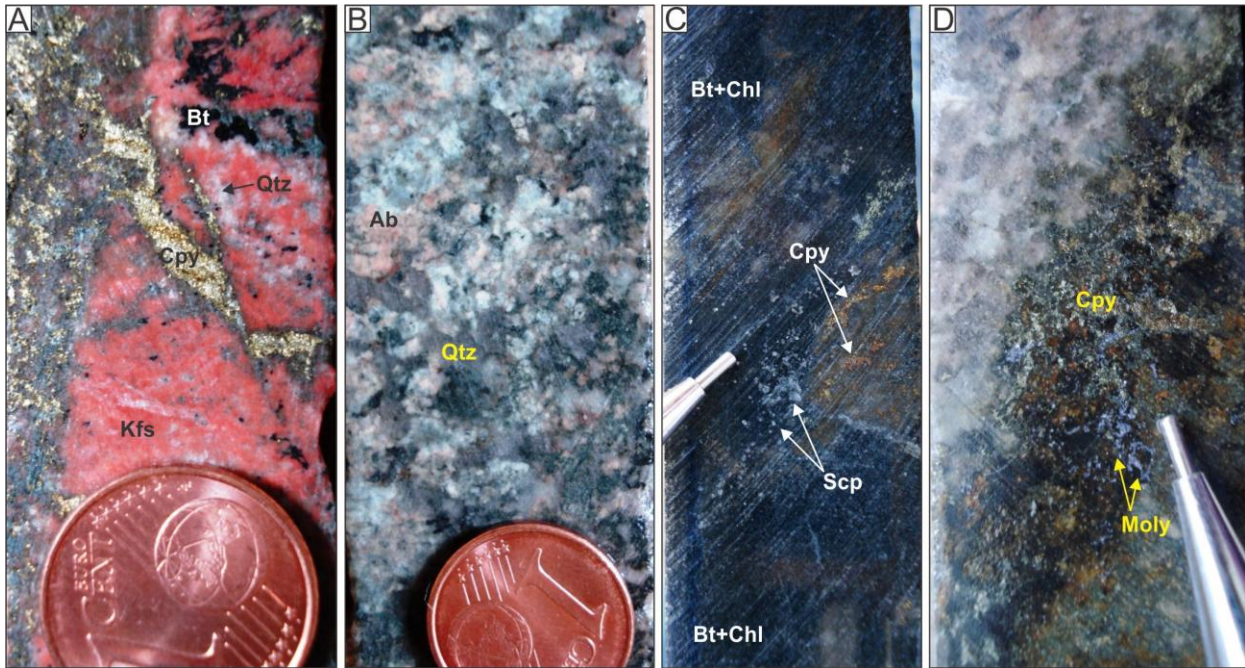


Fig. 7. Characteristic features of the ore and hydrothermally altered samples selected for geochronological studies. A) Ore from the Bacaba deposits hosted by the Bacaba Tonalite (sample BACD 25/229.25); B) Serra Dourada Granite in the Bacaba deposit area intensively affected by albite alteration and silicification (sample BACD 15/237.4); C) Sample from the Bacuri deposit pervasively affected by chlorite and biotite alteration, and with chalcopyrite and scapolite disseminations (sample BRID 07/115.42); D) Serra Dourada Granite in the Bacuri deposit area altered by silicification, and by discrete biotite and chlorite alteration (sample BRID 01/45). Molybdenite and chalcopyrite are coeval with biotite formation. Mineral abbreviations: Ab: albite, Bt: biotite, Chl: chlorite, Cpy: chalcopyrite, Kfs: potassium feldspar, Moly: molybdenite, Qtz: quartz, Scp: scapolite.

6.9.2 Castanha deposit

At the Castanha deposit (Fig. 5B), ore occurs in veins, veinlets, stockwork, and breccias (Pestilho, 2011). Mineralized breccias are structurally-controlled and present deformed clasts of the altered host rocks. Pyrrhotite-rich breccias, described only at Castanha, have pentlandite, Co-pentlandite, chalcopyrite, and sphalerite. The main ore, however, comprises chalcopyrite (up to 75%), molybdenite, pyrite, and marcasite, with associated quartz and monazite. Chalcopyrite-epidote-magnetite-allanite veinlets crosscut zones of sodic-calcic alteration. Other accessory minerals include uraninite, galena, monazite, Pd-melonite, sugakiite, and Ni-pyrite.

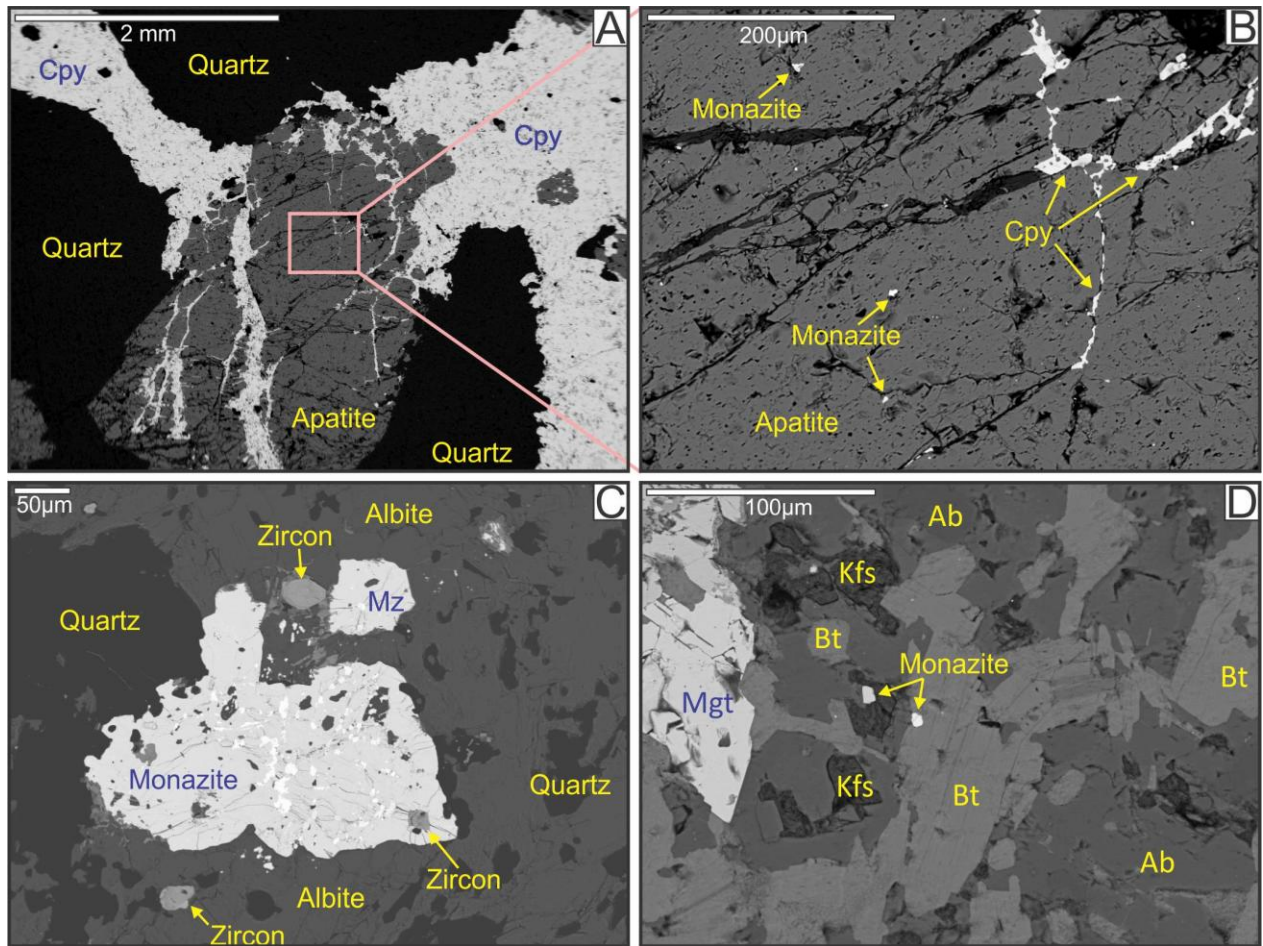


Fig. 8. BSE images showing monazite crystals in hydrothermally altered and ore samples from the Bacaba and Bacuri deposits. A) and B) Monazite inclusions in apatite crystals. Chalcopyrite and apatite fills the matrix of the copper ore breccia. Bacaba deposit (sample BACD 25/229.25); C) Large monazite crystal ($> 200 \mu\text{m}$) included in hydrothermal albite. Serra Dourada Granite affected by sodic alteration and silification (BACD 15/237.4); D) Monazite included in hydrothermal albite and biotite from sodic and potassic alteration, respectively. Sample from the Bacuri deposit pervasively affected by chlorite and biotite alteration (BRID 07/115.42). Mineral abbreviations: Ab: albite, Bt: biotite, Cpy: chalcopyrite, Kfs: potassium feldspar, Mgt: magnetite, Mz: monazite.

6.9.3 Bacuri deposit

In the Bacuri deposit (Fig. 5C), ore is strongly controlled by mylonitic foliation (Melo et al., submitted). Chalcopyrite, the main copper mineral, occurs disseminated in zones of intense potassic (potassium feldspar) and chlorite alteration. Chalcopyrite also occurs in veinlets with associated potassium feldspar, and minor apatite, monazite, epidote, allanite, clinozoisite, chlorite, pyrite and magnetite, or alternatively with quartz.

Monazite grains were selected from a hydrothermally altered sample (BRID 07/115.42) for U-Pb LA-MC-ICPMS dating, whereas molybdenite was selected for Re-Os NTIMS from part

of the Serra Dourada Granite (BRID 01/45) with a few chalcopyrite disseminations. Sample BRID 07/115.42 (Fig. 7C), which the protolith nature is uncertain, is intensively affected by chlorite and biotite alteration that completely obliterates the igneous characteristic of the rock. Scapolite and chalcopyrite also occurs as millimeter-scale disseminations. Late veins with quartz and chalcopyrite cut the rock. The pervasive chlorite and potassic alteration from this sample were formed concomitantly with the main stage of ore precipitation. Monazite crystals occur as inclusions in hydrothermal biotite and albite (Fig. 8D).

Sample BRID 01/45 (Fig. 7D) corresponds to the foliated Serra Dourada Granite affected by pervasive silicification and albite alteration, and by less developed biotite and chlorite alteration. Fine-grained molybdenite and chalcopyrite are associated with calcite and occur in centimeter-wide veins deformed along the mylonitic foliation. These sulfides are spatially unrelated to the main zone of copper ore, and may be coeval with local discrete potassic alteration. Late undeformed veins of malachite cut the sulfide-bearing veins.

7. U-Pb and Re-Os results

The isotopic data obtained in this study by different methods is summarized in Table 4.

Table 4 Synthesis of geochronological data obtained in this study

<i>Rock</i>	<i>Mineral</i>	<i>Method</i>	<i>Age (Ma)</i>	<i>MSWD</i>
<i>Host and country rocks</i>				
Quartz-feldspar porphyry (GMCL 54A)	zircon	U-Pb SHRIMP IIe	$2,740.9 \pm 4.7$	1.08
Castanha quartz-feldspar porphyry (CASD 02/424.90)	zircon	U-Pb SHRIMP IIe	$2,744.8 \pm 4$	0.18
Serra Dourada Granite (GMCL 40A)	zircon	U-Pb SHRIMP IIe	$2,848 \pm 5.5$	1.5
Campina Verde Tonalite (GMCL 01)	zircon	U-Pb SHRIMP IIe	$2,876 \pm 6.8$	5.6
Campina Verde Tonalite (GMCL 66)	zircon	U-Pb SHRIMP IIe	$2,876 \pm 5.2$	6.9
<i>Bacaba deposit</i>				
Ore hosted by the Bacaba Tonalite (BACD 25/229.25)	monazite	U-Pb LA-MC-ICPMS	$2,681 \pm 11$	3
Albite altered and silicified Serra Dourada Granite (BACD 15/237.4)	monazite	U-Pb LA-MC-ICPMS	$2,054.1 \pm 8.8$	10.2
<i>Bacuri deposit</i>				
Chlorite, biotite and scapolite altered rock (BRID 07/115.42)	monazite	U-Pb LA-MC-ICPMS	$2,703.0 \pm 5.8$	3.9
Ore hosted by the Serra Dourada Granite (BRID 01/45)	molybdenite	Re-Os NTIMS	$2,758 \pm 11$	-

7.1 Host rocks

7.1.1 Quartz-feldspar porphyries

Zircon crystals from the quartz-feldspar porphyry (Figs. 9A-C), sample GMCL 54A (Fig. 3B), are light pink to white, euhedral, and display either prismatic shape with pyramid terminations, or squared to rectangular shape with flat terminations. Crystal lengths are < 150 μm , and aspect ratios (length/width) around 1:1 to 1.5:1. Oscillatory zoning is observed in some grains in CL images (Fig. 9B), whereas in others there is a predominance of textureless areas comprising almost the whole grain (Fig. 9A). Th/U ratios vary from 0.48 to 0.96, with a mean value of 0.73. The zircon grains analyzed by U-Pb SHRIMP IIe produced 8 concordant analyses, resulting in a concordia age of $2,740.9 \pm 4.7$ Ma (MSWD= 1.08; Fig. 10A; Supplementary Table 1).

The zircon grains from the Castanha quartz-feldspar porphyry, sample CASD 02/424.90 (Fig. 3E), are pink, euhedral, and have pyramidal forms with flat terminations (Figs. 9D-F). Crystal lengths range from 50 to 150 μm , and aspect ratios (length/width) from 1:1.5 to 2:1. In terms of internal textures, CL images show that some grains have large textureless areas (Fig. 9E); nevertheless, other grains have weak oscillatory zoning (Fig. 9D). Th/U ratios range from 0.38 to 0.67 with a mean value of 0.53. Eleven concordant analyses by U-Pb SHRIMP IIe rendered the concordia age of $2,744.8 \pm 4$ Ma (MSWD = 0.18; Fig. 10B, Supplementary Table 1).

7.1.2 Serra Dourada Granite

Zircon grains (Figs. 9G-I) from sample GMCL 40A (Fig. 4C) are light pink, euhedral, have prismatic shapes with pyramidal terminations or slightly ovoid forms with flat terminations. Crystal lengths range from 50 to 220 μm , with aspect ratios (length/width) between 1:1 and 3:1. Some zircon grains exhibit xenocrystic cores, in which the core appears lighter (lower U content) than the rim (higher U content) in CL images. The oscillatory zoning is present in several grains (Figs. 9H and I), although sector or complex zonings (Fig. 9G) are also common. Additionally, some grains show textureless cores. Th/U ratios vary from 0.18 to 1.28, with a mean value of 0.53. Sample GMCL 40A was analyzed by U-Pb SHRIMP IIe and 5 spot analyses produced the concordia age of $2,848 \pm 5.5$ Ma (MSWD= 1.5; Fig. 10C, Supplementary Table 1).

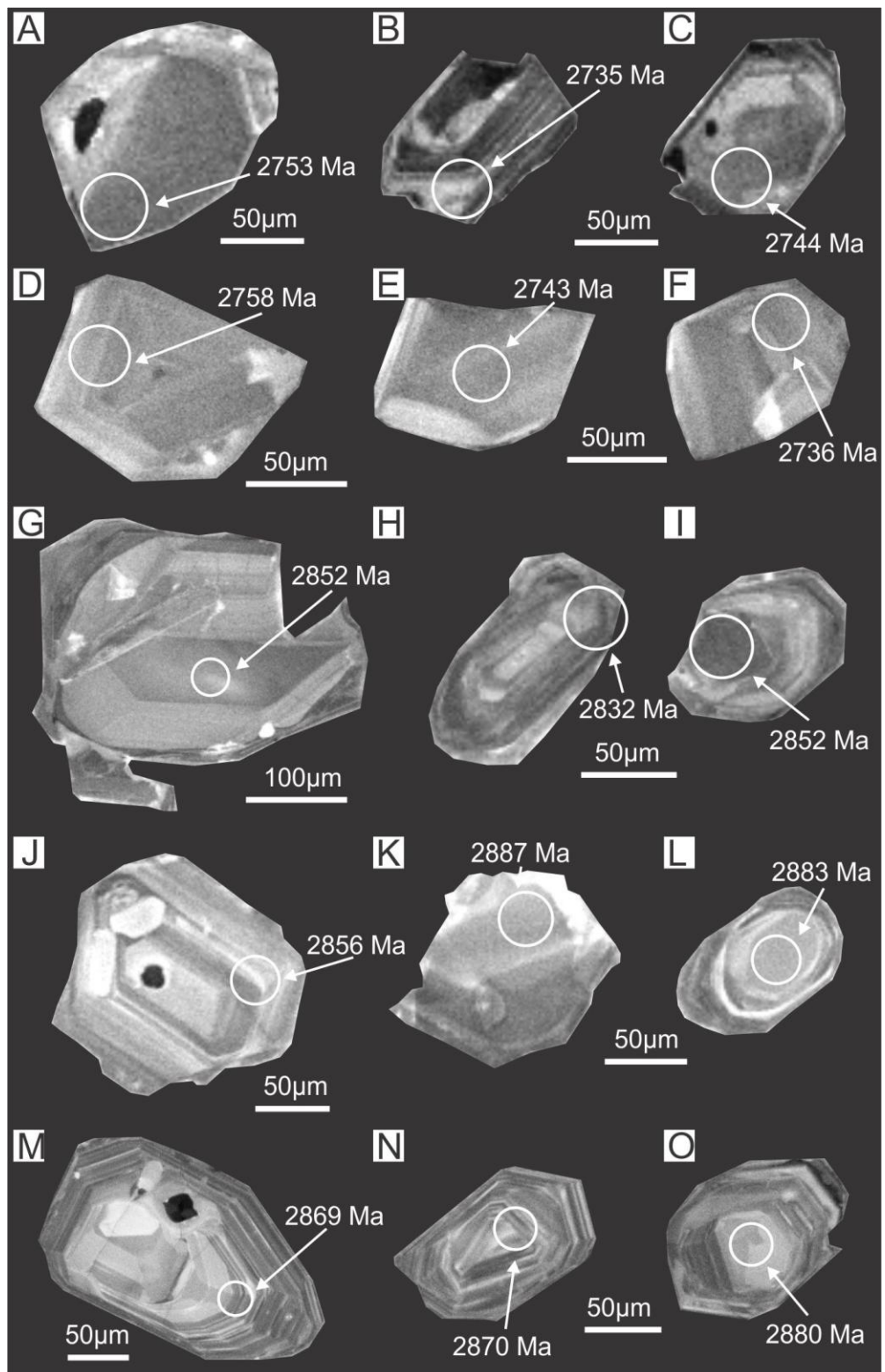


Fig. 9. CL images of zircon from the felsic rocks dated by U-Pb SHRIMP IIe. $^{207}\text{Pb}/^{206}\text{Pb}$ ages are indicated in the image where analyses were done. A-C) Quartz-feldspar porphyry (sample GMCL 54A); D-F) Castanha quartz-feldspar porphyry (sample CASD 02/424.9); G-I) Serra Dourada Granite (sample GMCL 40A); J-L) Campina Verde Tonalite (sample GMCL 01); M-O) Campina Verde Tonalite (sample GMCL 66).

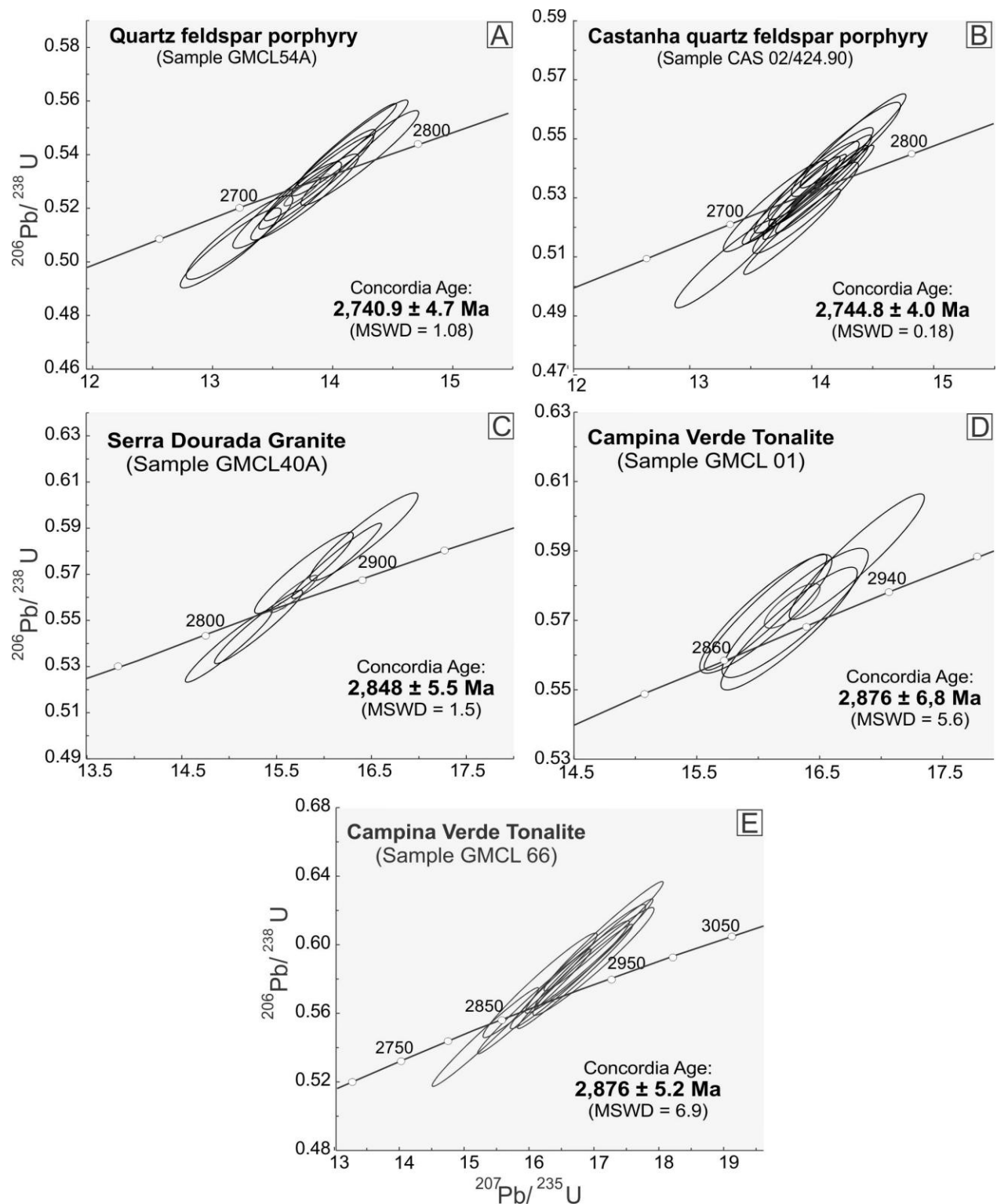


Fig. 10. $^{206}\text{Pb}/^{238}\text{U}$ vs. $^{207}\text{Pb}/^{235}\text{U}$ diagrams for zircon from the felsic rocks dated by U-Pb SHRIMP IIe. A) Quartz-feldspar porphyry (sample GMCL 54A); B) Castanha quartz-feldspar porphyry (sample CASD 02/424.9); C) Serra Dourada Granite (sample GMCL 40A); D) Campina Verde Tonalite (sample GMCL 01); E) Campina Verde Tonalite (sample GMCL 66).

7.1.3 Campina Verde Tonalite

Zircon grains from sample GMCL 01 (Figs. 4I) are pink, euhedral to subhedral, and have prismatic to ovoid shapes and rounded to flat terminations. Crystal lengths range from 40 a 200 μm , with aspect ratios (length/width) of 1:1 to 3:1. CL images (Figs. 9J-L) shows whether oscillatory and sector zoning in entire grains (Figs. 9J and L), or only in the rims. In these cases, zircon cores do not display any internal texture. Th/U ratios vary from 0.49 to 0.98, with a mean value of 0.67. Sample GMCL 01 was analyzed by U-Pb SHRIMP IIe and 5 spot analyses provided the concordia age of $2,876 \pm 6.8$ Ma (MSWD= 5.6; Fig. 10D, Supplementary Table 1).

Zircon grains from sample GMCL 66 (Fig. 4J) are pink, euhedral, and have predominant ovoid shapes with rounded to flat terminations, although a few prismatic grains are also present. Crystal lengths range from 30 a 190 μm , with aspect ratios (length/width) of 1:1 to 2:1. CL images (Figs. 9M-O) show oscillatory zoning patterns (Figs. 9M and N), but also brighter textureless cores (lower U content) with oscillatory zoning only in the rims (Fig. 9O). Additionally, zircons rims with sector zoning are also identified. Th/U ratios vary from 0.50 to 0.85, with a mean value of 0.64. Sample GMCL 66 was analyzed by U-Pb SHRIMP IIe and 9 spot analyses provided the concordia age of $2,876 \pm 5.2$ Ma (MSWD= 6.9; Fig. 10E; Supplementary Table 1).

7.2 IOCG deposits

7.2.1 Bacaba deposit

The monazite grains from the ore sample hosted by the Bacaba Tonalite (BACD 25/229.25; Fig. 7A) are light yellow, subhedral, and ovoid to pyramidal with rounded terminations. Internal textures in monazite grains are not observed in CL or BSE images. The crystals length varies from 20 to 250 μm , and aspect ratios (length/width) from 1:1 to 1.8:1. The monazite grains provided two distinct age populations, notwithstanding the fact that no differences were observed regarding structure, morphology, size, and color. Nine U-Pb LA-MC-ICPMS spot analyses in seven monazite grains rendered the concordia age of $2,681 \pm 11$ Ma (MSWD= 3; Fig. 11A, Supplementary Table 2), whereas nineteen spot analyses in fourteen grains yielded a concordia age of $2,054.1 \pm 8.8$ Ma (MSWD= 10.2; Fig. 11B, Supplementary Table 2). The older age was not restricted to monazite cores, like the younger age, which was not limited to the monazite rims.

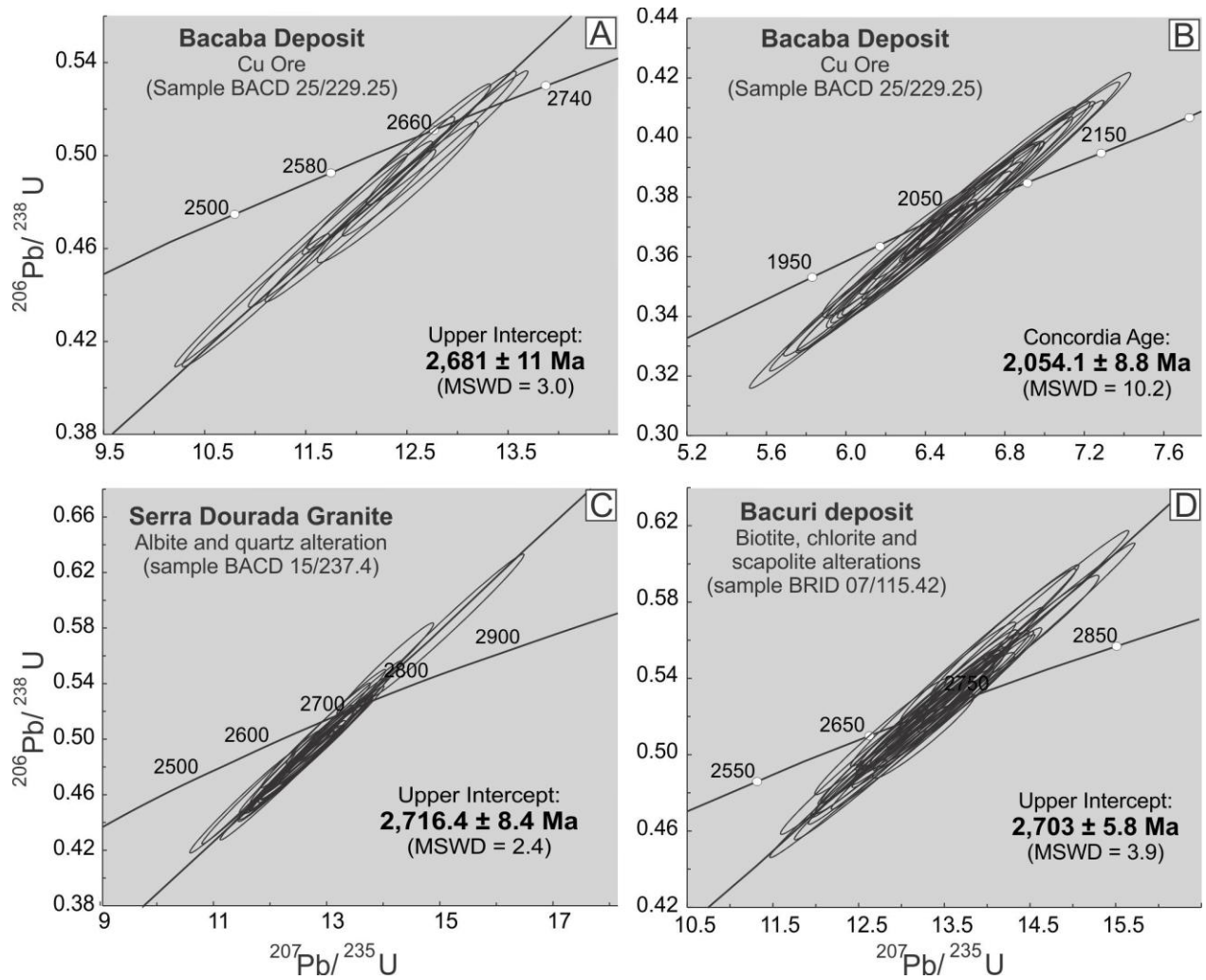


Fig. 11. $^{206}\text{Pb}/^{238}\text{U}$ vs. $^{207}\text{Pb}/^{235}\text{U}$ diagrams for monazite from hydrothermally altered rocks and ore from the Bacaba and Bacuri deposits. A) and B) Cu ore from the Bacaba deposit (sample BACD 25/229.25). Two different concordia ages (diagrams A and B) from distinct monazite populations were obtained for this sample; C) Serra Dourada Granite affected by sodic alteration (albite) and silification (BACD 15/237.4); D) Sample from the Bacuri deposit with biotite, chlorite and scapolite alteration (BRID 07/115.42).

Monazite grains from sodically altered Serra Dourada Granite (BACD 15/237.4; Fig. 7B) are light yellow, subhedral, and rounded to prismatic with triangular terminations. Some fractures and inclusions are present in a few grains. Internal textures are also absent in CL and BSE images. Crystals vary from 30 to 220 μm , and have aspect ratios (length/width) from 1:1 to 1.5:1. Twenty-four analyses by U-Pb LA-MC-ICPMS in nineteen grains yielded a concordia age of $2,716.4 \pm 8.4$ Ma (MSWD= 2.4; Fig. 11C, Supplementary Table 2).

7.2.2 Bacuri deposit

The monazite grains from the hydrothermally altered (chlorite and potassic alteration) sample BRID 07/115.42 (Fig. 7C) are yellow with few dark yellow areas, euhedral to subhedral, with pyramidal to prismatic forms. Several inclusions are present and no internal textures are observed in CL or BSE images. Crystal length varies from 40 to 190 µm, and aspect ratios (length/width) from 1:1 to 1.5:1. Thirty spot analyses by U-Pb LA-MC-ICPMS in seventeen grains provided a concordia age of $2,703.0 \pm 5.8$ Ma (MSWD= 3.9; Fig. 11D, Supplementary Table 2).

Molybdenite from mineralized sample BRID 01/45 (Fig. 7D) has Re abundance of 20.73 ppm, and radiogenic ^{187}Os concentration of 612.7 ppb. The molybdenite crystals from this sample yielded Re-Os age of $2,758 \pm 11$ Ma (Table 5).

Table 5 Summary of Re-Os molybdenite data from the Bacuri deposit

Re (ppm)	$\pm 2\sigma$	^{187}Re (ppb)	$\pm 2\sigma$	^{187}Os (ppb)	$\pm 2\sigma$	Total common Os (pg)	Age (Ma)	$\pm 2\sigma$ with λ (Ma)
<i>Molybdenite (BRID 01/45)</i>								
20.73	0.05	13029	33	612.7	0.4	2.1	2758	11

8. Discussion

8.1 Meso- and Neoarchean magmatism in the Southern Copper Belt

Detailed mapping in the Southern Copper Belt allowed the individualization and characterization of felsic subvolcanic rocks, mafic intrusive and volcanic rocks, meta-ultramafic rocks, granites, and migmatites. Moreover, some of these rocks, particularly the felsic subvolcanic and meta-ultramafic rocks, have their occurrence limited to small meter-scale outcrops that could be easily not noticed in less detailed mapping.

The felsic subvolcanic rocks, exemplified by quartz-feldspar porphyries, were not previously described in the Carajás region. Although these porphyries occur as small subcircular bodies in the field, various drill holes in the Castanha deposit area have intercepted several meters of these rocks, suggesting that these intrusions can be causative in subsurface. The U-Pb SHRIMP IIe ages of $2,740.9 \pm 4.7$ and $2,744.8 \pm 4$ Ma are interpreted as the igneous

crystallization ages of the quartz-feldspar porphyries and the Castanha quartz-feldspar porphyry, respectively.

These ca. 2.74 Ga ages obtained for the felsic subvolcanic rocks are slightly younger than the predominant ca. 2.76 Ga felsic and mafic volcanic magmatism of the Itacaiúnas Supergroup (Gibbs et al., 1986; DOCEGEO, 1988; Machado et al., 1991; Trendall et al., 1998; Galarza and Macambira, 2002a) that filled the Carajás Basin. Nonetheless, the 2.74 Ga ages are similar to those obtained for the Sossego granophyric granite ($2,740 \pm 26$ Ma; U-Pb LA-ICPMS; Moreto et al., submitted), which is one of the host rock of the Sossego orebody (Sossego deposit), and gabbro to gabbronorite ($2,739 \pm 5.9$ Ma; U-Pb SHRIMP IIe; Moreto et al., submitted) that host the Sequeirinho and Curral orebodies (Sossego deposit).

Additionally, the ca. 2.74 Ga age is coeval to that of the Neoarchean granite magmatism widely recognized in the Carajás Domain (e.g., 2.75-2.74 Ga Estrela and Serra do Rabo granites; Barros et al., 2004; Sardinha et al., 2006) and the Transition Subdomain (e.g., 2.75 Ga Pedra Branca Granite and 2.74 Ga Planalto Granite, Huhn et al., 1999b; Feio et al., 2012b). The 2.74 Ga ages are also close to the ages of emplacement of gabbro from the Pium diopside Norite ($2,735 \pm 5$ Ma, U-Pb zircon; Feio et al., 2012b), and the Cristalino Diorite (2738 ± 6 Ma, Pb-Pb zircon, Huhn et al., 1999b). All this data, including the subvolcanic rocks from this study and the host rocks of the Sossego deposit (granophyric granite and gabbronorite; Moreto et al., submitted), not only reinforce the widespread occurrence of the 2.74 Ga magmatism, but also strongly suggest a bimodal character for this Neoarchean magmatism in the Carajás Domain.

Nonetheless, preliminary geochemistry data (Silva, 2011) show that the quartz-feldspar porphyries are calk-alkaline and meta- to peraluminous, differing from the 2.74 Ga granites of the Carajás Domain (e.g., Estrela, Serra do Rabo, Planalto and Pedra Branca), which have an accentuated alkaline affinity and are metaluminous (Barros et al., 1997, Sardinha et al., 2006, Feio et al., 2012a).

The $2,848 \pm 5.5$ Ma age obtained for the Serra Dourada Granite (Moreto et al. 2011) is interpreted as the timing of igneous crystallization age for this unit. This age is close to the ages obtained previously for this rock, such as $2,860 \pm 22$ Ma (zircon U-Pb LA-MC-ICPMS, Moreto et al. 2011) and $2,831 \pm 6$ Ma (zircon U-Pb LA-ICPMS, Feio et al. 2012a). The $2,876 \pm 5.2$ and $2,876 \pm 6.8$ Ma ages obtained for the Campina Verde Tonalite are also interpreted as representing the igneous crystallization for this rock. The Serra Dourada Granite is slightly younger (ca. 30

Ma) than the Campina Verde Tonalite, which is consistent with field observation. The Campina Verde Tonalite is coeval with the 2.86 Ga event of migmatization and granulitization that affected the Xingu basement complex and the Chicrim-Cateté Orthogranulites (Machado et al., 1991, Pidgeon et al., 2000), although this unit does not have evidence of high-grade metamorphism.

The 2.87 Ga ages for the Campina Verde Tonalite are similar to the age of the widespread magmatism at the southern Rio Maria Domain. In this domain, magmatism shows different compositions and geochemical nature, varying from TTG suites (Água Fria Trondhjemite, Leite et al., 2004, Almeida et al., 2011), Archean granites (e.g., Xinguara, Mata Surrão and Guarantã granites; Lafon et al. 1994, Leite et al., 2004, Almeida et al., 2010), and sanukitoid rocks (Rio Maria Granodiorite, Macambira and Lancelot, 1996; Oliveira et al., 2009, 2011). Nonetheless, geochemistry data from Feio et al. (2012a) indicates that the Campina Verde Tonalite is calc-alkaline, and does not have geochemical affinity with TTG suites, such as those from the Rio Maria Domain.

In addition to the ca. 2.87-2.84 Ga and Neoarchean (2.74 Ga) ages obtained in this study, the Southern Copper Belt also contains the oldest rocks of the Carajás Province. Such rocks correspond to the Bacaba Tonalite ($3,001.2 \pm 3.6$ Ma, zircon U-Pb LA-MC-ICPMS; Moreto et al. 2011), which host the Bacaba deposit, and the Sequeirinho Granite ($3,010 \pm 21$ Ma, zircon U-Pb LA-ICPMS; Moreto et al., submitted), which host the Sossego deposit (Sequeirinho orebody). Similar ca. 3.0 Ga ages in the Carajás Province were attributed to the crystallization of the igneous protolith of enderbites and charnockites of the Chicrim- Cateté Orthogranulites (Rodrigues et al., 1992; Pidgeon et al., 2000; Vasquez et al. 2008a), in addition to metadacites ($3,002 \pm 3$ Ma; zircon U-Pb; Tassinari et al., 2005) from the Gradaús Group, which is a greenstone belt sequence of the Rio Maria Domain.

Other Mesoarchean rocks from the Southern Copper Belt were crystallized at ca. 2.97-2.96 Ga, and correspond to the Pista felsic metavolcanic rock ($2,968 \pm 15$ Ma and $2,979 \pm 5.3$ Ma, zircon U-Pb SHRIMP IIe, Moreto et al. submitted), which host the Sossego deposit (Pista orebody), and the Canaã dos Carajás Granite ($2,959 \pm 6$ Ma, zircon U-Pb LA-ICPMS, Feio et al. 2012a).

Based on the new geochronological data and the data available in the literature, at least six magmatic events can be constrained at the Southern Copper Belt. The oldest event, at 3.01-

2.99 Ga was responsible for the crystallization of the Bacaba Tonalite, the Sequeirinho Granite, and the igneous protolith of granulites from the Chicrim- Cateté Orthogranulites. At 2.97- 2.96 Ga the Pista felsic volcanic rock and the Canaã dos Carajás Granite were formed. During the third event, at 2.87 Ga, the Campina Verde Tonalite and the Rio Verde Trondhjemite were crystallized. Approximately 30 Ma years after the emplacement of these rocks, the large 2.84 Ga Serra Dourada Granite intruded the preexisting basement (e.g., Bacaba and Campina Verde tonalites). At 2.74 Ga the emplacement of the quartz-feldspar porphyries, granophyric granite, gabbro, the Planalto Granite, the Pium diopside Norite, and the Cristalino Diorite took place. Finally at 1.88 Ga the Rio Branco Granite was emplaced.

The 3.0, 2.87 and 2.84 Ga Mesoarchean rocks found in the Southern Copper Belt possibly corresponds to the basement of the Carajás Basin. The Mesoarchean (3.1 to 2.8 Ga) is characterized by a important interval for mantle–crust differentiation at the Carajás Province, which is evidence by T_{DM} model ages of ca. 3.0 Ga for rocks with different ages and compositions (Macambira and Lancelot, 1996; Sato and Tassinari, 1997; Tassinari and Macambira, 1999; Dall’Agnol et al., 1999b; Souza et al., 2001; Teixeira et al., 2002, Galarza and Macambira, 2002b). These rocks formed at ca. 3.0 Ga were possibly intensively reworked in the Neoarchean (ca. 2.76-2.74 Ga) when the Carajás Basin was installed and when several granite suites were emplaced (e.g., Estrela, Planalto and Serra do Rabo granites; Huhn et al., 1999b; Barros et al., 2004; Sardinha et al., 2006). Based on Sm-Nd systematic, Barros et al. (2009) also suggest that the magma responsible for forming the Estrela Granite were most probably produced by partial melting of ca. 3.0 Ga rocks. This fact could justify the scarcity of the 3.0 Ga rocks in the Carajás Domain.

8.2 Significance of the meta-ultramafic rocks

The presence of meta-ultramafic rocks in the area is notable, and these rocks occur as mylonites tectonically imbricated along shear zones cutting several units (e.g., Serra Dourada Granite, mafic intrusive and metavolcanic rocks). The meta-ultramafic rocks are often found along shear zones where copper (malachite) prospects are located. Moreover, this association is also observed in some IOCG deposit from the Southern Copper Belt, such as the Bacaba, Visconde and Pista orebody (Sossego deposit).

The relation between ultramafic rocks and Cu occurrences should be carefully evaluated. The world-class Olympic Dam IOCG deposit, in Australia, is hosted by a granite (Roxby Downs Granite) and cut by several mafic-ultramafic dikes, similar to lamprophyres and kimberlites (Johnson, 1993). Nd systematic conducted by Johnson and McCulloch (1995), showed that the ultramafic rocks may have contributed with a significant amount (approximately 50%) of Nd and Cu to the Olympic Dam deposit. Differently, the smaller and weakly mineralized copper prospects and barren iron oxide breccias from the Olympic Dam district, show Nd and Cu contribution exclusively from crustal sources, with no input of primitive Nd (Skirrow et al., 2007). Additionally, a comparison between initial $^{187}\text{Os}/^{188}\text{Os}$ ratios of iron oxides and sulfides from world-class IOCG deposits from the Chilean Iron Belt (e.g., Candelaria, Manto Verde, and Bronce deposits), and iron oxides from magnetite-apatite deposits in the same region was made (Mathur et al., 2002). The world-class IOCG deposits showed Os isotope signature of mantle-crust mixture, whereas the apatite-magnetite revealed radiogenic sources of Os, consistent with crustal sources (Mathur et al., 2002).

The meta-ultramafic lenses along shear zones that cut the area are interpreted to be allochthonous. The provenance area for these rocks could have been the volcanic rocks that filled the Carajás Basin, due to their proximity to the Southern Copper Belt. However, the existence of ultramafic rocks in the Carajás Domain is not common, and restricted to some parts of the Rio Novo Group (Fig. 1), close to the Serra Pelada gold deposit area (Fig. 1). Meta-ultramafic volcanic rocks are also described in the greenstone belts from the Rio Maria Domain, such as the Gradaús, Serra do Inajá, Babaçu, Lagoa Seca, and Sapucaia sequences (Ianhez et al., 1980; Cordeiro and Saueressig, 1980; Macambira et al., 1986; DOCEGEO, 1988; Araújo and Maia, 1991). The ages of these greenstone belts vary from 3.0 Ga (Gradaús Group; Tassinari et al., 2005) to 2.9 Ga (Lagoa Seca Group; Macambira and Lancelot, 1996).

Other ultramafic occurrences, plutonic in origin, which could be related to the tectonically imbricate mylonites correspond to the Luanga complex (Fig. 1), which hosts Cr-EGP mineralization, and is located approximately 50 km northeast from the studied area. The Luanga intrusive complex, which is composed of two NE-SW mafic-ultramafic bodies (Luanga and Lago Grande; Vasquez et al., 2008a) shows evidence for deformation and (low-grade) metamorphism (Ferreira Filho et al., 2007). On the other hand, in the Cateté Suite (E-W and N-S-trending Serra da Onça, Serra do Puma, Serra do Jacaré, Serra do Jacarezinho and Vermelho bodies; Vasquez et

al., 2008a), tectonic transport is ruled out due to evidence for neither deformation nor metamorphism (Macambira and Vale, 1997).

8.3 Geochronological data from the Bacaba and Bacuri deposits

The new geochronological data from this study (Table 4) point to a complex evolution of the Bacuri and Bacaba deposits, with evidence for multiple discrete hydrothermal events responsible for hydrothermal alteration and/or ore genesis.

For the Bacuri deposit, the $2,758 \pm 11$ Ma age was obtained for molybdenite associated with minor chalcopyrite disseminations spatially unrelated to the main ore zone. Additionally, monazite from an intensively hydrothermally altered rock (chlorite and biotite alteration) yielded the $2,703.0 \pm 5.8$ Ma age. In the Bacuri deposit, the chlorite and biotite formation was synchronously to the main stage of copper ore deposition. Both the 2.76 Ga and 2.70 Ga ages are interpreted as evidence of distinct episodes of hydrothermal fluid circulation and alteration in the Bacuri deposit. Only the younger age, however, is interpreted as related to the main stage of copper mineralization at the Bacuri deposit. Even if the analytical errors are considered, these ages could not overlap in time and show at least a 40 Ma difference. Since the duration and episodicity of ore-forming activity in different environments encompasses no more than a few million years (Cathles et al., 1997; Stein and Cathles 1997; Marsh et al., 1997; Ballard et al., 2001; Quadt et al., 2005), it is doubtful that the two distinct ages encompass a single and long-term hydrothermal event.

Monazite grains from a mineralized sample from the Bacaba deposit (BACD 25/229.25) hosted by the Bacaba Tonalite provided two distinct ages. The older corresponded to $2,681 \pm 11$ Ma, whereas the younger yielded a $2,054.1 \pm 8.8$ Ma age, which are 630 Ma separated in time. Since these ages were acquired in both cores and rims of different monazite grains, they likely represent distinct monazite populations. Igneous zircon grains from this ore sample were also dated in $2,990.9 \pm 5.8$ Ma (U-Pb LA-MC-ICPMS) by Moreto et al. (2011). Both the Neoarchean (2.68 Ga) and the Paleoproterozoic (2.05 Ga) ages are interpreted as two distinct and overprinted hydrothermal systems recorded in the Bacaba deposit. Nonetheless, only the 2.68 Ga event is interpreted as related to the main IOCG system responsible for ore formation at the Bacaba deposit. Hydrothermal fluids associated with the younger 2.05 Ga episode could have been responsible of new monazite growing, in spite of the fact that this event is not necessarily related

to new ore formation. In fact, the fluids from this Paleoproterozoic hydrothermal pulse may have remobilized ore and ore related minerals.

Additionally, monazite grains from sodically altered and silicified Serra Dourada Granite found in drill holes from the Bacaba deposit yielded the $2,716.4 \pm 8.4$ Ma age. Igneous zircon grains from this sample (BACD 15/237.4) were previously analyzed by U-Pb LA-MC-ICPMS and yielded a projected upper intercept age of $2,860 \pm 22$ Ma (Moreto et al., 2011). The zircon grains from this sample were intensively metamictized, evidenced by the great number of fractures and oxide inclusion, and had prominent lead loss. Differently, the monazite grains yielded a concordia age with no lead loss. This newly obtained 2.71 Ga age is interpreted to date the sodic alteration in the Bacaba deposit, which slightly precedes the main Neoarchean (2.68 Ga) event of IOCG ore formation.

Based on the new geochronological data (Table 4) is suggested that multiple temporally discrete hydrothermal events (Neoarchean and Paleoproterozoic) may have been responsible for the hydrothermal alteration and/or ore genesis at the Bacuri and Bacaba deposits. Dating of hydrothermally phases indicates that the older hydrothermal event took place at 2.76 Ga, and was responsible for local metassomatism and molybdenite formation at the Bacuri deposit. At 2.71-2.70 Ga, the IOCG-forming pulse was responsible for alteration and mineralization at the Bacuri deposit, and also related to the development of extensive zones of sodic alteration in the Bacaba deposit and surrounding areas. The 2.68 Ga monazite ages registered in the Bacaba ore might correspond, within analytical error, to the 2.70 Ga IOCG event, or differently (and unlikely) represent a distinct hydrothermal event. Finally, at ca. 2.05 Ga another hydrothermal pulse was responsible for new monazite crystallization and possibly ore remobilization at the Bacaba deposit.

Although a Pb closure temperature of about 700-750°C is suggested for monazite (Copeland et al., 1988; Smith and Giletti, 1997), several studies demonstrated that the U-Pb system can be highly disturbed in monazite by later relative lower-temperature hydrothermal events (Poitrasson et al., 1996; Townsend et al., 2000; Rasmussen et al., 2005, Li et al., 2011). These authors reported dissolution-reprecipitation process in presence of a fluid phase with temperatures not exceeding the 350-400°C. Additionally, Rasmussen et al. (2001) also reported monazite growth during low-temperature metamorphism of shales. These examples suggest that

disturbance and new growth of monazite can occur in temperatures below the Pb closure temperature, which is commonly considered the normal lower limit temperature for resetting.

8.4 Timing and evolution of the IOCG hydrothermal systems of the Southern Copper Belt

The geochronological results from this study (Table 4) combined with also reliable data from the Sossego (Re-Os in molybdenite and U-Pb in hydrothermal monazite; Moreto et al., submitted) and Alvo 118 deposits (U-Pb in hydrothermal xenotime; Tallarico, 2003), and Pb-Pb results (chalcopyrite) from the Cristalino and Visconde deposits (Soares et al., 2001; Silva et al., 2012) indicate that the IOCG deposits from the Southern Copper Belt were formed during several discrete hydrothermal and/or ore-related IOCG episodes during the Neoarchean and the Paleoproterozoic.

These multiple hydrothermal events, which are also illustrated in Figure 12, took place at:

- 2.76 Ga, recorded in molybdenite crystals from the Bacuri deposit that predate the main stage of ore formation in this deposit;
- 2.71-2.70 Ga, registered in hydrothermal monazite crystals from the Bacuri and Bacaba deposits, and the Sequeirinho orebody (Sossego deposit), and also recorded in molybdenite concentrates from the Pista orebody (Sossego deposit) (Moreto et al., submitted);
- 2.68 Ga, obtained in hydrothermal monazite grains and molybdenite aliquots from the Bacaba deposit and Pista orebody (Sossego deposit) (Moreto et al., submitted), respectively;
- 2.05 Ga, recorded in hydrothermal monazite crystals from the Bacaba deposit;
- 1.90 Ga, evidenced by hydrothermal monazite grains crystallized at the Sossego orebody (Sossego deposit) (Moreto et al., submitted);
- 1.88-1.87 Ga, suggested by hydrothermal monazite ages from the Sossego and Curral orebodies (Moreto et al., submitted), and hydrothermal xenotime from the Alvo 118 deposit.

The $2,747 \pm 140$ Ma (MSWD = 12) and $2,700 \pm 29$ Ma (MSWD = 656) Pb-Pb (chalcopyrite) ages from the Visconde and Cristalino deposit (Soares et al., 2001; Silva et al., 2012) are very imprecise due to their large errors, and for this reason were not associated with any interval of a hydrothermal event as shown above. However, the data possibly indicate that the

event (s) responsible for ore genesis likely took place in the Neoarchean instead of the Paleoproterozoic.

Although the recurrence of several hydrothermal systems in time is evidenced at the Southern Copper Belt, it is interpreted that the 2.71-2.68 Ga and 1.90-1.88 Ga intervals are, indeed, responsible for IOCG ore formation in the area. The other hydrothermal events are not necessarily associated with the precipitation of ore and ore-related minerals. Instead, they possibly led to the development of new hydrothermal mineral assemblage, and may have caused remobilization and overprint of new systems in previous altered zones. These non-mineralized events, however, allowed the growing of new monazite and/or molybdenite crystals. Based on these evidence, it is suggested a strong recurrence of hydrothermal systems, even in a single deposit scale, in the Southern Copper Belt.

Several temporally discrete hydrothermal and IOCG events over a larger range in time (500 Ma) have also been proposed for deposits from the Selwyn-Mount Dore corridor (e.g., Starra, Mount Elliot, SWAN, Mount Dore and Lady Ella), Mount Isa Inlier, Australia (Duncan et al., 2011). The geochronological data (Re-Os in molybdenite and U-Pb in titanite) from Duncan et al. (2011) suggest that these deposits were formed at different moments, and could be related to igneous activity (Mount Elliot and SWAN deposit), metamorphic processes (Starra deposit), but also related to evolved magmatic fluids (Lady Ella and Mount Dore deposits). In the Mount Elliot deposit, molybdenite provided different Re-Os ages, suggesting that the deposit was formed at different stages (Duncan et al., 2011). This is similar to the scenario at the Southern Copper Belt, where distinct hydrothermal monazite and molybdenite ages were obtained.

Furthermore, geochronological studies (U-Pb dating of allanite and titanite) conducted in several IOCG and Fe oxide-apatite deposits from the Kiruna district, Sweden showed that the main stage of Fe mineralization took place at 1890-1870 Ma (Smith et al., 2009), which is similar to the Orosianian IOCG-mineralizing interval at the Southern Copper Belt. Additionally, the isotopic data from Smith et al., (2009) reveal the existence of a second hydrothermal alteration event, at 1800-1750 Ma, which caused significant reworking of the initial phase of mineralization alongside further fluid flow episodes along major structural features.

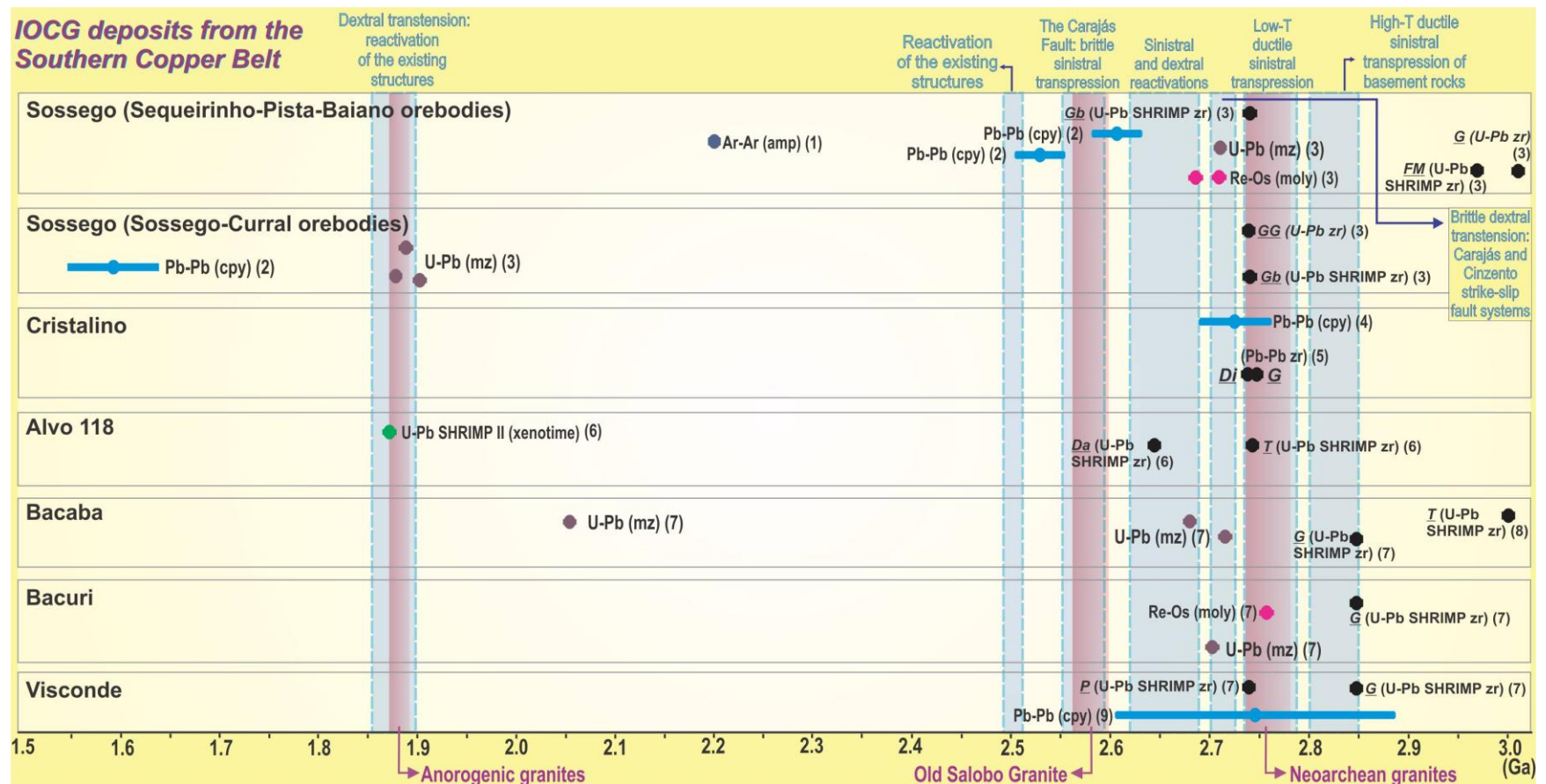


Fig. 12. A summary of geochronological data for IOCG deposits from the Southern Copper Belt and their host rocks, and the main tectonic and magmatic events recorded in the Carajás province. The data obtained in this study is included. Data source: (1) Marschik et al. (2003); (2) Neves (2006); (3) Moreto et al. (submitted); (4) Soares et al. (2001); (5) Huhn et al. (1999b); (6) Tallarico (2003); (7) Moreto et al. (this study); (8) Moreto et al. (2011); (9) Silva et al. (2012). amp amphibole; cpy chalcopyrite; Da dacite; Di diorite; FM felsic metavolcanic rock; G granite; GG granophyric granite; Gb gabbro; mz monazite; moly molybdenite; P quartz-feldspar porphyry; T tonalite; zr zircon.

In IOCG deposits worldwide, the genetic models point to diverse fluid and metals sources, with magmatic, non-magmatic and hybrid components (Barton and Johnson, 1996; 2000, 2004; Pollard, 2001, 2006; Hunt et al., 2007; Groves et al., 2010). The 2.76 Ga molybdenite age for the Bacuri deposit, which is interpreted as the oldest evidence for hydrothermal activity in the Southern Copper Belt, is similar to the age of deposition of the thick (~4-6 km; Gibbs et al., 1986) metavolcanic-sedimentary sequence (Itacaiúnas Supergroup) that filled the Carajás Basin. The latter has its southern edge located only hundreds of meters north of the Bacuri deposit. During the Itacaiúnas Supergroup deposition, hydrothermal fluids from the basin may have circulated through crustal weaknesses, such as the WNW-ESE trending shear fabrics present at the basement rocks (e.g., Serra Dourada Granite), and caused the hydrothermal alteration with molybdenite formation in the area of the Bacuri deposit.

The continental rift model proposed for the evolution of the Carajás Domain (Gibbs et al., 1986; DOCEGEO, 1988; Olszewski et al., 1989; Tallarico, 2003), suggest that a 2.76 Ga thermal source, possibly related to the ca. 2.7 Ga mantle-plume event registered worldwide (Condie, 1998; Isley and Abbott, 1999, 2002) caused a continental rift, the scenario in which the Carajás Basin would have installed. Moreover, Tallarico (2003) argue that the 2.76 Ga thermal event would have caused the underplating of mafic magma in lower crust, that would have ascend and generate differentiate magmatic chambers (2.76 Ga Luanga mafic-ultramafic igneous layered complex), and the metavolcanic-sedimentary Itacaiúnas Supergroup when the magma reached the surface. Trace element, Sr and Nd isotopic data from bimodal volcanic rocks of the Grão Pará Group (Itacaiúnas Supergroup) are also consistent with contamination of mantle-derived melts by older continental crust (Gibbs et al., 1986; Olszewski et al., 1989).

Following the genetic models for IOCG deposits from Groves and Bierlin (2007) and Groves et al. (2010), Precambrian IOCG deposits would be associated with magmatism and related hydrothermal activity driven by mantle underplating and/or plumes. Plume-induced partial melting of subcontinental lithospheric mantle previously metasomatized during earlier subduction probably produced basic to ultrabasic magmas that melted overlying continental crust and mixed with resultant felsic melts, controlling composition of magmatic fluids responsible by formation of IOCG deposits (Groves et al., 2010).

Based on: i) the existence of a 2.76 Ga hydrothermal event in the Bacuri deposit; ii) the continental rift model for the Carajás Domain related to a ca. 2.7 Ga mantle-plume event (Gibbs

et al., 1986; DOCEGEO, 1988; Olszewski et al., 1989; Tallarico, 2003); and iii) the genetic model for Precambrian IOCG deposit from Groves et al. (2010), hydrothermal fluids with mantle-derived components circulating and leaching metals from the Carajás Basin in a intracratonic setting cannot be ruled out.

On the other hand, the ca. 2.71-2.68 Ga IOCG mineralizing interval, registered by hydrothermal monazite from the Bacuri and Bacaba deposits, and the Sequeirinho orebody, and by molybdenite from the Pista orebody does not overlap in time with any significant magmatism recorded at the Carajás Province. This fact was also pointed out by Moreto et al. (submitted) when discussing the timing for IOCG formation at the Sossego deposit. Magmatic manifestations in the Carajás Domain during the 2.71-2.68 Ga interval, although obtained by Pb-Pb systematic, correspond to the Geladinho Granitic Stock (Table 1), located approximately 50 km northeast of the studied area, to the southwest of the Cigano Granite (Fig. 1). However, the $2,688 \pm 11$ Ma obtained age is interpreted as the minimum age for crystallization, and the granite is possibly older (Barbosa et al., 2001).

As suggested for the Sequeirinho-Pista-Baiano orebodies (Moreto et al., submitted), it is likely that alternative sources of heat, different to those from magmatism, caused the circulation of hydrothermal fluids in regional scale through major crustal discontinues, leading to metal leaching from the country rocks (basement and Itacaiúnas Supergroup) and subsequent ore deposition at ca. 2.7 Ga. The heat engine that may have triggered the circulation of hydrothermal fluids could be related to reactivation processes of previously formed ductile regional shear zones, especially those in the southern contact of the Carajás Basin with its basement, where the IOCG deposits from the Southern Copper Belt are located. The WNW-ESE trending high-temperature shear fabrics present at the basement rocks, which were likely formed during ca. 2.85 Ga ductile sinistral transpression, would have experienced several phases of ductile and brittle transpressional and transtensional reactivations in the Archean and the Paleoproterozoic (Pinheiro and Holdsworth, 1997) (Fig. 12). According to Domingos (2009), the tectonic inversion of the Carajás Basin, which was initiated at about 2.7 Ga, involved a regional phase of sinistral transpression controlled by a NNE-directed oblique shortening and caused the reactivation of the Carajás and Cinzento strike-slip fault systems. During this major tectonic event, WNW-ESE trending shear fabrics had their nucleation controlled by the pre-existing weakness planes parallel to the early ductile foliation (Domingos, 2009). These structural weaknesses in basement rocks

may have facilitated the percolation of sulfide-bearing hydrothermal fluids that would be responsible for the deposition of IOCG mineralization. Figure 13 illustrate the magmatic and metallogenetic evolution of the Southern Copper Belt.

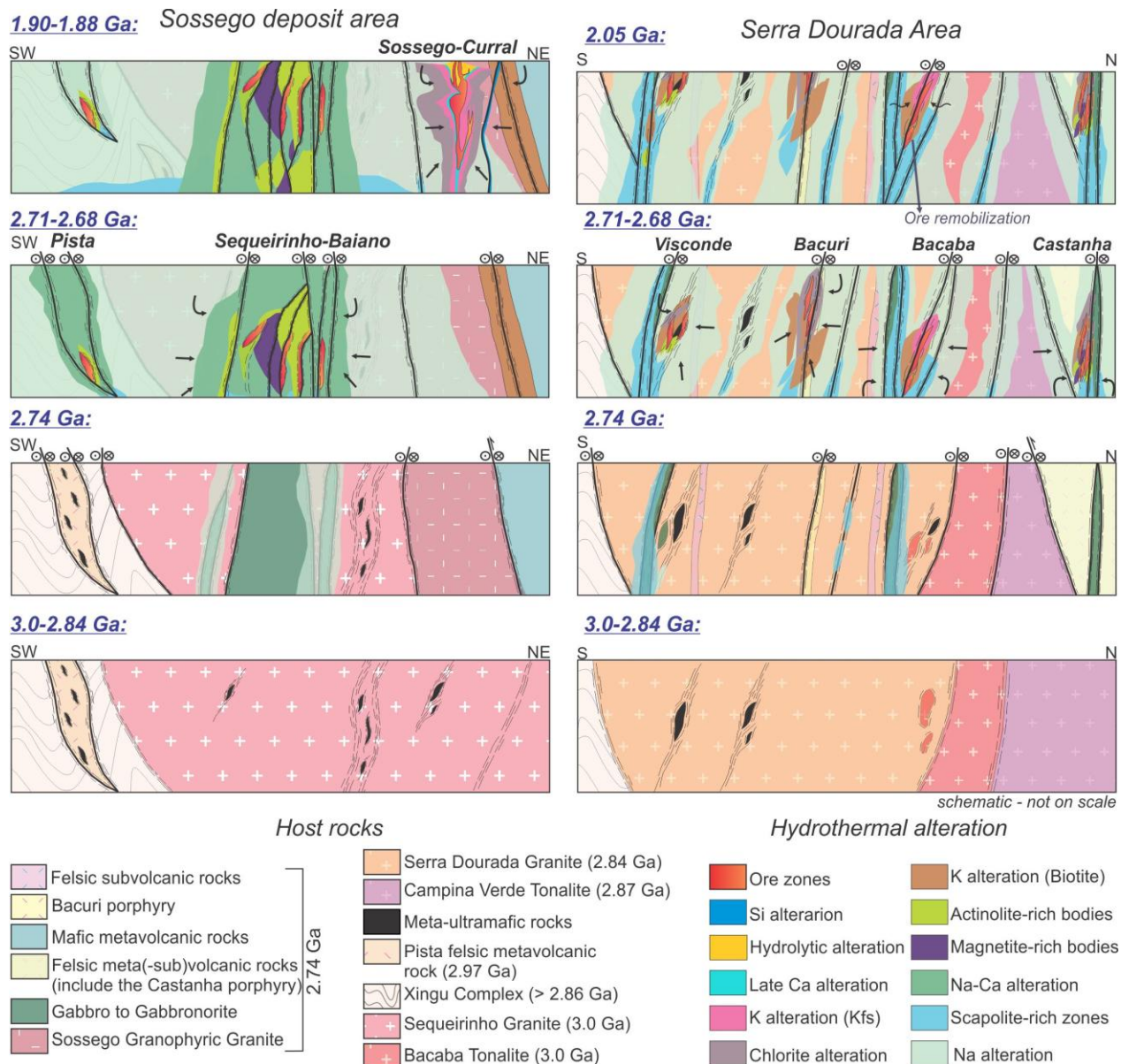


Fig. 13. Schematic diagram showing the magmatic and metallogenetic evolution of the Southern Copper Belt in time, from 3.0 to 1.88 Ga.

The major IOCG-forming interval at 2.71-2.68 Ga may be characterized by deeper-emplaced IOCG systems and associated with extensive zones of chlorine-bearing marialitic scapolite alteration in the rocks from the Southern Copper Belt, which are remarkably present at

the Bacaba, Castanha and Bacuri deposits (Augusto et al., 2008; Moreto et al., 2011). Scapolite-rich alteration zones are broadly identified in IOCG districts worldwide, such as the Fennoscandian Shield, Sweden (Smith et al., 2013), Wernecke Mountains, Yukon, Canada (Hunt et al., 2005), and the Eastern Mount Isa Block, Australia (Oliver et al., 2004). The marialitic scapolite represents a particularly sensitive indicator of fluid hypersalinity (Orville, 1975; Mora and Valley, 1989; Satish-Kumar et al., 2006), and its abundance could reveal the predominance of hot (>500°C; Vanko and Bishop, 1982) hypersaline fluids during early system evolution. Additionally, marialite formation requires buffered activity gradients in chlorine in the hydrothermal fluids (Mora and Valley, 1989).

Since the hydrothermal events occurred episodically in the Southern Copper Belt, hot hydrothermal fluids (e.g., ~ 400°C; early sodic alteration zones; Sossego orebody; Monteiro et al., 2008a) circulating through, and leaching the areas with widespread marialite alteration possibly released chlorine and sodium to the hydrothermal fluid, increasing its total salinity. Thus, scapolite dissolution due to interaction with externally-derived fluids in shallow-emplaced systems could have contributed to improve the capacity of metal (Cu) transport and might have played an important role in the recurrence and overprint of hydrothermal and ore systems.

The hydrothermal event responsible for the 2.05 Ga age for hydrothermal monazite at the Bacaba deposit should also be evaluated. This Rhyacian age notably differs (ca. 150 Ma) from the well-constraint 1.90-1.88 Ga Orosinian interval for IOCG formation, registered at the Sossego-Currall orebodies, and the Alvo 118 deposit (Torresi et al., 2012; Moreto et al., submitted). In this sense, is it implausible that these deposits would have formed simultaneously. According to Moreto et al., (submitted), it is not possible to affirm whether the genesis of the Sossego-Currall orebodies is directly related to the 1.88 Ga A-type granite magmatism registered in the province (e.g., Serra dos Carajás Intrusive Suite; Machado et al., 1991). In fact, these authors suggest that this felsic magmatism could have acted as source of heat that caused the circulation of hydrothermal fluids in regional scale, including the areas previously metasomatized by the Neoarchean IOCG hydrothermal events. Thus, the 1.90-1.88 Ga interval for IOCG mineralization represents a recurrence of superimposed hydrothermal systems along the Southern Copper Belt (Fig. 13). Stable isotopic signatures, fluid inclusion data, and distribution and style of hydrothermal alteration zones (Monteiro et al., 2008a,b; Pestilho, 2011; Torresi et al., 2012) suggest that the Paleoproterozoic IOCG systems (Sossego-Currall orebodies and Alvo 118

deposit) were formed at higher structural levels than the Neoarchean IOCG deposits (e.g., Sequeirinho-Pista-Baiano orebodies, Castanha, Bacaba and Bacuri deposits). A probable explanation is that the Paleoproterozoic deposits were installed after the exhumation of the Neoarchean systems (Fig. 13). The overprint of the 1.90-1.88 Ga IOCG forming interval, associated with the shallow-emplaced deposits, was not widely record in the Neoarchean IOCG deposits, pointing to channeled and structurally-controlled fluid migration.

The 2.05 Ga hydrothermal event also does not overlap in time with any magmatism recorded until the present at the Carajás Province. Like the model proposed for the genesis of the ca. 2.70 Ga IOCG deposits, this Rhyacian event could have also been triggered by heat sources alternative to those related to magmatism, such as heat generated by reactivation of regional shear zones (Fig. 12). This hypothesis, supported by the reactivation model from Pinheiro and Holdsworth (1997), suggest a weak tectonic inversion of the Carajás Basin between 2.0 to 1.8 Ga, under dextral transtension, which would have allowed the emplacement of the ca. 1.88 Ga A-type granites. This tectonic inversion would have also caused the reactivation of crustal discontinuities nucleated during the Archean, such as the Carajás Fault (Fig. 1) and the shear zone close to the Bacaba, Bacuri and Sossego IOCG deposits.

Although unlikely, the influence of the Trans-Amazonian orogenic cycle in the Southern Copper Belt should also be appraised. The Trans-Amazonian cycle was an important Paleoproterozoic rock-forming event in South America, generating voluminous juvenile and reworked fractions of continental crust (Cordani and Sato, 1999; Macambira et al., 2009). The Bacajá Domain, which comprises the southern part of the Paleoproterozoic (2.2–1.95 Ga) Maroni-Itacaiúnas Province (Cordani et al., 1979; Tassinari and Macambira, 1999, 2004) or Trans-Amazonian Province (Santos et al., 2000; Santos, 2003), display its present-day configuration due to collision (s) against the southern Archean Carajás Province at the end of the Trans-Amazonian orogenic cycle. Recent studies (Vasquez et al., 2008b; Macambira et al., 2009) propose a multi-stage evolution for the Bacajá domain, starting during the Neoarchean and ending at the Rhyacian, at 2.08-2.07 Ga. These Rhyacian ages are similar to the 2.05 Ga hydrothermal event registered at the Bacaba deposit. Although the Southern Copper Belt and the Bacajá Domain are distant approximately 70 km, the amalgamation of these two blocks at the end of the Trans-Amazonian orogenic cycle cannot be completely ruled out as being related to the formation of 2.05 Ga hydrothermal system, mainly because in these continental events large

quantities of hydrothermal fluids are released and circulates in the crust through crustal discontinuities.

9. Conclusions

The characterization of the lithotypes and hydrothermal alteration in the Southern Copper Belt, combined with geochronological data (Re-Os in molybdenite, and U-Pb in zircon and hydrothermal monazite), allow a more detailed comprehension on the metallogenetic and crustal evolution of the Southern Copper Belt, as listed below:

- The magmatism in the Southern Copper Belt varies in composition and age and mainly comprises: (1) ca. 3.0 Ga Bacaba Tonalite and Sequeirinho Granite, in addition to the protolith of the Xingu migmatite; (2) ca. 2.97-2.96 Ga Pista felsic metavolcanic rock and Canaã dos Carajás Granite; (3) the ca. 2.87 Ga Campina Verde Tonalite and the Rio Verde Trondhjemite; (4) 2.84 Ga Serra Dourada Granite; (5) 2.74 Ga quartz feldspar porphyries, including the Castanha porphyry, and the Sossego granophyric granite; gabbronorite, Planalto Granite, Cristalino Diorite and the Pium Diopside Norite; and the (6) 1.88 Ga Rio Branco Granite. Moreover, other units that were not dated until the present are also widely recognized at the Southern Copper Belt, such as volcanic and meta-ultramafic rocks.
- The meta-ultramafic rocks occur as mylonites tectonically imbricated along shear zones that cut entire area and as small boudins within the ca. 2.97 Ga Pista metavolcanic rock. These meta-ultramafic lenses are interpreted to be allochthonous, and are spatially related to copper (malachite) prospects and some IOCG deposits, such as the Bacaba and Visconde deposits and the Pista orebody, which are located along shear zones. The role of these ultramafic occurrences in the genesis of the IOCG deposits should be better evaluated in future studies, mainly because high copper content in world-class IOCG deposits has been attribute to ultramafic sources in several mineral provinces worldwide.
- Combining the reliable geochronological results from this study with other available data for IOCG deposits, it is strongly suggested for the Southern Copper Belt episodicity and overprint of hydrothermal and IOCG-forming systems during the Neoarchean and Paleoproterozoic.

- These hydrothermal events, responsible for hydrothermal alteration and/or IOCG ore formation correspond to: 1) 2.76 Ga (Bacuri deposit); 2) 2.71-2.68 Ga (Bacuri, Bacaba and Cristalino deposits, Sequeirinho-Pista orebodies, and probably the Visconde and Cristalino deposits); 3) 2.05 Ga (Bacaba deposit); 4) 1.90-1.88 Ga (Sossego and Curral orebodies, and Alvo 118 deposits). Genesis of IOCG mineralization in the Southern Copper Belt is attributed to the 2.71-2.68 Ga and 1.90-1.88 Ga intervals. The other non-mineralizing hydrothermal events possibly led to the development of new hydrothermal mineral assemblage, but not necessarily the precipitation of ore minerals.
- The older 2.76 Ga hydrothermal event, which is the oldest evidence for hydrothermal activity in the Southern Copper Belt, is contemporary with the deposition of the metavolcanic (-sedimentary) sequence of the Itacaiúnas Supergroup. Hydrothermal fluids from the basin may have circulated through crustal weaknesses, causing hydrothermal alteration in the Bacuri deposit area, which is located only hundreds of meters south of the Carajás Basin.
- The major 2.71-2.68 Ga IOCG mineralizing interval has been responsible for large-scale development of IOCG systems along the Southern Copper Belt. The new geochronological data indicate that deep-emplaced IOCG systems, characterized by extensive scapolite-rich halos, massive magnetite-(apatite) and calcic-sodic alteration (albite-actinolite) overprinted by potassic alteration (biotite-scapolite-tourmaline), have mainly been developed during the Neoarchean. These deposits encompass the Bacaba, Bacuri, and possibly the Castanha, Cristalino and Visconde deposits, which share a common metallogenetic evolution with the Sequeirinho-Baiano-Pista orebodies (Sossego deposit).
- The 2.71-2.68 Ga IOCG interval is apparently not directly related to a magmatic event in the Southern Copper Belt. For these events are proposed that regional circulation of hot (> 500°C) and saline hydrothermal fluids, causing metal leaching from the country rocks and subsequent ore deposition, is related to the ca. 2.7 Ga tectonic inversion of the Carajás Basin, in response to a regional phase of sinistral transpression controlled by a NNE-directed oblique shortening. This tectonic event caused the reactivation of the Carajás and Cinzento strike-slip fault systems, and likely the ductile shear zone where the IOCG deposits are located.

- The late Rhyacian (2.05 Ga) hydrothermal event also does not overlap in time with any magmatism recorded in the Carajás Province until the present. This event could have also been triggered by heat sources related to another reactivation of the regional shear zones nucleated during the Archean, in response to a weak tectonic inversion of the Carajás Basin between 2.0 to 1.8 Ga, under dextral transtension.
- Finally, the Orosinian event (1.90-1.88 Ga) was responsible for the development of shallow-emplaced IOCG deposits (Alvo 118 deposit and the Sossego-Currall orebodies) after exhumation of the Neoarchean systems. It is likely that the widespread 1.88 Ga anorogenic magmatism in the Carajás Province provided heat sufficiently high to cause the circulation of hydrothermal fluids in regional scale, along the crustal discontinuities. These hot ($> 400^{\circ}\text{C}$) and saline fluids may have caused reworking of the Neoarchean IOCG deposits, leading to elements remobilization and additional hydrothermal alteration and ore deposition.
- The recurrence of hydrothermal systems in the same area, even in the same deposit scale (e.g., Sossego deposit), imply in leaching and reworking of previously hydrothermally altered areas, including the widespread scapolite (marialite)-rich zones. This fluid/rock interaction may have caused modification of the fluid composition, leading to an increase in the total salinity, since the leaching of marialitic scapolite releases chlorine and sodium to the hydrothermal system. This high-salinity characteristic would have increased the fluid efficiency in carrying metals, especially Cu, as chlorine-complexes. The hydrothermal fluids were possibly channelled along major crustal structures, resulting occasionally in overprinting and mineralization focused in structurally controlled fluid discharge zones.

Acknowledgments

We are very grateful to Vale company for the continuous support provided to the researchers and students of the Institute of Geosciences, UNICAMP. We are particularly indebted to Márcio Godoy, Benevides Aires and Cleive Ribeiro for their invaluable support. We would also like to thank Erica Tonetto for her assistance with the SEM imaging. This research was funded by CNPq (grants 555065/2006-5, 472549/2009-0), FAPESP (grants 03/09584-3, 03/07453-9, 03-11163-603/01159-1), FAPESPA/VALE, and INCT/GEOCIAM (CNPq/MCT

/FAPESPA). Carolina P. N. Moreto also thanks FAPESP for the PhD scholarship (grant 2009/18371-0).

REFERENCES

- Almeida, J.A.C., Dall'Agnol, R., Dias, S.B., and Althoff, F.J., 2010, Origin of the Archean leucogranodiorite–granite suites: Evidence from the Rio Maria terrane and implications for granite magmatism in the Archean. *Lithos*, 187: 201–221.
- Almeida, J.A.C., Dall'Agnol, R., Oliveira, M.A., Macambira, M.J.B., Pimentel, M.M., Rämö, O.T., Guimarães, F.V., and Leite, A.A.S., 2011, Zircon geochronology and geochemistry of the TTG suites of the Rio Maria granite-greenstone terrane: Implications for the growth of the Archean crust of Carajás Province, Brazil. *Precamb. Res.* 120: 235–257.
- Althoff, F.J., Barbey, P., and Boullier, A.M., 2000, 2.8-3.0 Ga plutonism and deformation in the SE Amazonian craton: the Archean granitoids of Marajoara (Carajás Mineral Province, Brazil). *Precambrian Research*, v. 104, p. 187–206.
- Araújo O.J.B., Maia R.G.N., Jorge-João, X.S. Costa, and J.B.S., 1988, A megaestruturação da folha Serra dos Carajás. In: Congresso Latino Americano de Geologia., 7, pp. 324–333.
- Araújo, O.J.B. and Maia, R.G.N., 1991 - Serra dos Carajás, folha SB.22-ZA, Estado do Pará. Programa Levantamentos Geológicos Básicos do Brasil. Companhia de Pesquisa de Recursos Minerais. 136 p.
- Augusto, R.A., Monteiro, L.V.S., Xavier, R., and Souza Filho, C.R., 2008, Zonas de alteração hidrotermal e paragênese do minério de cobre do Alvo Bacaba, Província Mineral de Carajás (PA). *Rev. Brasil. Geoci.* 38(2): 263–277.
- Avelar, V.G., Lafon, J.M., Correia JR, F.C., and Macambira, E.M.B., 1999, O Magmatismo arqueano da região de Tucumã-Província Mineral de Carajás: novos resultados geocronológicos. *Revista Brasileira de Geociências*. 29(4): 453–460
- Ballard, J.R., Palin, J.M., Williams, I.S., and Campbell, I.H., 2001, Two age of porphyry intrusion resolved for the super-giant Chuquicamata copper deposit of northern Chile by ELA-ICP-MS and SHRIMP. *Geology* 29 (5): 383–386
- Barbosa, J.P.O., 2004, Geologia estrutural, geoquímica, petrografia e geocronologia de granitóides da região do Igapó Gelado, norte da Província Mineral de Carajás: Unpublished Master Thesis, Universidade Federal do Pará, Belém, 112 p.
- Barbosa, J.P.O., Barros, C.E.M., Macambira, M.J.B., and Vale, A.G., 2001, Geologia e Geocronologia do Stock Granítico Geladinho, região de Parauapebas, Província Mineral de Carajás. In: Simpósio de Geologia da Amazônia, 7, Belém. SBG-NO. CD-ROM.
- Barros, C.E.M., Dall'Agnol, R., Lafon, J.M., Teixeira, N.P. and Ribeiro, J.W., 1992, Geologia e geocronologia Rb-Sr do Gnaisse Estrela, Curionópolis, PA. *Bol. Mus. Par. Em. Goeldi, Ciênc. da Terra*, 4:83-102.
- Barros, C.E.M., Dall'agnol, R., Barbey, P., and Boullier, A.M., 1997, Geochemistry of the Estrela Granite Complex, Carajás region, Brazil: an example of an Archean A-type granitoid. *Journal of South American Earth Sciences*, 10(3-4): 321–330.
- Barros, C.E.M., Macambira, M.J.B., Barbey P., and Scheller, T., 2004, Dados isotópicos Pb–Pb em zircão (evaporação) e Sm–Nd do Complexo Granítico Estrela, Província Mineral de Carajás, Brasil: implicações petrológicas e tectônicas. *Rev. Brasil. Geoci.* 34, 531–538.
- Barros, C.E.M., Sardinha, A.S., Barbosa, J.P.O., and Macambira, M.J.B., 2009, Structure, Petrology, Geochemistry and zircon U/Pb and Pb/Pb geochronology of the synkinematic Archean (2.7 Ga) A-type granites from the Carajás Metallogenic Province, northern Brazil, *The Canadian Mineralogist*. 47: 1423–1440

- Barton M.D., and Johnson D.A., 1996, Evaporitic source model for igneous-related Fe oxide-(REE-Cu-Au-U) mineralization. *Geology* 24, 259–262.
- Barton, M. D., and Johnson D. A., 2000, Alternative brine sources for Fe oxide (-Cu-Au) systems: implication for hydrothermal alteration and metals. In: Porter, T. M. (ed) *Hydrothermal iron oxide copper-gold and related deposits: A global perspective*. Adelaide, Australian Mineral Foundation, vol. 1. p43-60
- Barton, M.D. and Johnson, D.A., 2004, Footprints of Fe-oxide(-Cu-Au) systems. SEG 2004: Predictive Mineral Discovery Under Cover. Centre for Global Metallogeny, Spec. Pub. 33, The University of Western Australia, 112-116.
- Carvalho, E.R., 2009, Caracterização geológica e gênese das mineralizações de óxido de Fe-Cu-Au e metais associados na Província Mineral de Carajás: estudo de caso do depósito de Sossego: Unpublished PhD Dissertation, Universidade Estadual de Campinas, 141 p.
- Cathles, L.M., Erendi, A.H.J., and Barrie, T., 1997, How long can a hydrothermal system be sustained by a single intrusive event? *Economic Geology*, v. 92, p. 766–771.
- Condie, K. C., 1998, Episodic continental growth and supercontinents: A mantle avalanche connection? *Earth Planetary Science Letters*, 163: 97–108.
- Cordani, U., 1981, Comentários sobre as determinações geocronológicas da região da Serra dos Carajás. Report, Universidade de São Paulo-Docegeo.
- Cordani, U.G., and Sato, K., 1999, Crustal evolution of the South American Platform, based on Nd isotopic systematics on granitoid rocks. *Episodes* 22, 167–173.
- Cordani, U.G., Tassinari, C.C.G., Teixeira, W., Basei, M.A.S., and Kawashira, K., 1979, Evolução tectônica da Amazônia com base nos dados geocronológicos. 11º Congresso Chileno de Geología, Arica, Chile pp. 137-148.
- Cordeiro, A.A.C., and Saueressig, R., 1980, Serra das Andorinhas: geologia e principais ocorrências de ouro. In: Congresso Brasileiro de Geologia, 31., 1980, Camboriú. Resumos das comunicações... Camboriú: SBG, 1980. p. 344.
- Copeland, P., Parrish, R.R., Harrison, T.M., 1988, Identification of inherited Pb in monazite and its implications for U-Pb systematics. *Nature* 333, 760–763.
- Craveiro, G.S., Villas, R.N., and Silva, A.R.C., 2012a, Depósito Cu-Au Visconde, Carajás (PA): geologia e alteração hidrotermal das rochas encaixantes. *Revista Brasileira de Geociências* 42(3):453-470.
- Craveiro, G.S., Villas, R.N., and Silva, A.R.C., 2012b, Depósito Visconde: fluidos hidrotermais e implicações metalogenéticas. In 46º Congresso Brasileiro de Geologia, Santos.(CD-ROM)
- Dall'Agnol, R., and Oliveira, D.C., 2007, Oxidized, magnetite-series, rapakivi-type granites of Carajás, Brazil: implications for classification and petrogenesis of A-type granites. *Lithos* 93, 215–233.
- Dall'Agnol, R., Costi, H.T., Leite, A.A., Magalhães, M.S., and Teixeira, N.P., 1999a, Rapakivi granites from Brazil and adjacent areas. *Precambrian Research* 95, 9–39.
- Dall'Agnol, R., Rämö, O.T., Magalhães, M.S., and Macambira, M.J.B., 1999b, Petrology of the anorogenic, oxidised Jamon and Musa granites, Amazonian craton: implications for the genesis of Proterozoic A-type granites. *Lithos* 46, 431–462.
- Dall'Agnol, R., Teixeira, N.P., Rämö, O.T., Moura, C.A.V., Macambira, M.J.B., and Oliveira, D.C., 2005, Petrogenesis of the Paleoproterozoic, rapakivi, A-type granites of the Archean Carajás Metallogenic Province, Brazil. *Lithos* 80: 101–129.
- Dall'Agnol, R., Oliveira, M.A., Almeida, J.A.C., Althoff, F.J., Leite, A.A.S., Oliveira, D.C., and Barros, C.E.M., 2006, Archean and paleoproterozoic granitoids of the Carajás Metallogenic Province, eastern Amazonian craton. In: Symposium on magmatism, crustal evolution and metallogenesis of the Amazoniam Craton, Belém, Excursion Guide, p.: 99-150.
- Dardenne, M.A., and Schobbenhaus, C.S., 2001, Metalogênese do Brasil. Editora Universidade de Brasília/CNPq, Brasília, 392 p.
- Dardenne, M.A., Ferreira Filho, C.F. and Meirelles, M.R., 1988, The role of shoshonitic and calc-alkaline suites in the tectonic evolution of the Carajás district, Brazil. *Journal of South American Earth Sciences*, 1: 363–372.

- Dias, G.S., Macambira, M.B., Dall'Ágnol, R., Soares, A.D.V., and Barros, C.E.M., 1996, Datações de zircões de sill de metagabro: comprovação de idade arqueana da Formação Águas Claras, Carajás, Pará. In: Simpósio de Geologia da Amazônia, 5, SBG, Belém, pp. 376-378.
- DOCEGEO, 1988, Revisão litoestratigráfica da Província Mineral de Carajás – Litoestratigrafia e principais depósitos minerais. 35º Congresso Brasileiro de Geologia, Belém, SBG, Proceedings, 11-54.
- Domingos, F., 2009, The structural setting of the Canaã dos Carajás region and Sossego-Sequeirinho deposits, Carajás, Brazil: Unpublished Ph.D. Dissertation, Durham University, 483 p. Available at Durham E-Theses Online: <http://etheses.dur.ac.uk/144/>.
- Duncan, R., Stein, H., Evans, K., Hitzman, M., Nelson, and Kirwin, D. 2011, A new geochronological framework for mineralization and alteration in the Selwyn-Mount Dore corridor, eastern fold belt, Mt. Isa Inlier, Australia: Genetic implications for iron oxide-copper-gold deposits: Econ. Geol., 106: 169-192.
- Feio, G.R.L., Dall'Agnol R., Dantas E.L., Macambira M.J.B., Santos J.O.S., Althoff F.J., and Soares J.E.B., 2012a, Archean granitoid magmatism in the Canaã dos Carajás area: Implications for crustal evolution of the Carajás province, Amazonian craton, Brazil. Precambrian Research in press, Corrected Proof.
- Feio, GRL, Dall'Agnol, R, Dantas, EL, Macambira, MJB, Gomes, ACB, Sardinha, AS, Oliveira, DC, Santos, RD, and Santos, PA., 2012b, Geochemistry, geochronology, and origin of the Neoarchean Planalto Granite suite, Carajás, Amazonian craton: A-type or hydrated charnockitic granites?. Lithos, 151: 57-73
- Ferreira Filho, C.F., 1985, Geologia e mineralizações sulfetadas do Prospecto Bahia, Província Mineral de Carajás, PA. Unpublished Master Thesis, Universidade de Brasília, 112p
- Ferreira Filho, C.F., Cançado, F., Correa, C., Macambira, E.M.B., Junqueira-Brod, T.C., and Siepierski, L. 2007, Mineralizações estratiformes de PGE-Ni associadas a complexos acamadados em Carajás: os exemplos de Luanga e Serra da Onça. In: Rosa-Costa, L. T., Klein, E.L., Viglio, E.P. (Ed.). Contribuições à geologia da Amazônia. Belém: SBG-Núcleo Norte, v. 5, p. 1-14.
- Figueiredo e Silva, R., Lobato, L.M., Rosière, C.A., Zucchetti, M., Hagemann, S., Zucchetti, M., Baars, F.J., Morais, R., and Andrade, I., 2008, Hydrothermal origin for the jaspilite-hosted, giant Serra Norte iron ore deposits in the Carajás mineral province, Para State, Brazil: Reviews in Economic Geology, v. 15, p. 255–290.
- Galarza, M.A., and Macambira, M.J.B., 2002a, Petrologia e geocronologia das rochas encaixantes do depósito de Cu–Au Igarapé Bahia, Província Mineral de Carajás, Pará, Brasil, in: Kein, E.L., Vasquez, M.L., Rosa-Costa, L.T., Contribuições à Geologia da Amazônia, v. 3, SBG/NN, Belém, p. 153–168.
- Galarza, M.A., and Macambira, M.J.B., 2002b, Geocronologia e Evolução Crustal da Área do Depósito de Cu–Au Gameleira, Província Mineral de Carajás (Pará), Brasil: Geologia USP Série Científica v. 2, p. 143–159.
- Galarza, M.A., Macambira, M.J.B. and Moura, C.A.V., 2003, Geocronologia Pb–Pb e Sm–Nd das rochas maficas do depósito Igarapé Bahia, Província Mineral de Carajás (PA). VII Simpósio de Geologia da Amazônia, SBG, [CD-ROM]
- Gibbs, A.K., Wirth, K.R., Hirata, W.K., and Olszewski Jr., W.J., 1986, Age and composition of the Grão Pará Group volcanics, Serra dos Carajás. Revista Brasileira de Geociências, 16: 201–211.
- Gomes, A.C.B., 2003, Geologia, petrografia e geoquímica dos granítóides de Canaã dos Carajás, SE do Estado do Pará. Belém. Dissertação de Mestrado, UFPA, 160p.
- Gonçalez, M.G.B., Dall'agnol, R., Angelim, E.P.V., Macambira, Mj.B., and Della Senta, N. 1988, Geologia do Maciço anorogênico Cigano, vale do Rio Parauapebas-PA. In: Cong. Bras. Geol., 35, Anais, Belém, SBG–Núcleo Norte, v. 3, p. 1132-1146
- Grainger, C.J., Groves, D.I., Tallarico, F.H.B, and Fletcher, I.R. 2008, Metallogenesis of the Carajás Mineral Province, Southern Amazon Craton, Brazil: Varying styles of Archean through

- Paleoproterozoic to Neoproterozoic base- and precious-metal mineralization. *Ore Geology Reviews*, 33: 451-489.
- Groves, D.I., and Bierlein, F.K., 2007, Geodynamic settings of mineral deposit systems. *Journal of the Geological Society, London*, 164, 19–30.
- Groves, D.I., Bierlein, F.P., Meinert, L.D., and Hitzman, M.W., 2010, Iron Oxide Copper-Gold (IOCG) Deposits through Earth History: Implications for Origin, Lithospheric Setting, and Distinction from Other Epigenetic Iron Oxide Deposits: *Economic Geology*, v. 105, p. 641-654.
- Hirata, W.K., Rigon, J.C., Kadekaru, K., Cordeiro, A.A.C., and Meireles, E.A., 1982, Geologia Regional da Província Mineral de Carajás. In: *Simpósio de Geologia da Amazônia*, 1, Belém, SBG/NO, p. 100–110.
- Holdsworth, R. and Pinheiro, R., 2000, The anatomy of shallow-crustal transpressional structures: insights from the Archean Carajás fault zone, Amazon, Brazil. *Journal of Structural Geology* 22: 1105–1123.
- Huhn, S.B., Macambira, M.J.B., and Dall'Agnol, R., 1999b, Geologia e geocronologia Pb-Pb do Granito Alcalino Planalto, Região da Serra do Rabo, Carajás-PA. In: SBG, *Simpósio de Geologia da Amazônia*, 6, Boletim de Resumos, p. 463-466.
- Huhn, S.R.B., Souza, C.I.J., Albuquerque, M.C., Leal, E.D., Brustolin, V., 1999a, Descoberta do depósito Cu(Au) Cristalino: Geologia e mineralização associada região da Serra do Rabo - Carajás – PA. SBG/NO, *Simpósio de Geologia da Amazônia*, 6, pp 140–143.
- Hunt J., Baker T., Thorkelson D. 2005. Regional-scale Proterozoic IOCG-mineralized breccia systems: examples from the Wernecke Mountains, Yukon, Canada. *Mineralium Deposita*, 40:492-514.
- Hunt, J.A., Baker, T., and Thorkelson, D.J., 2007, A review of iron oxide copper- gold deposits, with focus on the Wernecke Breccias, Yukon, Canada, as an example of a non-magmatic end member and implications for IOCG genesis and classification: *Exploration and Mining Geology*, v. 16, p. 209–232.
- Ianhez, A.C., Sousa A.M.S., and Montalvão, R.M.G., 1980, Geologia da sequência vulcâno-sedimentar da Serra do Inajá – Santana do Araguaia. In: *Congresso Brasileiro de Geologia*, 31., 1980, Camboriú. Anais... Camboriú: SBG, 1980. v. 5, p. 2918-2928.
- Isley, A. E., and Abbott, D. H., 1999, Plume-related mafic volcanism and the deposition of banded iron formation. *J. Geophys. Res.*, 104: 15,461–15,477.
- Isley, A. E., and Abbott, D. H., 2002, Implication for the temporal distribution of high-Mg magmas for mantle plume volcanism through time. *J. Geol.*, 110: 141–158.
- Johnson, J.P., 1993, The geochronology and radiogenic isotope systematics of the Olympic Dam copper-uraniumgold- silver deposit, South Australia. Unpublished Ph.D. Dissertation, Australian National University, Canberra, A.C.T.
- Johnson, J.P., and McCulloch, M.T., 1995, Sources of mineralising fluids for the Olympic Dam deposit (South Australia): Sm-Nd isotopic constraints. *Chemical Geology* 121, 177–199.
- Klein, E.L., and Carvalho, J.M. de A., 2008, Recursos Minerais. In: M.L Vasquez, L.T. Rosa-Costa. (Orgs) *Geologia e Recursos Minerais do Estado do Pará: SIG: Texto explicativo dos Mapas Geológico e Tectônico e de Recursos Minerais do Estado do Pará*. Escala 1:1.000.000. Belém: CPRM.
- Krymsky, R.S., Macambira, J.B. and Macambira, M.J.B., 2002, Geocronologia U-Pb em zircão de rochas vulcânicas da Formação Carajás, Estado do Pará. II Simpósio de Vulcanismo e Ambientes Associados, SBG/NO, 2: 41.
- Lafon, J.M., Macambira, M.J.B., and Pidgeon, R.T. 2000, Zircon U-Pb SHRIMP dating of Neoarchean magmatism in the southwestern part of the Carajás Province (eastern Amazonian Craton, Brazil). In: *International Geological Congress*, 31., Abstracts, Rio de Janeiro, [CD-ROM].
- Lafon, J.-M., Rodrigues, E., and Duarte, K.D., 1994, Le granite Mata Surrão: un magmatisme monzogranitique contemporain des associations tonalitiques-trondhjé-mítiques-granodioritiques archeennes de la région de Rio Maria (Amazonie orientale, Brésil). *C. R. Acad. Sci. Paris* 318, 643–649.

- Lancaster Oliveira, J., Fanton, J., Almeida, A.J., Leveille, R.A., and Vieira, S., 2000, Discovery and geology of the Sossego copper-gold deposit, Carajás District, Pará State, Brazil: International Geology Congress, 31st, Proceedings, International Union of Geological Sciences, [CD-ROM].
- Leite, A.A.S., Dall'Agnol, R., Macambira, M.J.B., and Althoff, F.J., 2004, Geologia e geocronologia dos granítoides arqueanos da região de Xinguara (PA) e suas implicações na evolução do Terreno Granito-Greenstone de Rio Maria. *Revista Brasileira de Geociências*. 34, 447–458.
- Li, N., Chen, Y.-J., Fletcher, I., Zeng, Q.-T., 2011, Triassic mineralization with Cretaceous overprint in the Dahu Au-Mo deposit, Xiaoqinling gold province: Constraints from SHRIMP monazite U-Th-Pb geochronology. *Gondwana Research* 20, 543–552.
- Lindenmayer, Z.G., Pimentel, M.M., Ronchi, L.H., Althoff, F.J., Laux, J.H., Araújo, J.C., Fleck A., Bortowski, D.C., Nowatzki, A.C., 2001. Geologia do depósito de Cu–Au do Gameleira, Serra dos Carajás, Pará. In: Jost H, Brod JA, Quieroz ET (eds) *Caracterização de Depósitos Auríferos Brasileiros*, ADIMB-DNPM, Brasília, pp. 79–139
- Lobato, L.M., Roaière, C.A., Silva, R.C.F., Zucchetti, M., Baars, F.J., Seoane, J.C.S., Rios, F.J., Pimentel, M., Mendes, G.E. and Monteiro, A.M., 2005, A mineralização hidrotermal de ferro da Província Mineral de Carajás - controle estrutural e contexto na evolução metalogenética da Província. In: Marini, J.O.; Queiróz, E.T.; Ramos, W.B. (eds.), *Caracterização de distritos mineiros da Amazônia*. DNPM-CT-Mineral-ADIMB, 25–92.
- Ludwig K.R. 2003. User's Manual for Isoplot/Ex v. 3.00. A Geochronological Toolkit for Microsoft Excel. BGC Special Publication 4, Berkeley, 71 pp.
- Macambira, J.B., 2003, O ambiente deposicional da Formação Carajás e uma proposta de modelo evolutivo para a Bacia Grão Pará. Unpublished Ph.D Dissertation, Universidade Estadual de Campinas, 217p.
- Macambira, E.M.B., and Vale, A.G., 1997, São Félix do Xingu: folha SB.22-Y-B, Estado do Pará, escala 1:250.000. Texto Explicativo. Brasília: CPRM. 344 p., il. Programa Levantamentos Geológicos Básicos do Brasil (PLGB).
- Macambira, E.M.B., and Ferreira Filho, C.F., 2002, Fracionamento magmático dos corpos máfico-ultramáficos da Suíte Intrusiva Cateté – sudeste do Pará. In: Klein, E.L., Vasquez, M.L., Rosa-Costa, L.T. (Ed.). Contribuições à geologia da Amazônia. Belém: SBG-Núcleo Norte. v. 3, p. 105–114.
- Macambira, J.B., Kotschoubey, B., Santos, M.D., Moura, C.A.V., and Ramos, J.F.F., 1986, Estratigrafia e mineralizações primárias de ouro da aba sul do sinclínorio de Gradas-Sul do Pará. In: Congresso Brasileiro de Geologia, 34, Goiânia, 1986. Anais... Goiânia, SBG. v.5, p.1956-1964.
- Macambira, J.B., Macambira, M.J.B., Scheller, T., and Gomes, A.C.B., 1996, Geocronologia Pb/Pb e tipologia de zircões de rochas vulcânicas da Formação Carajás-Pará: indicador da idade dos BIFs. In: SBG/NE, Congresso Brasileiro de Geologia, 39, Boletim de Resumos Expandidos, pp. 516–518.
- Macambira, M.J.B., and Lancelot, J., 1996, Time constraints of Archean Rio Maria crust, Southeastern Amazonian Craton, Brazil. *International Geology Review*, 38 (12): 1134–1142.
- Macambira, M.J.B., Vasquez, M.L., Silva, D.C.C., Galarza, M.A., Barros, C.E.M., and Camelo, J.F., 2009, Crustal growth of the central-eastern Paleoproterozoic domain, SW Amazonian craton: Juvenile accretion vs. reworking. *Journal of South American Earth Sciences* 27 (2009) 235–246.
- Machado, N., Lindenmayer, D.H., Krough, T.E., and Lindenmayer, Z.G., 1991, U-Pb geochronology of Archean magmatism and basementreactivation in the Carajás area, Amazon Shield, Brazil. *Precambrian Research*, 49:329-354
- Markey, R.J., Stein, H.J., and Morgan, J.W., 1998, Highly precise Re-Os dating for molybdenite using alkaline fusion and NTIMS. *Talanta* 45, 935–946.
- Markey, R.J., Stein, H.J., Hannah, J.L., Selby, D. and Creaser, R.A., 2007, Standardizing Re-Os geochronology: A new molybdenite Reference Material (Henderson, USA) and the stoichiometry of Os salts". *Chemical Geology*, 244, 74-87.

- Marschik, R., Spangenberg, J.E., Leveille, R.A., and de Almeida, A.J., 2003, The Sossego iron oxide-Cu-Au deposit, Carajás, Brazil. In: Eliopoulos D et al (eds) Mineral Exploration and Sustainable Development v 1. Millpress, Rotterdam, p. 331–334
- Marsh, T.M., Einaudi, M.T., and McWilliams, M., 1997, $^{40}\text{Ar}/^{39}\text{Ar}$ geochronology of Cu-Au and Au-Ag mineralization in the Potrerillos district, Chile: Economic Geology, v. 92, p. 784–806
- Mathur, R., Marschik, R., Ruiz, J., Munizaga, F., Leveille, R.A., and Martin, W., 2002, Age and mineralization of the Candelaria Fe oxide Cu-Au deposit and the origin of the Chilean iron belt, based on Re-Os isotopes: Economic Geology, v. 97, p. 59–71.
- Meirelles, M.R., 1986, Geoquímica e petrologia dos jaspilitos e rochas vulcânicas associadas, Grupo Grão-Pará, Serra dos Carajás. Unpublished Master Thesis, UnB, pp.
- Meirelles, M.R., and Dardenne, M.A., 1991, Vulcanismo basáltico de afinidade shoshonítica em ambiente de arco arqueano, Grupo Grão Pará, Serra dos Carajás, PA. Revista Brasileira de Geociências, 21: 41-50.
- Melo, G.H.C., Monteiro, L.V.S., Xavier, R.P., Moreto, C.P.N., and Silva, M.A.D., submitted, Bacuri copper deposit: host rocks, hydrothermal alteration and characterization of the copper ore, Carajás Province (PA). Revista Brasileira de Geociências, 15pp.
- Melo, G.H.C., 2010. Estudo de inclusões fluidas do depósito de cobre Alvo Bacaba, Província Mineral de Carajás. Unpublished undergraduate essay. 19 p.
- Montalvão, R.M.G., Tassinari, C.C.G., and Bezerra, P.E.L, 1984, Geocronologia dos granitóides e gnaisses das regiões do Rio Maria, Fazenda Mata Geral e Rio Itacaiúnas, Sul do Pará (Distrito Carajás Cumaru): Actas do XXXIII Congresso Brasileiro de Geologia, Rio de Janeiro, SBG, v. 6, pp. 2757-2766.
- Monteiro, L.V.S., Xavier, R.P., Carvalho, E.R., Hitzman, M.W., Johnson, C.A., Souza Filho, C.R., and Torresi, I., 2008a, Spatial and temporal zoning of hydrothermal alteration and mineralization in the Sossego iron oxide–copper–gold deposit, Carajás Mineral Province, Brazil: paragenesis and stable isotope constraints. Mineralium Deposita, 43:129–159.
- Monteiro, L.V.S., Xavier, R.P., Hitzman, M.W., Juliani, C., Souza Filho, C.R., and Carvalho, E.R., 2008b, Mineral chemistry of ore and hydrothermal alteration at the Sossego iron oxide–copper–gold deposit, Carajás Mineral Province, Brazil. Ore Geology Reviews, 34:317–336.
- Monteiro, L.V.S., Xavier, R.P., Pestilho, A.L.S., Moreto, C.P.N., Juliani, C., Torresi, I., and Souza Filho, C.R., 2011, O Cinturão Sul do Cobre na Província Mineral de Carajás: reconstituição do paleossistema hidrotermal associado aos depósitos de óxido de ferro-cobre-ouro. In: Frantz J.C.; Marques J.C.; Jost H.. (Org.). Contribuições à metalogenia do Brasil. 1ed. Porto Alegre: UFRGS/Instituto de Geociências, 2011, v. 1, p. 41-70.
- Mora, C.I., and Valley, J.W., 1989, Halogen-rich scapolite and biotite: implications for metamorphic fluid-rock interactions. Am. Mineral. 74:721–737.
- Moreto, C.P.N., 2010, O depósito de óxido de ferro-cobre-ouro Bacaba, Província Mineral de Carajás: Geocronologia U-Pb das rochas hospedeiras. Unpublished Master Thesis. Universidade Estadual de Campinas. 85p.
- Moreto, C.P.N., Monteiro L.V.S., Xavier R.P., Amaral W.S., Santos T.J.S., Juliani C., and Souza Filho C.R., 2011, Mesoarchean (3.0 and 2.86 Ga) host rocks of the iron oxide-Cu-Au Bacaba deposit, Carajás Mineral Province: U-Pb geochronology and metallogenetic implications. Mineralium Deposita V. 46, pps. 789-811. DOI: 10.1007/s00126-011-0352-9.
- Moreto, C.P.N., Monteiro, L.V.S., Creaser, R., Xavier, R.P., Dufrane, A., Tassinari, C.G., Sato, K., Kemp, A.I.S., and Amaral, W.S., submitted, Overprinting of Paleoproterozoic on Archean iron oxide - copper-gold system at the Sossego deposit, Carajás Province: Re-Os and U-Pb geochronological evidences.
- Moreto, C.P.N., Monteiro, L.V.S., Xavier, R.P., Torresi, I., and Souza Filho, C.R., 2009. Caracterização geoquímica do minério e das zonas de alteração hidrotermal do depósito de óxido de ferro-cobre-ouro Alvo 118, Província Mineral de Carajás. II Simpósio Brasileiro de Metalogenia, Gramado-RS, Brazil [CD-ROM]

- Moroni, M., Girardi, V.A.V., and Ferrario, A., 2001, The Serra Pelada Au–PGE deposit, Serra dos Carajás (Pará State, Brazil): geological and geochemical indications for a composite mineralising process: Mineralium Deposita, v. 36, p. 768–785.
- Mougeot, R., Respaut, J.P., Brique, L., Ledru, P., Milesi J.P., Lerouge, C., Marcoux, E., Huhn, and S.B., Macambira, M.J.B., 1996b, Isotope geochemistry constrains for Cu, Au mineralizations and evolution of the Carajás Province (Para, Brazil). In: SBG, Congresso Brasileiro de Geologia, 39, Salvador, Anais, 7, 321-324 (in Portuguese).
- Mougeot, R., Respaut, J.P., Briqueu, L., Ledru, P., Milesi, J.P., Macambira, M.J.B., and Huhn S.B. 1996a, Geochronological constrains for the age of the Águas Claras Formation (Carajás Province, Pará, Brazil). In: Congresso Brasileiro de Geologia, 39, Salvador, 1996. Anais., Salvador, SBG. 6:579-581.
- NCL Brasil, 2005, Revision de La Estimación de Recursos del Proyecto Cristalino. Vale S.A Internal Report, 1-103.
- Neves, M.P., 2006, Estudos isotópicos (Pb-Pb, Sm-Nd, C e O) do depósito Cu-Au do Sossego, Província Mineral de Carajás. Master Thesis. Universidade Federal do Pará. 116 p.
- Nogueira, A.C.R., Truckenbrod, W., Costa, J.B.S., and Pinheiro, R.V.L., 1994, Análise faciológica e estrutural da Formação Águas Claras, Pré-Cambriano da Serra dos Carajás. 4 Simpósio de Geologia da Amazônia, pp. 363–364.
- Nogueira, A.C.R., Truckenbrod, W., Pinheiro, R.V.L., 2000, Storm and tide-dominated siliciclastic deposits of the Archean Águas Claras Formation, Serra dos Carajás, Brazil. 31st International Geological Congress, Rio de Janeiro. Sociedade Brasileira de Geologia. Abstract volume CD-ROM.
- Nogueira, A.C.R., Truckenbrodt, W., and Pinheiro, R.V.L., 1995, Formação Águas Claras, Pré-Cambriano da Serra dos Carajás: redescricao e redefinição litoestratigráfica. Boletim do Museu Paraense Emílio Goeldi, Ciências da Terra, (7), pg. 177-277.
- Oliveira, C.G., and Leonardos, O.H., 1990, Gold mineralization in the Diadema shear belt, northern Brazil. Economic Geology, 85: 1034-1043.
- Oliveira, D.C., Santos, P.J.L., Gabriel, E.O., Rodrigues, D.S., Faresin, A.C., Silva, M.L.T., Sousa, S.D., Santos, R.V., Silva, A.C., Souza, M.C., Santos, R.D., and Macambira, M.J.B., 2010, Aspectos geológicos e geocronológicos das rochas magmáticas e metamórficas da região entre os municípios de Água Azul do Norte e Canaã dos Carajás – Província Mineral de Carajás, In: SBG, Congresso Brasileiro de Geologia, 45, CDrom (in Portuguese).
- Oliveira, M.A., Dall'Agnol, R., Althoff, F.J., and Leite, A.A.S., 2009, Mesoarchean sanukitoid rocks of the Rio Mari Granite-Greenstone Terrane, Amazonian craton, Brazil. Journal of South American Earth Sciences 27: 146-160
- Oliveira, M.A., Dall'Agnol, R., and Almeida, J.A.C. de., 2011, Petrology of the Mesoarchean Rio Maria Suite and the discrimination of the sanukitoid series. Lithos, 127: 192-209.
- Oliver, N.H.S., Cleverley, J.S., Mark, G., Pollard, P., Fu, B., Marshall, L.J., Rubenach, M.J., Williams, P.J., and Baker, T., 2004, Modeling of the role of sodic alteration in the genesis of iron oxide-copper-gold deposits, Eastern Mount Isa Block, Australia. Economic Geology, p. 1145-1176.
- Olszewski, W.J., Wirth, K.R., Gibbs, A.K., and Gaudette, H.E., 1989, The age, origin, and tectonics of the Grão Pará Group and associated rocks, Serra dos Carajás, Brazil: Archean continental volcanism and rifting. Precambrian Research, 42, 229-254.
- Orville, P. M., 1975, Stability of scapolite in the system Ab-An-NaCl-CaCO₃ at 4 kb and 750 °C. Geochimica et Cosmochimica Acta, 39, 1091–1105.
- Pestilho, A.L.S. and Monteiro, L.V.S., 2008, Caracterização petrográfica das zonas de alteração hidrotermal e paragêneses do minério de cobre e ouro do Alvo Castanha, Província Mineral de Carajás. Simpósio de vulcanismo e Ambientes Associados, 4, Foz do Iguaçu [CD-ROM].
- Pestilho, A.L.S., 2008, Depósito de Cu-(Zn-Ni) do Alvo Castanha, Província Mineral de Carajás, PA: Evolução paragenética e dos fluidos mineralizantes. Unpublished honours thesis, 86p.

- Pestilho, A.L.S., 2011, Sistemática de isótopos estáveis aplicada à caracterização da evolução dos paleo-sistemas hidrotermais associados aos depósitos cupríferos Alvo Bacaba e Alvo Castanha, Província Mineral de Carajás, PA. Unpublished Master Dissertation. 71p.
- Pidgeon, R.T., Macambira, M.J.B., and Lafon, J.M. 2000, Th–U–Pb isotopic systems and internal structures of complex zircons from an enderbite from the Pium Complex, Carajás Province, Brazil: evidence for the ages of granulite facies metamorphism and the protolith of the enderbite. *Chemical Geology* 166, 159–171.
- Pimentel, M.M., and Machado, N., 1994, Geocronologia U–Pb dos terrenos granito-greenstone de Rio Maria, Pará. In: Cong. Bras. Geol., Anais, Sociedade Brasileira de Geologia, vol. 2, pp. 390–391.
- Pimentel, M.M., Lindenmayer, Z.G., Laux, J.H., Armstrong, R. and Araújo, J.C., 2003, Geochronology and Nd geochemistry of the Gameleira Cu-Au deposit, Serra dos Carajás, Brazil: 1.8–1.7 Ga hydrothermal alteration and mineralization. *Journal of South American Earth Sciences*, 15: 803–813.
- Pinheiro, R.V.L., and Holdsworth, R.E., 1997, Reactivation of Archaean strike-slip fault systems, Amazon region, Brazil. *Journal of the Geological Society of London* 154, 99–103.
- Poirras, F., Chereny, S., Bland, D.J., 1996, Contrasted monazite hydrothermal alteration mechanisms and their geochemical implications. *Earth and Planetary Science Letters* 145, 79–96.
- Pollard, P.J., 2001, Sodic-(calcic) alteration in Fe-oxide–Cu–Au districts: an origin via unmixing of magmatic H₂O–CO₂–NaCl + CaCl₂–KCl fluids. *Mineralium Deposita* 36: 93–100.
- Pollard, P.J. 2006, An intrusion-related origin for Cu–Au mineralization in iron oxide–copper–gold (IOCG) provinces. *Mineralium Deposita*, 41: 179–187.
- Quadt, A. v., Moritz, R., Peytcheva, I., and Heinrich, C. A., 2005, Geochronology and geodynamics of Late Cretaceous magmatism and Cu–Au mineralization in the Panagyurishte region of the Apuseni-Banat-Timok-Srednogorie belt, Bulgaria. *Ore Geology Reviews*, 27 (2005) 95–126.
- Rasmussen, B., Fletcher, I.R., McNaughton, N.J., 2001, Dating low-grade metamorphic events by SHRIMP U–Pb analysis of monazite in shale. *Geology* 39, 963–966.
- Rasmussen, B., Fletcher, I.R., Sheppard, S., 2005, Isotopic dating of the migration of a low-grade metamorphic front during orogenesis. *Geology* 33, 773–776.
- Ribeiro, A.A., 2008, Litogeocquímica e geologia isotópica estável (C, S, O) do depósito Cupro-aurífero do Alvo Cristalino Sul, Província Mineral de Carajás, Pará, Unpublished Master Thesis, Universidade Federal de Ouro Preto, 142 p.
- Ricci, P.S.F., Carvalho, M.A., 2006, Rocks of the Pium-Area, Carajás Block, Brazil – A Deep seated High-T Gabbroic Pluton (Charnockitoid-Like) with Xenoliths of Enderbitic Gneisses Dated at 3002 Ma – The Basement Problem Revisited. In: Simpósio de Geologia da Amazônia, 8, [CD-ROM]
- Rigon, J.C., Munaro, P., Santos, L.A., Nascimento, J.A.S. and Barreira, C.F., 2000, Alvo 118 copper–gold deposit: geology and mineralization, Serra dos Carajás, Pará, Brazil. 31st International Geological Congress, Rio de Janeiro. SBG, Abstract Volume, [CD-ROM].
- Rios, F.J., Villas, R.N., and Fuzikawa, K., 2003, Fluid Evolution in the Pedra Preta wolframite ore deposit, Paleoproterozoic Musa Granite, eastern Amazon craton, Brazil. *Journal of South American Earth Sciences*, 15: 787–802.
- Rios, F.J., Villas, R.N., Fuzikawa, K., Sial, A.N., and Mariano, G., 1998, Isótopos de oxigênio e temperatura de formação dos veios mineralizados com wolframita da jazida Pedra Preta, sul do Pará. *Revista Brasileira de Geociências* 28(3):253–256
- Rodrigues, E.S., Lafon, J.M., and Scheller, T., 1992, Geocronologia Pb-Pb da Província Mineral de Carajás: primeiros resultados. In: Congresso Brasileiro de Geologia, 37, Boletim Resumos Expandidos, SBG, São Paulo, vol. 2, pp. 183–184.
- Roscito, F.G., 2009, Caracterização geoquímica e balanço de massa das zonas de alteração hidrotermal do depósito cuprífero de Alvo Bacaba, Província Mineral de Carajás. Unpublished Honours Thesis, Universidade Estadual de Campinas, 82p.

- Santos, J.O.S., 2003, Geotectônica dos Escudos da Guiana e Brasil Central. In: Buzzi, L.A., Schobbenhaus, C., Vidotti, R.M., Gonçalves, J.H., (Eds.), Geologia, Tectônica e Recursos Minerais do Brasil. Texto, Mapas e SIG. CPRM-Serviço Geológico do Brasil, vol. 4, pp. 169–226.
- Santos, J.O.S., Hartmann, L.A., Gaudette, H.E., Groves, D.I., McNaughton, N.J., and Fletcher, I.R., 2000, A new understanding of the provinces of Amazon Craton based on field mapping and U-Pb and Sm-Nd geochronology. *Gondwana Research*, 3: 453-488.
- Santos, M.G.S., 2002, Estudo dos isótopos de Pb e Nd do depósito de Cu– Au (U-Etr) Alemão, Província Mineral de Carajás (PA). Unpublished Master Thesis, Universidade Federal do Pará, 126p.
- Sardinha, A.S., Barros, C.E. de M., Krymsky, M., 2006, Geology, geochemistry and U–Pb geochronology of the Archean (2.74Ga) Serra do Rabo granite stocks, Carajás Metallogenetic Province, northern Brazil. *Journal of South American Earth Sciences* 20, 327–339.
- Sardinha, A.S., Dall’Agnol, R., Gomes, A.C.B., Macambira, M.J.B., and Galarza, M.A., 2004, Geocronologia Pb-Pb e U-Pb em zircão de granitóides arqueanos da região de Canaã dos Carajás, Província Mineral de Carajás. 42º Congresso Brasileiro de Geologia, Araxá (MG), SBG, [CD-ROM].
- Satish-Kumar, M., Hermann, J., Tsunogae, T., Osanai, Y., 2006, Carbonation of Cl-rich scapolite boudins in Skallen, East Antarctica: evidence for changing fluid condition in the continental crust. *Journal of Metamorphic Geology* 24 (3), 241-261.
- Sato, K., and Tassinari, C.C.G., 1997, Principais eventos de acreção continental no Cráton Amazônico baseados em idademodelo Sm-Nd, calculada em evoluções de estágio único e estágio duplo. In: Costa M.L.C. & Angélica R.S. (coords.) Contribuição à Geologia da Amazônia. SBG-NO, p. 91–142.
- Selby, D, and Creaser, R.A., 2004, Macroscale NTIMS and microscale LA-MC-ICP-MS Re-Os isotopic analysis of molybdenite: Testing spatial restrictions for reliable Re-Os age determinations, and implications for the decoupling of Re and Os within molybdenite. *Geochimica et Cosmochimica Acta* (2004), 68, 3897-3908.
- Silva, C.M.G., and Villas, N.R., 1998, The Águas Claras Cu-sulfide ± Au deposit, Carajás region, Pará, Brazil: geological setting, wall-rock alterationand mineralizing fluids: *Revista Brasileira de Geociências*, v. 28, p. 315-326.
- Silva, M.A.D, 2011, O Domínio de Transição da Província Mineral de Carajás: Contexto geológico e litoquímica das unidades hospedeiras de mineralizações cúpro-auríferas. Honours Thesis. Universidade Estadual de Campinas. 74p.
- Silva, A.R.C., Villas, R.N.N., Lafon, J.M., and Craveiro, G.S., 2012, Idade da alteração e mineralização do depósito de Cu-Au Visconde, Província Mineral de Carajás (Pará), Brasil. 46º Congresso Brasileiro de Geologia, Santos. (CD-ROM).
- Silva, M.G., Teixeira, J.B.G., Pimentel, M.M., Vasconcelos, P.M., Arielo, A. and Rocha, W.J.S.F., 2005, Geologia e mineralizações de Fe-Cu-Au do Alvo GT46 (Igarapé Cinzento, Carajás). In: Marini, O.J., Queiroz, E.T., Ramos, B.W. (eds.), Caracterização de Depósitos Minerais em Distritos Mineiros da Amazônia, 94-151.
- Simonetti, A., Heaman ,L.M., Hartlaub, R.P., Creaser, R.A., Machattie, T.G., and Bohm, C. 2005, U-Pb zircon dating by laser ablation MC-ICP-MS using a new multiple ion counting Faraday collector array. *Journal of Analytical Atomic Spectrometry* 20: 677-686.
- Simonetti, A., Heaman, L.M., Chacko, T. and Banerjee, N.R., 2006, In situ petrographic thin section U-Pb dating of zircon, monazite, and titanite using laser ablation-MC-ICP-MS. *International Journal of Mass Spectrometry*, 253(1-2): 87-97.
- Skirrow, R.G., Bastrakov, E.N., Barovich, K., Fraser, G., Creaser, R.A., Fanning, C.M., Raymond, O.L., and Davison, G.J., 2007, Timing of Iron Oxide Cu-Au-(U) hidrotermal activity and Nd isotope constrains on metal sources in the Gawler Craton, South Australia. *Economic Geology*, vol.102, pp. 1441-1470.
- Smith, H.A., Giletti, B.J., 1997, Lead diffusion in monazite. *Geochimica et Cosmochimica Acta* 61, 1047–1055.

- Smith, M.P., Storey, C.D., Jeffries, T.E., and Ryan, C., 2009, In situ U-Pb and trace element analysis of accessory minerals in the Kiruna district, Norrbotten, Sweden: New constraints on the timing and origin of mineralization. *Journal of Petrology*, vol 50 (11), pp. 2063-2094.
- Smith, M.P., Gleeson, S.A., and Yardley, B.W.D., 2013, Hydrothermal fluid evolution and metal transport in the Kiruna district, Sweden: Contrasting metal behavior in aqueous and aqueous-carbonic brines. *Geochimica et Cosmochimica Acta*, 102: 89-112.
- Soares, A.D.V., Macambira, M.J.B., Santos, M.G.S., Vieira, E.A.P., Massoti, F.S., Souza, C.I.J., Padilha, J.L., and Magni, M.C.V., 2001, Depósito Cu-(Au) Cristalino, Serra dos Carajás, PA: Idade da mineralização com base em análises Pb-Pb em sulfetos (dados preliminares): Simpósio de Geologia da Amazônia, VII, Belém, Sociedade Brasileira de Geologia, [CD-ROM].
- Souza, S.R.B., Macambira, M.J.B., Sheller, T., 1996, Novos dados geocronológicos para os granitos deformados do Rio Itacaiúnas (Serra dos Carajás, PA); implicações estratigráficas. V Simpósio de Geologia da Amazônia, Belém, Anais, 380–383.
- Souza, L.J., Vieira, E.A., 2000, Salobo 3 Alpha deposit: geology and mineralization. In: Porter TM (ed) *Hydrothermal iron oxide copper-gold and related deposits: a global perspective*. Australian Mineral Foundation, Adelaide, pp 213–224
- Souza, Z.S., Potrel, H., Lafon, J.M., Althoff, F.J., Pimentel, M.M., Dall'Agnol, R., and Oliveira, C.G., 2001, Nd, Pb and Sr isotopes of the identidade belt, an Archaean greenstone belt of the Rio Maria region (Carajás Province, Brazil): implications for the archaean geodynamic evolution of the Amazonian craton. *Precambrian Research* 109: 293–315
- Stein, H.J., and Cathles, L.M., 1997, Preface: A special issue on the timing and duration of hydrothermal events: *Economic Geology*, v. 92, p. 763–765.
- Tallarico, F.H.B., 2003, O cinturão cupro-aurífero de Carajás, Brasil. Unpublished Ph.D. Dissertation, Universidade Estadual de Campinas, 229p
- Tallarico, F.H.B., Figueiredo B.R., Groves D.I., Kositcin N., McNaughton N.J., Fletcher I.R., and Rego J.L., 2005, Geology and SHRIMP U-Pb geochronology of the Igarapé Bahia deposit, Carajás copper-gold belt, Brazil: an Archean (2.57 Ga) example of iron-oxideCu-Au-(U- REE) mineralization. *Economic Geology* 100:7–28.
- Tallarico, F.H.B., McNaughton, N.J., Groves, D.I., Fletcher, I.R., Figueiredo, B.R., Carvalho, J.B., Rego, J.L., Nunes, A.R., 2004, Geological and SHRIMP II U-Pb constraints on the age and origin of the Breves Cu-Au-(W-Bi-Sn) deposit, Carajás, Brazil. *Mineralium Deposita*. 39, 68-86.
- Tallarico, F.H.B., Oliveira, C.G., and Figueiredo, B.R., 2000, The Igarapé Bahia Cu-Au mineralization, Carajás Province: *Revista Brasileira de Geociências*, v. 30, p. 230-233.
- Tassinari C.C.G., and Macambira M.J.B., 1999, Geochronological Provinces of the Amazonian Craton. *Episodes*, 22 (3):174-182.
- Tassinari, C. C. G., Hirata, W. K., and Kawashita, K., 1982, Geologic evolution of the Serra dos Carajás, Pará, Brazil: *Revista Brasileira de Geociências*, v. 12, nos. 1-3, pp. 263-267
- Tassinari, C.C.G., 1996, O mapa geocronológico do Cráton Amazônico no Brasil: revisão dos dados isotópicos. Tese de Livre Docência, IG-USP, 139p.
- Tassinari, C.C.G., and Macambira, M., 2004, A evolução tectônica do Cráton Amazônico. In: Mantesso-Neto, V., Bartorelli, A., Carneiro, C.D.R., Brito Neves, B.B. (eds.). *Geologia do Continente Sul-Americano: Evolução da obra de Fernando Flávio Marques Almeida*. São Paulo, Beca, p. 471-485
- Tassinari, C.C.G., Tachibana, J., Tulio, M., Livio, R., and Gaia, C., 2005, Geologia isotópica aplicada nas mineralizações de Cu-Au do greenstone belt da Serra dos Gradaús, Província Mineral de Carajás, Cráton Amazônico: exemplo de mineralizações policíclicas. In: *Simpósio Brasileiro de Metalogenia*, 1, [CD-ROM]
- Tavaza, E., 1999, Mineralização de Au-Cu-(ETR-U) associada às brechas hidrotermais do depósito de Igarapé Bahia, província Mineral de Carajás, PA. Unpublished Master Thesis, Ouro Preto, Brazil, Universidade Federal de Ouro Preto. 81p.

- Teixeira, W., Tassinari, C.C.G., Cordani, U.G., and Kawashita, K., 1989, A review of the geochronological of the Amazonian Craton: tectonic implications. *Precambrian Research*, 42: 213-227.
- Teixeira, J.B.G., 1994, Geochemistry, petrology, and tectonic setting of archean basaltic and dioritic rocks from the N4 Iron deposit, Serra dos Carajás, Pará, Brazil. 1994. 161p. Unpublished Ph.D Dissertation.
- Teixeira, J.B.G., Lindenmayer, Z.G., and Silva, M.G., 2010, Depósitos de Óxido de Fe, Cu-Au de Carajás. In: R.S.C. Brito, M.G. Silva, R.M. Kuyumjian. (Org.). Modelos de depósitos de cobre do Brasil e sua resposta ao intemperismo. 1 ed. Brasilia: CPRM, p. 15-48.
- Teixeira, N.P., Bettencourt, J.S., Moura, C.A.V., Dall'Agnol, R., and Macambira, E.M.B., 2002, Archean crustal sources for Paleoproterozoic tin-mineralized granites in the Carajás Province, SSE Pará, Brazil: Pb-Pb geochronology and Nd isotope geochemistry. *Precamb. Res.* 119: 257-275.
- Torresi, I., Bortholoto, D.F.A., Xavier, R.P., and Monteiro, L.V.S., 2012, Hydrothermal alteration, fluid inclusions and stable isotope systematics of the Alvo 118 iron oxide-copper-gold deposit, Carajás Mineral Province (Brazil): implications for ore genesis. *Mineralium Deposita*, 47: 299-323.
- Townsend, K.J., Miller, C.F., D'Andrea, J.L., Ayers, J.C., Harrison, T.M., Coath, C.D., 2000, Low temperature replacement of monazite in the Ireteba granite, Southern Nevada: geochronological implications. *Chemical Geology* 172, 95-112.
- Trendall, A.F., Basei, M.A.S., De Laeter, J.R., and Nelson, D.R., 1998, SHRIMP U-Pb constraints on the age of the Carajás formation, Grão Pará Group, Amazon Craton. *Journal of South American Earth Sciences* 11, 265-277.
- Vale. 2012. Vale obtains operation license for Salobo. [http:// saladeimprensa.vale.com /en/release/interna.asp?id=22000](http://saladeimprensa.vale.com/en/release/interna.asp?id=22000). Accessed in february 04, 2013.
- Vanko, D.A., Bishop, F.C., 1982, Occurrence and origin of marialitic scapolite in the Humboldt Lopolith, N.W. Nevada. *Contrib. Mineral. Petrol.* 81:277-289.
- Vasquez, L.V., Rosa-Costa, L.R., Silva, C.G., Ricci, P.F., Barbosa, J.O., Klein, E.L., Lopes, E.S., Macambira, E.B., Chaves, C.L., Carvalho, J.M., Oliveira, J.G., Anjos, G.C., and Silva, H.R., 2008a, Geologia e Recursos Minerais do Estado do Pará: Sistema de Informações Geográficas – SIG: Texto Explicativo dos Mapas Geológico e Tectônico e de Recursos Minerais do Estado do Pará. Organizadores: M.L Vasquez, L.T. Rosa-Costa. Escala 1:1.000.000. Belém: CPRM.
- Vasquez, M.L., Macambira, M.J.B., and Armstrong, R.A., 2008b, Zircon geochronology of granitoids from the western Bacajá domain, southeastern Amazonian craton, Brazil: Neoarchean to Orosirian evolution. *Precambrian Research* 161, 279-302
- Villas, R.N., and Santos, M.D., 2001, Gold deposits of the Carajás Mineral Province: deposit types and metallogenesis. *Mineralium Deposita*, 36:300-331.
- Williams I.S., 1998, U-Th-Pb geochronology by ion microprobe. In: McKibben, M.A. Shanks, W.C. and Ridley W.I. (eds) Applications of Microanalytical Techniques to Understanding Mineralizing Processes. *Reviews in Economic Geology* 7: 1-35.
- Wirth, K.R., Gibbs, A.K., and Olszewski, W.J.Jr., 1986, U-Pb ages of zircons from the Grão Pará Group and Serra dos Carajás granite, Pará, Brasil. *Revista Brasileira de Geociências* 16: 195-200.
- Xavier, R.P., Araújo, C.E.G., Dreher, A.M., Nunes, and A.R., Rêgo, J.L, 2003, Fluid evolution in the Paleoproterozoic Intrusion-related Breves Cu-Au (Mo-W-Bi) deposit, Carajás Mineral Province, Northern Brazil. In VIII Simpósio de Geologia da Amazônia. Manaus, Amazonas.
- Xavier, R.P., Monteiro, L.V.S., Souza Filho, C.R., Torresi, I., Carvalho, E.R., Dreher, A.M., Wiedenbeck, M., Trumbull, R.B., Pestilho, A.L.S., and Moreto, C.P.N., 2010, The iron oxide copper-gold deposits of the Carajás Mineral Province, Brazil: an updated and critical review. In: Porter TM (ed) *Hydrothermal Iron Oxide Copper-Gold & Related Deposits: A Global Perspective*. Australian Miner. Fund, Adelaide, Vol 3, pp. 285-306.
- Zuchetti, M., 2007, Rochas maficas do grupo Grão Pará e sua relação com a mineralização de ferro dos depósitos N4 E N5, Carajás, PA: Unpublished Ph.D. Dissertation, Universidade Federal de Minas Gerais, 165p.

Appendix

Supplementary Table 1 Summary of U-Pb SHRIMP IIe zircon data

Zircon Grain	% 206 comm	Isotopic ratios						Ages (²⁰⁴ corr)						
		U (ppm)	Th (ppm)	²³² Th/ ²³⁸ U	²⁰⁷ Pb/ ²³⁵ U	1σ	²⁰⁶ Pb/ ²³⁸ U	1σ	err corr	²⁰⁶ Pb/ ²³⁸ U	1σ	²⁰⁷ Pb/ ²⁰⁶ Pb	1σ	% disc
<i>Quartz-feldspar porphyry (GMCL 54A)</i>														
Zr-1.1	-0.08	212	182	0.888	13.91	2.3	0.5295	2.2	0.961	2739.5	48.8	2746	10	0
Zr-3.1	0.01	121	86	0.738	13.27	2.2	0.5087	2.0	0.915	2651.1	44.1	2735	15	3
Zr-5.1	0.35	201	163	0.837	14.27	2.3	0.5385	2.2	0.953	2777.2	48.9	2761	11	-1
Zr-6.1	-0.34	163	142	0.903	13.81	2.1	0.5240	2.0	0.940	2716.0	44.8	2753	12	1
Zr-7.1	0.17	139	94	0.698	13.67	2.2	0.5210	2.0	0.934	2703.3	45.1	2744	13	2
Zr-8.1	-0.18	337	312	0.955	13.94	2.2	0.5323	2.1	0.963	2751.0	47.3	2742	10	0
Zr-10.1	-0.02	395	150	0.391	14.17	1.9	0.5436	1.9	0.973	2798.6	42.3	2734	7	-2
Zr-11.1	-0.27	207	174	0.868	14.19	2.3	0.5422	2.2	0.961	2792.8	49.3	2740	10	-2
<i>Castanha quartz-feldspar porphyry (CAS 02/424.9)</i>														
Zr-1.1	-0.11	307	167	0.56	13.98	2.0	0.5309	1.98	0.97	2745.4	44.2	2751	8	0
Zr-1.2	0.32	158	84	0.55	14.23	2.1	0.5455	1.93	0.93	2806.6	44.0	2735	13	-3
Zr-2.1	0.00	232	129	0.57	14.02	2.0	0.5349	1.91	0.96	2762.1	43.0	2743	9	-1
Zr-3.1	0.22	162	60	0.38	13.66	2.1	0.5263	1.94	0.94	2725.9	43.1	2726	12	0
Zr-4.1	0.01	179	74	0.43	13.90	2.1	0.5257	1.94	0.94	2723.4	43.1	2758	11	1
Zr-5.1	0.14	363	209	0.60	13.78	1.9	0.5282	1.86	0.97	2734.1	41.4	2736	8	0
Zr-6.1	-0.02	216	100	0.48	14.03	2.0	0.5374	1.91	0.94	2772.4	43.2	2736	11	-1
Zr-8.1	-0.06	261	151	0.60	14.29	2.0	0.5484	1.92	0.96	2818.6	43.8	2734	10	-3
Zr-9.1	-0.07	223	121	0.56	13.91	2.0	0.5327	1.92	0.94	2752.9	43.1	2737	11	-1
Zr-10.1	0.12	489	255	0.54	14.06	1.9	0.5321	1.84	0.97	2750.3	41.2	2756	7	0
Zr-11.1	-0.02	526	311	0.61	13.84	1.9	0.5291	1.84	0.98	2737.8	41.0	2740	7	0
<i>Serra Dourada Granite (GMCL 40A)</i>														
Zr-1.1	-0.22	146	181	1.28	16.41	2.3	0.5857	2.1	.934	2972.0	51.1	2852	13	-4
Zr-3.1	-0.19	330	114	0.36	16.13	1.9	0.5756	1.9	.967	2930.7	44.1	2852	8	-3
Zr-4.1	0.77	271	153	0.58	15.77	2.2	0.5700	2.0	.935	2908.0	47.7	2832	13	-3
Zr-6.1	0.04	273	233	0.88	14.99	2.0	0.5385	1.9	.954	2777.3	43.5	2841	10	2
Zr-10.1	0.06	282	60	0.22	15.30	2.0	0.5469	1.9	.957	2812.1	43.8	2850	9	1
<i>Campina Verde Tonalite (GMCL 01)</i>														
Zr-1.1	0.10	91	59	0.67	16.30	2.4	0.5721	2.15	0.89	2916.6	50.4	2879	18	-1
Zr-2.1	-0.19	174	166	0.98	16.80	2.2	0.5884	2.03	0.94	2982.7	48.5	2883	12	-3
Zr-3.1	0.34	120	75	0.65	16.25	2.3	0.5676	2.06	0.91	2898.1	48.0	2887	15	0
Zr-4.1	0.69	178	84	0.49	16.06	2.2	0.5719	1.97	0.89	2915.5	46.3	2856	16	-2
Zr-5.1	0.04	240	135	0.58	16.06	2.1	0.5724	1.93	0.94	2917.6	45.2	2854	12	-2
<i>Campina Verde Tonalite (GMCL 66)</i>														
Zr-1.1	-0.12	100	77	0.79	16.98	3.6	.5906	3.5	.967	2991.9	84.1	2894	15	-3
Zr-3.1	0.07	107	79	0.76	16.84	3.6	.5916	3.5	.971	2996.0	84.7	2878	14	-4
Zr-4.1	0.10	125	75	0.62	16.14	3.6	.5761	3.5	.971	2932.8	82.4	2852	14	-3
Zr-5.1	0.25	251	121	0.50	15.29	3.5	.5456	3.5	.982	2807.0	79.3	2852	11	2
Zr-7.1	-0.05	199	113	0.59	17.13	3.5	.6051	3.5	.982	3050.5	84.6	2869	11	-6
Zr-8.1	0.06	143	118	0.85	16.60	3.7	.5823	3.6	.976	2958.2	84.7	2880	13	-3
Zr-9.1	0.11	282	147	0.54	16.05	3.6	.5667	3.6	.986	2894.1	82.9	2870	10	-1
Zr-10.1	0.00	219	120	0.57	16.98	3.5	.5955	3.5	.984	3011.6	83.5	2881	10	-4
Zr-12.1	0.00	244	119	0.51	16.69	3.5	.5815	3.5	.985	2955.0	81.9	2891	10	-2

Supplementary Table 2 Summary of the U-Pb LA-MC-ICPMS monazite data

Zircon Grain	Isotopic ratios								Ages									
	^{206}Pb	^{204}Pb	$^{207}\text{Pb}/^{206}\text{Pb}$	2σ	$^{207}\text{Pb}/^{235}\text{U}$	2σ	$^{206}\text{Pb}/^{238}\text{U}$	2σ	$^{207}\text{Pb}/^{206}\text{Pb}$	2σ	$^{207}\text{Pb}/^{235}\text{U}$	2σ	$^{206}\text{Pb}/^{238}\text{U}$	2σ	% disc	r		
Bacaba deposit – ore (BACD 25/229.25)																		
M5B	86964	297	0.1277	0.0013	6.952	0.3946	0.3948	0.0221	2067	17	2105	49	2145	101	-4.4	0.985		
M6A	137153	163	0.1271	0.0013	6.750	0.3923	0.3851	0.0220	2059	18	2079	50	2100	102	-2.4	0.985		
M4A	290595	163	0.1272	0.0012	6.748	0.3228	0.3848	0.0181	2059	16	2079	41	2099	83	-2.2	0.981		
M4B	266369	138	0.1265	0.0012	6.650	0.4163	0.3814	0.0236	2049	17	2066	54	2083	109	-1.9	0.989		
M6B	56061	148	0.1277	0.0014	6.731	0.5307	0.3822	0.0298	2067	19	2077	67	2086	138	-1.1	0.990		
M3A	57800	786	0.1271	0.0012	6.645	0.2871	0.3793	0.0160	2058	17	2065	37	2073	74	-0.8	0.974		
M5A	140758	206	0.1275	0.0013	6.616	0.5201	0.3763	0.0293	2064	18	2062	67	2059	136	0.3	0.991		
M8B	89216	126	0.1283	0.0012	6.688	0.5004	0.3782	0.0281	2074	17	2071	64	2068	130	0.4	0.992		
M8A	129703	122	0.1269	0.0014	6.523	0.3715	0.3730	0.0209	2055	19	2049	49	2043	97	0.7	0.982		
M24A	387517	90	0.1262	0.0012	6.374	0.3880	0.3663	0.0220	2046	16	2029	52	2012	103	1.9	0.988		
M10A	123810	133	0.1273	0.0012	6.463	0.4407	0.3682	0.0248	2061	17	2041	58	2021	116	2.3	0.990		
M25A	37121	61	0.1258	0.0015	6.268	0.3166	0.3615	0.0177	2040	22	2014	43	1989	83	2.9	0.970		
M14A	168625	110	0.1274	0.0012	6.423	0.3812	0.3656	0.0214	2063	17	2035	51	2009	100	3.0	0.987		
M23A	184829	84	0.1268	0.0012	6.286	0.5471	0.3597	0.0311	2053	17	2016	74	1981	146	4.1	0.994		
M7B	70369	108	0.1274	0.0013	6.291	0.4424	0.3583	0.0249	2062	19	2017	60	1974	117	5.0	0.989		
M7A	43731	102	0.1276	0.0015	6.282	0.3104	0.3571	0.0171	2065	21	2016	42	1968	81	5.4	0.971		
M12A	105043	73	0.1272	0.0012	6.207	0.3694	0.3538	0.0208	2060	17	2005	51	1953	98	6.0	0.987		
M21A	270712	94	0.1264	0.0012	6.035	0.2845	0.3463	0.0160	2048	16	1981	40	1917	76	7.4	0.981		
M19A	120333	107	0.1268	0.0012	5.998	0.3945	0.3431	0.0223	2054	17	1976	56	1902	106	8.5	0.989		
M2A	221896	143	0.1835	0.0018	12.841	0.6075	0.5074	0.0235	2685	16	2668	44	2646	100	1.8	0.979		
M2B	303721	150	0.1851	0.0017	12.781	0.7511	0.5009	0.0291	2699	15	2664	54	2618	124	3.7	0.988		
M9A	53913	112	0.1820	0.0019	12.399	0.7638	0.4941	0.0300	2671	17	2635	56	2588	128	3.8	0.986		
M18A	107111	120	0.1819	0.0017	12.244	0.5972	0.4881	0.0233	2670	16	2623	45	2563	100	4.9	0.980		
M9B	121353	118	0.1859	0.0023	12.411	0.6517	0.4842	0.0247	2706	20	2636	48	2545	107	7.2	0.973		
M16A	216446	89	0.1826	0.0018	11.843	0.7446	0.4704	0.0292	2676	17	2592	57	2485	127	8.6	0.987		
M20A	260567	122	0.1844	0.0018	11.943	0.6905	0.4698	0.0268	2693	16	2600	53	2483	116	9.4	0.986		
M15A	459154	94	0.1811	0.0017	11.358	0.9432	0.4550	0.0376	2663	15	2553	75	2417	164	11.0	0.994		
M22A	140973	111	0.1824	0.0017	11.007	0.5969	0.4377	0.0234	2675	15	2524	49	2340	104	14.9	0.985		
Bacaba deposit – Albite altered and silicified Serra Dourada Granite (BACD 15/237.4)																		
M9B	184434	151	0.1842	0.0017	12.769	0.7944	0.5027	0.0309	2691	15	2663	57	2625	131	3.0	0.989		
M10B	307676	151	0.1843	0.0018	13.996	0.6989	0.5507	0.0270	2692	16	2749	46	2828	111	-6.2	0.981		
M9A	186755	175	0.1845	0.0017	13.129	0.7195	0.5161	0.0279	2694	16	2689	50	2683	117	0.5	0.985		
M16A	231049	97	0.1855	0.0017	12.423	0.8209	0.4857	0.0318	2703	15	2637	60	2552	136	6.7	0.990		
M7B	129457	176	0.1857	0.0018	12.445	0.6796	0.4860	0.0261	2705	16	2639	50	2553	112	6.8	0.984		
M14A	198894	301	0.1862	0.0017	13.325	0.7966	0.5191	0.0307	2709	15	2703	55	2695	129	0.6	0.988		
M11A	406621	151	0.1867	0.0017	12.662	0.6743	0.4919	0.0258	2713	15	2655	49	2579	111	6.0	0.985		
M2B	430405	213	0.1867	0.0018	13.140	0.7384	0.5103	0.0283	2714	15	2690	52	2658	120	2.5	0.986		
M5A	682771	188	0.1870	0.0018	12.588	0.8923	0.4881	0.0343	2716	16	2649	65	2562	147	6.9	0.991		
M19A	252120	100	0.1873	0.0017	12.435	0.5362	0.4815	0.0203	2719	15	2638	40	2534	88	8.2	0.978		
M5B	417436	530	0.1875	0.0018	12.743	0.5639	0.4930	0.0213	2720	15	2661	41	2584	91	6.1	0.977		
M4B	291953	206	0.1875	0.0017	12.596	0.8617	0.4871	0.0330	2721	15	2650	62	2558	142	7.2	0.991		
M20A	266759	101	0.1876	0.0017	12.359	0.7651	0.4778	0.0292	2721	15	2632	57	2518	126	9.0	0.989		
M12A	178563	148	0.1878	0.0017	12.545	0.7797	0.4845	0.0298	2723	15	2646	57	2547	128	7.8	0.989		
M8B	197884	157	0.1878	0.0017	12.462	0.5318	0.4812	0.0201	2723	15	2640	39	2533	87	8.5	0.977		
M1B	192192	211	0.1878	0.0018	12.769	0.7926	0.4931	0.0302	2723	16	2663	57	2584	129	6.2	0.988		
M18A	420969	99	0.1879	0.0017	12.294	0.7300	0.4746	0.0278	2723	15	2627	54	2504	121	9.7	0.988		
M1A	254076	190	0.1879	0.0019	12.769	0.8306	0.4929	0.0317	2724	16	2663	59	2583	135	6.3	0.988		
M8A	188932	199	0.1880	0.0017	12.419	0.6614	0.4791	0.0251	2725	15	2637	49	2524	109	8.9	0.985		
M17A	274934	117	0.1881	0.0017	12.918	0.6594	0.4981	0.0250	2726	15	2674	47	2605	107	5.4	0.984		

Supplementary Table 2 (continued)

Zircon Grain	Isotopic ratios								Ages							
	^{206}Pb	^{204}Pb	$^{207}\text{Pb}/^{206}\text{Pb}$	2σ	$^{207}\text{Pb}/^{235}\text{U}$	2σ	$^{206}\text{Pb}/^{238}\text{U}$	2σ	$^{207}\text{Pb}/^{206}\text{Pb}$	2σ	$^{207}\text{Pb}/^{235}\text{U}$	2σ	$^{206}\text{Pb}/^{238}\text{U}$	2σ	% disc	r
<i>Bacaba deposit – Albite altered and silicified Serra Dourada Granite (BACD 15/237.4)</i>																
M6B	188749	167	0.1882	0.0017	12.064	0.8058	0.4650	0.0308	2726	15	2609	61	2461	134	11.7	0.990
M13A	295568	158	0.1882	0.0017	12.807	0.9575	0.4936	0.0366	2726	15	2666	68	2586	156	6.2	0.993
M10A	235625	172	0.1882	0.0017	12.716	0.8793	0.4900	0.0336	2727	15	2659	63	2571	144	6.9	0.991
M15A	381189	131	0.1883	0.0017	12.890	0.6119	0.4966	0.0231	2727	15	2672	44	2599	99	5.7	0.981
<i>Bacuri deposit – chlorite, biotite and scapolite altered rock (BRID 07/115.42)</i>																
M8A	287334	5	0.1819	0.0017	12.760	0.6296	0.5087	0.0246	2670	16	2662	45	2651	104	0.9	0.981
M7B	447060	10	0.1826	0.0019	13.740	1.0894	0.5458	0.0429	2676	17	2732	72	2808	177	-6.1	0.992
M16A	269854	3	0.1827	0.0017	13.660	0.5523	0.5423	0.0214	2677	15	2726	38	2793	89	-5.3	0.974
M5A	528116	18	0.1827	0.0017	14.193	0.6910	0.5633	0.0269	2678	15	2763	45	2880	110	-9.4	0.982
M8B	241373	18	0.1837	0.0017	12.455	0.7077	0.4917	0.0276	2687	15	2639	52	2578	118	4.9	0.987
M7A	433983	58	0.1841	0.0017	14.409	1.0185	0.5675	0.0398	2690	16	2777	65	2898	161	-9.6	0.991
M10B	406313	12	0.1842	0.0018	13.409	0.7709	0.5279	0.0299	2691	16	2709	53	2733	125	-1.9	0.985
M10A	330831	32	0.1843	0.0017	13.340	1.0731	0.5248	0.0419	2692	15	2704	73	2720	175	-1.2	0.993
M12A	422658	7	0.1846	0.0017	13.027	0.7928	0.5119	0.0308	2695	15	2682	56	2665	130	1.4	0.988
M18A	300205	5	0.1850	0.0018	13.510	0.5580	0.5295	0.0213	2699	16	2716	38	2740	89	-1.9	0.973
M1B	1305657	54	0.1851	0.0018	13.194	0.5418	0.5169	0.0206	2699	16	2694	38	2686	87	0.6	0.973
M9B	1382162	20	0.1851	0.0018	13.426	0.7820	0.5260	0.0302	2699	16	2710	54	2724	126	-1.1	0.987
M14A	278019	9	0.1853	0.0018	13.572	0.4839	0.5313	0.0182	2701	16	2720	33	2747	76	-2.1	0.962
M6B	1076099	20	0.1857	0.0018	13.038	0.9023	0.5093	0.0349	2704	16	2682	63	2653	147	2.3	0.990
M11B	921983	12	0.1857	0.0018	13.381	0.6077	0.5226	0.0232	2704	16	2707	42	2710	98	-0.3	0.978
M1A	1349882	61	0.1857	0.0018	12.891	0.7348	0.5033	0.0283	2705	16	2672	52	2628	120	3.5	0.986
M4B	1008648	47	0.1859	0.0017	13.400	0.7142	0.5228	0.0275	2706	15	2708	49	2711	115	-0.2	0.985
M13A	330538	55	0.1861	0.0018	13.802	0.5662	0.5379	0.0214	2708	16	2736	38	2775	89	-3.0	0.971
M3A	1148481	17	0.1863	0.0017	13.253	0.6904	0.5160	0.0264	2709	15	2698	48	2682	111	1.2	0.984
M6A	1310813	45	0.1866	0.0018	12.720	1.0266	0.4943	0.0396	2713	16	2659	73	2589	169	5.5	0.993
M4A	1354247	37	0.1867	0.0017	13.053	0.9313	0.5071	0.0359	2713	15	2683	65	2644	152	3.1	0.992
M3B	1284766	31	0.1870	0.0018	14.199	1.2479	0.5509	0.0481	2716	16	2763	80	2829	197	-5.2	0.994
M11A	1547809	21	0.1870	0.0018	14.567	0.6045	0.5650	0.0228	2716	16	2787	39	2887	93	-7.8	0.971
M2A	1078492	60	0.1870	0.0017	13.486	0.8667	0.5230	0.0333	2716	15	2714	59	2712	139	0.2	0.989
M17A	1149293	2	0.1873	0.0017	13.375	0.5765	0.5179	0.0218	2719	15	2707	40	2690	92	1.3	0.977
M5B	1544003	19	0.1874	0.0018	12.848	0.8970	0.4972	0.0344	2720	15	2669	64	2602	146	5.3	0.991
M9A	1415687	22	0.1876	0.0019	13.726	0.7466	0.5308	0.0284	2721	16	2731	50	2745	118	-1.1	0.983
M15A	1071401	11	0.1876	0.0019	13.758	0.4620	0.5318	0.0170	2721	17	2733	31	2749	71	-1.3	0.952
M2B	1383993	31	0.1877	0.0017	13.371	0.9724	0.5165	0.0373	2722	15	2706	66	2684	157	1.7	0.992
M20A	1240731	10	0.1889	0.0019	13.260	0.4864	0.5091	0.0179	2733	17	2698	34	2653	76	3.6	0.960

8. CONSIDERAÇÕES FINAIS: Síntese da evolução metalognética do Cinturão Sul do Cobre

A caracterização geológica detalhada de parte do Cinturão do Sul do Cobre aliada aos estudos geocronológicos possibilitou uma compreensão dos principais eventos magmáticos e hidrotermais que atuaram nesse importante cinturão metalogenético. Unidades litológicas como rochas subvulcânicas félsicas, rochas vulcânicas e intrusivas máficas, rochas metaultramáficas, granitos (*latu sensu*) e migmatitos foram caracterizados.

Com base nos dados apresentados nos dois artigos, e outros disponíveis na literatura (e.g., Huhn *et al.*, 1999b; Feio *et al.*, 2012a,b) foi possível identificar ao menos 6 eventos magmáticos que teriam atuado na porção centro-oeste do Cinturão Sul do Cobre:

- I. 3,0 Ga, relacionado à colocação do Granito Sequeirinho e do Tonalito Bacaba. Esse evento corresponde às idades de cristalização mais antigas registradas na Província Carajás. Idades semelhantes foram obtidas nos protólitos das rochas granulíticas da Suíte Chicrim-Cateté;
- II. 2,97-2,96 Ga, associado à formação da rocha metavulcânica Pista e do Granito Canaã dos Carajás. A rocha metavulcânica Pista corresponde à rocha vulcânica mais antiga do Domínio Carajás. Contudo, rochas vulcânicas tão antigas são identificadas no Domínio Rio Maria (e.g., *greenstone belts* Lagoa Seca e Gradaús; Macambira e Lancelot, 1996; Pimentel e Machado, 1994; Tassinari *et al.*, 2005). Apesar de especulativo, a rocha vulcânica hospedeira do corpo Pista poderia representar uma lasca tectônica associada a esses *greenstones belts* de 3,0-2,97 Ga do Domínio Rio Maria ou, alternativamente, sugerir uma história evolutiva semelhante para os dois domínios anterior à instalação da Bacia Carajás;
- III. 2,87 Ga, representado pelo Tonalito Campina Verde e pelo Trondjemito Rio Verde. De acordo com Feio *et al.* (2012a), o Trondjemito Rio Verde teria afinidade geoquímica similar à rochas TTG do Domínio Rio Maria, enquanto que o Tonalito Campina Verde seria cálcio-alcalino. Essa idade ao redor de 2,87 Ga é contemporânea ao evento de migmatização que afetou o migmatito do Complexo Xingu e ao evento de granulitização da Suíte Chicrin-Cateté, e é próxima à idade de ca. 2,86-2,84 Ga atribuída à estabilização tectônica do Domínio Rio Maria;

- IV. 2,84 Ga, caracterizado pela colocação do Granito Serra Dourada, com afinidade cálcio-alcalina e características pós-colisionais;
- V. 2,74 Ga, representado pelo magmatismo neoarqueano registrado unicamente no Domínio Carajás. Esse evento é evidenciado pela intrusão de corpos graníticos (granito granofílico Sossego, quartzo-feldspato pórfiros, Suítes Planalto e Pedra Branca) e gabróicos (gabronorito, diopsídio Norito Pium, Diorito Cristalino), apontando para um importante magmatismo bimodal de ampla ocorrência, que poderia ser típico de limite de blocos crustais;
- VI. 1,88 Ga, associado aos granitos alcalinos do tipo-A, a exemplo do Granito Rio Branco.

Em relação aos eventos metalogenéticos responsáveis pela alteração hidrotermal e mineralização no Cinturão Sul do Cobre, os dados isotópicos apresentados nos dois artigos (depósito Sossego, Bacaba e Bacuri) somados aos dados presentes na literatura (depósitos Alvo 118, Visconde e Cristalino; Soares *et al.*, 2001; Tallarico, 2003; Silva *et al.*, 2012) apontam para a superposição de múltiplos eventos hidrotermais e/ou mineralizantes durante o Neoarqueano e Paleoproterozóico. De maneira resumida, esses diversos eventos hidrotermais teriam ocorrido em:

- i. 2,76 Ga - formação de molibdenita, presente em vênula mineralizada hospedada pelo Granito Serra Dourada no depósito Bacuri, que precede o estágio principal de mineralização nesse depósito;
- ii. 2,71-2,70 Ga - precipitação de monazita hidrotermal associada a calcopirita dos corpos de minério nos depósitos Bacuri, Bacaba, e Corpo Sequeirinho, e formação de molibdenita no corpo Pista;
- iii. 2,68 Ga - evidenciado pela ocorrência de monazita hidrotermal no depósito Bacaba e molibdenita no corpo Pista;
- iv. 2,05 Ga - formação de monazita hidrotermal no depósito Bacaba;
- v. 1,90 Ga - caracterizado pela cristalização de monazita hidrotermal no corpo Sossego;
- vi. 1,88-1,87 Ga - sugerido a partir da datação de monazita hidrotermal nos corpos Sossego e Curral, e xenotima hidrotermal no depósito Alvo 118.

As idades Pb-Pb em calcopirita dos depósitos Cristalino (2.700 ± 29 Ma, MSWD = 656, Soares *et al.*, 2001) e Visconde (2.747 ± 140 Ma, MSWD=12, Silva *et al.*, 2012) não foram

mencionadas acima em função dos grandes erros associados. Contudo, esses dados sugerem que o evento responsável pela formação do minério é de idade neoarqueana.

Apesar das diversas idades obtidas em minerais hidrotermais, os intervalos entre 2,71-2,68 e 1,90-1,88 Ga são interpretados como os eventos mineralizantes IOCG responsáveis pelo minério cupro-aurífero no Cinturão Sul do Cobre. Os demais eventos hidrotermais não necessariamente estariam relacionados com a precipitação de novos corpos de minério, mas sim ao desenvolvimento de novas assembleias hidrotermais a partir do metassomatismo das rochas hospedeiras. Adicionalmente, estariam associados ao retrabalhamento das áreas previamente mineralizadas e hidrotermalizadas.

Nesse contexto, a recorrência de eventos hidrotermais é fortemente sugerida para o Cinturão Sul do Cobre. Esse processo implica na lixiviação e remobilização de elementos de áreas previamente afetadas pela alteração hidrotermal, incluindo as zonas com intensa alteração sódica com escapolita (marialita), presentes em extensas áreas do Cinturão Sul do Cobre. Essa interação, com elevadas razões fluido-rocha, seria responsável por modificações na composição dos fluidos hidrotermais, que se tornariam muito salinos em função da liberação de cloro e sódio presentes na marialita, e consequentemente eficientes no transporte de metais (Cu). As grandes estruturas regionais, a exemplo da zona de cisalhamento no contato sul entre a Bacia Carajás e as rochas do embasamento, teriam atuado com importantes condutos para a circulação desses fluidos hidrotermais.

O evento hidrotermal de 2,76 Ga é contemporâneo à deposição das rochas metavulcano-sedimentares que preencheram a Bacia Carajás. Durante a deposição do Supergrupo Itacaiúnas, fluidos hidrotermais provenientes da bacia teriam circulado ao longo de fraquezas crustais, a exemplo da foliação milonítica com direção WNW-ESE presente nas rochas do embasamento (e.g., Granito Serra Dourada). Esses fluidos modificados teriam sido responsáveis pela alteração hidrotermal e formação de molibdenita na área do depósito Bacuri.

O intervalo de formação de mineralizações IOCG entre 2,71-2,68 Ga, responsáveis pelos depósitos neoarqueanos (Sequeirinho, Pista, Bacaba, Bacuri, Cristalino e Visconde), aparentemente não está diretamente associado à eventos magmáticos registrados na Província Carajás. Fontes alternativas de calor possivelmente possibilitaram a circulação regional de fluidos hidrotermais, que estariam ligados aos sistemas mineralizantes neoarqueanos. Esse fluxo de calor poderia estar vinculado à reativações das zonas de cisalhamento regionais, especialmente àquela

próxima aos depósitos do Cinturão Sul do Cobre. Segundo Pinheiro e Holdsworth (1997), as rochas do embasamento da Bacia Carajás teriam sido deformadas sob regime dúctil de alta temperatura em 2,85 Ga (transpressão sinistral), e experimentado diversos eventos de reativações transcorrentes (dextrais e sinistrais) durante o Arqueano e Paleoproterozóico. Segundo Domingos (2009), a inversão tectônica da Bacia Carajás, iniciada em ca. 2,7 Ga, teria envolvido uma fase regional de transpressão sinistral controlada por encurtamento crustal na direção NNE. Essa inversão tectônica teria causado a reativação dos sistemas de falha *strike-slip* Carajás e Cinzento. Durante esse evento tectônico, o desenvolvimento da foliação milonítica WNW-ESE foi controlada por planos paralelos de fraqueza pré-existentes, formados durante evento dúctil anterior (2,85 Ga) (Domingos, 2009). Essas descontinuidades estruturais nas rochas do embasamento teriam facilitado a percolação de fluidos hidrotermais responsáveis pela precipitação do minério de cobre.

O evento hidrotermal riaciano (2,05 Ga), responsável pela cristalização de monazita no depósito Bacaba, também não se sobrepõe a nenhum evento magmático registrado na Província Carajás. Esse sistema hidrotermal também poderia ter sido desencadeado por novas reativações das zonas de cisalhamento regionais, relacionadas à fraca inversão tectônica da Bacia Carajás entre 2,0 e 1,8 Ga. Alternativamente, porém pouco provável, o evento hidrotermal de 2,05 Ga poderia estar relacionado ao evento Transamazônico. Estudos recentes (Vasquez *et al.*, 2008b; Macambira *et al.*, 2009) propõem uma evolução em diversos estágios para o Domínio Bacajá (situado ao norte do Domínio Carajás), tendo início durante o Neoarqueano e término no Riaciano, entre 2,08-2,07 Ga, com a colisão desse bloco com o Domínio Carajás. Durante a amalgamação de blocos continentais, grandes quantidades de fluidos hidrotermais são liberadas e circulam na crosta através das grandes falhas crustais.

Em relação ao evento IOCG de 1,88 Ga, responsável pela formação dos corpos Sossego e Curral e pelo depósito Alvo 118, é proposto nesse estudo que a intensa granitogênese paleoproterozóica do tipo-A (e.g., Suíte Intrusiva Serra dos Carajás; Fig. 1) teria fornecido calor suficiente para a circulação dos fluidos hidrotermais em escala regional, e posterior deposição dos corpos de minério. Alternativamente, esses granitos do tipo-A também poderiam ter fornecido os fluidos diretamente envolvidos na gênese dos depósitos. Nesse caso, entretanto, uma intensa interação e lixiviação das rochas hospedeiras regionais seria necessária para fornecer componentes metalíferos para o sistema hidrotermal, uma vez que granitos anorogênicos típicos

(e.g., reduzidos, com baixo conteúdo de água e colocação profunda) tem especialização metalogenética principalmente para depósitos de estanho e tungstênio, e não Cu-Au com expressivo conteúdo de hematita (e/ou magnetita).

O Cinturão Sul do Cobre difere, em termos de evolução metalogenética, do Cinturão Norte do Cobre, hospedeiro dos depósitos Salobo, Igarapé-Bahia, Gameleira, dentre outros. Nesse cinturão norte, métodos geocronológicos confiáveis, como Re-Os em molibdenita (depósito Salobo, Réquia *et al.*, 2003) e U-Pb SHRIMP II em monazita hidrotermal (depósito Igarapé-Bahia, Tallarico *et al.*, 2005) apontam para um importante evento mineralizante IOCG em 2,57 Ga. A circulação de fluidos hidrotermais ligada à esse evento neoarqueano possivelmente foi restrita à porção norte do Domínio Carajás, uma vez que nenhuma evidência para esse evento de 2,57 Ga foi encontrada no Cinturão Sul do Cobre.

REFERÊNCIAS BIBLIOGRÁFICAS

- Araújo O.J.B. & Maia R.G.N. 1991. - Serra dos Carajás, folha SB.22-ZA, Estado do Pará. Programa Levantamentos Geológicos Básicos do Brasil. Companhia de Pesquisa de Recursos Minerais. 136 p.
- Araújo O.J.B., Maia R.G.N., Jorge-João, X.S. Costa, J.B.S. 1988. A megaestruturação da folha Serra dos Carajás. In: Congresso Latino Americano de Geologia., 7, pp. 324–333.
- Augusto R.A., Monteiro L.V.S., Xavier R., Souza Filho C.R. 2008. Zonas de alteração hidrotermal e paragênese do minério de cobre do Alvo Bacaba, Província Mineral de Carajás (PA). Rev. Brasil. Geoci. 38(2): 263-277.
- Avelar V.G., Lafon J.M., Correia JR F.C., Macambira, E.M.B. 1999. O Magmatismo arqueano da região de Tucumã-Província Mineral de Carajás: novos resultados geocronológicos. Revista Brasileira de Geociências. 29(4): 453-460
- Barbosa J.P.O. 2004. Geologia estrutural, geoquímica, petrografia e geocronologia de granitóides da região do Igarapé Gelado, norte da Província Mineral de Carajás: Dissertação de Mestrado, Universidade Federal do Pará, Belém, 112 p.
- Barros C.E.M., Macambira M.J.B., Barbey P., Scheller T. 2004. Dados isotópicos Pb–Pb em zircão (evaporação) e Sm–Nd do Complexo Granítico Estrela, Província Mineral de Carajás, Brasil: implicações petrológicas e tectônicas. Rev. Brasil. Geoci. 34, 531–538.
- Barros C.E.M., Nascimento, V.M. do, Medeiros Filho, C.A. 2010. Revisão da estratigrafia das rochas da Serra Leste, Província Mineral de Carajás. Rev. Bras. Geoc., 40: 167-174
- Barros C.E.M., Sardinha A.S., Barbosa J.P.O., Macambira M.J.B. 2009. Structure, Petrology, Geochemistry and zircon U/Pb and Pb/Pb geochronology of the synkinematic Archean (2.7 Ga) A-type granites from the Carajás Metallogenic Province, northern Brazil, The Canadian Mineralogist. 47: 1423-1440
- Beisiegel V.R., Bernadelli A.L., Drummond N.F., Ruff A.W., Tremaine J.W. 1973. Geologia e recursos minerais da Serra dos Carajás. Rev. Bras. Geoc., 3: 215-242.
- Bortholoto D.F.A. 2007. O depósito de óxido de Fe-Cu-Au Alvo 118, Província Mineral de Carajás (PA): rochas hospedeiras, alteração hidrotermal e paragênese do minério. Trabalho de conclusão de curso, Universidade Estadual de Campinas, 47p.
- Carvalho E.R. 2009. Caracterização geológica e gênese das mineralizações de óxido de Fe-Cu-Au e metais associados na Província Mineral de Carajás: estudo de caso do depósito de Sossego: Tese de doutorado, Universidade Estadual de Campinas, 141 p.
- Craveiro G.S., Villas R.N., Silva A.R.C. 2012a. Depósito Cu-Au Visconde, Carajás (PA): geologia e alteração hidrotermal das rochas encaixantes. Revista Brasileira de Geociências 42(3):453-470.
- Craveiro G.S., Villas R.N., Silva A.R.C. 2012b. Depósito Visconde: fluidos hidrotermais e implicações metalogenéticas. In 46º Congresso Brasileiro de Geologia, Santos.(CD-ROM)
- Dall'Agnol R., Costi H.T., Leite A.A., Magalhães M.S., Teixeira N.P. 1999a. Rapakivi granites from Brazil and adjacent areas. Precambrian Research 95, 9– 39.
- Dall'Agnol R., Rämö O.T., Magalhães M.S., Macambira M.J.B. 1999b. Petrology of the anorogenic, oxidised Jamon and Musa granites, Amazonian craton: implications for the genesis of Proterozoic A-type granites. Lithos 46, 431– 462.
- Dall'Agnol R., Teixeira N.P., Rämö O.T., Moura C.A.V., Macambira, M.J.B., Oliveira, D.C. 2005. Petrogenesis of the Paleoproterozoic, rapakivi, A-type granites of the Archean Carajás Metallogenic Province, Brazil. Lithos 80: 101–129.
- Dall'Agnol R., Oliveira M.A., Almeida J.A.C., Althoff F.J., Leite A.A.S., Oliveira D.C., Barros C.E.M. 2006. Archean and paleoproterozoic granitoids of the Carajás Metallogenic Province, eastern Amazonian craton. In: Symposium on magmatism, crustal evolution and metallogenesis of the Amazoniam Craton, Belém, Excursion Guide, p.: 99-150.

- Dall'Agnol R., Oliveira D.C. 2007. Oxidized, magnetite-series, rapakivi-type granites of Carajás, Brazil: implications for classification and petrogenesis of A-type granites. *Lithos* 93, 215–233.
- Dardenne M.A., Ferreira Filho C.F. Meirelles M.R. 1988. The role of shoshonitic and calc-alkaline suites in the tectonic evolution of the Carajás district, Brazil. *Journal of South American Earth Sciences*, 1: 363–372.
- Dias G.S., Macambira M.B., Dall'Ágnol R., Soares A.D.V., Barros C.E.M. 1996. Datações de zircões de sill de metagabro: comprovação de idade arqueana da Formação Águas Claras, Carajás, Pará. In: Simpósio de Geologia da Amazônia, 5, SBG, Belém, pp. 376-378.
- DOCEGEO 1988. Revisão litoestratigráfica da Província Mineral de Carajás – Litoestratigrafia e principais depósitos minerais. 35o Congresso Brasileiro de Geologia, Belém, SBG, Proceedings, 11–54.
- Domingos F. 2009. The structural setting of the Canaã dos Carajás region and Sossego-Sequeirinho deposits, Carajás, Brazil: Tese de doutorado, Durham University, 483 p. Available at Durham E-Theses Online: <http://etheses.dur.ac.uk/144/>.
- Fabre S., Nédélec A., Poitrasson F., Strauss H., Thomazo C., Nogueira A. 2011. Iron and Sulphur isotopes from the Carajás mining province (Pará, Brazil): implications for the oxidation of the ocean and the atmosphere across the Archaean-Proterozoic transition: *Chemical Geology*, v. 289, p. 124-139.
- Feio G.R.L., Dall'Agnol R., Dantas E.L., Macambira M.J.B., Santos J.O.S., Althoff F.J., Soares J.E.B. 2012a. Archean granitoid magmatism in the Canaã dos Carajás area: Implications for crustal evolution of the Carajás province, Amazonian craton, Brazil. *Precambrian Research* In press, Corrected Proof.
- Feio G.R.L., Dall'Agnol R., Dantas EL, Macambira MJB, Gomes ACB, Sardinha AS, Oliveira DC, Santos RD, Santos PA. 2012b. Geochemistry, geochronology, and origin of the Neoarchean Planalto Granite suite, Carajás, Amazonian craton: A-type or hydrated charnockitic granites?. *Lithos*, 151: 57-73
- Ferreira Filho C.F., Cançado F., Correa C., Macambira E.M.B., Junqueira-Brod T.C., Siepierski L. 2007. Mineralizações estratiformes de PGE-Ni associadas a complexos acamadados em Carajás: os exemplos de Luanga e Serra da Onça. In: Rosa-Costa, L. T., Klein, E.L., Viglio, E.P. (Ed.). Contribuições à geologia da Amazônia. Belém: SBG-Núcleo Norte, v. 5, p. 1-14.
- Galarza M.A., & Macambira M.J.B. 2002a. Petrologia e geocronologia das rochas encaixantes do depósito de Cu–Au Igarapé Bahia, Província Mineral de Carajás, Pará, Brasil, in: Kein, E.L., Vasquez, M.L., Rosa-Costa, L.T., Contribuições à Geologia da Amazônia, v. 3, SBG/NN, Belém, p. 153–168.
- Galarza M.A., & Macambira M.J.B. 2002b. Geocronologia e Evolução Crustal da Área do Depósito de Cu–Au Gameleira, Província Mineral de Carajás (Pará), Brasil: *Geologia USP Série Científica* v. 2, p. 143–159.
- Galarza M.A., Macambira M.J.B. Moura C.A.V. 2003. Geocronologia Pb–Pb e Sm–Nd das rochas maficas do depósito Igarapé Bahia, Província Mineral de Carajás (PA). VII Simpósio de Geologia da Amazônia, SBG, [CD-ROM]
- Galarza M.A., Macambira M.J.B., Villas R.N. 2008. Dating and isotopic characteristics (Pb and S) of the Fe oxide–Cu–Au–U–REE Igarapé Bahia ore deposit, Carajás mineral province, Pará state, Brazil. *Journal of South American Earth Sciences*. 25:377-397.
- Gibbs A.K. Wirth K.R., Hirata W.K., Olszewski Jr. W.J. 1986. Age and composition of the Grão Pará Group volcanics, Serra dos Carajás. *Revista Brasileira de Geociências*, 16: 201–211.
- Gomes A.C.B. 2003. Geologia, petrografia e geoquímica dos granitóides de Canaã dos Carajás, SE do Estado do Pará. Belém. Dissertação de Mestrado, UFPA, 160p.
- Grainger C.J., Groves D.I., Tallarico F.H.B., Fletcher I.R. 2008. Metallogenesis of the Carajás Mineral Province, Southern Amazon Craton, Brazil: Varying styles of Archean through Paleoproterozoic to Neoproterozoic base- and precious-metal mineralization. *Ore Geology Reviews*, 33: 451-489.

- Groves D.I., Bierlein F.P., Meinert L.D., Hitzman M.W. 2010. Iron Oxide Copper-Gold (IOCG) Deposits through Earth History: Implications for Origin, Lithospheric Setting, and Distinction from Other Epigenetic Iron Oxide Deposits: *Economic Geology*, v. 105, p. 641-654.
- Hirata W.K., Rigon J.C., Kadekaru K., Cordeiro A.A.C., Meireles E.A. 1982. Geologia Regional da Província Mineral de Carajás. In: Simpósio de Geologia da Amazônia, 1, Belém, SBG/NO, p. 100–110.
- Hitzman M.W. 2000. Iron oxide–Cu–au deposits: what, where, when, and why. In: Porter TM (ed) *Hydrothermal iron oxide copper-gold and related deposits: a global perspective*. Australian Miner. Fund, Adelaide, Vol 1, p. 9–25.
- Hitzman M.W., Oreskes N., Einaudi M.T. 1992. Geological characteristics and tectonic setting of Proterozoic iron oxide (Cu–U–Au–REE) deposits. *Precambrian Research*, 58, 241–287.
- Holdsworth R. & Pinheiro R. 2000. The anatomy of shallow-crustal transpressional structures: insights from the Archean Carajás fault zone, Amazon, Brazil. *Journal of Structural Geology* 22: 1105–1123.
- Huhn S.R.B., Nascimento, J.A.S. 1997. São os depósitos cupríferos de Carajás do tipo Cu-Au-U-ETR? In: Costa, M.L., Angélica, R.S. (Coord.). *Contribuições à geologia da Amazônia*. Belém: SBG–Núcleo Norte, 1997. v. 1, p. 143–160.
- Huhn S.R.B., Souza C.I.J., Albuquerque M.C., Leal E.D., Brustolin V. 1999a. Descoberta do depósito Cu(Au) Cristalino: Geologia e mineralização associada região da Serra do Rabo - Carajás – PA. SBG/NO, Simpósio de Geologia da Amazônia, 6, pp 140–143.
- Huhn S.B., Macambira M.J.B., Dall’Agnol R. 1999b. Geologia e geocronologia Pb-Pb do Granito Alcalino Planalto, Região da Serra do Rabo, Carajás-PA. In: SBG, Simpósio de Geologia da Amazônia, 6, Boletim de Resumos, p. 463–466.
- Lafon J.M., Macambira M.J.B., Pidgeon R.T. 2000. Zircon U-Pb SHRIMP dating of Neoarchean magmatism in the southwestern part of the Carajás Province (eastern Amazonian Craton, Brazil). In: International Geological Congress, 31., Abstracts, Rio de Janeiro, [CD-ROM].
- Lancaster Oliveira J., Fanton J., Almeida A.J., Leveille R.A., Vieira S. 2000. Discovery and geology of the Sossego copper-gold deposit, Carajás District, Pará State, Brazil: International Geology Congress, 31st, Proceedings, International Union of Geological Sciences, [CD-ROM].
- Lindenmayer Z.G. 2003. Depósito de Cu–Au do Salobo, Serra dos Carajás: Uma revisão. In: L.H. Ronchi and F.J. Althoff (Eds.), *Caracterização e modelamento de depósitos minerais*. Editora Unisinos, São Leopoldo, 69–98.
- Lobato L.M., Roaière C.A., Silva R.C.F., Zucchetti M., Baars F.J., Seoane J.C.S., Rios F.J., Pimentel M., Mendes G.E. Monteiro A.M. 2005. A mineralização hidrotermal de ferro da Província Mineral de Carajás - controle estrutural e contexto na evolução metalogenética da Província. In: Marini, J.O.; Queiróz, E.T.; Ramos, W.B. (eds.), *Caracterização de distritos mineiros da Amazônia*. DNPM-CT-Mineral-ADIMB, 25–92.
- Macambira M.J.B., & Lancelot J. 1996. Time constraints of Archean Rio Maria crust, Southeastern Amazonian Craton, Brazil. *Intern. Geol. Rev.*, 38 (12): 1134–1142.
- Macambira E.M.B., & Vale A.G. 1997. São Félix do Xingu: folha SB.22-Y-B, Estado do Pará, escala 1:250.000. Texto Explicativo. Brasília: CPRM. 344 p., il. Programa Levantamentos Geológicos Básicos do Brasil (PLGB).
- Macambira E.M.B., & Ferreira Filho C.F. 2002. Fracionamento magmático dos corpos máfico-ultramáficos da Suíte Intrusiva Cateté – sudeste do Pará. In: Klein, E.L., Vasquez, M.L., Rosa-Costa, L.T. (Ed.). *Contribuições à geologia da Amazônia*. Belém: SBG-Núcleo Norte. v. 3, p. 105–114.
- Macambira J.B. 2003. O ambiente deposicional da Formação Carajás e uma proposta de modelo evolutivo para a Bacia Grão Pará. Tese de doutorado, Universidade Estadual de Campinas, 217p.
- Macambira M.J.B., Vasquez M.L., Silva D.C.C., Galarza M.A., Barros C.E.M., Camelo J.F. 2009. Crustal growth of the central-eastern Paleoproterozoic domain, SW Amazonian craton: Juvenile accretion vs. reworking. *Journal of South American Earth Sciences* 27 (2009) 235–246.

- Machado N., Lindenmayer D.H., Krough T.E., Lindenmayer Z.G. 1991. U-Pb geochronology of Archean magmatism and basement reactivation in the Carajás area, Amazon Shield, Brazil. *Precambrian Research*, 49:329-354
- Marschik R., Mathur R., Ruiz J., Leveille R., Almeida A.J. de 2005. Late Archean Cu-Au-Mo mineralization at Gameleira and Serra Verde, Carajás Mineral Province, Brazil: constraints from Re-Os molybdenite ages. *Mineralium Deposita* 39:983–991
- Marschik R., Spangenberg J.E., Leveille R.A., de Almeida, A.J. 2003. The Sossego iron oxide-Cu-Au deposit, Carajás, Brazil. In: Eliopoulos D et al (eds) *Mineral Exploration and Sustainable Development v 1*. Millpress, Rotterdam, p. 331–334
- Meirelles M.R., & Dardenne M.A. 1991. Vulcanismo basáltico de afinidade shoshonítica em ambiente de arco arqueano, Grupo Grão Pará, Serra dos Carajás, PA. *Revista Brasileira de Geociências*, 21: 41-50.
- Meirelles M.R. 1986. Geoquímica e petrologia dos jaspilitos e rochas vulcânicas associadas, Grupo Grão-Pará, Serra dos Carajás. Dissertação de Mestrado, UnB, pp.
- Melo G.H.C. 2010. Estudo de inclusões fluidas do depósito de cobre Alvo Bacaba, Província Mineral de Carajás. Unpublished undergraduate essay. 19 p.
- Melo G.H.C., Monteiro L.V.S., Xavier R.P., Moreto C.P.N., Silva M.A.D., Submetido, Bacuri copper deposit: host rocks, hydrothermal alteration and characterization of the copper ore, Carajás Province (PA). *Revista Brasileira de Geociências*, 15pp.
- Monteiro L.V.S., Xavier R.P., Carvalho E.R., Hitzman M.W., Johnson C.A., Souza Filho C.R., Torresi I. 2008a. Spatial and temporal zoning of hydrothermal alteration and mineralization in the Sossego iron oxide-copper-gold deposit, Carajás Mineral Province, Brazil: paragenesis and stable isotope constraints. *Mineralium Deposita*, 43:129–159.
- Monteiro L.V.S., Xavier R.P., Hitzman M.W., Juliani C., Souza Filho C.R., Carvalho E.R. 2008b. Mineral chemistry of ore and hydrothermal alteration at the Sossego iron oxide-copper-gold deposit, Carajás Mineral Province, Brazil. *Ore Geology Reviews*, 34:317-336.
- Morais R.P.S., & Alkmim F.F. 2005. O controle litoestrutural da mineralização de cobre do Depósito Sequeirinho, Canaã dos Carajás, PA. In: I Simpósio Brasileiro de Metalogenia, Gramado, [CD-ROM]
- Moreto C.P.N. 2010. O depósito de óxido de ferro-cobre-ouro Bacaba, Província Mineral de Carajás: Geocronologia U-Pb das rochas hospedeiras. Dissertação de mestrado. UNICAMP. 85p.
- Moreto C.P.N., Monteiro L.V.S., Xavier R.P., Amaral W.S., Santos T.J.S., Juliani C., and Souza Filho C.R. 2011. Mesoarchean (3.0 and 2.86 Ga) host rocks of the iron oxide-Cu-Au Bacaba deposit, Carajás Mineral Province: U-Pb geochronology and metallogenetic implications. *Mineralium Deposita* V. 46, pps. 789-811. DOI: 10.1007/s00126-011-0352-9.
- Mougeot R., Respaut J.P., Briqueu L., Ledru P., Milesi J.P., Macambira M.J.B., Huhn S.B. 1996a. Geochronological constrains for the age of the Águas Claras Formation (Carajás Province, Pará, Brazil). In: Congresso Brasileiro de Geologia, 39, Salvador, 1996. Anais., Salvador, SBG. 6:579-581.
- Mougeot R., Respaut J.P., Brique L., Ledru P., Milesi J.P., Lerouge C., Marcoux E., Huhn S.B., Macambira M.J.B. 1996b. Isotope geochemistry constrains for Cu, Au mineralizations and evolution of the Carajás Province (Para, Brazil). In: SBG, Congresso Brasileiro de Geologia, 39, Salvador, Anais, 7, 321-324 (in Portuguese).
- NCL Brasil. 2005. Revision de La Estimación de Recursos del Proyecto Cristalino. Vale S.A Internal Report, 1-103.
- Neves M.P. 2006. Estudos isotópicos (Pb-Pb, Sm-Nd, C e O) do depósito Cu-Au do Sossego, Província Mineral de Carajás. Dissertação de Mestrado. Universidade Federal do Pará. 116 p.
- Nogueira A.C.R., Truckenbrodt W., Pinheiro R.V.L. 1995. Formação Águas Claras, Pré-Cambriano da Serra dos Carajás: redescricao e redefinição litoestratigráfica. *Boletim do Museu Paraense Emílio Goeldi, Ciências da Terra*, (7), pg. 177-277.

- Oliveira D.C., Santos P.J.L., Gabriel E.O., Rodrigues D.S., Faresin A.C., Silva M.L.T., Sousa S.D., Santos R.V., Silva A.C., Souza M.C., Santos R.D., Macambira M.J.B. 2010. Aspectos geológicos e geocronológicos das rochas magmáticas e metamórficas da região entre os municípios de Água Azul do Norte e Canaã dos Carajás – Província Mineral de Carajás, In: SBG, Congresso Brasileiro de Geologia, 45, CDrom (in Portuguese).
- Pestilho A.L.S. 2008. Depósito de Cu-(Zn-Ni) do Alvo Castanha, Província Mineral de Carajás, PA: Evolução paragenética e dos fluidos mineralizantes. Trabalho de graduação, 86p.
- Pestilho A.L.S. 2011. Sistemática de isótopos estáveis aplicada à caracterização da evolução dos paleo-sistemas hidrotermais associados aos depósitos cupríferos Alvo Bacaba e Alvo Castanha, Província Mineral de Carajás, PA. Dissertação de mestrado. 71p.
- Pidgeon R.T., Macambira M.J.B., Lafon J.M. 2000. Th–U–Pb isotopic systems and internal structures of complex zircons from an enderbite from the Pium Complex, Carajás Province, Brazil: evidence for the ages of granulite facies metamorphism and the protolith of the enderbite. Chemical Geology 166, 159–171.
- Pimentel M.M., & Machado N. 1994. Geocronologia U–Pb dos terrenos granito-greenstone de Rio Maria, Pará. In: Cong. Bras. Geol., Anais, Sociedade Brasileira de Geologia, vol. 2, pp. 390–391.
- Pimentel M.M., Lindenmayer Z.G., Laux J.H., Armstrong R. Araújo J.C. 2003. Geochronology and Nd geochemistry of the Gameleira Cu-Au deposit, Serra dos Carajás, Brazil: 1.8–1.7 Ga hydrothermal alteration and mineralization. Journal of South American Earth Sciences, 15: 803-813.
- Pinheiro R.V.L., & Holdsworth R.E. 1997. Reactivation of Archaean *strike-slip* fault systems, Amazon region, Brazil. Journal of the Geological Society of London 154, 99–103.
- Pinheiro R.V.L., & Nogueira A.C.R. 2003. Carajás: Bacia transtensiva invertida em fl or positiva ou segmento de bacia extensional localmente invertida por transpressão? In: Simpósio de Geologia da Amazônia., 8, Res. Exp., SBG Núcleo Norte, [CD-ROM].
- Réquia K., Stein H., Fontboté L., and Chiaradia M. 2003. Re-Os and Pb-Pb geochronology of the Archean Salobo iron oxide copper–gold deposit, Carajás Mineral Province, northern Brazil: Mineralium Deposita, v. 38, p. 727-738.
- Ribeiro A.A. 2008. Litogequímica e geologia isotópica estável (C, S, O) do depósito Cupro-aurífero do Alvo Cristalino Sul, Província Mineral de Carajás, Pará, Dissertação de Mestrado, Universidade Federal de Ouro Preto, 142 p.
- Ricci P.S.F., Carvalho M.A. 2006. Rocks of the Pium-Area, Carajás Block, Brazil – A Deep seated High-T Gabbroic Pluton (Charnockitoid-Like) with Xenoliths of Enderbitic Gneisses Dated at 3002 Ma – The Basement Problem Revisited. In: Simpósio de Geologia da Amazônia, 8, [CD-ROM]
- Rigon J.C., Munaro P., Santos L.A., Nascimento J.A.S. Barreira C.F. 2000. Alvo 118 copper–gold deposit: geology and mineralization, Serra dos Carajás, Pará, Brazil. 31st International Geological Congress, Rio de Janeiro. SBG, Abstract Volume, [CD-ROM].
- Rosa A.G.N. 2006. Rochas encaixantes, alteração hidrotermal e caracterização dos fluidos relacionados à formação do Corpo Sequeirinho do Depósito Cu-Au do Sossego, região de Carajás: Dissertação de Mestrado, Universidade Federal do Pará.
- Rosière C.A., Baars F.J., Seoane J.C.S., Lobato L.M., Silva L.L. da, Mendes G.E. 2006. Structure and iron mineralization of the Carajás Province. T I Min Metall B, 115: 126-133.
- Santos J.O.S. 2003. Geotectônica dos Escudos da Guiana e Brasil Central. In: Bizzi, L.A., Schobbenhaus, C., Vidotti, R.M., Gonçalves, J.H., (Eds.), Geologia, Tectônica e Recursos Minerais do Brasil. Texto, Mapas e SIG. CPRM-Serviço Geológico do Brasil, vol. 4, pp. 169–226.
- Santos J.O.S., Hartmann L.A., Gaudette H.E., Groves D.I., McNaughton N.J., Fletcher I.R. 2000. A new understanding of the provinces of Amazon Craton based on field mapping and U-Pb and Sm-Nd geochronology. Gondwana Research, 3: 453-488.
- Sardinha A.S., Barros C.E. de M., Krymsky M. 2006. Geology, geochemistry and U–Pb geochronology of the Archean (2.74Ga) Serra do Rabo granite stocks, Carajás Metallogenetic Province, northern Brazil. Journal of South American Earth Sciences 20, 327–339.

- Silva G.G., Lima M.I.C., Andrade A.R.F., Issler R.S., Guimarrães G. 1974. Geologia. In: Levantamento de recursos naturais. Projeto Rodam: Folha SB.22 Araguaia e pane da Folha SC.22 Tocantins. Rio de Janeiro, MME-DNPM. v. 4, 143 p.
- Silva A.R.C., Villas R.N.N., Lafon J.M., Craveiro G.S. 2012. Idade da alteração e mineralização do depósito de Cu-Au Visconde, Província Mineral de Carajás (Pará), Brasil. 46º Congresso Brasileiro de Geologia, Santos. (CD-ROM).
- Silva M.A.D. 2011. O Domínio de Transição da Província Mineral de Carajás: Contexto geológico e litoquímica das unidades hospedeiras de mineralizações cúpro-auríferas. Trabalho de Conclusão de Curso. UNICAMP. 74p.
- Silva M.G., Teixeira J.B.G., Pimentel, M.M., Vasconcelos, P.M., Arielo, A. and Rocha, W.J.S.F. 2005. Geologia e mineralizações de Fe-Cu-Au do Alvo GT46 (Igarapé Cinzento, Carajás). In: Marini, O.J., Queiroz, E.T., Ramos, B.W. (eds.), Caracterização de Depósitos Minerais em Distritos Mineiros da Amazônia, 94-151.
- Soares A.D.V., Macambira M.J.B., Santos M.G.S., Vieira E.A.P., Massoti F.S., Souza C.I.J., Padilha J.L., Magni M.C.V. 2001. Depósito Cu-(Au) Cristalino, Serra dos Carajás, PA: Idade da mineralização com base em análises Pb-Pb em sulfetos (dados preliminares): Simpósio de Geologia da Amazônia, VII, Belém, Sociedade Brasileira de Geologia, [CD-ROM].
- Souza S.R.B., Macambira M.J.B., Sheller T. 1996. Novos dados geocronológicos para os granitos deformados do Rio Itacaiúnas (Serra dos Carajás, PA); implicações estratigráficas. V Simpósio de Geologia da Amazônia, Belém, Anais, 380–383.
- Tallarico F.H.B. 2003. O cinturão cupro-aurífero de Carajás, Brasil. Tese de doutorado, Universidade Estadual de Campinas, 229p
- Tallarico F.H.B., Figueiredo B.R., Groves D.I., Kositcin N., McNaughton N.J., Fletcher I.R., and Rego J.L. 2005. Geology and SHRIMP U-Pb geochronology of the Igarapé Bahia deposit, Carajás copper-gold belt, Brazil: an Archean (2.57 Ga) example of iron-oxideCu-Au-(U- REE) mineralization. Economic Geology 100:7–28.
- Tassinari C.C.G. 1996. O mapa geocronológico do Cráton Amazônico no Brasil: revisão dos dados isotópicos. Tese de Livre Docência, IG-USP, 139p.
- Tassinari C.C.G., & Macambira M.J.B. 1999. Geochronological Provinces of the Amazonian Craton. Episodes, 22 (3):174-182.
- Tassinari C.C.G., Mellito M.K. and Babinski M. 2003. Age and origin of the Cu (Au-Mo-Ag) Salobo 3A ore deposit, Carajás Mineral Province, Amazonian Craton, Northern Brazil. Episodes 26 (1), 2–9.
- Tassinari C.C.G., & Macambira M. 2004 A evolução tectônica do Cráton Amazônico. In: Mantesso-Neto, V., Bartorelli, A., Carneiro, C.D.R., Brito Neves, B.B. (eds.). Geologia do Continente Sul-Americano: Evolução da obra de Fernando Flávio Marques Almeida. São Paulo, Beca, p. 471-485
- Tassinari C.C.G., Tachibana J., Túlio M., Lívio R., Gaia C. 2005. Geologia isotópica aplicada nas mineralizações de Cu-Au do greenstone belt da Serra dos Gradaús, Província Mineral de Carajás, Cráton Amazônico: exemplo de mineralizações policíclicas. In: Simpósio Brasileiro de Metalogenia, 1, [CD-ROM]
- Tavaza E. 1999. Mineralização de Au-Cu-(ETR-U) associada às brechas hidrotermais do depósito de Iagarapé Bahia, província Mineral de Carajás, PA. Dissertação de Mestrado, Ouro Preto, Brazil, Universidade Federal de Ouro Preto. 81p.
- Teixeira J.B.G. 1994. Geochemistry, petrology, and tectonic setting of archean basaltic and dioritic rocks from the N4 Iron deposit, Serra dos Carajás, Pará, Brazil. 1994. 161 f. Tese de doutorado.
- Teixeira J.B.G., Lindenmayer Z.G., Silva M.G. 2010. Depósitos de Óxido de Fe, Cu-Au de Carajás. In: R.S.C. Brito, M.G. Silva, R.M. Kuyumjian. (Org.). Modelos de depósitos de cobre do Brasil e sua resposta ao intemperismo. 1 ed. Brasília: CPRM, p. 15-48.
- Teixeira W., Tassinari C.C.G., Cordani U.G., Kawashita K. 1989. A review of the geochronological of the Amazonian Craton: tectonic implications. Precambrian Research, 42: 213-227.

- Torresi I, Bortholoto D.F.A., Xavier R.P., Monteiro L.V.S. 2012. Hydrothermal alteration, fluid inclusions and stable isotope systematics of the Alvo 118 iron oxide–copper–gold deposit, Carajás Mineral Province (Brazil): implications for ore genesis. *Mineralium Deposita*, 47: 299–323.
- Vale. 2012. Vale obtains operation license for Salobo. <http://saladeimprensa.vale.com/en/release/interna.asp?id=22000>. Acessado em 04 fevereiro de 2013.
- Vasquez L.V., Rosa-Costa L.R., Silva C.G., Ricci, P.F., Barbosa, J.O., Klein, E.L., Lopes, E.S., Macambira, E.B., Chaves, C.L., Carvalho, J.M., Oliveira J.G., Anjos G.C., Silva H.R. 2008. *Geologia e Recursos Minerais do Estado do Pará: Sistema de Informações Geográficas – SIG: Texto Explicativo dos Mapas Geológico e Tectônico e de Recursos Minerais do Estado do Pará*. Organizadores: M.L Vasquez, L.T. Rosa-Costa. Escala 1:1.000.000. Belém: CPRM.
- Vasquez M.L., Macambira M.J.B., Armstrong R.A. 2008b. Zircon geochronology of granitoids from the western Bacajá domain, southeastern Amazonian craton, Brazil: Neoarchean to Orosirian evolution. *Precambrian Research* 161, 279–302
- Williams P.J., Barton M.D., Johnson D.A, Fontboté L., de Haller A., Mark G., Oliver N.H.S., Marschik R. 2005. Iron oxide-copper-gold deposits: Geology, space-time distribution, and possible modes of origin: in Hedenquist, J.W., Thompson, J.F.H., Goldfarb, R.J., and Richards, J.P., eds., *Economic Geology, 100th Anniversary Volume*, Society of Economic Geologists, p. 371-405.
- Wirth K.R., Gibbs A.K., Olszewski W.J.Jr. 1986. U–Pb ages of zircons from the Grão Pará Group and Serra dos Carajás granite, Pará, Brasil. *Revista Brasileira de Geociências* 16: 195–200.
- Xavier R.P., Wiedenbeck M., Trumbull R.B., Dreher A.M., Monteiro L.V.S., Rhede D., Araújo C.E.G., Torresi I. 2008a. Tourmaline B-isotopes fingerprint marine evaporites as the source of high-salinity ore fluids in iron oxide-copper-gold deposits, Carajás Mineral Province (Brazil): *Geology* 36: 743-746.
- Xavier R.P., Torresi I., Bortholoto D.F.A., Monteiro L.V.S., Souza Filho C.R. 2008b. Shallow iron oxide – copper-gold hydrothermal systems in the Carajás Mineral Province, Brazil: Example of the Alvo 118 deposit. 44º Congresso Brasileiro de Geologia, Curitiba, [CD-ROM].
- Xavier R.P., Monteiro L.V.S., Souza Filho C.R., Torresi I., Carvalho E.R., Dreher A.M., Wiedenbeck M., Trumbull R.B., Pestilho A.L.S., Moreto C.P.N. 2010. The iron oxide copper– gold deposits of the Carajás Mineral Province, Brazil: an updated and critical review. In: Porter TM (ed) *Hydrothermal Iron Oxide Copper-Gold & Related Deposits: A Global Perspective*. Australian Miner. Fund, Adelaide, Vol 3, pp. 285-306.
- Zuchetti M. 2007. Rochas maficas do grupo Grão Pará e sua relação com a mineralização de ferro dos depósitos N4 E N5, Carajás, PA: Tese de doutorado, Universidade Federal de Minas Gerais, 165p.

